THE UNIVERSITY OF QUEENSLAND

AUSTRALIA

Metabolomic Study of Baculovirus Infected Insect Cells to Identify Metabolite Based Strategies for Improving Virus Yields

Trinh Thi Bich Tran

Masters of Biotechnology (The University of Queensland, Australia)

Bachelors of Science (University of Natural Science, Vietnam)

A thesis submitted for the degree of Doctor of Philosophy at

The University of Queensland in 2014

Australian Institute for Bioengineering and Nanotechnology

Abstract

The baculovirus insect cell system has been used widely for biopesticide applications and for the production of recombinant proteins, vaccines and vectors for gene delivery. To be commercially viable, especially for the low margin applications of biopesticides and veterinary vaccines, the yield of this production system needs to be improved. One of the important approaches is the infection of insect cell cultures at high cell densities in order to maximize volumetric production. However, the cell specific yield gradually reduces with increasing infection cell density (ICD). As a result, the volumetric production can not improve further regardless of efforts to increase the uninfected cell density in batch or fed-batch cultures. The phenomenon known as “the cell density effect” appears not only during the late stage of protein production, but also during the early stage of virus replication and transcription. Discovering the changes in intra and extracellular metabolites between low and high ICDs may reveal evidence for improving yields. This PhD thesis focuses on the development of an intracellular metabolite extraction protocol for infected insect cell cultures and for measuring intra and extracellular metabolites of infected cells of different baculovirus infected insect cell systems.

Prior to analyzing the intracellular metabolites of low and high ICDs, an extraction protocol was developed and validated for insect cell cultures, especially infected insect cells. The ice-cold saline quenching solution developed for mammalian cells did not work well for insect cells, especially for infected cultures. Therefore, a modification of the quenching solution was made by an addition of 0.2% Pluronic® F-68 that successfully protected the cell membrane during quenching and washing procedures. In addition, one wash was found to be enough for removal of medium originated metabolites adhering on the surface of cell membranes. The ATP recovery (over the direct extract) of the extraction protocol using ice-cold saline quenching solution plus 0.2% Pluronic® F-68 after one wash was almost 90% for *Spodoptera frugiperda* (Sf9) cells infected with a recombinant *Autographa californica* multiple nucleopolyhedrovirus (rAcMNPV) and *Helicoverpa zea* (HzAM1) cells infected with a wild-type *Helicoverpa armigera* single nucleopolyhedrovirus (HearNPV) at 24 hours post infection (hpi).

The intracellular metabolite patterns and substrate consumption rates of low versus high ICDs was first investigated for the Sf9/rAcMNPV system in Sf900™III medium. A preliminary study was conducted to identify how late post-infection the cell membrane integrity was maintained during the quenching and washing processes. The result showed that the extraction protocol is efficient up to 48 hpi for infected Sf9 cells. Levels of intracellular nucleotides (tri-phosphates), amino acids (AA), and TCA cycle intermediates

(α-ketoglutarate, pyruvate) during an infection at a low ICD (2×10^6 cells/mL) were shown to be higher than those during an infection at a high ICD (6×10^6 cells/mL) with significant differences being found in many cases. Some evidence of AA uptake rates of infected Sf9 cells at a low ICD being higher than those at a high ICD was also found. Reductions in intracellular metabolite concentrations and AA consumption rates with increasing ICD were more severe at late infection stages.

The use of a chemically defined medium (CDM) allows improved intra and extracellular metabolite studies. Although some achievements in cell metabolism have been obtained from insect cells propagated in hydrolysate containing media, a CDM is useful for gaining additional insights into the metabolism of the cells. Results from the current study using a prototype CDM from Life Technologies shows that Sf9 cells grew well in the CDM and the infected Sf9 cells in this medium can produce recombinant protein (β-Gal) at a level (per cell basis) that is slightly higher than that for infected Sf9 cells in the control Sf900™III medium. The differences in intracellular metabolite concentrations between low and high ICDs for infected Sf9 cells in the CDM followed similar trends to those for infected Sf9 cells in Sf900™III. However, the differences in AA consumption rates between low and high ICDs for infected Sf9 cells in the CDM were much larger than those for the infected Sf9 cells in Sf900™III. The presence/absence of peptides in the medium is most likely the main reason for the difference between these two media. An underestimation of AA consumption rates post-infection was suggested from a comparison of the AA uptake data for cells infected in the CDM medium versus those infected in the peptide containing medium (Sf900™III).

Intracellular metabolite concentrations and substrate consumption patterns of the HzAM1cell/HearNPV system in Sf900™III medium was also investigated as a comparison to the Sf9 cells/rAcMNPV system. This system is important for the production of a biopesticide to target the major heliothis caterpillar pest. A preliminary study showed that the metabolite extraction protocol developed was efficient for infected HzAM1 until 48-60 hpi. As found for infected Sf9 cells, many intracellular metabolite concentrations for infected HzAM1 also significantly reduced with increasing ICD. Reduction in intracellular nucleotide tri-phosphates with increasing cell density prior to infection may be a key limiting factor leading to the decline in viral DNA and mRNA production and consequently, the drop in protein yield found with increasing ICD. In addition, consumption of AAs also reduced when the ICD increased especially at late infection stages. Furthermore, a reduction in the intracellular concentration of some of the TCA cycle intermediates associated with an increasing ICD might also contribute to the cell density effect.

This thesis makes an important contribution to the methodology for quantifying intracellular metabolites of insect cells in culture and of virus infected cells in general. It identifies a number of metabolites, in particular some nucleotides that may be limiting baculovirus yields during high cell density infections.

Declaration by author

This thesis *is composed of my original work, and contains* no material previously published or written by another person except where due reference has been made in the text. I have clearly stated the contribution by others to jointly-authored works that I have included in my thesis.

I have clearly stated the contribution of others to my thesis as a whole, including statistical assistance, survey design, data analysis, significant technical procedures, professional editorial advice, and any other original research work used or reported in my thesis. The content of my thesis is the result of work I have carried out since the commencement of my research higher degree candidature and does not include a substantial part of work that has been submitted *to qualify for the award of any* other degree or diploma in any university or other tertiary institution.

I acknowledge that an electronic copy of my thesis must be lodged with the University Library and, subject to the General Award Rules of The University of Queensland, immediately made available for research and study in accordance with the *Copyright Act 1968*.

I acknowledge that copyright of all material contained in my thesis resides with the copyright holder(s) of that material. Where appropriate I have obtained copyright permission from the copyright holder to reproduce material in this thesis.

Publications during candidature

Peer-reviewed papers

1. Trinh T.B. Tran, Stefanie Dietmair, Leslie C.L. Chan, Hoai T. Huynh, Lars K. Nielsen and Steven Reid (2012). Development of quenching and washing protocols for quantitative intracellular metabolite analysis of uninfected and baculovirus-infected insect cells. *Methods*, 56: 396-407.
2. Trinh T.B. Tran, Hoai T. Huynh, Mark Hodson, Leslie C.L. Chan, Lars K. Nielsen and Steven Reid (2014). Studies of the cell density effect on the metabolism of baculovirus infected Sf9 cells in Sf900™III medium. *Applied Microbiology and Biotechnology*. Submission pending.
3. Trinh T.B. Tran, Hoai T. Huynh, Lars K. Nielsen and Steven Reid. Studies of the cell density effect on the metabolism of the baculovirus HzAM1/HearNPV System (2014). *Archives Virology*. Submission pending
4. Trinh T.B. Tran, Hoai T. Huynh, Lars K. Nielsen and Steven Reid. Influence of medium on the nutrient consumption and intracellular metabolite profiles of baculovirus infected insect cells at low and high infection cell densities**.** Under preparation.

Conference papers

1. Tran, T.T.B, Huynh, H.T, Chan, L.C, Nielsen, L., Reid, S. (2012). Evaluation of an intracellular metabolite extraction protocol for baculovirus-infected insect cells. Poster presentation at the ComBio Conference. Held in Adelaide, Australia on 24-27/9/2012.
2. Tran, T.T.B, Huynh, H.T, Chan, L.C, Nielsen, L., Reid, S. (2012). Evaluation of an intracellular metabolite extraction protocol for Sf9 infected insect cells**.** Poster presentation at the first International Conference on BioNano Innovation. Held in Brisbane, Australia on 18-20/7/2012.
3. Reid, S., Tran, T.T.B, Huynh, H.T, Chan, L.C, Nielsen, L. (2011). Metabolomics study of infected insect cells. The 10th Conference on Protein Expression in Animal Cells (10th PEACe) on September 25-29/2011, Cascais, Portugal.

Publications included in this thesis

1. **Trinh T.B. Tran**, Stefanie Dietmair, Leslie C.L. Chan, Hoai T. Huynh, Lars K. Nielsen and Steven Reid (2012). Development of quenching and washing protocols for quantitative intracellular metabolite analysis of uninfected and baculovirus-infected insect cells. *Methods*, 56: 396-407.

   This publication is incorporated as Chapter 3.

Contributor	Statement of contribution
Tran, T.T.B (Candidate)	Designed experiments (80%)
	Conducted experiments (95%)
	Wrote the paper (90%)
Dietmair, S.	Designed experiments (5%)
Chan, L.C.	Designed experiments (5%)
	Wrote and edited paper (5%)
Huynh, H.T.	Conducted experiments (5%)
Nielsen, L.	Designed experiments (5%)
Reid, S.	Designed experiments (5%)
	Wrote and edited paper (5%)

Contributions by others to the thesis

No contributions by others

Statement of parts of the thesis submitted to qualify for the award of another degree

None

Acknowledgements

First of all, I would like to thank my principal supervisor, Dr. Steven Reid for giving me his valuable advice, support, and encouragement to complete my PhD project. I am grateful for the financial support from Dr. Reid for the last 3 months of my candidature.

I also would like to thank Dr. Leslie Chan, my co-supervisor for his advice and support during my project.

A special thanks to Professor Lars Nielsen for his valuable advice and support.

Thanks go to Mr. Bob Simpson for his assistance in using the real time PCR equipment.

My work has received help and support from other members in our biopesticide research group, especially Mr. Hoai Huynh who supported and helped me in some of my experiments, so I would like to thank them all. Thanks for help and friendship of staff and students from the Nielsen group. In particular I would like to thank Mark Hodson for his help in conducting a wide range of analytical procedures.

I would like to thank Mr. Tony Miscamble, AIBN Research Higher Degree Manager and Ms. Laurie Sendra, AIBN Research Higher Degree Program Administrator, for their guidance and assistance during my candidature.

Finally, I would like to express my thankfulness to the University of Queensland for awarding me the UQ Vietnam-Australia 35 Year Commemorative Research Higher Degree Scholarship.

Most importantly, that is my family. Without their continuing love and support this thesis would not be possible. Very special thanks to my husband and my little daughter. Their accompanying love provided endless support for me and allowed me to complete this thesis.

Keywords

Baculovirus, Insect cell culture, *Spodoptera frugiperda*, *Heliothis zea*, Cell density effect, Intracellualr metabolite extraction, Metabolomics, Consumption rates, β-Galactosidase, Occlusion body

Australian and New Zealand Standard Research Classifications (ANZSRC)

ANZSRC code: 100302, Bioprocessing, Bioproduction and Bioproducts, 80%
ANZSRC code: 060506, Virology, 20%

Fields of Research (FoR) Classification

FoR code: 1001, Agricultural Biotechnology, 50%
FoR code: 1003, Industrial Biotechnology, 50%

Table of Contents

List of Figures & Tables

producing wild-type HaSNPV at a TOI of 0.75×10^6cells/mL and an MOI of 17 PFU/cell. Error bars show the standard deviation of biological triplicates.

Fig. 3.3 Intracellular concentrations of ATP, ADP and AMP (adenosine phosphates, AdoP) and recoveries of total AdoP and ATP (R-Total AdoP, R-ATP), from uninfected and baculovirus-infected insect cells after being direct extracted (DE), quenched but not washed (Q0W), quenched and washed one or two times (Q1W, Q2W) and unquenched (UQ). Ice-cold NaCl+P (0.5-1^{o}C) was used for both quenching and washing, while room temperature NaCl+P was used for the UQ case. 100% acetonitrile (-40^{o}C) was used for direct extraction of cell cultures, while 50 %v/v acetonitrile in deionized water (-40^{o}C) was used to extract quenched and unquenched cell pellets. (A) Uninfected Sf9 cells, sampled at 1×10^6 cells/mL. (B) Infected Sf9 cells, with rβ-Gal-AcMNPV at a TOI of 1.5×10^6 cells/mL and an MOI of 20 PFU/cell, sampled at24 hpi (C) Uninfected HzAM1 cells, sampled at 1×10^6 cells/mL. (D) Infected HzAM1 cells, with wtHearNPV at a TOI of 0.75×10^6 cells/mL and an MOI of 17 PFU/cell, sampled at 24 hpi. Error bars show the standard deviation of biological triplicates.

Fig. 3.4 Intracellular concentrations of amino acids from uninfected and baculovirus-infected insect cells after being quenched but not washed (Q0W), and quenched with one, two or three wash steps (Q1W, Q2W, Q3W), using ice-cold NaCl+P as the quenching solution (QS). Non-standard Norvaline (Nva) was spiked into the QS as a means of gauging washing efficiency. Ice-cold NaCl+P (0.5-1^{o}C) was used for both quenching and washing, and 50%v/v acetonitrile in deionized water (-40^{o}C) was used to extract the cell pellets. (A) Uninfected Sf9 cells, sampled at 1×10^6 cells/mL. (B) Infected Sf9 cells, with rAcMNPV at a TOI of 1.5×10^6 cells/mL and an MOI of 20 PFU/cell, sampled at 24 hpi (C) Uninfected HzAM1 cells, sampled at 1×10^6 cells/mL. (D) Infected HzAM1 cells, with wtHearNPV at a TOI of 0.75×10^6 cells/mL and an MOI of 17 PFU/cell, sampled at 24 hpi. Error bars show the standard deviation of biological triplicates.

Fig. 4.1 The kinetics of cell growth, cell size expansion and viability (a), specific vDNA and β-Gal production (b), intracellular levels and the recovery at different times post-infection (c) and the intracellular amino acids (AAs) (d) of Sf9 cells infected with a recombinant baculovirus (rAcMNPV) at an MOI of 10 PFU/cell. Infections were conducted in Sf900™III serum free medium at infection cell densities (ICD) of 2.5×10^6 cells/mL, and a multiplicity of infection (MOI) of 10 PFU/cell. The experiment was conducted in shaker-flask suspension cultures. Each data point is the average from three biological replicates, and

the error bars represent the standard deviation. Abbreviations, TCD: total cell density, Via: viability, Dia: cell diameter, INF: infected, UINF: uninfected.

Fig. 4.2 Total cell density and cell hypertrophy (a), specific vDNA and β-Gal production (b), and total cell protein vs β-Gal (c) of Sf9 cells infected with a rAcMNPV. Infections were conducted in Sf900™III serum free medium at low (2×10^6) and high (6×10^6 cells/mL) ICDs and at an MOI of 10 PFU/cell. The experiment was conducted in shaker-flask suspension cultures. Each data point is the average from three biological replicates, and the error bars represent the standard deviation. Abbreviations, TCD: total cell density, Via: viability, Dia: cell diameter, LICD: low infection cell density, HICD: high infection cell density

Fig. 4.3 Multivariate analysis of intracellular metabolite concentrations of Sf9 infected cells at low ($2x10^6$ cells/mL) and high ($6x10^6$ cells/mL) ICDs. Orthogonal projection to latent structures–discriminant analysis (OPLS-DA) scores (a) and loadings (b) plots of the 5 time points post-infection at low and high ICDs, classified by cell density. OPLS-DA model metrics: Predictive component R2X = 0.197; R2 = 0.913; Q2 = 0.869; R2Y = 1: Orthogonal component R2X = 0.278.

Fig. 4.4 Intracellular concentrations of organic acids and UDP sugars for infected Sf9 cells at low (2×10^6) and high (6×10^6 cells/mL) ICDs. Infections were conducted in Sf900™III serum free medium at an MOI of 10 PFU/cell in shaker-flask suspension cultures. Each data point is the average from three biological replicates, and the error bars represent the standard deviation.

Fig. 4.5 Stacked bar charts of (a) adenosine, (b) uridine, (c) guanosine and (d) cytidine nucleotide concentrations of Sf9 infected cells over 5 time points post-infection at low ($2x10^6$ cells/mL) and high ($6x10^6$ cells/mL) ICDs. Infections were conducted in Sf900™III serum free medium at an MOI of 10 PFU/cell. The experiment was conducted in shaker-flask suspension cultures. Each data point is the average from three biological replicates, and the error bars represent the standard deviation.

Fig. 4.6 Intracellular AA concentration of infected Sf9 cells at various times post-infection at low (a) and high (b) ICDs, and the comparison between low and high ICD for intracellular AA levels at 0 hpi (c) and 36 hpi (d). Infections were conducted in Sf900™III at low (2×10^6) and high (6×10^6 cells/mL) ICDs and at an MOI of 10 PFU/cell. The experiment

was conducted in shaker-flask suspension cultures. Each data point is the average from three biological replicates, and the error bars represent the standard deviation.

Fig. 4.7 AA consumption rates between early (0-24 hpi) and late (24-60 hpi) infection stages for low (a) and high ICD (b) and between low and high ICDs for early (c) and late infection (d) of Sf9 cells infected with a rAcMNPV. Infections were conducted in Sf900™III at low (2×10^6) and high (6×10^6 cells/mL) ICDs and at an MOI of 10 PFU/cell. The experiment was conducted in shaker-flask suspension cultures. Each data point is the average from three biological replicates, and the error bars represent the standard deviation.

Fig. 4.8 AA consumption rates (mmol/mm^3 cell biomass/hour) between early (0-24 hpi) and late (24-60 hpi) infection stages for low (a) and high ICD (b) and between low and high ICDs for early (c) and late infection (d) of Sf9 cells infected with a rAcMNPV. Infections were conducted in Sf900™III at low (2×10^6) and high (6×10^6 cells/mL) ICDs and at an MOI of 10 PFU/cell. The experiment was conducted in shaker-flask suspension cultures. Each data point is the average from three biological replicates, and the error bars represent the standard deviation.

Fig. 4.9 Ratios of AA levels between high versus low ICDs for extra- and intra-cellular AAs at 0 hpi (a) and 36 hpi (b) and ratios between intra- versus extra-cellular AA levels for low and high ICDs at 0 hpi (c) and 36 hpi (d) of Sf9 cells infected with a recombinant baculovirus (rAcMNPV). Infections were conducted in Sf900™III at low (2×10^6) and high (6×10^6 cells/mL) ICDs and at an MOI of 10 PFU/cell. The experiment was conducted in shaker-flask suspension cultures. Each data point is the average from three biological replicates, and the error bars represent the standard deviation.

Fig. 4.10 Extracellular concentrations of sugars and organic acids for infected Sf9 cells at low (2×10^6) and high (6×10^6 cells/mL) ICDs over various times post-infection. Infections were conducted in Sf900™III serum free medium at an MOI of 10 PFU/cell in shaker-flask suspension cultures. Each data point is the average from three biological replicates, and the error bars represent the standard deviation.

Fig. 5.1 Free AA concentrations of Sf900™III and CDM media. Sf900™III would be expected to contain other AAs in the form of small peptides from the yeast hydrolysate

present in the medium. However the AA levels shown for the CDM are expected to represent the total AA concentration present in the medium.

Fig. 5.2 Stock cell maintenance of Sf9 cells propagated either in Sf900™III (blue) or CDM (red) over 50 days (a). Cells were passaged every 3-4 days at a seeding cell density of 4-5×10^5 cells/mL. The growth curve of Sf9 cells propagated either in Sf900™III (blue) or CDM (red) over 168 hours post-inoculation (b). Cell specific β-Gal yield of Sf9 cells infected at an MOI of 10 PFU/cell either in Sf900™III or CDM at low (1×10^6 cells/mL) and high (6×10^6 or 5×10^6 cells/mL for Sf900™III or CDM, respectively) ICDs, (c). Cell cultures were maintained in shaker flasks with three biological replicates and the error bars are the standard deviation of the triplicates.

Fig. 5.3 The kinetics of cell growth and cell viability (a), cell size expansion (b) and specific β-Gal yield (c) of infected Sf9 cells propagated in CDM at low (1×10^6 cells/mL) and high (5×10^6 cells/mL) ICDs. Infections were conducted at a multiplicity of infection (MOI) of 10 PFU/cell in shaker-flask suspension cultures. Each data point is the average from three biological replicates, and the error bars represent the standard deviation.

Fig. 5.4 Multivariate analysis of intracellular metabolite concentrations of infected Sf9 cells propagated in CDM at low (1×10^6 cells/mL) and high (5×10^6 cells/mL) ICDs. Orthogonal projection to latent structures–discriminant analysis (OPLS-DA) scores (a) and loadings (b) plots of the 4 time points post-infection at low and high ICDs, classified by cell density. OPLS-DA model metrics: Predictive component R2X = 0.279; R2 = 0.987; Q2 = 0.907; R2Y = 1: Orthogonal component R2X = 0.203. Infections were conducted at a multiplicity of infection (MOI) of 10 PFU/cell in shaker-flask suspension cultures.

Fig. 5.5 Stacked bar charts of (a) adenosine, (b) uridine, and (c) cytidine nucleotide concentrations for four time points post-infection of infected Sf9 cells propagated in CDM at low (1×10^6 cells/mL) and high (5×10^6 cells/mL) ICDs. Infections were conducted at an MOI of 10 PFU/cell in shaker-flask suspension cultures. Each data point is the average from two biological replicates, and the error bars represent the standard deviation.

Fig. 5.6 Intracellular AA concentrations of infected Sf9 cells at four times post-infection for low (a) and high (b) ICDs, and the comparison between low and high ICDs for intracellular AA levels at 0 hpi (c) and 36 hpi (d). Infections were conducted in CDM at low (1×10^6 cells/mL) and high (5×10^6 cells/mL) ICDs and at an MOI of 10 PFU/cell. The experiment

was conducted in shaker-flask suspension cultures. Each data point is the average from two biological replicates, and the error bars represent the standard deviation. (*) indicates significant differences in the levels observed.

Fig. 5.7 Comparison of AA consumption rates (mmol/cell/hour) between early (0-24 hpi) and late (24-60 hpi) infection stages for low (a) and high ICDs (b) and between low and high ICDs for early (c) and late infection stages (d) of Sf9 cells infected with a rAcMNPV. Infections were conducted in CDM at low (1×10^6 cells/mL) and high (5×10^6 cells/mL) ICDs and at an MOI of 10 PFU/cell. The experiment was conducted in shaker-flask suspension cultures. Each data point is the average from two biological replicates, and the error bars represent the standard deviation. (*) indicates significant differences in the levels observed.

Fig. 5.8 Comparison of AA consumption rates (mmol/mm^3 of cell volume/hour) between early (0-24 hpi) and late (24-60 hpi) infection stages for low (a) and high ICDs (b) and between low and high ICDs for early (c) and late infection stages (d) of Sf9 cells infected with a rAcMNPV. Infections were conducted in CDM at low (1×10^6 cells/mL) and high (5×10^6 cells/mL) ICDs and at an MOI of 10 PFU/cell. The experiment was conducted in shaker-flask suspension cultures. Each data point is the average from two biological replicates, and the error bars represent the standard deviation. (*) indicates significant differences in the levels observed.

Fig. 5.9 Ratios of AA levels between high versus low ICDs for extra- and intra-cellular AAs at 0 hpi (a) and 36 hpi (b), and ratios between intra- versus extra-cellular AA levels for low and high ICDs at 0 hpi (c) and 36 hpi (d) of Sf9 cells infected with a recombinant baculovirus (rAcMNPV). Infections were conducted in CDM at low (1×10^6 cells/mL) and high (5×10^6 cells/mL) ICDs, at an MOI of 10 PFU/cell. The experiment was conducted in shaker-flask suspension cultures. Each data point is the average from two biological replicates, and the error bars represent the standard deviation. (*) indicates significant differences in the levels observed. The ratios of alanine are off scale in some cases in the above figure and so are listed here: 3.7, 2.6 and 3.2 for extra and intracellular at 0 hpi and extracellular at 36 hpi, respectively.

Fig. 5.10 Ratios of specific β-Gal yield between high and low ICDs for infected Sf9 cells in Sf900™III and CDM media. The ratio was calculated from the average values (from biological triplicates) for high and low ICDs and the error bar is the standard deviation

calculated from standard deviations of the dividend and divisor. Data for infected Sf9 cells in Sf900™III medium was from the dataset in Chapter 4.

Fig. 5.11 Ratios of intracellular ATP (a), total adenosine (b), UTP (c) and CTP (d) between high and low ICDs for infected Sf9 cells in Sf900™III and CDM media. The ratio was calculated from the average values (from biological duplicates) for high and low ICDs and the error bar is the standard deviation calculated from standard deviations of the dividend and divisor. Data for infected Sf9 cells in Sf900™III medium was from the dataset in Chapter 4.

Fig. 5.12 Ratios of intracellular KGA (a), FUM (b), UDPG (c) and UDPGA (d) between high and low ICDs for infected Sf9 cells in Sf900™III and CDM media. The ratio was calculated from the average values (from biological triplicates) for high and low ICDs and the error bar is the standard deviation calculated from standard deviations of the dividend and divisor. Data for infected Sf9 cells in Sf900™III medium was from the dataset in Chapter 4.

Fig. 5.13 Ratios between high/low ICDs forintracellular AAs at various time post-infection of infected Sf9 cells in Sf900™III (a) and CDM (b), and the comparison of these ratios for infected Sf9 cells in Sf900™III and CDM at 0 hpi (c) and 36 hpi (d). The ratio was calculated from the average values (from biological triplicates) for high and low ICDs and the error bar is the standard deviation calculated from standard deviations of the dividend and divisor. Data for infected Sf9 cells in Sf900™III medium was from the dataset in Chapter 4.

Fig. 5.14 Comparison of AA consumption rates of uninfected cultures between Sf9 cells propagated in Sf900™III and CDM over the exponential period of 0-72 hours post-innoculation. The values were the average of biological triplicates and the error bar is the standard deviation of the triplicates. Data for infected Sf9 cells in Sf900™III medium was from the dataset in Chapter 4.

Fig. 6.1 The kinetics of cell growth, cell size expansion and viability (a), specific vDNA and OB yields (b) and intracellular ATP levels and the recovery over various times post-infection (c) of HzAM1 cells infected with a wide-type baculovirus (HearNPV) at a multiplicity of infection (MOI) of 5 PFU/cell. Infections were conducted in Sf900™III medium at infection cell densities (ICD) of 1×10^6 cells/mL. The experiment was conducted

in shaker-flask suspension cultures. Each data point is the average from three biological replicates, and the error bars represent the standard deviation.

Fig. 6.2 Total cell density (a), cell hypertrophy (b), specific vDNA (c) and OB production (d) of HzAM1 cells infected with a wild-type HearNPV. Infections were conducted in Sf900™III serum free medium at various ICDs from 0.5-4×10^6 cells/mL at an MOI of 5 PFU/cell. The experiment was conducted in shaker-flask suspension cultures. Each data point is the average from three biological replicates, and the error bars represent the standard deviation. For OB yield, measurement was conducted only one at 168 hpi due to the low accuracy of OB counts at earlier stages.

Fig. 6.3 Correlations between the peak yields (volumetric or specific) of vDNA (a, b) or OB(c, d) and the peak cell density (PCD) from HzAM1 cell cultures infected with a wild-type baculovirus (HearNPV) at various ICDs of 0.5 to 4×10^6 cells/mL, and a MOI of 5 PFU/cell. The experiment was conducted in shaker-flask suspension cultures. Each data point is the average from three biological replicates, and the error bars represent the standard deviation. Significance testing was performed separately for each experimental set of data points with different letters indicating values that are significantly different according to Tukey's HSD (α=0.05).

Fig. 6.4 Intracellular concentrations of adenosine (a), uridine (b) and cytidine (c) nucleotides and amino acids of uninfected HzAM1 cell cultures at various cell densities from 0.5 to 8×10^6 cells/mL. Cultures were propagated in Sf900™III serum free medium. The experiment was conducted in shaker-flask suspension cultures. Each data point is the average from three biological replicates, and the error bars represent the standard deviation. Significance testing was performed separately for each experimental set of data points with different letters indicating cases that are significantly different according to Tukey's HSD (α=0.05).

Fig. 6.5 Multivariate analysis of intracellular metabolite concentrations of infected HzAM1 at low (0.5x10^6 cells/mL) (green) and moderate high (2x10^6 cells/mL) (blue) ICDs. Orthogonal projection to latent structures–discriminant analysis (OPLS-DA) scores (a) and loadings (b) plots of the 6 time points post-infection at low and high ICDs, classified by cell density. OPLS-DA model metrics: Predictive component R2X = 0.124; R2 = 0.857; Q2 = 0.685; R2Y = 1: Orthogonal component R2X = 0.26. Infections were conducted in

Sf900™III serum free medium at an MOI of 5 PFU/cell. The experiment was conducted in shaker-flask suspension cultures.

Fig. 6.6 Stacked bar charts of (a) adenosine, (b) uridine, and (c) cytidine nucleotide concentrations of 6 time points post-infection of infected HzAM1 cells at low ($0.5x10^6$ cells/mL) and moderate high ($2x10^6$ cells/mL) ICDs. Infections were conducted in Sf900™III medium at an MOI of 5 PFU/cell (HearNPV). The experiment was conducted in shaker-flask suspension cultures. Each data point is the average from three biological replicates, and the error bars represent the standard deviation.

Fig. 6.7 Intracellular AA concentrations at 6 times post-infection at low (a) and high (b) ICDs , and the comparison between low and high ICDs for intracellular AA levels at 0 (c) and 36 hpi (d) of infected HzAM1 cells. Infections were conducted in Sf900™III at low ($0.5x10^6$ cells/mL) and high ($2x10^6$ cells/mL) ICDs and at an MOI of 5 PFU/cell (HearNPV). The experiment was conducted in shaker-flask suspension cultures. Each data point is the average from three biological replicates, and the error bars represent the standard deviation. Data from the same AA with an (*) was significant difference according to Tukey's HSD test (α=0.05).

Fig. 6.8 Comparison of AA consumption rates (mmol/cell/hour) between early (0-18 hpi) and late (18-72hpi) infection stages for 3 different infection cell densities of 0.5×10^6 (a) 2×10^6 (b), and 4×10^6 cells/mL (c) of infected HzAM1 cells. Infections were conducted in Sf900™III at an MOI of 5 PFU/cell (HearNPV). The experiment was conducted in shaker-flask suspension cultures. Each data point is the average from three biological replicates, and the error bars represent the standard deviation. Data from the same AA with an (*) was significant difference according to Tukey's HSD test (α=0.05).

Fig. 6.9 Comparison of AA consumption rates (mmol/cell/hour) among 3 infection cell densities of 0.5×10^6, 2×10^6, and 4×10^6 cells/mL at either early (0-18 hpi) (a) or late (18-72hpi) (b) infection stagesof infected HzAM1. Infections were conducted in Sf900™III at an MOI of 5 PFU/cell (HearNPV). The experiment was conducted in shaker-flask suspension cultures. Each data point is the average from three biological replicates, and the error bars represent the standard deviation.

Fig. 6.10 Comparison of AA consumption rates (mmol/mm^3 of cell biomass/hour) among 3 infection cell densities of 0.5×10^6 cells/mL, 2×10^6 cells/mL, and 4×10^6 cells/mL at either

early (0-18 hpi) (a) or late (18-72 hpi) (b) infection stages of infected HzAM1 cells. Infections were conducted in Sf900™III at an MOI of 5 PFU/cell (HearNPV). The experiment was conducted in shaker-flask suspension cultures. Each data point is the average from three biological replicates, and the error bars represent the standard deviation.

Fig. 6.11 Ratios of AA levels between high versus low ICDs for extra- and intra-cellular AAs at 0 hpi (a) and 36 hpi (b) and ratios between intra- versus extra-cellular AA levels for low and high ICDs at 0 hpi (c) and 36 hpi (d) ofinfected HzAM1 cells. Infections were conducted in Sf900™III at low (0.5×10^6 cells/mL) and high (2×10^6 cells/mL) ICDs and at an MOI of 5 PFU/cell (HearNPV). The experiment was conducted in shaker-flask suspension cultures. Each data point is the average from three biological replicates, and the error bars represent the standard deviation.

Table 4.4 Comparison of sugar and AA consumption rates ($\times 10^{-6}$ mmol/mm^3 cell biomass/hour) between uninfected and infected cells at low (2×10^6) and high (6×10^6 cells/mL) ICDs. Detailed description is presented in Table 4.3.

Table 5.1.Intracellular metabolites concentrations (mM) over various times post-infection for Sf9 cells infected with a recombinant baculovirus (rAcMNPV) in a chemically defined medium at either low (1×10^6) or high (5×10^6 cells/mL) infection cell densities (ICDs). Data represented as an average of biological duplicates. The metabolites listed were selected on the basis of showing significant variations in levels between different ICDs or times post infection following the analysis shown in Fig. 5.4.

Table 5.2 Glucose and amino acid consumption rates ($\times 10^{-12}$ mmol/cell/hour) of uninfected and infected Sf9 cells infected with a rAcMNPVat low (1×10^6) and high (5×10^6 cells/mL) ICDs in a chemically defined medium (CDM). Uninfected and infected cultures were set up at 0.5×10^6 cells/mL. For the case of uninfected cultures no infection was made and sampling was conducted at every 24 hours during the 24-hour doubling time period. For infected cases, cultures were infected with a baculovirus at an MOI of 10 PFU/cell at 1×10^6 and 5×10^6 cells/mL and sampling was conducted every 12 hours until 60 hours post-infection. Data is the average of biological duplicates.

Table 5.3 Comparison of AA consumption rates ($\times 10^{-6}$ mmol/mm^3 cell volume/hour) between uninfected and infected Sf9 cells infected with a rAcMNPV at low (1×10^6 cells/mL) and high (5×10^6 cells/mL) ICDs in a chemically defined medium (CDM). Further description details are as shown in Table 2.

Table 6.1 Intracellular metabolite concentrations (mM) for HzAM1cells infected with a wild-type baculovirus (HearNPV) at either low (0.5×10^6) or moderately high (2×10^6 cells/mL) infection cell densities (ICDs) over various times post-infection. Data represented as an average of biological triplicates. The metabolites listed were selected on the basis of showing significant variations in levels between different ICDs or times post infection following the analysis shown in Fig. 6.5.

Table 6.2 Glucose and amino acid consumption rates ($\times 10^{-12}$ mmol/cell/hour) of uninfected and infected HzAM1 cells infected with a wide-type HearNPV at various ICDs. Uninfected and infected cultures were set up at 0.5×10^6 cells/mL. For the case of uninfected cultures no infection was made and sampling was conducted every 24 hours during the period that

the culture maintained a 24-hour doubling time. For infected cultures, cultures were infected with an MOI of 5 PFU/cell at 0.5, 2 and 4×10^6 cells/mL and sampling was conducted every 12 hours until 60 hours post-infection. Data is the average of biological triplicates.

Table 6.3 Comparison of AA consumption rates ($x10^{-6}$mmol/mm^3 cell volume/hour) of uninfected and infected HzAM1 cells infected with a wild-type HearNPV at various ICDs. Further details are as described in Table 6.2.

List of Abbreviations

AA	Amino acid
AcMNPV	*Autographa californica* multiple nucleopolyhedrovirus
AdoP	Adenosine phosphates
ADP	Adenosine di-phosphate
AMP	Adenosine mono-phosphate
ALA	Alanine
ARG	Arginine
ASN	Asparagine
ASP	Aspartate
ATP	Adenosine tri-phosphate
BEVS	Baculovirus expression vector system
β-Gal	β-Galactosidase
BCA	Bicinconinic acid assay
BSA	Bovine serum albumin
BV	Budded virus
CIT	Citrate
CDP	Cytidine di-phosphate
CMP	Cytidine mono-phosphate
CTP	Cytidine tri-phosphate
DE	Derect extract
dpi	Days post infection
dCTP	Deoxycitidine tri-phosphate
dNTP	Deoxyribonucleoside tri-phosphate
dRNs	Deoxyribonucleotides
dTTP	Deoxythymidine tri-phosphate
dUTP	Deoxyuridine tri-phosphate
FUM	Fumarate
GDP	Guanosine di-phosphate
GLN	Glutamine
GLU	Glutamate
GLY	Glycine
GMP	Guanosine mono-phosphate
GTP	Guanosine tri-phosphate

HearNPV	*Helicoverpa armigera* nucleopolyhedrovirus
HIS	Histidine
hpi	Hour post infection
HSD	Honestly Significant Difference
HzAM1	*Helicoverpa zea* cell line
ICD	Infection cell density
ILE	Isoleucine
IPM	Integrated Pest Management
KGA	α-ketoglutarate
LAC	Lactate
LEU	Leucine
LYS	Lysine
MET	Methionine
MOI	Multiplicity of infection
NPV	Nucleopolyhedrovirus
OB	Occlusion body
ODV	Occlusion body derived virus
ONPG	o-nitrophenyl-β-D-galactopyranoside
P	Passage
PBS	Phosphate buffered saline
PCD	Peak cell density
PTCD	Peak total cell density
PCR	Polymerase chain reaction
PHE	Phenylalanine
PRO	Proline
PYR	Pyruvate
RT-PCR	Real time polymerase chain reaction
SDS	Sodium dodecyl sulphate
SER	Serine
Sf9	*Spodoptera frugiperda* cell line
Sf900™II/III	Commercial medium for insect cell culture
SUC	Succinate
SY	Specific yield
TCA cycle	Tricarboxylic acid cycle

TCD	Total cell density
TCV	Total cell volume
THR	Threonine
TRP	Tryptophan
TYR	Tyrosine
UDP	Uridine di-phosphate
UDPG	Uridine di-phosphate glucose
UDPGA	Uridine di-phosphate gluconic acid
UDPNAG	Uridine di-phosphate N-acetylglucosamine
UMP	Uridine mono-phosphate
UTP	Uridine tri-phosphate
VAL	Valine
VLP	Virus like particle
VY	Volumetric yield

Chapter 1

Introduction

1.1 Introduction

This chapter presents an overview of the background related to the research project. It includes highlights of the application of baculovirus insect cell systems, the biology of baculoviruses, *in vitro* production of baculoviruses and a description of the cell density effect, an overview of insect cell metabolism and metabolomics approaches used to study metabolism. The end of this chapter presents a thesis outline which lists the key research questions to be investigated in this thesis.

1.2 The application of baculovirus insect cell expression systems

The baculovirus insect cell expression systems have become a useful tool for efficient production of recombinant eukaryotic proteins (Jarvis, 2009; Kost et al., 2005; Mena and Kamen, 2011), and have evolving applications in human biologics such as humanized N-glycoproteins, baculovirus display immunogens and gene delivery vectors for mammalian cells (Aucoin et al., 2010; Kost et al., 2005). Recently, baculovirus-expression has gained considerable momentum as a regulatory-approved manufacturing platform for human (Cervarix®, Provenge®) and veterinary (Ingelvac®, Porcilis®) vaccines (Mena and Kamen, 2011).

Besides being a valuable commercial tool for recombinant protein production, the baculovirus insect cell systems have been extensively studied for the production of baculoviruses which can be developed as effective biopesticides to control various types of insect pests (Chakraborty et al., 1996; Chakraborty et al., 1999; Pedrini et al., 2006), especially as part of an integrated pest management program (Moscardi et al., 2011; Szewczyk et al., 2009).

1.2.1 Baculovirus insect cell systems and recombinant protein production

As mentioned above, the baculovirus insect cell systems have been used widely for recombinant protein production. In fact, baculoviruses have been employed to express a wide variety of heterologous proteins in insect cell cultures (Buerger et al., 2007; Caron et al., 1990; Chan et al., 1998; Hink et al., 1991; Hitchman et al., 2010; Nishikawa et al., 2003; Possee et al., 1999; Weiss, 1992). The reasons for using baculovirus insect cell systems include high levels of post translational modifications, potentially high expression levels by using the baculovirus polyhedrin promoter, stability of vector constructs and a large genome capacity (Mena and Kamen, 2011). In fact, insect cells possess pathways that facilitate the folding, modification, and assembly of the protein product (Kost et al.,

2005). It has been proven in many studies that insect cells are able to carry out many of the processing events such as glycosylation, phosphorylation, fatty acid acylation, amidation, proteolytic processing and cellular targeting required for the formation of biologically active, heterologous proteins that are antigenetically, immunogenically and functionally similar to their native proteins (Luckow and Summers, 1988; O'Reilly et al., 1994).

In addition, there is an interest in using the baculovirus insect cell expression system as a research tool for producing human and veterinary vaccines (Mena and Kamen, 2011; van Oers, 2006), and as vectors for gene delivery (Hitchman et al., 2010; Hu, 2008). Being well-documented as safe for vertebrates and the ability to transduce mammalian cells, baculoviruses are being evaluated as efficient vectors to deliver antigens for vaccination (Yang et al., 2007). The cervical cancer vaccine (from GlaxoSmithKline) is the first human vaccine produced in insect cells with a baculovirus vector that has been marketed. Another human product, a prostate cancer vaccine (Provence^{TM}) approved by the Federal Drug Administration (USA) is also made using the baculovirus expression system. Other human vaccines in the late stage of clinical development include the recombinant hemagglutinin based influenza vaccine, FluBlok®, developed by Protein Sciences Corporation (Meriden, Connecticut, USA), and the therapeutic vaccine for diabetic type 1 treatment, Diamyd®, developed by Diamyd Medical AB (Stockholm, Sweden) (Mena and Kamen, 2011).

Furthermore, baculoviruses show an ability to enter a wide range of mammalian cells and thus, may be useful to use as vectors for gene delivery. By the 1990s, numerous cell lines had been transduced successfully (Boyce and Bucher, 1996; Hofmann et al., 1995). Since then, the use of baculoviruses as vectors for gene therapy has gradually gained in popularity for use in this area (Kost and Condreay, 2002; Kost et al., 2005). The inability to replicate in mammalian cells and the low cytotoxicity property of baculoviruses make them good candidates for gene therapy *in vitro* (Airenne et al., 2009). Recently, baculovirus vectors have been developed as potential vectors for gene therapy (Airenne et al., 2010), either as a gene carrier or as a production system for other gene therapy vectors such as adeno-associated viruses (Hu, 2006; Shan et al., 2006). It can be used for *in vivo* targeting of genes to several organs such as brain and liver (Hu, 2008) and to stem cells for tissue engineering (Lin et al., 2010).

1.2.2 Baculovirus biopesticides

Insect pests cause severe damage to crops worldwide and are one of the major causes of loss of agricultural yield. Chemical pesticides have been used widely to control

pests in agriculture for many years with premium efficiency. However, increasing resistance to existing chemical pesticides (Franzmann et al., 2008; Jacobson et al., 2009), increasing concern about the environment and food safety issues, and the desire of farmers to use safer pesticides are all reasons for the interest in biopesticides. The use of biological approaches as alternatives for pest control is the smart choice of modern agriculture towards sustainable agriculture and organic farming practices.

Biological approaches as alternatives for chemical pesticides include the use of environmentally friendly biological agents and/or genetic modification of crops to ensure pest resistance. Transgenic crops have been developed and are used widely, with the most common transgenic crops for insect pest control being *Bt* cotton and maize. However, field evolved insect resistance to transgenic crops even with gene pyramiding (Tabashnik et al., 2009), the high cost of development and registration, the resistance of the public to gene modification of crops (Moscardi et al., 2011), and limited access of farmers to such biotech crops due to intellectual property issues are all limitations for the widespread use of this pest control measure. Therefore, biological agents, especially baculoviruses remain of interest as alternatives to the use of chemical pesticides.

Baculoviruses, among other insect viruses, are regarded as safe and selective bioinsecticides, restricted to invertebrates (Moscardi, 1999). Baculoviruses are one of the most promising biocontrol agents, with a low chance of resistance development and proven high safety levels (Szewczyk et al., 2006). More than 50 baculovirus-based pesticides have been registered and used worldwide (Moscardi et al., 2011). In fact, baculoviruses have been used to control caterpillar pests that affect major crops such as soybean, sorghum, maize, tomato, cotton, pigeon pea, and pepper in many countries including Brazil, China, India, America, and Australia (Buerger et al., 2007; Szewczyk et al., 2009). It is considered as an ideal tool for Integrated Pest Management (IPM) programs (Buerger et al., 2007; Moscardi et al., 2011).

1.3 Baculovirus biology and infection cycle

Baculoviruses belong to the family of *Baculoviridae*, which are a diverse group of viruses found mostly in insects and they appear as pathogens of several insects. They are known to infect arthropods and are not known, so far, to have any non-arthropod hosts (O'Reilly et al., 1994). They are characterized by rod-shaped occluded viruses with circular, double-strand DNA ranging from 80 to 200 kbp (Pan et al., 2007; Szewczyk et al., 2009). The family is composed of 4 genera of *Alphabaculovirus* (Lepidopteran nucleopolyhedrovirus), *Betabaculovirus* (Lepidopteran granulovirus), *Gammabaculovirus*

(Hymenopteran nucleopolyhedrovirus) and *Deltabaculovirus* (Dioteran nucleopolyhedrovirus) (Jehle et al., 2006; Moscardi et al., 2011; Szewczyk et al., 2009). The majority of baculoviruses used as biological agents for pest control are in the genus of nucleopolyhedrovirus (NPVs) (Pedrini et al., 2006). These viruses are excellent candidates for use as biopesticides due to their high virulence to their specific host, narrow host range, and the fact that they cause little damage to beneficial insects, and result in minimal disruption to other biological control measures (Burges et al., 1980; Moscardi, 1999; Teakle, 1995). The NPVs are usually divided into two morphotypes: based on single (SNPVs) or multiple (MNPVs) nucleocapsids packaged into each envelope (Granados and Hashimoto, 1989; Shuler et al., 1995; Szewczyk et al., 2006; Vlak, 1992).

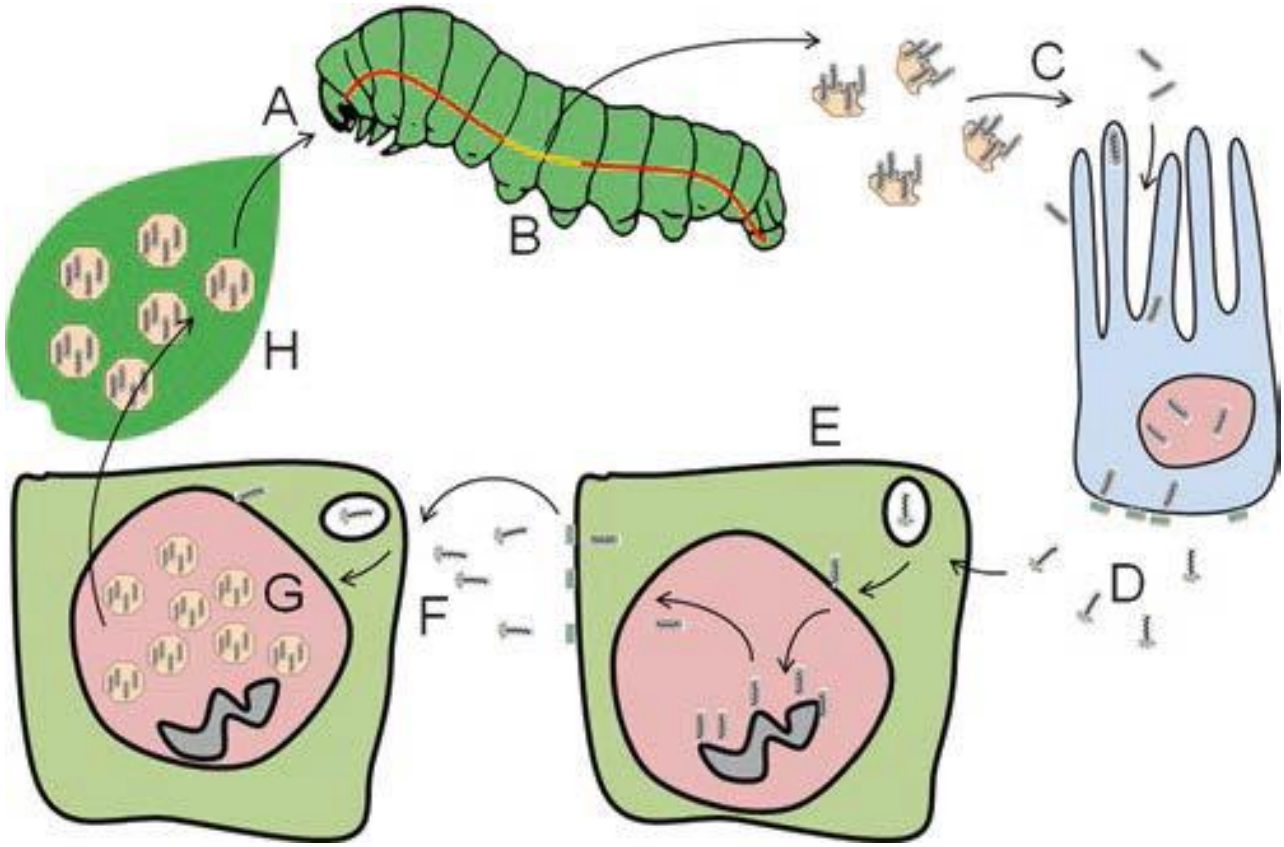

Fig. 1.1 Diagram of a baculovirus infection cycle in nature (Moscardi et al., 2011). OBs enter a caterpillar through ingestion along with plant material (A) and the high alkaline environment (pH 9.5-11.5) of the midgut (B) degrades OBs and releases ODVs to infect midgut epithelial cells (C). Infected cells produce BVs, which bud out (D) and infect other cells (E). After secondary infection (F), virus accumulates in occlusion bodies (G). Finally, the larval body disintegrates and millions of polyhedra are released to the environment (H).

Baculoviruses have been isolated from more than 700 invertebrates (Tanada and Kaya, 1993), and are widely known as safe and effective microbial insecticides. The baculovirus life cycle involves two virus forms, the occlusion-derived virus (ODV)

contained within occlusion bodies (OB) and the budded virus (BV). Primary infections are initiated when caterpillars ingest OBs, which dissolve in the alkaline midgut to release ODVs. Midgut cells then release BVs which transmit secondary infection to other cell-types. Numerous OBs are then produced, which are released into the environment upon caterpillar liquefaction. Fig. 1.1 represents the natural life cycle of baculoviruses.

These two virus phenotypes (BV and ODV) have different roles and are generated at different stages during the baculovirus life cycle (Faulkner and Carstens, 1986; Rohrmann, 1992). BVs are produced during the late stages of viral infection and spread the infection from cell to cell within the insect and are highly infectious to cultured cells. ODVs are produced very late in the viral replication cycle, in which virions remain within insect cell nuclei, accumulate and are occluded in polyhedra. These occluded virions are released upon disintegration of dead insects and contaminated foliage is ingested by other susceptible insects (Funk et al., 1997). ODVs only spread infection from insect to insect but do not normally spread the infection within insect tissues.

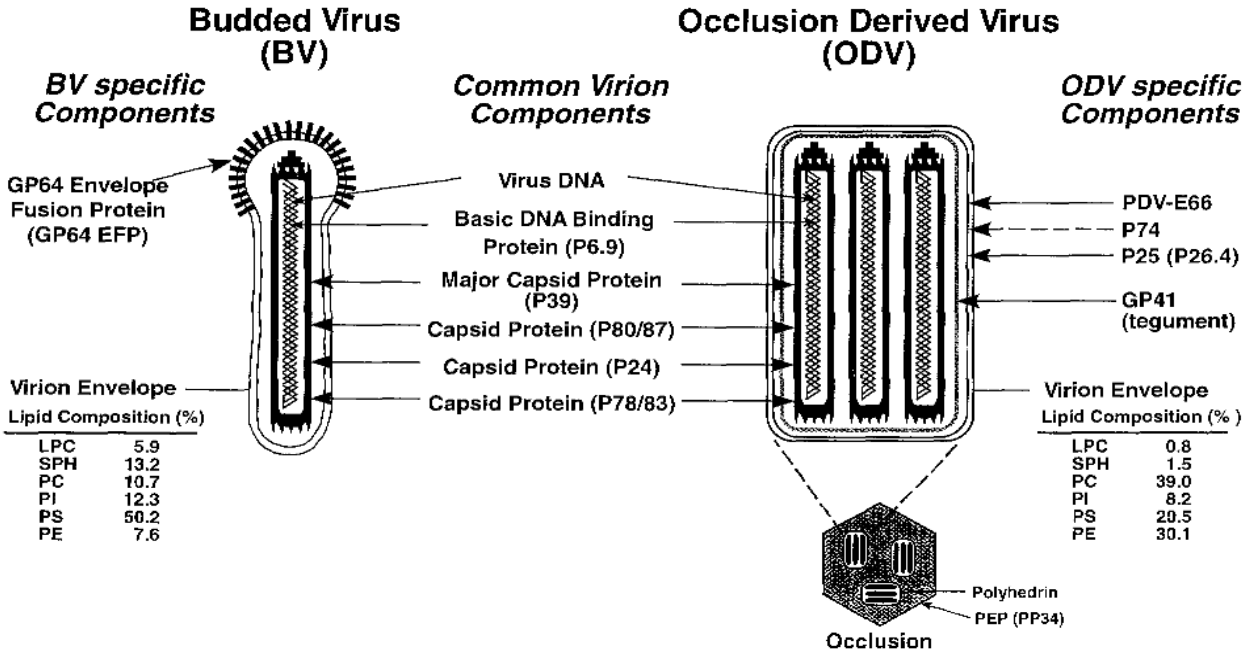

Fig. 1.2 The two phenotypes of baculovirus: budded virus (BV) and occlusion derived virus (ODV) (Blissard, 1996).

Since the infection process of these two forms of NPVs is different, the structure of the envelope is clearly different. Every polyhedron is surrounded by a polyhedron envelope that is alkali-soluble, which allows them to dissolve under the high pH environment of the insect midgut, releasing virions. However, the occluded viral form is highly stable in the external environment (Szewczyk et al., 2006), which is a major factor in allowing persistence of the virus and subsequent initiation of sporadic infections of insect

populations at intervals of one year or more (Funk et al., 1997; Rohrmann, 1999). Therefore, OB is the form of the virus for use as a biopesticide (Rohrmann, 1999; Slack and Arif, 2007). In contrast, BVs acquire an envelope when they bud through the cytoplasmic membrane which has been modified by a viral-encoded glycoprotein called *gp*64, and it is adapted for movement and infection of tissues within the insect (Funk et al., 1997). The structure of both phenotypes of NPVs is shown in Fig. 1.2.

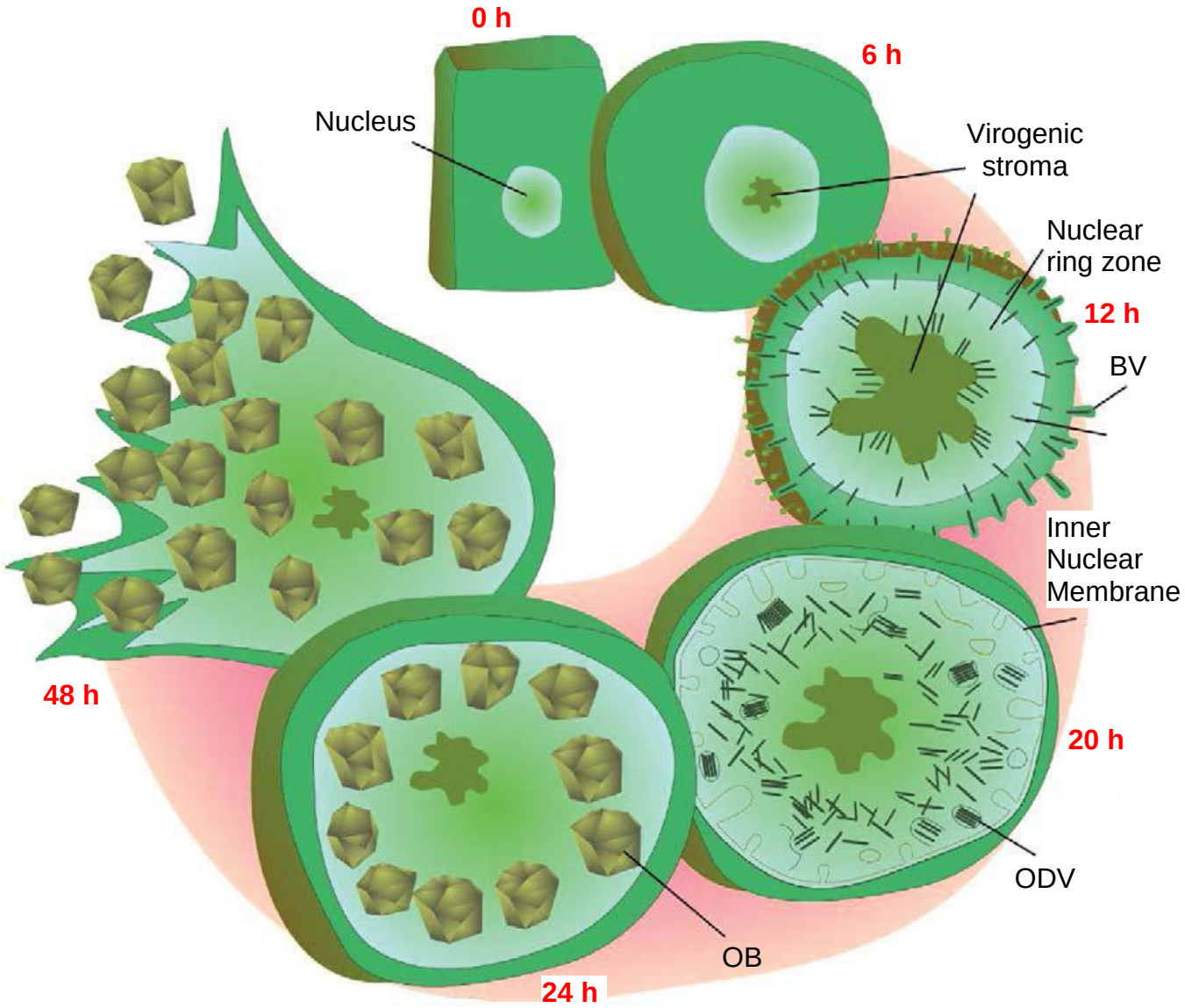

Fig. 1.3 Baculovirus infection cycle in cell culture (Slack and Arif, 2007). Several phases of virus replication are illustrated beginning with the rounding of newly infected cells and finishing with the lytic release of OBs. Indicated times are relative to the infection cycle of AcMNPV.

In cell culture, the infection cycle takes place in three basic phases: early, late and very late. These three phases correspond biologically to 1) the early phase that entails reprogramming of the cell for virus replication; 2) the late phase that involves producing

BV's; and 3) the very late phase involving production of OB's (O'Reilly et al., 1994; Slack and Arif, 2007). The infection cycle in cell culture is illustrated in Fig. 1.3.

Understanding changes inside the cells corresponding to various phases in the infection cycle may reveal the cause of the drop in the cell specific yield during high cell density infections and provide options for improving virus yields. For example, during the very late phase that involves polyhedra protein/OB production, there is likely to be a high demand for energy and amino acids, but at this stage the cell is entering a death phase and so the uptake of nutrients at this time may be compromised.

1.4 *In-vitro* production and the cell density effect

1.4.1 *In vitro* production of baculovirus biopesticides

Baculoviruses have been produced *in vivo* for commercial use as biopesticides. To date, over 50 baculovirus biopesticide products against different insect pests worldwide are produced *in vivo* either in the field or in the laboratory using caterpillars raised in insectaries (Moscardi et al., 2011). The *in vivo* production of baculoviruses, however, is associated with several disadvantages including being labour intensive and costly (Agathos, 1991; Black et al., 1997), and it is difficult to have quality control over the purity of products especially when requiring large scale production (Powell and Faull, 1989). In contrast, *in vitro* production of baculoviruses using insect cell culture offers several advantages including higher purity of product (Shuler et al., 1995) as well as the possibility to select desirable cell clones which may provide greater viral yield (Weiss et al., 1994). Thus, *in vitro* production has been indicated as a key element in making biopesticides more desirable in the market (Szewczyk et al., 2006).

In addition, *in vitro* production of baculoviruses also avoids the complexity of rearing insect larvae for virus infection and production *in vivo*. Moreover, hundreds of cell lines have been developed and the specific cell strains can be stored for later use leading to great potential for the production of baculoviruses *in vitro* (Moscardi et al., 2011). In general, it is possible to develop an efficient process to harvest biologically active OB free from contaminants that would be cheap compared with virus produced *in vivo* (Weiss et al., 1994).

While *in vivo* production is simple and low cost at small scale, it becomes costly as scale increases and it is widely believed that *in vitro* production is essential for baculoviruses to be more broadly commercialized. Baculoviruses display genetic instability in culture which is a limitation to *in vitro* production that is caused by the accumulation of mutant few polyhedra, FP phenotypes (de Rezende et al., 2009; Pedrini et al., 2004), and

the formation of Defective Interfering Particles (DIPs) (Moscardi et al., 2011). These limitations can be minimized by a production process developed by Dr Reid's laboratory (Reid and Lua, 2005). The current method of producing baculoviruses starting with caterpillar ODVs is capable of producing of 2×10^{12} OB/L. However, *in vitro* baculovirus yields still need to be increased 4 fold over current yields (to 8×10^{12} OB/L) to be commercially successful. In order to increase the yield, it is necessary to infect the cell at high cell densities. Unfortunately, the specific yield drops when increasing the cell density at the time of infection. Cells infected at lower cell densities, (0.5×10^{6} to 1×10^{6} cells/mL), have been shown to produce 600 OB/cell, but the yield drops in half to about 300 OB/cell for infections at high cell densities ($3\text{-}4\times10^{6}$ cells/mL). Hence, if the yield of 600 OB/cell can be achieved for high density infections, it is feasible to increase the yields to be more commercially successful. In other words, it is necessary to overcome the challenge for improving yields that is related to the cell density effect.

1.4.2 The cell density effect

The cell density effect is the phenomenon of the reduction in cell specific yield with increasing infection cell density (ICD), and it is well documented for baculovirus infected insect cells. The cell density effect has been reported mainly for Sf9 cells (Carinhas et al., 2009; Caron et al., 1990; Doverskog et al., 2000; Jesionowski and Ataai, 1997; Radford et al., 1997; Reuveny et al., 1993; Taticek and Shuler, 1997; Wong et al., 1996; Yamaji et al., 1999). There are a few investigations conducted in other cell lines such as *Anticarsia gemmatalis* (saUFL-AG-286) (Micheloud et al., 2009), *Trichopulsia ni* (Hi5) (Chico and Jager, 2000; Ikonomou et al., 2004; Taticek and Shuler, 1997; Yang et al., 1996), and *Heliothis zea* (HzAM1) (Chakraborty et al., 1996), which show that the cell density effect applies generally to baculovirus infected insect cell systems.

There have been many speculations on the cause of the cell density effect including nutrient limitation, toxic compound accumulation, cell-to-cell contact inhibition, but the reasons for this drawback remain unidentified (Doverskog et al., 1997; Taticek and Shuler, 1997). It has been suggested that the cause of the drop in productivity at high cell densities for baculovirus infection processes is related to nutrient limitations rather than accumulation of toxins (Drews et al., 1995; Radford et al., 1997; Wong et al., 1996). This is supported by the fact that there is an increase in the cell specific yield with an improvement of the nutrient supply through fed-batch strategies (Chan et al., 1998; Elias et al., 2000; Jardin et al., 2007) or fresh medium replacement (Chakraborty et al., 1996; Doverskog et al., 2000; Ikonomou et al., 2004; Jesionowski and Ataai, 1997; Lindsay and

Betenbaugh, 1992; Radford et al., 1997; Reuveny et al., 1993). The nutrient limitation may involve micronutrients such as vitamins or trace elements, some of which are cofactors for enzymes involved in critical processes such as catabolism (e.g. pyruvate dehydrogenase) and DNA replication (e.g. DNA polymerase). These limitations may also result in the limiting of nucleotides for viral DNA replication and transcription. However, the process limitation for the cell density effect may not be entirely related to nutrient supply, and there could be many factors involved in this issue and the mechanism causing the cell density effect is not fully understood. There could be complex interactions between the virus infection process, cellular physiology and the physio-chemical environment. Recently, the reduction in recombinant protein production at high cell densities has been shown to be strongly correlated with limitations in the upstream processes of virus replication and transcription (Huynh et al., 2013). Other possible factors causing low productivity in high density cultures have been suggested including oxygen limitations (Lecina et al., 2006; Palomares et al., 2004; Taticek and Shuler, 1997), the cell cycle phase at the time of infection (Calles et al., 2006; Doverskog et al., 2000) and the history of the culture (Doverskog et al., 2000).

In order to identify the cause of the cell density effect and to overcome this bottleneck, many attempts have been made. These include the measurement of extracellular metabolites to identify the limiting nutrients in the medium (Caron et al., 1990; Drews et al., 1995; Reuveny et al., 1993); the measurement of consumption rates and fluxomics analysis (Bernal et al., 2009); and supplementing culture media with glucose, glutamine, complex nutrient mixtures, and key intermediate metabolites (Carinhas et al., 2010; Reuveny et al., 1993). However, the limitation of these approaches is that the metabolite levels in the media do not necessarily reflect intracellular metabolite levels. For many reasons, some metabolites may not get into the cells even if they are available in the culture medium at reasonable levels. Therefore, intracellular metabolite measurements can provide a better understanding of what happens inside the cells and consequently, appropriate actions may be taken to improve yields.

The metabolite environment inside the cells at low and high cell densities at the time of infection may reveal the cause of the cell density effect. In particular, intracellular metabolite measurements in combination with consumption rates of key metabolites may identify limitations during high cell density infections. It is possible for example that poor transport into cells of key metabolites at high cell densities post-infection contribute to the cell density effect, rather than a limitation of metabolites in the medium.

1.5 Insect cell metabolism

The metabolism of different insect cell lines has been reported by many research groups. In particular, the metabolism of *Spodoptera frugiperda* (Sf9) and *Trichoplusia ni* (Tn5B1-4 or High Five) cell lines have been studied thoroughly (Bedard et al., 1993; Benslimane et al., 2005; Drews et al., 1995; Drews et al., 2000; Ferrance et al., 1993; Ohman et al., 1995; Reuveny et al., 1993; Rhiel et al., 1997; Sugiura and Amann, 1996), as these two cell lines have been extensively used for recombinant protein production. In addition to Sf9 and High Five cells, the metabolism of other cell lines including *Helicoverpa zea* (Lua and Reid, 2003) and *Anticarsia gemmatalis* (de Rezende et al., 2009; Gioria et al., 2006) have also been investigated to a significant degree.

Generally, there are some common aspects of insect cell metabolism including the utilization of sugars, peptides, amino acids, organic acids, vitamins, lipids and organic salts (Agathos 1991), and the production of alanine, lactate and ammonium ions as by-products (Rhiel et al., 1997; Sugiura and Amann, 1996). Glucose is usually the preferred carbon and energy source of insect cells (Bedard et al., 1993; Rhiel et al., 1997). Several studies with *Spodoptera frugiperda* cell lines demonstrated the importance of glucose for cell growth (Bedard et al., 1993; Bhatia et al., 1997; Drews et al., 1995; Mendonca et al., 1999; Reuveny et al., 1993). The high level of glucose consumption in Sf9 cell cultures is indicative of the presence of an active glycolytic pathway (Neermann and Wagner, 1996; Raghunand and Dale, 1999). Consumption of maltose usually occurs during the early growth phase in media containing both glucose and maltose (Bedard et al., 1993; Ferrance et al., 1993), while fructose was only consumed after glucose depletion (Ikonomou et al., 2003). Sucrose, on the other hand, is not consumed by either Sf9 (Bedard et al., 1993; Drews et al., 1995; Reuveny et al., 1993) or Hi5 (Rhiel et al., 1997) cells.

It has been reported in many studies that glutamine is a key nutrient for insect cells (Bedard et al., 1993; de Rezende et al., 2009; Ferrance et al., 1993; Reuveny et al., 1993; Wang et al., 1993). The main by-product of insect cell metabolism is alanine (Bedard et al., 1993; Drews et al., 1995; Ohman et al., 1995; Reuveny et al., 1993), but no inhibitory effect related to alanine has been reported (Doverskog et al., 1997). Lactate and ammonia production levels are minimal even at high substrate concentrations and not inhibitory unless other culture conditions become adversely inhibitory (Bedard et al., 1993; Benslimane et al., 2005; Drews et al., 2000; Ferrance et al., 1993; Ikonomou et al., 2003; Rhiel et al., 1997; Sugiura and Amann, 1996; Wang et al., 1993). These are only some

common aspects of insect cell metabolism, the specific consumption level and preference of substrates as well as by-product formation level are different between cell lines and depend on the cultivation conditions.

It is suggested that different insect cell lines have different nutrient requirements as well as different levels of waste product accumulation during cell culture. The consumption of glutamine is considered as the most significant compared to the other amino acids for Sf9 cells, and this suggests that glutamine may have a possible role in the energy metabolism of Sf9 cells. Unlike Sf9 cells, HzAM1cells show a preference for asparagine over glutamine (Lua and Reid, 2003), and this is similar for the High Five cells. It has been reported for Sf9 cells that the production levels of lactate and ammonia are minimal even at high substrate concentrations (Bedard et al., 1993; Benslimane et al., 2005; Drews et al., 2000; Ferrance et al., 1993; Ikonomou et al., 2003; Rhiel et al., 1997; Sugiura and Amann, 1996; Wang et al., 1993). In contrast, HzAM1 cells showed a significant level of ammonia production in Sf900™II medium, which is an asparagine and glutamine rich medium (Lua and Reid, 2003). However, given the absence of asparagine and glutamine in the medium, there is no accumulation of ammonia (Lua and Reid, 2003). Insect cells may consume ammonium ions as a nitrogen source in glutamine free media (Ohman et al., 1995), and when infected with a baculovirus (Wang et al., 1993; Wang et al., 1996). These studies indicate that the by-product formation pattern observed is not only characterized by the cell line used but also is strongly influenced by the cultivation conditions (Drews et al., 2000). Similarly, it has been shown that alanine accumulated at very high levels as a metabolic byproduct (Bedard et al., 1993; Drews et al., 2000; Ohman et al., 1995; Rhiel et al., 1997). However, no alanine was formed by Sf9 cells during glucose limitations (Ohman et al., 1995), indicating that much of the glucose in culture is utilized for biosynthesizing precursors (Bhatia et al., 1997).

The metabolism of insect cells before and after infection with a baculovirus is different, and it has been suggested that post infection cell metabolism increases. Several groups found a higher consumption of glucose, glutamine and other amino acids, an increase in alanine production, and a higher oxygen uptake, up to 80% (Palomares et al., 2004) during the post infection period. Nevertheless, there is no report on the growth inhibition of Sf9 cell lines related to alanine (Doverskog et al., 1997), and the reduced yield in insect cell cultures at high cell densities is most likely caused by nutrient depletion rather than inhibition by waste products (Drews et al., 1995).

1.6 Metabolomics approach

1.6.1 Definition of metabolomics

The definition of metabolomics was first introduced by Fiehn (2002), although studies on the metabolome had been done earlier (Oliver et al., 1998; Tweeddale et al., 1998). According to Fiehn, metabolomics addresses the identification and quantification of all the metabolites in a living system. However, the study of the complete metabolome is unachievable because of the complexity of the metabolome in chemical and structural diversity as well as its broad dynamic range. In other words, there is no analytical technique that is able to measure the complete set of metabolites. Therefore, several terms are used to distinguish different types of analysis as shown below. Definitions and their application in metabolomic studies can be different from group to group.

Definitions of common terms used in the field of metabolomics are listed below:

Metabolome: A complete set of metabolites present in a biological system that participate or are generated in its metabolism (Dettmer et al., 2007; Oldiges et al., 2007).

Metabolic fingerprinting: Global screening approach to classify crude samples with minimal sample preparation based on metabolite patterns or “fingerprints” (Dettmer et al., 2007; Dunn, 2008). Identification and quantification is limited and the strategy is employed as a tool for discrimination of samples from different biological origins or status. It is also defined as the study of the intracellular metabolome (Dunn, 2008).

Metabolic footprinting: Analysis of the extracellular metabolites in cell culture medium. Unlike intracellular metabolite analysis, there is no requirement for quenching and extraction of metabolites (Dunn, 2008; Oldiges et al., 2007).

Metabolite profile: Analysis of a set of metabolites related to a class of compounds (carbohydrates, amino acids) or a specific biochemical pathway (Dettmer et al., 2007; Dunn, 2008; Fiehn, 2001; Villas-Boas et al., 2005b). The analysis uses a particular analytical technique, together with an estimate of quantity (Castrillo et al., 2003; Roessner et al., 2000).

Metabolite targeted analysis: Quantitative analysis of a small number of identified metabolites related to a specific part of the metabolism (Dunn, 2008; Fiehn, 2002; Mashego et al., 2007; Villas-Boas et al., 2005b).

1.6.2 The application of metabolomics and its challenges

Metabolomic approaches, which offer an analysis of metabolite levels in biological samples, have been employed widely recently. Metabolomic studies have been done in

yeast and bacteria (Allen et al., 2003; Bhattacharya et al., 1995; Buchholz et al., 2002; Castrillo et al., 2003; Chassagnole et al., 2002; de Koning and van Dam, 1992; Gonzalez et al., 1997; Markuszewski et al., 2003; Tweeddale et al., 1998; Villas-Boas et al., 2005a). These approaches have also been applied for the investigation of the metabolome in plants and animals with a particular focus on metabolomic studies in mammalian systems. Several metabolomic studies in mammalian cells have been conducted such as with adherent cultured human fibroblasts (Bennett et al., 2008), Madin–Darby canine kidney (MDCK) (Ritter et al., 2008) and hepatic cells (Hofmann et al., 2008), human breast cancer cell lines (Teng et al., 2009), as well as suspension cultured Chinese hamster ovary (CHO) and mouse NS0 myeloma cells (Dietmair et al., 2010; Sellick et al., 2009).

In comparison to transcriptomics or proteomics, the study of metabolomics offers some advantages. Firstly, the metabolome reflects the functional level of the cell more appropriately because the metabolome is the downstream product of the genome. Changes in the metabolome are expected to be amplified relative to the proteome or the transcriptome (Urbanczyk-Wochniak et al., 2003). Secondly, the metabolome is a highly discriminatory system for studying changes in biology. It has been shown in certain situations that although alterations in the concentrations of proteins or transcripts are neither significant nor detectable, the concentration of metabolites can significantly change (Dunn and Ellis, 2005). Finally, the metabolome is a high-throughput strategy because costs for metabolomics experiments are low compared to proteomic and transcriptomic experiments (Dunn, 2008; Fiehn, 2002; Goodacre et al., 2004). In short, metabolomic studies are ‘complementary’ to transcriptomic and proteomic studies in order to determine gene functions of an organism (Dunn and Ellis, 2005; Fiehn, 2002; Urbanczyk-Wochniak et al., 2003). However, metabolomic approaches face particular challenges resulting from properties of the metabolites. These properties include rapid turnover, structure diversity, wide range of metabolite concentrations, and a huge number of metabolites.

Rapid turnover

Many metabolites are extremely labile, such as cytosolic glucose, with a turnover rate of approximately 1 mM/s and ATP at the rate of 1.5 mM/s (de Koning and van Dam, 1992; Theobald et al., 1997; Weibel et al., 1974). Due to the rapid turnover of metabolites, samples must be quenched immediately upon sampling to ensure that the measured metabolite concentration reflects the metabolic state of the sample at the sampling time point.

Diversity of metabolite structure

Different atomic arrangements form a diverse set of metabolites of low molecular weight (less than 1000 Da). The diversity in molecular structure is expressed in the number of atoms in the molecule, the carbon skeleton, the number and location of active groups, the presence of stable and unstable atomic bonds as well as the geometric structure of the molecule. Variability in atomic structure provides wide variations in chemical (molecular weight, polarity, solubility) and physical (volatility) properties. This structure diversity makes the determination of the complete metabolome simultaneously impossible (Villas-Boas et al., 2005b). Therefore, all sample preparation and analytical techniques for metabolite determination have been developed to target classes of metabolites and to achieve as much information as possible. There is no unique extraction procedure for metabolome analysis that will cover all intracellular metabolites.

Wide range of metabolite concentrations

It is estimated that the range of metabolite concentrations inside a cell can vary approximately 7-9 orders of magnitude (pmol–mmol) (Dunn and Ellis, 2005; Ryan and Robards, 2006). The large range of abundance together with the large variation in the nature of metabolites provides additional challenges to the analytical technologies employed in metabolomic studies.

Huge number of metabolites

The total number of metabolites varies depending on the biological system investigated. Several hundred metabolites are postulated to be present in microorganisms, while much higher numbers, up to thousands of metabolites are expected in more complex organisms. The metabolome of yeast (*Saccharomyces cerevisiae*) is estimated to be around 600 metabolites, whereas, more than 200,000 metabolites are expected in plants and humans (Dunn and Ellis, 2005; Mungur et al., 2005; Ryan and Robards, 2006). In addition, (Schwab, 2003), reported that microorganisms generally have fewer metabolites than genes, whereas complex organisms such as plants, have more metabolites than genes in a biological system. Multiple mRNAs could be formed from a single gene, multiple proteins from one mRNA, and multiple metabolites may be formed from one enzyme, because many enzymes may accept more than one substrate, although enzymes generally have high selectivity. Therefore, as indicated above, it is impossible to date to

isolate and measure all metabolites together as desired for a comprehensive metabolomic study.

1.6.3 Sample preparation for metabolome analysis

Sample preparation is one of critical steps in metabolome analysis. According to Ritter et al. (2008), the most difficult part in a metabolomic study is the identification of an appropriate sample preparation method. It is because sample preparation is affected by many factors including the organism under investigation, the cultivation mode, the medium composition, and the assay used to quantify the metabolites. The differences in cell wall or cell membrane structure and cell size may influence the efficiency of quenching and the rate of metabolite leakage (Sellick et al., 2009). Undoubtedly quenching and extraction methods are sample- and cell-dependent (Sellick et al., 2009; Sellick et al., 2010), and they need to be validated for each organism of interest (Faijes et al., 2007); otherwise, extractions can lead to enormous errors (Bolten et al., 2007).

Sample preparation and cell extraction makes the intracellular metabolites accessible to the different analytical methods employed, but it is almost impossible to avoid losses, mainly due to the diverse chemical and physical properties of the metabolome (Villas-Boas et al., 2005a). Fig. 1.4 illustrates the key steps required for a sample preparation procedure to measure intracellular metabolites. The two most important steps in this scheme are the quenching and extraction. They are the most critical technical features for characterization of the intracellular metabolites (Sellick et al., 2009).

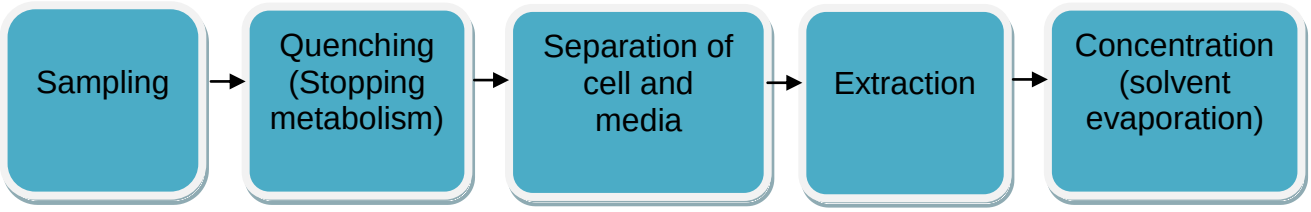

Fig. 1.4 Schematics of sample preparation steps for intracellular metabolite analysis

In most sample preparation protocols for metabolome analysis, an initial quenching of the cells to stop metabolism, followed by extraction of the metabolites are included. Some extraction protocols, for suspension culture cells, quench cell activity directly with a cold extraction solution before removal of the medium. This approach presumes that the majority of the cellular metabolites will not be present in the medium and hence, can be presumed to have an intracellular localization (Sellick et al., 2009). However, there are a large number of metabolites that are present in both the culture medium and inside the

cells, (e.g., amino acids), or that may be secreted to the extracellular medium during growth. Consequently, direct extraction approaches are associated with the risk of overestimating intracellular pools, because the metabolites present in the extracellular medium are not removed (Canelas et al., 2008). This is a particular restriction for animal cells, which are grown in complex and "metabolite-rich" media (Sellick et al., 2009). Therefore, extraction approaches must remove, or minimize as much as possible, contamination of intracellular metabolites by those in the medium when dealing with animal cells in culture.

"Quenching" or stopping cellular metabolism

As many metabolites turnover rapidly such as cytosolic glucose and ATP as mentioned above, quenching cells upon sampling is necessary to stop cellular metabolism and to prevent metabolite turnover. It is ideal if the time between sampling and quenching is shorter than the turnover rates of such metabolites to prevent alteration in the intracellular metabolite concentrations, and to ensure that measured metabolite levels are accurate at the time of sampling. Otherwise, the measured metabolite concentration does not reflect a snapshot of the sample at the sampling time point. In order to shorten the interval between sampling of the cells and their metabolic inactivation, cells should be quenched immediately together with their culture medium upon sampling (Villas-Boas and Bruheim, 2007). If separation of cells from medium is conducted upon sampling without quenching, it is difficult to get an accurate metabolite level at the sampling time point as the cells cannot be filtered or centrifuged fast enough to prevent alteration in the intracellular metabolite levels (Villas-Boas and Bruheim, 2007).

Because of the rapid turnover rate of many primary metabolites, in the range of 1mM/s to 1.5mM/s, an efficient quenching method should be employed to allow assessing a reliable metabolite profile. According to Mashego et al. (2007) and Alvarez-Sanchez (2010), quenching should meet the following criteria. Firstly, inactivation of the metabolism in samples should be faster than the turnover rates of such metabolites. Secondly, the integrity of the cell membrane should be retained during quenching to eliminate the leakage of intracellular metabolites from the cells. Thirdly, the chemical and physical properties of metabolites and their concentration should not be changed during the quenching process. Finally, metabolites extracted from quenched samples should be tractable for subsequent analysis.

Two strategies which have usually been applied for inactivation of metabolism include instant changes of temperature or pH of the sample (Alvarez-Sanchez, 2010;

Villas-Boas et al., 2005a). Traditionally, rapid quenching of microbial metabolic activity has been achieved by a rapid change of sample temperature to either low (<-40^{0}C) or high (>80^{0}C) or by applying instantly a change to extreme pH, either low (by adding acids) or high (by adding alkali solutions), (Mashego et al., 2007). In addition, automated quenching using special equipment has been reported (Wiendahl et al., 2007). These are based on using an on-line coupling of a fast sampling device for a bioreactor, and rapidly cooling down the sampled cell suspension. With this automated approach, the sampling device is pre-cooled at -50^{0}C, which is ideal for ceasing cellular metabolism. However, this quenching method requires a special device which is a limitation for general use.

By changing the temperature, instantaneous inactivation of metabolism is often achieved by rapidly decreasing the culture temperature to values far below 0°C (Faijes et al., 2007). Other authors, (Wittmann et al., 2004), claimed that quenching is mainly carried out by cooling at values usually lower than -20^{o}C, assuming that such a low temperature does not severely affect sample integrity by cold shock. The lower temperature leads to the slower turnover rate of all the enzymes within the cell and it results in an efficient quenching process (Sellick et al., 2009). Another approach of quenching is applying a fast increase of temperature, which also interrupts cell metabolism as in the addition of ethanol at 94^{o}C (Faijes et al., 2007). However, this method generates potential degradation of thermo-labile metabolites and increases cell permeability (Winder et al., 2008). Therefore, a quenching solution with a low melting point, (far below 0^{o}C), is often preferred.

The most common quenching solution is cold methanol (usually 60% v/v in water, at –40^{o}C), which stops metabolism of the cells in a very short time (Bolten and Wittmann, 2008; Lu et al., 2008; Ritter et al., 2008; Sellick et al., 2009). Methanol possesses several advantages of a good quenching solution including miscibility with water, low melting point, and low viscosity (Canelas et al., 2008). Cold methanol quenching, (non-buffered or buffered with HEPES or AMBIC or NaCl), has been used widely for yeast and bacteria (Bolten and Wittmann, 2008; Canelas et al., 2008; de Koning and van Dam, 1992; Faijes et al., 2007; Gonzalez et al., 1997; Hans et al., 2001; Loret et al., 2007). However, it has been reported that there is a leakage of intracellular metabolites from yeast and bacteria due to cellular membrane disruption during quenching such cells with non-buffered or even buffered cold methanol (Bolten et al., 2007; Villas-Boas et al., 2005a; Winder et al., 2008; Wittmann et al., 2004). That is why it is not used frequently for animal cells, which lack a cell wall, and are more prone to cell membrane damage.

For mammalian cells, the use of AMBIC, (0.85%), supplemented in cold methanol (60%,-40^{o}C), improved significantly intracellular metabolite concentrations over the use of

methanol alone (Sellick et al., 2009). However, Dietmair et al., (2010), pointed out the use of cold methanol, with or without AMBIC, induces leakage of intracellular metabolites from CHO cells. These authors found that, cold sodium chloride, (0.9%), is the most appropriate quenching solution for fragile mammalian cells. Animal cells, (mammalian cells and insect cells), are highly sensitive to osmolarity changes and the cellular membrane is rapidly disrupted by organic solvents. Therefore, higher melting point quenching solutions, (around 0^{o}C), that cause minimal cell membrane damage, would be most suitable for animal cells.

Separation of cells from spent medium

Following quenching, the cells should be separated from the spent medium-quenching solution mixture. This step aims to minimize the dilution effect of extracting the cells in the presence of the medium/quenching solution and allows separate quantification of intracellular and extracellular metabolites (Bolten et al., 2007; Villas-Boas et al., 2005a). The separation step is usually done by fast filtration or cold centrifugation. Fast filtration usually takes several seconds (Bolten et al., 2007), and hence metabolite levels can change during the filtration. Thus, fast filtration is only a suitable approach for metabolites with low turnover rates (de Koning and van Dam, 1992). Cold centrifugation tends to be used frequently because sample handling is conducted at low temperatures and hence the turnover of metabolites is eliminated or minimized (Mashego et al., 2007; Villas-Boas et al., 2005a). Cold centrifugation tends to be the preferred choice among these two cell separation methods (Mashego et al., 2007).

In the separation step, additional washes may be included to get rid of metabolites derived from the culture medium, especially for animal cells which are grown in a complex and rich medium. However, the introduction of additional washes increases damage of the cells (Dietmair et al., 2010), and results in leakage of intracellular metabolites from the cells (Sellick et al., 2009), or results in metabolite turnover and a change in the metabolite profile (Plassmeier et al., 2007). Therefore, the application of additional washes should be considered carefully and often involves a compromise between the benefits derived from the wash and the loss of intracellular metabolites following washing. In the case of washing being unavoidable, such as in the measurement of intracellular metabolites for insect cells grown in a very rich medium, development of a quenching solution that can protect the cells during the quenching and washing process is required.

Metabolite extraction

Following the quenching and separation steps, metabolites are usually extracted from cell pellets using extraction solvents. The extraction is performed to lyse the cells and release the intracellular metabolites. Ideally, the extraction method should extract all or the maximum number of metabolites as possible in the sample with the highest efficiency and minimum degradation (Faijes et al., 2007; Maharjan and Ferenci, 2003; Sellick et al., 2009; Villas-Boas and Bruheim, 2007). However, it is difficult to develop an extraction procedure suitable for all metabolites due to their physical and chemical diversity. There is no unique extraction procedure for metabolome analysis, among many different procedures, that is optimal for extraction of all metabolites (Faijes et al., 2007; Villas-Boas et al., 2005b).

A series of extraction methods using different solutions have been employed to extract intracellular metabolites of different living organisms from bacteria and yeast to plant and animal cells and tissues. To be selected as an extraction agent, the agent should neither physically nor chemically modify the metabolites targeted for analysis (Mashego et al., 2007). Furthermore, extraction solvents should be compatible with the subsequent analytical procedures (Villas-Boas et al., 2005b). A wide range of different extraction solutions have been reported including alcohols, water, acids, bases and organic solvents at high or low temperature (de Koning and van Dam, 1992; Dietmair et al., 2010; Faijes et al., 2007; Grob et al., 2003; Maharjan and Ferenci, 2003; Ritter et al., 2008; Sellick et al., 2009; Shryock et al., 1986; Villas-Boas et al., 2005a; Villas-Boas et al., 2005b; Winder et al., 2008), and each solution is only suitable for specific classes of metabolites and certain cell types (Canelas et al., 2009; de Koning and van Dam, 1992; Grob et al., 2003; Maharjan and Ferenci, 2003; Rabinowitz and Kimball, 2007; Shryock et al., 1986; Tomiya et al., 2001; Villas-Boas et al., 2005b). Therefore, the extraction protocol is selected depending on the aim of study and the target biological sample (Alvarez-Sanchez, 2010), as well as being based on the nature and level of metabolites extracted (Dunn and Ellis, 2005). While targeted analysis requires a highly selective extraction that provides clean and concentrated extracts, metabolic profiling is possible using a non-selective extraction procedure (Alvarez-Sanchez, 2010). The selection of an extraction method in particular depends on the cell type to be studied. Cell size and cellular composition can significantly affect the extraction procedure required (Sellick et al., 2010).

A huge number of publications report on optimized quenching and extraction procedures for yeast and bacterial cells (Bolten et al., 2007; de Koning and van Dam, 1992; Faijes et al., 2007; Maharjan and Ferenci, 2003; Villas-Boas et al., 2005a; Winder et

al., 2008). Whereas, there are comparatively few papers comparing quenching and extraction methods in mammalian cells (Dietmair et al., 2010; Grob et al., 2003; Ritter et al., 2008; Sellick et al., 2009; Sellick et al., 2010). Ritter et al., (2008) did a screening of different extraction protocols for Madin–Darby canine kidney, (MDCK), cells and recommended that methanol/chloroform (MeOH/CHCl3) and MeOH/Boil are promising candidates for the investigation of a large number of intracellular metabolites by anion exchange chromatography analysis. Sellick et al., (2010) reported that the extraction of metabolites from CHO cells using two 100% methanol extractions followed by a final water extraction recovered the greatest range of metabolites. Dietmair et al., (2010), evaluated the efficiency of 12 different extraction protocols from the literature and found that cold (-40^{o}C) acetonitrile at 50% in water is the most efficient extraction solution for CHO cells. Previously, Grob et al., (2003), also concluded 20 to 60% acetonitrile in water is the best solvent for extracting nucleotides in mouse lymphoma cells.

Sample concentration

After extraction, cell extracts need to be concentrated before analysis because they are diluted in a large volume of extraction solvents. In addition, extraction solvents should be removed from the sample prior to analysis since the solvents may interfere with the analytical methods used to quantify the metabolites (Villas-Boas et al., 2005b). Solvent removal can be done using solvent evaporation under vacuum. However, this method is relatively time consuming and the temperature required for solvent evaporation does not favor many metabolites (Ferreira et al., 1995). Freeze drying is most suitable due to the avoidance of thermal degradation during the concentration since metabolites are dried from a frozen solution. Furthermore, being free of water, many metabolites usually show good stability, which allows storage almost indefinitely (Villas-Boas et al., 2005b).

1.6.4 Analysis of metabolites

Following sample preparation, metabolites in the samples are quantified using different analytical techniques. Due to the natural complexity of metabolites and the convoluted nature of metabolism, various analytical approaches have been applied recently in an effort to measure multiple metabolites. In principle, almost every analytical technique or detection method can be employed for different parts of a metabolomic analysis. However, highly selective and sensitive multifunctional methods are obviously favoured since they allow the reliable detection of a large spectrum of compounds

requiring only small sample volumes (Oldiges et al., 2007). Analytical methods used for analyzing metabolites include thin-layer chromatography (Maharjan and Ferenci, 2003; Tweeddale et al., 1998), high-performance liquid chromatography (HPLC) (Dietmair et al., 2010; Groussac et al., 2000; Meyer et al., 1999; Ritter et al., 2006; Wittmann et al., 2004), nuclear magnetic resonance spectroscopy (Raamsdonk et al., 2001; Tang et al., 2004) and chromatography coupled to mass spectrometry (MS) (Buchholz et al., 2001; Koek et al., 2006; Ramautar et al., 2006).

HPLC is a common analytical technique used to analyze metabolites. For nucleotides and nucleotide sugars, HPLC is one of the most simple and rapid methods for measuring a range of these metabolites at the same time (Kochanowski et al., 2006). In addition, the accuracy of this technique for quantification of a wide range of substances is very reliable. However, only compounds with similar characteristics can be analyzed simultaneously, and co-eluting peaks often cannot be distinguished. Another disadvantage is that only very abundant metabolites can be detected with HPLC as the detection limit requires analyte concentrations to be in the micromolar range and in addition unknown metabolites are difficult to identify.

The application of mass spectrometry (MS) for analysis of cellular metabolites has grown dramatically over the last two decades, and today it is the single most important detector method in biotechnology (Villas-Boas et al., 2005b). Chromatography (gas and liquid chromatography), and more recently capillary electrophoresis, coupled to MS stands out for its potential for high sensitivity and specificity (Bajad et al., 2006), which provides a very powerful analytical system (Oldiges et al., 2007). These combinations offer tremendous opportunities for analysis of complex biological samples since they are able to determine and identify a large number of metabolites in a single analysis (Villas-Boas et al., 2005b).

It is impossible today to measure all of the intracellular metabolites due to the nature and complexity of metabolites inside the cells. The current analytical protocols available allow analyzing a selected number of metabolites relating to the provision of energy and materials for the generation of cell biomass and production of waste products, including nucleotides, amino acids, sugars, and organic acids.

1.7 Insect cell culture medium

Medium for insect cell cultures is very complex (Castro et al., 1992). Originally, insect cell culture medium was developed based on the composition of hemolymph, which was used to design a chemically-defined basal medium containing inorganic salts, vitamins,

amino acids, organic acids and sugars (Wyatt, 1956). However, it is necessary to add heat-treated hemolymph or vertebrate serum into the basal medium to supply undefined substrates which are thought to be essential to support insect cell growth. Serum is a more suitable medium supplement than hemolymph, and it provides an ideal condition for cell growth and virus infection (Goodwin, 1991; Hewlett, 1991). However, the presence of serum in insect cell culture medium is associated with many limitations due to its high cost, lot-to-lot variability, inconsistent supply, the risk of disease transmission, and contamination with adventitious agents (Schlaeger, 1996). Moreover, the protein content in serum can potentially interfere with downstream processes (Reid et al., 2013). Hence, the next breakthrough in insect cell media was the development of serum-free and protein-free media (abbreviated as SFM).

The development of SFM has involved the replacement of growth factors, lipids and shear protectants in serum by protein hydrolysates and a manufactured lipid emulsion which contains the shear protectant Pluronic F-86 (Inlow et al., 1989; Schlaeger, 1996). By this way, the basis of the well-established IPL41 SFM for lepidopteran insect cell lines was developed (Inlow et al., 1989), and its improved commercial derivatives including EX-CELL® 401 (Sigma-Aldrich) and Sf900™II (Life Technologies) SFM (Schlaeger, 1996). Further improvement of SFM with the reduction in hydrolysate content has resulted in next-generation formulations such as Sf900™III SFM (Life Technologies).

The use of hydrolysates in insect cell culture medium is considered as a revolution in SFM development. However, the reliance on hydrolysates for supplying amino acids and growth factors has disadvantages in terms of the lot-to-lot variability of these undefined components (Reid et al., 2013). The variations of materials and processes for hydrolysate production lead to the variations of the end product and the medium and ultimately the cell culture process (Pasupuleti and Braun, 2010). Although ultrafiltration processes may help to improve the consistency, the underlining variability in chemical composition is still present (Reid et al., 2013). In addition, hydrolysates also provide an amount of undesirable components together with desirable ones. Desirable components include amino acids, peptides and low molecular weight growth factors while undesirable components include high levels of inorganic salts (Pasupuleti and Braun, 2010), and possibly some undefined components imparting cellular toxicity (Lu et al., 2007). Other problems associated with protein hydrolysates include a wide divergence in aqueous solubility that limits their inclusion at high levels, especially in concentrated feeds. The problem associated with hydrolysates may be addressed by the development of a chemically defined medium (CDM). CDM are also useful for further metabolomics and fluxomics studies. Currently,

CDM formulations are well established for mammalian cell culture, but are not yet available for insect cell culture (Reid et al., 2013).

1.8 The thesis outline

The improvement of the yield of baculovirus-insect cell expression systems is essential for commercial viability of the products from these systems. The challenge for improving the yield of baculovirus insect cell systems is that protein yield (per cell basis) drops when cells are infected at a high cell density, which is known as “the cell density effect”. Many research groups have investigated the extracellular environment through the measurement of extracellular metabolites to identify the limiting nutrients in the medium (Caron et al., 1990; Drews et al., 1995; Reuveny et al., 1993), the measurement of consumption rates and fluxomics analysis (Bernal et al., 2009), the supplement of glucose, glutamine, complex nutrient mixtures, and key intermediate metabolites to culture media (Carinhas et al., 2010; Reuveny et al., 1993), in order to overcome the cell density effect. However, the limitation of these approaches is that the metabolite levels in the media might not necessarily reflect intracellular metabolite levels. For many reasons, some metabolites may not get into the cells at high cell densities post-infection, although they are available in the culture medium at reasonable levels. Therefore, the metabolite environment inside the cells at low and high cell densities at the time of infection provides a better understanding of what happens inside the cells and may reveal the cause of the cell density effect. In particular, intracellular metabolite measurements in combination with consumption rates of key metabolites may identify limitations during high cell density infections. Especially, at the very late phase of infection which involves a high level of protein production, it is likely that a high demand for energy and amino acids is placed upon the cell, but the cell is entering a death phase at this time and so the uptake of nutrients may be compromised. Thus, a key research question is whether the intracellular levels of key metabolites (e.g. amino acids) are low during the late stage of high density infections compared to appropriate controls (low ICDs)?

In order to address the issue regarding possible intracellular limitations during high cell density infections, key metabolites involved in the supply of energy and substrates for DNA, RNA, and protein synthesis such as intracellular nucleotides and amino acids should be measured. However, there is no sample preparation protocol for quantitative intracellular metabolite analysis available for insect cells. Thus, a methodology for quantitative intracellular metabolite analysis of insect cells was developed and optimized (Chapter 3). In this chapter, two particular baculovirus applications were tested,

representing recombinant protein production (*Autographa californica* nucleopolyhedrovirus (AcMNPV) in *Spodoptera frugiperda* (Sf9) cells) and biopesticide production (*Helicoverpa armigera* nucleopolyhedrovirus (HearNPV) in *Heliothis zea* (HzAM1) cells).

Following the development of a methodology for quantitative intracellular metabolite analysis of insect cells (Chapter 3), the limitations related to the drop in specific yield for a high cell density infection of Sf9 cells in Sf900™III medium was investigated using a metabolomics approach (Chapter 4). In this chapter, substrate consumption rates as well as intracellular metabolite levels of infected cells at low and high cell densities at the time of infection were measured and compared between these two infection conditions. Reasons for studying the Sf9 system prior to the HzAM1 system include the vast amount of information on cell metabolism, and the well documented cell density effect for the Sf9 system. In addition, recombinant AcMNPV viruses produce high titer stocks and the production of certain recombinant proteins is easily quantified. Finally there are strong commercial interests for this system for the production of recombinant proteins, vaccines and vectors for gene therapy.

Ideally, the cells should be cultured using a fully chemically defined medium (CDM) for the investigation of extra- and intra-cellular environments. However, a CDM for insect cells is not commercially available and the development of such a CDM is beyond the scope of a research laboratory. Fortunately, a prototype CDM for insect cell culture was made available for testing by Life Technologies. This CDM contains no peptides, and the free amino acid levels are higher than in Sf900™III. It is interesting to investigate any differences in intracellular metabolite levels of the Sf9 cells in the CDM compared to that for cells in Sf900™III, especially for high cell density infections. Substrate consumption rates and intracellular metabolite levels of infected cells at low and high infection cell densities were measured and compared between these two infection conditions using the available CDM as a comparison to the results obtained in Chapter 4 using the commercially available Sf900™III medium (Chapter 5).

Following the investigation of limitations related to the drop in specific yields for high cell density infections of Sf9 cells in Sf900™III/CDM media (Chapters 4 & 5), it was of interest to investigate limitations related to the decline in cell specific yield with increasing ICD for another cell line/virus system, such as the wild-type HearNPV infected HzAM1 system (Chapter 6). It is interesting to explore whether there are any differences in terms of limitations related to the cell density effect between different cell lines infected with different viruses when using the same medium for both cell lines.

The following chapter (Chapter 2) provides details of general materials and methods used in this research project. The techniques for insect cell culture and maintenance, preparation of budded virus stocks, and bioassays are included. The specific techniques/ methods used for particular experiments of the results chapters are described in the relevant chapters. Finally, Chapter 7 contains a general discussion, conclusions and provides recommendations for future investigations.

Chapter 2

Materials and Methods

2.1 Insect cell culture and maintenance

2.1.1 Insect cell lines

The insect cell lines used in this study are a *Helicoverpa zea* cell line (BCIRL-HzAM1) and a *Spodoptera frugiperda* clone 9 cell line (Sf9; ATCC CRL 1711).

The HzAM1 cell line was derived from the pupal ovarian tissue of *H. zea* (Lepidoptera: Noctuidae) (McIntosh and Ignoffo, 1981). This cell line was originally obtained from CSIRO, Division of Entomology, Canberra, Australia. In our lab, the cells were adapted to a low cost, home-made, serum free medium, VPM3 medium, which was disclosed in the PCT patent, WO/2005/045014 (Reid and Lua, 2005). The cells were then adapted to the serum-free medium Sf900™II (Gibco, Life Technologies, New York, USA) in suspension cultures using Erlenmeyer flasks (Corning Incorporate, NJ, USA) prior to being used in this study.

The Sf9 cell line was originally purchased from the American Type Culture Collection (ATCC CRL 1711). This cell line was cloned from the Sf21 cell line by Smith et al. (1983). The Sf21 cell line originated from the ovarian tissue of several fall armyworm pupae (*Spodoptera frugiperda*) (Vaughn et al., 1977). The cells were adapted to Sf900™II medium by previous students in our laboratory and have been passaged 75 to 100 times prior to generation of the frozen stock used in this study.

2.1.2 Insect cell serum free media

The media used in this study are Sf900™II and Sf900™III. Both are commercially available serum-free media designed for insect cells (Gibco, Life Technologies, New York, USA). In addition to Sf900™II and Sf900™III, a fully chemically defined medium (CDM) is also used for testing (Life Technologies). This prototype CDM contains no peptides, and was designed for insect cells.

2.1.3 Maintaining of working stock cells

For the HzAM1 cell line, working stock cells were grown in 25 mL suspension cultures in 125mL Erlenmeyer flasks (Corning Incorporation, USA), on a Bioline Orbital Shaker (Edwards Instrument Company, Australia), operated at 120 rpm, inside a refrigerated incubator (Thermoline, Australia), at 28^{o}C. Stock cells were passaged every 3 to 4 days with seeding cell densities of 0.4×10^{6} and 0.25×10^{6} cells/mL, respectively. The final cell densities at the time for the next passage were around 3 to 4×10^{6} cells/mL. All

cell passaging was conducted in a Biological Safety Cabinet Class II (Email Westinghouse Pty Ltd, Australia), using aseptic techniques. The working stock cells were maintained for about 30 passages after thawing.

For the Sf9 cell line, working stock cells were maintained as for the HzAM1 cell line. However, the peak cell density of Sf9 cells is much higher than that of HzAM1 cells in culture (around 1.8×10^7 cells/mL compared to 8×10^6 cells/mL, respectively), thus they were seeded at 0.3×10^6 and 0.5×10^6 cells/mL for stock cells maintained for 4 and 3 days, respectively. The final cell density at the time for the next passage was around 4 to 5×10^6 cells/mL. Stock cells were also used for up to 30 passages after thawing.

2.1.4 Cell density and cell viability determination

Manual cell count using a microscope

Cell density and viability of working stock cells were determined by manual counts using a microscope (Olympus, Japan). The cells were serially diluted with Sf900™II medium and then 1:1 with 0.1% Trypan Blue (Sigma-Aldrich) to give around 100 cells on each side of a haemocytometer (Weber, England). The dilution factor D of the original culture is calculated using the following equation to achieve the above counting cell density:

$$\mathbf{D} = CD\frac{cells}{ml}x\frac{\mathbf{1.8x10^{-3}ml\ (18\ squares)}}{\mathbf{200}\ cells\ (\mathbf{18}\ squares)}$$

In cases where the cell density (CD) was unknown before counting, its value was estimated based on the initial seeding cell density and the culture period with the assumption that cells double every 24 hours.

Samples were counted immediately upon diluting with Trypan Blue to avoid the uptake of Trypan Blue by viable cells. In Trypan Blue, viable cells remain with a pale yellow colour, while dead cells uptake Trypan Blue and become blue. Both sides of a haemocytometer (18 squares) were measured as a single count. The volume enclosed in the 18 counting squares is exactly 1.8×10^{-3} ml when the cover slip is placed on top of the haemocytometer prior to loading the sample. Triplicate counts (3 haemocytometers) of each sample were performed each time to estimate cell density with the random relative error of 15% (Nielsen et al., 1991). Cell viabilities were determined by dividing the number of viable cells by the number of total cells counted (including viable and dead cells).

Manual cell counts using a microscope were conducted for determination of the cell density and viability of working stock cells and the viability of experiments. The total cell densities of all of the experiments were measured using a Multisizer™4 Coulter Counter (Beckman Coulter Inc., Fullerton, CA, USA).

Cell count using the Multisizer™4 Coulter Counter

A Multisizer™ Coulter Counter was used to measure total cell densities and cell volumes for all experiments. Although the viability cannot be measured by the Multisizer™4 Coulter Counter, measurements of cell densities using such a machine is more objective and less time consuming than are manual counts. The particle size that the machine can count ranges from 0 to 60 µm. For insect cells (HzAM1 cells with an average cell size of 17-18 µm, and 14-15 µm for Sf9 cells), the range for cell counts was set from 9 to 60 µm. Cell densities obtained using this range matched the result of manual cell counts using a microscope.

Samples need to be serially diluted with fresh medium to get the total cell density to around 0.5×10^6 cells/mL. The sample was then diluted a further 101X with IsoFlow™ (Beckman Coulter Pty. Ltd., Gladesville, Australia), in a special clear plastic vial Accuvette (add 0.2 mL culture into 20 mL IsoFlow), before counting using the Multisizer™4 Coulter Counter.

2.2 Baculoviruses

The viruses used in this study were the wild type *Helicoverpa armigera* single nucleopolyhedrovirus (HearNPV) and the recombinant *Autographa californica* multiple nucleopolyhedrovirus (rAcMNPV).

The wild type HearNPV (strain H25EA1) used in this study was obtained from CSIRO (Entomology Division, Canberra, Australia), and is an Australian field isolate. These OB working stocks were harvested from later stage HearNPV infected caterpillars. These stocks were harvested from *Helicoverpa armigera* caterpillar colonies maintained by the Queensland Department of Primary Industries (QDPI), Brisbane, Australia.

A recombinant rAcMNPV which expresses the *Escherichia coli* LacZ gene for producing the β−Galactosidase (β-Gal) protein under the control of the polyhedrin promoter was used to infect Sf9 cells in this study. This virus was from old frozen virus stocks which then underwent a plaque purification process to pick up a good virus isolate for producing a fresh working virus stock.

2.2.1 Preparation of budded virus stocks

Wild type HearNPV virus

Passage 1 (P1) virus stock was generated by infection of HzAM1 cultures (in Sf900™II or Sf900™III media), with the ODVs derived from caterpillar OB's. In order to get ODVs, the OB's were digested by adding a 40 µL alkaline solution (0.5M Na_2CO_3 and 1M NaCl) into an aliquot of 0.5 mL of caterpillar OB containing 10^{10} OB in an eppendorf tube, and vortexed to mix well. The tube was incubated at 28^{o}C for 30 minutes to destroy the polyhedron matrix to release the ODVs, and then transferred into a Petri dish and mixed with 10.5 mL of medium by gentle pipetting. The mixture of the virus (ODVs) and the medium was filtered by using 0.22 µm syringe filters (Sartorious, Australia), into a sterile 10 ml tube. This filtered virus solution (~10 ml) was used to infect 90 ml of cell culture to get the final volume to 100 ml with a cell density of 0.5×10^6 cells/mL. The passage 1 infected culture (P1) was incubated at 28^{o}C and 120 rpm. P1 budded virus stock (BV) was harvested at 4 days post-infection and used for P2 infections.

Passage 2 (P2) virus stock was prepared from the P1 virus stock. P2 virus was prepared by infecting the early exponential phase of an HzAM1 culture at 1×10^6 cells/mL (cultures were set up at 0.5×10^6 cells/mL and infection was conducted 24 hours later), with 30% (v/v) P1 virus stock (whole culture). The P2 virus infected culture was incubated at 28^{o}C, 120 rpm. After 3 days of infection, the infected P2 culture was collected and centrifuged at 1000×g for 10 minutes (room temperature centrifugation). The P2 budded virus (BV) supernatant was harvested in the biosafety cabinet into 10ml tubes (~10ml each) and kept in the fridge (4^{o}C) for quick use or stored in a -80^{o}C freezer (Sanyo, Japan), for longer term use. Prior to use for infection, P2 supernatant virus was assayed to determine the virus titer using a suspension culture method. All experiments were conducted using P2 virus to initiate P3 infections.

Recombinant AcMNPV virus

The recombinant AcMNPV virus stocks were prepared by infecting early exponential phase Sf9 cell cultures (in Sf900™II or Sf900™III media) at the infection cell density (ICD) of 1.5×10^6 cells/mL and an MOI of 0.1 PFU/cell using a plaque purified virus stock, which had undergone 1 passage after the plaque purification process to generate the P1 virus stock. The infected culture was incubated at 28^{o}C, 120 rpm for 3-4 days. The P2 virus stock was harvested when the total cell density reached around 5×10^6 cells/mL with a viability of around 60-70%. The supernatant was harvested by spinning the infected culture

at 1000×g for 10 minutes. The P2 supernatant virus was then stored at 4^{o}C in the dark, as it is UV sensitive. The virus titer was determined by an endpoint assay prior to being used for infection. The P2 virus stock was used for experiments only when the BV titer was at least 1×10^{9} PFU/mL.

2.2.2 Virus titration

Wild type HearNPV virus

Fresh and frozen supernatant P2 virus was assayed to determine the virus titer using a suspension culture method as described by Matindoost et al. (2012). The titration involved 2 infected flasks at an ICD of 0.5×10^{6} cells/mL infected with 2.5% of P2 virus (v/v) and 1 uninfected control flask at a seeding cell density of 0.5×10^{6} cells/mL. Viable and total cell densities of the three shaker flasks were determined at 0, 2, 3 and 4 days post infection by manual counts using a microscope. The multiplicity of infection (MOI) was estimated based on the viable cell density at the time of infection and the total peak cell density (either at 3 or 4 days post infection) by a model using Matlab software (MathWorks Inc., USA). The budded virus titer was then calculated based on the initial viable cell density, MOI and the volume of virus used for infection. The model used was based on a model developed by (Power et al., 1994) and adapted to wild-type HearNPV infections based on virus kinetic data generated by Marcia Pedrini (Pedrini, 2003).

Recombinant AcMNPV virus

The virus titer of the rAcMNPV P2 stocks were estimated using an endpoint titration assay (Nielsen et al., 1992). The procedure of the assay is as follows. A Sf9 cell culture in Sf900™II or Sf900™III media was freshly prepared with a seeding cell density of about 0.5×10^{6} cells/mL the day before the assay, and was grown up to a cell density of around 1×10^{6}cells/ml. The virus sample was serially diluted (10-fold, nine times, from 10^{-1} to 10^{-9}) with fresh medium. Each dilution of the serial virus dilutions from 10^{-5} to 10^{-9} were mixed with an equal volume of cell culture (at a cell density of 1×10^{6} cells/mL) using a vortex mixer. Each virus cell mixture (at each virus dilution), was then placed into 20 wells of 60-well plates (Nalge Nunc) with 10 µL/well. The plates were then incubated in a humidified plastic box (filled with moist paper towels) at 28°C for 7 days in an incubator. After incubation of the virus titer plates, 8 µL X-gal (Progen, Brisbane, Australia) dissolved at 0.8 mg/mL in water with 4% v/v DMSO (Sigma-Aldrich) was added to each well. X-gal (5-bromo-chloryl-4-indyl-β-D-galactopyraniside) is a chromogenic substrate which is cleaved

by β-Gal to form a blue coloured compound. The plates were then left in the dark for 2-4 hours for colour development. The wells containing virus will become blue because they contain β-Gal which was produced during the cell infection. The number of blue (positive) and clear (negative) wells were recorded and converted into plaque-forming units per milliliter (PFU/mL) using software developed by Nielsen et al. (1992).

2.3 Cryopreservation

2.3.1 Preparation for freezing cell stocks

Master stocks of Sf9 and HzAM1 cells were cryopreserved in liquid nitrogen for long term storage and to ensure the continuation of research as master stock cells are not passaged beyond 30 times after thawing. In order to achieve successful freezing, the cells being frozen should be in an exponential phase of growth and have at least 98% of viability.

For the Sf9 cell line, the procedure for freezing stock cells is as follows.

1. Prepare cells prior to freezing: 100 mL of cell culture was prepared in a 250 mL shaker flask and incubated to a cell density of 4-6×10^6 cells/mL. The culture prepared for freezing must be growing optimally, with a doubling time of 24 hours or lower and viability of at least 95%, and definitely without sign of contamination. Otherwise, the culture was not used for making frozen stock cells and another fresh culture had to be prepared. At the time the desired cell density of stock cells was reached, the culture was aliquoted into two 50 mL sterile tubes and centrifuged at a low speed, 200×g, for 5 minutes to get the cell pellet. The cell pellet in each tube was then re-suspended with 2.75 mL of conditioned medium, which is collected from the centrifugation step to separate the cells and the supernatant (conditioned medium). The two re-suspended cell pellets (about 2.75 mL each) were pooled together and diluted with 5.5 mL of fresh medium containing 15% (v/v) DMSO (Sigma-Aldrich, St. Louis, USA) to give a final volume of 11 mL.

2. Freezing: The 11 mL of cell suspension prepared in step 1 was aliquoted into 11 cryogenic ampoules (1 mL each) and then sealed with screw caps. The ampoules were placed on ice, and encased in an air-tight protective sheath (Cryoflex, Nalge Nunc). Then, the ampoules were inserted onto a slow freezing container, “Mr. Frosty” (Nagle Nunc International, USA), containing isopropanol. “Mr. Frosty” containers were placed in a fridge at 4^{o}C for 1 hour and then kept in a -80^{o}C freezer (Sanyo, Japan) overnight. After this, the frozen ampoules were transferred from the “Mr. Frosty” containers into canes, and the canes were stored in a dewar filled with liquid nitrogen.

For the HzAM1 cell line, the procedure for freezing stock cells also includes the steps as described above. The only difference is that the cell density of the culture at the time of the freezing step is lower (2.5-3×10^6 cells/mL) and a frozen volume of 1.8 mL was used instead of 1mL.

2.3.2 Thawing frozen cells

The frozen stock cells were thawed using the following procedure:

1. A frozen ampoule was retrieved from the liquid nitrogen dewar and then the cryoflex was removed
2. The ampoule was rapidly thawed in a 27^{o}C water bath
3. After thawing, decontaminate the outside of the ampoule using ethanol 70%
4. Then, the cell suspension from the ampoule was transferred into a sterile 250ml flask, which contains 48 mL of fresh medium, using a transfer pipette.
5. The culture was incubated at 28^{o}C, 120 rpm
6. Count the cells and check viability every day and passage the cells when the cell density reaches 2-3×10^6 cells/mL with a viability of around 90%, then passage the cells as usual as for stock cells. The growth of the new thawed cells was monitored for a few passages to ensure they were growing well before use as a working stock.

2.4 Bioassays

2.4.1 β-Galactosidase (β-Gal) assay

The amount of β-Gal was measured using a spectrophotometric assay (Miller, 1972). In this method, the enzymatic activity was measured based on the ability of the enzyme to catalyze cleavage of o-nitrophenyl-β-D-galactopyranoside (ONPG) to produce galactose and the yellow coloured compound o-nitrophenol. The absorbance of the latter compound was measured at 420 nm using a Spectramax M5 microplate reader (Molecular Devices Inc., USA). The colour development is linearly related to the concentration of hydrolyzed ONPG, (hence the activity of β-Gal), and the reaction time.

The protocol for the β-Gal assay is described as follows. Samples were diluted with MiliQ water to the point that provides an absorbance at 420 nm in the range of 0.3 to 0.8. 50 μL of diluted sample was mixed with 950 μL of Z buffer (0.06 M Na_2HPO_4, 0.04 M NaH_2PO_4, 0.001M $MgSO_4$, 0.01 M KCl, 0.035% v/v β-mercaptoethanol in water) and 200 μL of ONPG (4 mg/L) in a 10 mL tube (Sarstedt, Australia). A blank was prepared as above with 50 μL water instead of diluted sample being added. The mixture was incubated

at 37^{0}C for 30 minutes in a water bath. After this time, 500 μL of stop buffer (1M Na_2CO_3) was added to cease the reaction. The reaction solution (1700 μL) was transferred into a cuvette (Sarstedt, Australia) and the absorbance measured at 420 nm. The absorbance of sample was corrected with the blank sample to exclude the background.

The β-Gal activity was calculated as follows:

$$\mathbf{VY} = \frac{\mathbf{10^6}\ x\ A}{\varepsilon\ x\ l\ x\ t}\ \mathbf{x\ D\ x}\ \frac{Vtotal}{Vsample}$$

Where: VY : Volumetric yield of β-Gal (Units/mL)

A : Absorbance at 420 nm

ε : Absorbance coefficient of o-nitrophenol at 420nm (4500 L/mole/cm)

l : Cuvette path length (1 cm)

t : Incubation time (30 minutes)

D : Dilution factor

V_{total} : Final volume in cuvette (1700 μL)

V_{sample}: Sample volume (50 μL)

2.4.2 Polyhedra extraction and enumeration

Polyhedra were extracted from infected cells using 1% sodium dodecyl sulphate (SDS). An equal volume of SDS 1% was added to an infected culture. The mixture was mixed well and incubated at 28^{0}C for 30 minutes to dissolve the cell membrane and release the polyhedra. The mixture was then diluted serially with MiliQ water to an appropriate dilution to allow a count of 25-30 OBs per small square of a haemocytometer. A total of 5 small squares (out of 25 squares) were counted on each side of the haemocytometer. Each sample was counted in 3 haemocytometers (both sides) using an optical microscope (Olympus, Japan), at a 400X magnification. Diluted samples were counted 10 minutes after loading to allow the polyhedra to settle to the base of the haemocytometer. The polyhedra concentration was determined as follows:

OB/mL = number counted in 5 small squares x 5 x dilution factor x 10^4

where 10^{-4} ml is the volume of diluted sample in 25 small squares.

OB/mL of each sample was the average of the OB/mL obtained from each side (6 sides in total) of the haemocytometer counts. The cell specific yield (polyhedra per cell)

was obtained by dividing the volumetric yield (polyhedra per mL) by the total peak cell density (cell/mL).

2.4.3 ATP assay

Intracellular ATP concentrations were determined using an ATPlite assay kit (Thermo scientific, USA). Dried cell extract samples were first re-suspended in MiliQ water and then diluted 4 times with ultrapure water. The ATP concentration of the samples was determined based on the ATP standard by measuring the luminescence at 500 ms integration using the Spectramax M5 microplate reader (Molecular Devices Inc., USA). ATP standard dilution series, (0-0.01 mM) were prepared by serial dilution of an ATP standard, 10 mM stock solution. The concentrations of standard include 0.01 mM, 0.005 mM, 0.0025 mM, 0.00125 mM, 0.000625 mM, 0.0003125 mM and 0 mM (blank).

First, 50 µL of cell lysis solution was loaded into each well of 96 well microplates (Costar black, Corning incorporated, NY, USA). Then samples or ATP standards were added into the wells, at 100µL/well. Three replicates were performed for each sample or ATP standard concentration. The plate was then mixed on a plate shaker for 5 minutes at 700 rpm. Finally, 50 µL of enzyme/substrate (Luciferase/Luciferin) solution (which was reconstituted with substrate buffer solution), was added into each well. The plate was mixed again on a plate shaker for 5 minutes at 700 rpm. The plate was placed in the dark for 10 minutes before being measured for luminescence using the Spectramax M5.

2.4.4 Total protein assay

Total protein from the cells was analyzed using a BCA protein assay kit (Thermo Fisher Scientific, Rockford, IL, USA). About 1×10^6 cells were used for this analysis, so the volume of cell culture samples was taken depending on the cell density of the culture. In order to get the sample volume accurately, samples were measured by weighing (subtract the weight of tubes after adding the culture to empty tubes). The samples were spun down at 1000×g for 5 minutes (Eppendorf AG, Hamburg, Germany), to separate the cell pellets from the medium. The cell pellets were then washed twice with PBS solution (osmolarity of PBS was adjusted to 360 mOsmol/Kg). The cell pellets were frozen (-20^{o}C) for the total protein assay to be performed later. Prior to analysis, the cell pellet was lysed using sodium hydroxide 0.1M at 40^{o}C in a water bath for 20 minutes. Cell lysis samples were diluted further with ultrapure water. The total protein concentration of samples was determined based on a BSA (bovine serum albumin) standard as follows. Standards and

unknown samples were added into clear bottom 96-well plates at 25 µL/well in duplicate. A working reagent, containing 50 parts of reagent A (sodium carbonate, sodium bicarbonate, bicinchoninic acid and sodium tartrate in 0.1M sodium hydroxide) and 1 part of reagent B (cupric sulfate 4%), was added into each well at 200 µL each. The filled plate was covered, mixed thoroughly on a plate shaker for 30 seconds and then incubated at 37^{o}C for 30 minutes in a water bath. After that, the plate was cooled down to room temperature and then the absorbance at 562 nm was measured using a Spectramax M5 (Molecular Devices Inc., USA). The BSA standard curve was generated under a sigmoidal logistics plot using SigmaPlot 12.3 (Systat Software Inc., Chicago, IL, USA).

2.4.5 Measurement of viral DNA copies

Recombinant AcMNPV

Quantitative real time polymerase chain reaction (qRT-PCR) was developed to quantify targeted DNA by Heid *et al.* (1996). The method has been developed by Rosinski *et al.*, (2002) and optimized further by Haas (2004) for quantifying viral DNA (vDNA) copies of recombinant β-Gal-AcMNPV (rAcMNPV) infected Sf9 cells. The primers were designed to amplify the vDNA polymerase gene. The required primers and probe were designed based on the published sequence (Accession number L22858) of the vDNA polymerase gene (Rosinski et al., 2002). The length of the amplicon was 67 bp. The annealing temperature for the primers is 60°C and for the probe 72°C, which ensure all target DNA sequences have probe bound prior to the extension commencing. The sequences of primers and probe are as follows:

Forward primer: 5'-ATTAGCGTGGCGTGCTTTTAC-3'

Reverse primer: 5'-GGGTCAGGCTCCTCTTTGC-3'

DNA-probe: 5'-FAM-CAAACACGCGCATTAACGAGAGCACC-TAMRA-3'

Prior to measuring the vDNA copies of infected samples, the vDNA standard was prepared from budded virus stock. For vDNA standard preparation, 10 mL of P2 budded virus stock with a virus titer of more than 1×10^{9} PFU/mL was centrifuged at 100,000× g for 45 minutes at 4°C to pellet BV using an ultracentrifuge (Beckman Coulter Inc., Brea, CA, USA). Subsequently, the Qiagen genomic tip mini kit (Qiagen, Venlo, Netherlands) was used for the vDNA isolation from the pellet. The protocol for purifying vDNA is as follows. The above pelleted budded virus was re-suspended with 1 mL buffer G2. The pellet should be re-suspended as thoroughly as possible as this is the critical step for a good flow rate on the Qiagen genomic tip. Then 25 µL proteinase K stock solution (20 mg/mL) was added

into the re-suspended budded virus as the mixture was incubated at 50^0C for 30 minutes. The sample was now ready to load into the Qiagen genomic tip.

Before loading the sample, the Qiagen genomic tip 20/G was equilibrated with 1 mL buffer QBT and allowed to empty by gravity flow. Sample was applied to the equilibrated Qiagen genomic tip after vortexing at full speed for 10 seconds and allowed to enter the resin by gravity flow. The Qiagen genomic tip was washed 3 times with 1 mL buffer QC each time and left for the buffer QC to move out of the Qiagen genomic tip by gravity flow. Then the Qiagen genomic tip was placed over a clean 10 mL collection tube and the genomic DNA was eluted twice with 1 mL of buffer QF each time. The purified DNA was precipitated by adding 1.4 mL isopropanol into the eluted DNA solution. The mixture was mixed and centrifuged immediately at 5000×g for 15 minutes at 4^oC. The supernatant was removed carefully and the pellet was washed with 1 mL cold ethanol 70%. The mixture DNA in ethanol 70% was vortexed briefly and centrifuged at 5000×g for 10 minutes at 4^oC. The supernatant was removed carefully and the pellet was allowed to air-dry for 10 minutes. The purified DNA was then re-suspended in 0.2 mL TE buffer.

The purified vDNA was qualified by running in a 6% agarose gel with a 10 kb ladder. A clear band was observed above the 10kb band from the ladder indicating the integrity of the viral DNA fragment. The isolated DNA was then quantified using both a NanoDrop (Themoscientific) and a Picogreen DNA assay kit (Life Technologies). The protocol for quantifying purified viral DNA using the Picogreen DNA assay kit was as follows. The working solution of Lambda DNA standard (2 µg/mL) was prepared from the 100 µg/mL stock solution by diluting 50X with TE buffer. The purified vDNA sample prepared above was diluted by 100 and 200 fold with TE buffer. Sample (100 and 200 fold dilutions) and standard levels were loaded into each well of a Costar black clear bottom 96-well plate (Corning Inc., USA) at 100 µL/well in triplicate. The same volume of a working Quan-iT PicoGreen reagent, prepared from stock solution by 1/200 dilution with TE buffer, was added into each well of the plate. The plate was measured for fluorescence at 480/520 nm using a Spectramax M5 (Molecular Devices Inc., USA). A standard curve was generated from 6 levels of standard concentration from 0 to 2000 ng/mL under a sigmoidal logistics plot using SigmaPlot 12.3 (Systat Software Inc., USA).

The standard curve was generated from 6 points with the DNA concentration ranging from 3×10^{-1} to 3×10^{-6} ng vDNA/µL which corresponds to 2×10^6 to 20 vDNA copies/µL, assuming a molecular weight of 1.359×10^{-7} ng/genome (Rosinski, et al. 2002). A regression equation was generated between the vDNA copy number and the Ct value. vDNA copy number of each sample was then calculated based on its Ct value.

Samples were taken from infected cultures at 12 hour intervals post infection from 0 to 60 hours post infection (hpi) and preserved for subsequent analysis. Infected samples containing 1×10^6 cells/mL were pelleted by spinning down at 300x g for 5 minutes. The cell pellets were then stored at -20^0C until analysis. Accurate volumes of culture were obtained by weighing the empty tubes and tubes plus cell culture. Prior to measuring total vDNA using qRT-PCR, the cell pellet was digested for 15 hours in 1 mL digestion buffer at 50^oC to expose the naked DNA. Digestion buffer contains 100 mM NaCl; 10 mM Tris.HCl, pH 8.0; 25 mM EDTA, pH 8.0; 0.5 % sodium dodecyl sulphate (SDS); and 0.1 mg/mL Proteinase K. Proteinase K was prepared from a stock solution of 20 mg/mL (Amresco, Solon, OH, USA). The weight of tubes after adding digestion buffer was obtained to get accurate final volumes of samples. Digested samples were then subsequently diluted by a 10 times dilution series with injection water. Two dilution levels of 10^{-3} and 10^{-4} were used for measuring vDNA copies. Dilutions less than 100-fold were found to inhibit the PCR reaction which may be caused by the SDS (Haas, 2004).

The master mix for the PCR reaction was prepared in a laminar flow hood which is free from foreign DNA contamination. The master mix for each reaction contains 5µL Taq Man® Universal PCR Master Mix (2-fold concentrated; Life Technologies), 2 µL primers (forward and reverse) at the concentration of 1 µM and 1 µL probe of 1.25 µM. Template DNA was added at 2 µL to the above reaction mix to get a total volume of 10 µL for each reaction. The master mix and DNA template were added into each well of a 384 well plate automatically using an Eppendorf epMotion 5075 Robotics System (Eppendorf, Hamburg, Germany). Each sample or standard was added into triplicate wells in the same PCR plate. Prior to placing the loaded reaction plate into the ABI PRISM® 7900HT Sequence Detection System (Life Technologies) for amplification, detection and analysis, the plate was sealed and spun briefly to ensure that all liquid was collected at the bottom of the reaction wells. The cycling protocol was 2 minutes at 50°C, 10 minutes at 95°C and 45 cycles of 30 seconds at 95°C and 60 seconds at 60°C (data collection period) and then cooled to 25°C.

The signal from the qRT-PCR is the number of cycles used until the fluorescent intensity of FAM™ crossed an arbitrary cycle threshold (Ct) as determined from the amplification plot. Samples from the same experiment or those that need to be compared to each other were run in the same plate to avoid any discrepancies among plates. The vDNA copy number was back calculated from the average of the triplicate wells of each sample, the calibration curve of the used reaction plate, the sample dilution, the final digestion volume, and the initial sample volume. The cell specific vDNA copies were

determined from the copy number of the initial volume and the cell density of the culture post infection.

Wild-type HearNPV

The qRT-PCR reaction for measuring vDNA copies of the wild-type HearNPV generally follows the principle described for recombinant AcMNPV. vDNA polymerase gene of the wild-type HearNPV was also used as the target for the qRT-PCR reaction. The sequence of primers and probe were as described by Pedrini et al. (2011) as follows.

Forward primer: 5'-CATTGCCAACAGTATTTACGGATATT-3'

Reverse primer: 5'-TTCTCTACCGATCTTGGTGATGTAAT-3'

DNA-probe: 5'-FAM-TGGAATTTTTTTCAAACCGCTCGCC-TAMRA-3'

The viral DNA standard was prepared from 80 mL of budded virus stock with a virus titer of 4×10^7 PFU/mL and followed the procedure as described above.

2.4.6 HPLC analysis

Intracellular nucleotides and both intra-and extra-cellular amino acids were analyzed by High Performance Liquid Chromatography (HPLC) using an Agilent 1200 series system (Agilent, Forest Hill, VIC, Australia). This system includes a binary pump (G1312A), a Micro-Vacuum Degasser (G1379B), a high-performance autosampler (HiP-ALS, G1367B) with an FC/ALS thermostat (G1330B) for cooling samples, a thermostatted column compartment (G1316A) to control the temperature of the column, and a detector. A diode array detector (DAD, G1315C) was used to detect nucleotides; and a fluorescence detector (FLD, G1321A) was used for amino acid detection. The HPLC analyses for nucleotides and amino acids were carried out by Metabolomics Australia, Queensland node (AIBN).

Nucleotide analysis

The detail of the method for determination of nucleotides by HPLC was as described in Dietmair et al. (2010). The following is a brief description of the methods. The concentration of nucleotides was determined by ion-pairing reverse phase HPLC using a Gemini C18 column (3 µm, 150 x 4.6 mm, Phenomenex, Lane Cove, NSW, Australia). The column temperature was set at 30^0C, and the flow rate at 0.8 ml/minute. The gradient program used is presented in Table 2.1. Nucleotide concentrations were determined by measuring the absorbance over the whole ultraviolet (UV) spectrum with a diode array

detector (DAD, G1315C, Agilent). Compounds were detected and identified at the wavelengths of 254 and 280 nm by comparing their retention times and their 254/280 absorbance ratios or UV spectra with those of known standards.

Table 2.1 HPLC gradient for nucleotide quantification

Time (min)	%A	%B	Flow rate (mL/min)
0.0	100	0	0.8
8.0	100	0	0.8
27.0	65	35	0.8
42.0	62	38	0.8
44.0	0	100	0.8
54.0	0	100	0.8
56.0	100	0	0.8
54.0	100	0	0.8

Buffer A: *100mM KH2PO4/K2HPO4, 8mM Tetrabutylammoniumsulfate (TBAS), (pH 5.5)*

Buffer B: *75% buffer A: 25% MeOH (v/v)*

Amino acid analysis

Amino acids were quantified using a high-throughput method modified from previous work in the group (Dietmair et al., 2010). In brief, derivatised amino acids were analysed by RP-HPLC. Derivatisation was performed in a high-performance autosampler (Agilent HiP-ALS SL, G1367C). First, 0.5 uL of sample containing 250 uM of internal standards, sarcosine and 2-aminobutanoic acid, was added into 2.5 uL of borate buffer (0.4 N, pH 10.2, Agilent PN: 5061-3339), mixed and incubated for 20 s at 4^{o}C. Then 1 uL of OPA reagent (10 mg *o*-pthalaldehyde/mL in 3-mercaptopropionic acid, Agilent PN: 5061-3335) was added to initially derivatise primary amino acids. The reaction was mixed and incubated for 20 s at 4^{o}C. Next, 0.4 uL of FMOC reagent (2.5 mg 9-fluorenylmethyl chloroformate/mL in acetonitrile, Agilent PN: 5061-3337) was added, mixed and incubated for 20 s at 4^{o}C, to derivatise other amino acids. After that, 45.6 uL of Buffer A (40 mM Na_2HPO_4, 0.02% NaN_3, pH 7.8) was added to lower the pH of the reaction prior to injecting the 50 uL reaction onto an Agilent Zorbax Extend C-18 column (3.5 um, 4.6 x 150 mm, Agilent PN: 763953-902) with a guard column (SecurityGuard Gemini C18, Phenomenex PN: AJO-7597). Column temperature was kept at 37^{o}C in a thermostatted column compartment (Agilent TCC, G1316B). Chromatography was performed using an Agilent

1200-SL HPLC system, equipped with an active seal wash and a degasser (Agilent Degasser, G1379B). The HPLC gradient was 2-45% B from 0-18 min, 50-60% B from 18.1-20 min, 100% B from 20.1-24 min, and 2% B from 24.1-27 min – using a binary pump (Agilent Bin Pump SL, G1312B). Buffer B was 45% acetonitrile, 45% methanol and 10% water. Flow rate was 2 mL/min. Derivatised amino acids were monitored using a fluorescence detector (Agilent FLD, G1321A). OPA-derivatised amino acids were detected at 340_{ex} and 450_{em} nm from 1-18 min, and FMOC-derivatised amino acids at 266_{ex} and 305_{em} nm from 18-27 min. 2-aminobutanoic acid and sarcosine were used as internal standards for primary (0-18 min) and secondary (18-27 min) amino acids, respectively. Chromatograms were integrated using ChemStation (Rev B.03.02[341]).

Organic acid and sugar analysis

In addition to nucleotides and amino acids, extracellular organic acids (α-ketoglutarate, pyruvate, succinate, lactate, fumarate, acetate and propionate) and sugars (sucrose, glucose and maltose) were analyzed by HPLC (Agilent 1200 series, Agilent, Mulgrave, Victoria, Australia) using both MWD and RID detectors. Maltose and sucrose tend to co-elute on the column as both have similar molecular weight. Thus, prior to analyzing using a HPLC, samples were hydrolyzed with 6M HCl at 65^{o}C for 15 minutes in order to convert sucrose into glucose and fructose (Radford, 1995), while maltose is not hydrolyzed by this method (Lua and Reid, 2003). The samples were then separated on Phenomenex Rezex RHM Monosaccharide H^{+} 300×7.8mm 8microns + Guard column at 70^{o}C with the mobile phase of 100% 0.008N sulfuric acid and flow rate of 0.6 mL/min. Running time was 25 minutes. Injection volume was 30 µL with the injector program being set up as follows:

1 Draw 40 µL from sample, max. speed (100 µL/min), -1.5 mm offset
2 Wait 0.1 min
3 Draw 5 µL from air, max. speed (100 µL/min)
4 Needle wash in flush port, 10 sec
5 Eject 15µL into waste, max. speed (100 µL/min)
6 Inject

Four levels of calibration standard were used for the calibration curve: level 1 (1:10 dilution), level 2 (1:5 dilution), level 3 (1:2 dilution), and level 4 (undiluted). The amount of organic acids or sugars in samples was calculated from the regression equation derived from the known standard concentrations. The fructose level then equated to the sucrose

level, while the glucose level was the total glucose from the sample and from hydrolyzed sucrose (same amount as fructose). Glucose concentration in the sample was indirectly calculated by subtracting the fructose concentration from the total glucose.

Calculation of specific substrate consumption, and production rates

The overall cell and biomass specific rates of substrate consumption and production, q_S (mmol/10^3 cells/hour), and q_S (mmol/10^3 mm^3 cell biomass/hour), can be calculated using following equation:

$$\frac{dS}{dt} = -q_S X$$

where S is the substrate concentration (mM),

X is the average total cell density (cells/ mL) or cell volume (mm^3/mL).

As the substrate concentrations in the culture medium were measured at various times post-infection/inoculation, a plot of the substrate concentrations over the time post-infection/inoculation was generated. The slope of the line was used to calculate the substrate consumption rate as per the following equation:

$$\frac{Slope}{X} = q_S$$

where X is the average total cell density (cells/mL) or cell volume (mm^3/mL) over the above period post-infection/inoculation.

In the case of measuring the substrate concentrations at only 2 points at the beginning and end of the period, the substrate consumption rate was calculated as follows:

$$\frac{S_t - S_{t_0}}{X(t - t_0)} = q_S$$

where t is the time at the end of the period (hour), t_0 is the time at the beginning of the period, S_t and S_{t0} are substrate concentrations (mM) at t and t_0, respectively and X is the average total cell density (cells/mL) or cell volume (mm^3/mL) over the above period post-infection/inoculation.

2.4.7 LC-MS analysis

Intracellular nucleotides and TCA cycle intermediates were also measured by LC-MS/MS as described previously (Dietmair et al., 2012). Briefly, the Dionex UltiMate 3000 liquid chromatography system (Dionex, California, USA) coupled with the ABSciex 4000

QTRAP mass spectrometer (ABSciex, Concord, Canada) were used to measure concentrations of intracellular metabolites. A Gemini-NX C18 150×2.0mm, 3µm 100 Å particle column (Phenomenex, Aschaffenburg, Germany) was used to separate metabolites by chromatography. The column was maintained at 55^{o}C in the column oven. The mobile phase was 7.5 mM aqueous tributylamine solution adjusted with ice-cold acetic acid (eluent A) and acetonitrile (eluent B) to pH 4.95. The gradient profile is shown in Table 2.2. The injection volume was 10 µL. The flow rate of the mobile phase was 0.3 mL/min that was introduced directly into the mass spectrometer with no split.

Table 2.2 Gradient profile for LCMS/MS

Time (hours)	Eluent A (%)
0	100
8	100
20	80
30	73
31	0
33	0
34	100
50	100

The mass spectrometer, equipped with a Turbo V electro-spray ion source, was operated in negative ionization mode. The turbo ion spray voltage was set to -4500 V. The nebulizer (GS1), auxiliary (GS2), curtain (CUR) and collision (CAD) gases were 60, 20 and medium (arbitrary units), respectively that were generated from pressurized air in a N300DR nitrogen generator (Peak Scientific, Massachusetts, USA). Temperature of the auxiliary gas remained at 350^{o}C. All transitions were fixed at an entrance potential of -10V. Declustering potential, collision energy and collision cell exit potential were set up based on previously optimized settings for the individual analytes. The mass spectrometer was set to unit resolution and scheduled Multiple Reaction Monitoring mode after determining the updated retention time of each analyte under the chromatographic conditions described above to obtain adequate selectivity and sensitivity. Randomization has been applied for sample acquisition and 2 quality control (QC) samples were included randomly for every 10 samples injected. QC1 was the repeat injection of calibration level 3 (12.5 µM) and QC2 was a pooled sample for the entire sample set (Sangster et al., 2006). By this way, acquisition stability and reproducibility were monitored.

To achieve higher performance and accuracy of the LCMS/MS data the following modifications have been made to the above protocol. The analytical column was equipped with a pre-column Security Guard Gemini-NX C18 4 mm × 2 mm I.D. cartridge (Phenomenex, Aschaffenburg, Germany). The samples were run with sample- and analyte-relevant calibration standards and pooled QC samples (Hodson et al., 2009; Sangster et al., 2006) to control for reproducibility of data acquisition and to ensure data integrity. Analyte stock solutions were prepared in purified water (Veolia Water Solution & Technologies, Pyrmont, Australia) and aliquots of each solution were mixed to achieve a final calibrant solution at 200 µM. This calibrant solution was serially diluted and the dilutions used as calibration standards from 200 to 0.006 µM, constituting $9 \leq x \leq 20$ calibration points for all analytes to account for differential responses in the mass spectrometer. Data were processed and analysed in Analyst 1.5.2 and MultiQuant 2.1.1 (ABSciex, Canada).

2.5 Evaluation of insect cells grown in 50 mL tube bioreactors

Prior to developing a method for quenching and extraction of intracellular metabolites of cultured insect cells, the growth of insect cells in tube cultures was investigated. The advantage of tube cultures is that it allows conducting the quenching process quickly by pouring immediately the culture in each tube into a cold quenching solution. Since the working volume of the tube culture can be set up at 10 ml, this volume is sufficient for one intracellular extraction sample. As the whole culture can be sacrificed for analysis, sampling and quenching is achieved very rapidly (within seconds). The growth of cells in 50 ml tubes was tested for both HzAM1 and Sf9 cell lines compared with shaker flasks as controls.

Tube testing was conducted for both non-infected and infected cultures of HzAM1 and Sf9 cells with different shaking speeds 200, 220, 240, and 260 rpm, and different working volumes of 10ml and 20ml. The control was a culture in shaker flasks (25 ml working volume) at 120 rpm.

The testing showed that tube cultures worked well compared to the shaker controls for the HzAM1 cells but not for the Sf9 cells. Hence shaker cultures rather than tube cultures were used for Sf9 experiments.

Chapter 3

Development of intracellular metabolite extraction protocol for insect cells

Methods 56 (2012) 396–407

Contents lists available at SciVerse ScienceDirect

Methods

journal homepage: www.elsevier.com/locate/ymeth

Development of quenching and washing protocols for quantitative intracellular metabolite analysis of uninfected and baculovirus-infected insect cells

Trinh T.B. Tran, Stefanie Dietmair, Leslie C.L. Chan, Hoai T. Huynh, Lars K. Nielsen *, Steven Reid

Australian Institute for Bioengineering and Nanotechnology, The University of Queensland, St. Lucia, QLD 4072, Australia

ARTICLE INFO

Article history:
Available online 7 December 2011

Keywords:
Metabolomics
Quenching
Washing
Insect cell culture
Baculovirus expression system

ABSTRACT

Metabolomics refer to the global analysis of small molecule metabolites in a biological system, and can be a powerful tool to elucidate and optimize cellular processes, particularly when integrated into a systems biology framework. Determining the endometabolome in cultured animal cells is especially challenging, due to the conflicting demands for rapid quenching of metabolism and retention of membrane integrity, while cells are separated from the complex medium. The challenge is magnified in virus infected cells due to increased membrane fragility. This paper describes an effective methodology for quantitative intracellular metabolite analysis of the baculovirus–insect cell expression system, an important platform for the production of heterologous proteins and baculovirus-based biopesticides. These two applications were represented by *Spodoptera frugiperda* (Sf9) and *Helicoverpa zea* (HzAM1) cells infected with recombinant *Autographa californica* and wild-type *Helicoverpa armigera* nucleopolyhedroviruses (AcMNPV and HaSNPV), respectively. Specifically, an ice-cold quenching solution comprising 1.1% w/v NaCl and 0.2% w/v Pluronic® F-68 (NaCl + P) was found to be efficacious in preserving cell viability and minimizing cell leakage during quenching and centrifugation-based washing procedures (prior to extraction using cold 50% v/v acetonitrile). Good recoveries of intracellular adenosine triphosphate, total adenosine phosphates and amino acids were obtained after just one wash step, for both uninfected and infected insect cells. The ability to implement wash steps is critical, as insect cell media are metabolites-rich, while infected insect cells are much more fragile than their uninfected counterparts. Hence, a promising methodology has been developed to facilitate endometabolomic analysis of insect cell–baculovirus systems for bioprocess optimization.

1. Introduction

The baculovirus–insect cell expression system is widely used in research for efficient production of near-authentic recombinant eukaryotic proteins [1–3], and has evolving applications in human biologics such as humanized *N*-glycoproteins, baculovirus display immunogens and gene delivery vectors for mammalian cells [2,4]. Recently, baculovirus-expression has gained considerable momentum as a regulatory-approved manufacturing platform for human (Cervarix®, Provenge®) and veterinary (Ingelvac®, Porcilis®) vaccines [3]. Furthermore, baculoviruses can be developed as effective biopesticides for many agriculturally-important insect pests, especially as part of an integrated pest management program [5,6].

For commercial viability, baculovirus–insect cell bioprocesses have to be optimized for high protein product yields, and this likely involves a high cell density production process using fed-batch cultures in stirred-tank bioreactors [7]. However, scaling-up such a process is challenging, as insect cell–baculovirus interactions are complex, and may have variable outcomes depending on changes in the nutrient (medium and feed) and fluid-mechanical (bioreactor) environments. This is especially the case when nutrient levels in feeds are progressively increased for high cell density infections, leading to perturbations such as osmotic shock and toxin accumulation [7]. A systems biology approach, involving the integration of various omics platforms such as transcriptomics and metabolomics into genome-scale computational models, could bring about better elucidation of complex biological systems, and offer rational strategies towards bioprocess optimization [8,9]. With this in mind, a methodology was developed in this study for quantitative intracellular metabolite analysis of insect cells, to enable the application of metabolomics for the baculovirus–insect cell expression system. Two particular baculovirus applications were tested in this study, representing recombinant protein production (*Autographa californica* nucleopolyhedrovirus in *Spodoptera frugiperda* (Sf9) cells) and biopesticide production (*Helicoverpa armigera* nucleopolyhedrovirus in *Helicoverpa zea* (HzAM1) cells).

While the exometabolome of cell cultures has been well-researched in the past [10], it is the endometabolome that offers the most comprehensive information regarding cell metabolism [8]. However, quantitative intracellular metabolite analysis is the

* Corresponding author. Address: Australian Institute for Bioengineering and Nanotechnology, Building 75, Corner College/Cooper Road, The University of Queensland, St. Lucia, QLD 4072, Australia. Fax: +61 7 3346 3973.
E-mail address: lars.nielsen@uq.edu.au (L.K. Nielsen).

1046-2023/$ - see front matter Crown Copyright © 2011 Published by Elsevier Inc. All rights reserved.
doi:10.1016/j.ymeth.2011.11.009

most challenging aspect of a metabolomics study [11], as there is a requirement for efficient quenching and extraction procedures to preserve the metabolic state of cells at the point of sampling. An ideal quenching solution is one that rapidly terminates all enzymatic activities to avoid degradation of high-turnover metabolites (e.g. adenosine triphosphate), while an ideal extraction solution should be able to extract all intracellular metabolites – which have a wide range of chemistries, physical attributes and concentrations [12,13]. In reality, complete metabolome profiling remains an aspiration, while methodologies for metabolite recovery and analysis are still under active development [8].

Sample preparation protocols for endometabolome analysis have been developed for yeast [14–16], bacteria [17–20] and mammalian cells [11–13,21,22], but as yet not for insect cells. Dietmair et al. developed an optimized methodology for quantitative metabolomics of Chinese Hamster Ovary (CHO) cells, using ice-cold isotonic NaCl (0.9% w/v) and very cold 50% v/v acetonitrile (−40 °C) for effective quenching and extraction of intracellular metabolites, respectively [12]. This CHO cell methodology was anticipated to be applicable for insect cells, since both cell types are similar physically in terms of size and lack of cell walls. Hence in this study, quenching and washing procedures were optimized for uninfected and infected insect cells, using ice-cold saline and improved saline-based formulations as quenching solutions (at 1.1% w/v NaCl, which is isotonic for insect cells). After these procedures, the intracellular metabolites were extracted using acetonitrile and analyzed using HPLC using the same methodologies described by Dietmair et al. [12].

There was a particular focus on quenching and cell pellet washing procedures in this study for a number of reasons. Firstly, infected insect cell plasma membranes are likely to be more fragile than those of CHO cells, since baculovirus infection is a cell-lytic process [23,24]. Hence saline alone may not be able to prevent metabolite leakage, especially when the infected cells are subjected to fluid-mechanical shear stress during sample preparation. In this study, the cell-protectant Pluronic® F-68 [25] was tested as an additive in the default saline quenching solution, to determine its effectiveness in minimizing metabolite leakage. Secondly, insect cells are grown in complex media that contain high concentrations of certain metabolites (e.g. amino acids), hence one or more wash steps are necessary post quenching so that the measured intracellular metabolite content is free from media-contamination. Thirdly, the washing method itself has to be carefully evaluated for insect cells, since this step increased cell damage/leakage when applied to CHO cells [12,13], and cell separation via fast filtration resulted in much reduced metabolite recoveries when compared to that using centrifugation [12]. Hence, a centrifugation-based washing method was applied to insect cells, and the Pluronic® F-68-supplemented saline was tested as a promising leakage-minimizing washing solution.

2. Materials and methods

2.1. Cell lines, media and virus stocks

2.1.1. Sf9–rAcMNPV system

The *S. frugiperda* clone 9 cell-line (Sf9; ATCC CRL 1711) and recombinant β-Galactosidase-expressing *A. californica* multi-capsid nucleopolyhedrovirus (rβ-Gal AcMNPV) have been described previously [26]. Cell stocks were propagated in the commercial serum-free medium Sf-900 II (Invitrogen, Carlsbad, CA), and maintained by regular passaging every 3–4 days in 25 mL shaker flask cultures (125 mL single-use Erlenmeyer flasks; Corning, Lowell, MA) at seeding densities of 3–5 $\times$ 10^5 cells/mL. The shaker cultures were agitated at 120 rpm on an orbital shaker platform (Thermoline, NSW, Australia) and incubated at 28 °C in a refrigerated incubator (Thermoline).

The passage 1 (P1) virus stock was prepared by infecting Sf9 cells in Sf-900 II medium, at a Time of Infection (TOI) of 1.5 $\times$ 10^6 cells/mL and a Multiplicity of Infection (MOI) of 0.1 Plaque Forming Units (PFU)/cell, using frozen virus stocks [26]. At 4 days post-infection (d.p.i.), the infected culture was centrifuged (1000*g*, 10 min) to retrieve the supernatant as the virus stock (containing infectious budded virus, BV). The working virus stock (P2) was prepared from the P1 virus in a similar fashion, at a TOI of 0.5 $\times$ 10^6 cells/mL and a MOI of 0.001 PFU/cell. Virus stocks were stored at 4 °C, and were titered prior to use.

2.1.2. HzAM1–HaSNPV system

The *H. zea* cell-line (BCIRL-HZAM1) and wild-type *H. armigera* single-capsid nucleopolyhedrovirus (wtHaSNPV, strain H25EA1) have been described previously in the PCT patent by Lua and Reid, WO/2005/045014 [27]. HzAM1 cell stocks were maintained as described for the Sf9–rAcMNPV system, in Sf-900 II medium.

Passage 1 (P1) HaSNPV stock was prepared by extracting occlusion-derived virus (ODV) from caterpillar-produced occlusion bodies (OB) as described in the PCT patent WO/2005/045014 [27]. Briefly, 500 μL of OB suspension (10^{10} OBs/mL) was lyzed with 40 μL of alkaline saline (0.5 M Na_2CO_3, 1.0 M NaCl), at 28 °C for 30 min. The resulting ODV suspension was neutralized, sterilized with 0.2 μm syringe filters (Sartorius–Stedim Biotech, Aubagne, France), and then used to infect a 100 mL shaker culture seeded at 5 $\times$ 10^5 cells/mL (250 mL Erlenmeyer flask, Corning). The P1 infected culture was incubated for 4 d.p.i., and was then used to establish the P2 infection (5 $\times$ 10^5 cells/mL, 100 mL, 15% v/v virus inoculum). The P2 infected culture was incubated for 3 d.p.i. and then centrifuged (1000*g*, 10 min) to retrieve the BV-containing supernatant as the working virus stock, which was stored at 4 °C and was titered prior to use.

2.2. Analytical methods

2.2.1. Cell, virus and product quantification

For general cell passaging, viable and total cell densities were estimated from triplicated hemocytometer (Improved Neubauer; Brand, Germany) counts under a phase-contrast microscope (Olympus, Japan), which resulted in a relative error of 15% [28]. Cell viabilities were estimated using the 0.05% w/v Trypan Blue exclusion method [28]. For metabolomic experiments, total cell densities were enumerated using a Multisizer-4™ coulter counter (Beckman Coulter, Fullerton, CA), because it provided a much reduced count variability (1–2%). In this case, cell viabilities were determined via Propidium Iodide staining using the Cell Lab Quanta™ SC MPL flow cytometer (Beckman Coulter), or via Trypan Blue staining using a hemocytometer.

An endpoint dilution assay was used to estimate the titer (PFU/mL) of rAcMNPV virus stocks, which was based on a modified Reed and Muench protocol [29,30], and was described previously [31]. The HaSNPV virus stocks were titered using an in-house suspension culture (SC) titration assay [32], which was informed by the Power-Nielsen baculovirus infection model [33] and HaSNPV–HzAM1 infection kinetics [34]. The product of rAcMNPV infections (rβ-Gal) was quantified using a well-established colorimetric assay based on the enzymatic hydrolysis of *o*-nitrophenyl-galactopyranoside (ONPG), as described previously [26]. The product of wtHaSNPV infections (OBs) was quantified via triplicated hemocytometer counts under a phase-contrast microscope, after liberation from infected cells using 0.5% w/v SDS, as described previously [35].

2.2.2. Metabolite analysis

Intracellular nucleotide and amino acid concentrations were measured via high performance liquid chromatography (HPLC),

using an Agilent 1200 Series system (Agilent Technologies, Santa Clara, CA). In particular, nucleotides were measured via ion-pairing reverse phase HPLC, using a Gemini C18 column (3 μm, 150 × 4.6 mm, Phenomenex, Torrance, CA) and a diode array detector (DAD, G1315C, Agilent). Amino acids were measured via reverse phase HPLC, using a Gemini C18 column (as described above) and a fluorescence detector (FLD, G1321A, Agilent). Primary and secondary amines were precolumn-derivatized using the HPLC autosampler, with *o*-phthalaldehyde (OPA, PN5061-3335, Agilent) and 9-fluorenylmethyl chloroformate (FMOC, PN5061-3337, Agilent), respectively. The full methodologies have been comprehensively described by Dietmair et al. [12].

Intracellular ATP was also measured using the ATPlite luminescence ATP detection assay system (PerkinElmer Life Sciences, Boston, MA), particularly in the case of the quenching solution efficacy study. This assay is based on the production of light when ATP reacts with D-Luciferin in the presence of Luciferase, and was conducted according to the manufacturer's instructions.

2.2.3. Statistical analysis

One-way analysis of variance (ANOVA), incorporating Tukey's Honestly Significant Difference (HSD) test, was used to determine whether the means from two or more groups of data were significantly different at the 95% confidence level. Minitab 15 Statistical Software (Minitab, State College, PA) was used for all data analysis.

2.3. Metabolomics studies

2.3.1. Evaluating the efficacy of three NaCl-based quenching solutions for intracellular metabolite analysis of uninfected Sf9 cells

Three quenching solutions (QS) were tested in this study, to determine their efficacy in preserving the intracellular ATP levels of uninfected Sf9 cells. The first QS was 1.1% w/v NaCl (NaCl), which was based on the 0.9% w/v saline shown to be efficacious for quenching CHO cells in a previous study [12]. A higher concentration of NaCl was used for insect cells, as they require a higher optimum medium osmolality when compared to mammalian cells (350–385 vs 290 mOsmol/kg, respectively) [36]. The other two QSs were first developed in this study, being 1.1% w/v NaCl supplemented with 0.2% w/v Pluronic® F-68 (PF68) (NaCl + P), and 0.8% w/v NaCl supplemented with 0.2% w/v PF68, 1.65 g/L sucrose, 0.5 g/L $CaCl_2$, 0.918 g/L $MgSO_4$, 1.2 g/L KCl, 0.35 g/L $NaHCO_3$ and 1.16 g/L $NaH_2PO_4.H_2O$ (NaCl + P + S). All three QSs were adjusted to a final osmolality of around 365 mOsmol/kg, and NaCl + P + S was adjusted to a final pH of 6.0.

Uninfected Sf9 cell cultures were set up as follows, to ensure that the cells were in very good condition for metabolomics analysis (early-exponential growth phase). Multiple 30 mL shaker flask cultures (125 mL Erlenmeyer flasks, 120 rpm, 28 °C) were seeded at 5×10^5 cells/mL in Sf-900 II medium, and then allowed to double in cell density over 24 h. Taking out one flask at a time from the incubator, the contents of each flask (30 mL) were quickly poured into either 30 mL of very cold 100% acetonitrile (pre-cooled in a dry ice/ethanol bath to −40 °C), 120 mL of room temperature QS, or 120 mL of ice-cold QS (pre-cooled in an ice bath to 0.5–1 °C). These treatments were referred to as direct extracted (DE), unquenched (UQ) and quenched (Q).

The DE culture (in centrifuge tubes) was vortex-mixed and incubated for 10 min in an ice bath. The extracted cell lysate was then clarified by centrifugation (5000*g*, 5 min, 0 °C), frozen at −80 °C, and placed on a sample holder in the freeze-dryer (Alpha I-4 LSC, Martin Christ, Germany), with the tubes' screw-caps slightly loosened. The samples were freeze-dried according to the manufacturer's instructions, at settings of 0.021 mbar vacuum and −20 °C, and a duration of up to 24 h. The freeze-dried samples were then stored at −80 °C until analysis.

The UQ culture (in centrifuge tubes) was centrifuged (1000*g*, 1 min, 0 °C) and the cell pellet was then extracted by resuspension in very cold 50% v/v acetonitrile in deionized water (pre-cooled in a dry ice/ethanol bath to −40 °C, 0.5 mL/10^6 cells), vortex-mixing, and incubation for 10 min in an ice bath. The cell lysate was clarified by centrifugation (5000*g*, 5 min, 0 °C) and then freeze-dried as described for the DE protocol. The Q treatments had three cases: no wash (Q0W), one wash (Q1W) and two wash (Q2W) steps. The quenched cells from the Q0W case were extracted and freeze-dried as described for the UQ case. The Q1W and Q2W cases involved extra centrifugation steps (1000*g*, 1 min, 0 °C) to pellet and resuspend the quenched cells with an equal volume of ice-cold QS (washing), which were then extracted and freeze-dried as described for the UQ case. Cell pellet resuspension during wash steps was performed gently by multiple tube inversions. The freeze-dried cell extracts from all treatments were resuspended in deionized water just prior to analysis. Each treatment (UQ, Q0W, Q1W, Q2W) for the three quenching solutions being tested, and the DE case, were performed in three biological replicates.

Cold 50% acetonitrile was shown previously to be the most efficacious among a wide range of extraction solvents for the recovery of multiple types of metabolites in CHO cells [12]. In this study, a selection of extraction solvents (cold 50% acetonitrile, cold 50% methanol, hot 80% methanol, hot 75% ethanol and cold 75% ethanol) was tested for Sf9 insect cells, and cold 50% acetonitrile was found to be the best in terms of ATP recovery and reproducibility (data not reported), hence it was used as the default extraction solvent. Solvent/water removal from the cell extracts was a critical step, since solvents may interfere with the metabolite analysis procedure, and fully dried extracts exhibit excellent stability and can be stored almost indefinitely [37]. Freeze drying is the ideal method to achieve this, as the process of sublimation of frozen samples does not expose the metabolites to thermal degradation and concentration effects.

Intracellular ATP levels were measured using the ATPlite assay kit. This assay has been validated previously to demonstrate that it was not affected by the sample matrix. Briefly, reconstituted freeze-dried cell extracts were either spiked or not spiked with an ATP standard, then assayed to determine the measured spiked ATP concentration. The same amount of ATP standard was also added to deionized water, and the measured spiked ATP concentration in water was compared to that from the cell extract, and both were shown to be not significantly different ($P = 0.121$, one-way ANOVA).

2.3.2. Optimizing the washing procedure for intracellular metabolite analysis of uninfected and baculovirus-infected Sf9 and HzAM1 cells

Uninfected Sf9 cell cultures were set up in shaker flasks and processed for intracellular metabolite analysis, in exactly the same way as that described for the first study, except that quenching was performed only with NaCl + P, and a 3rd wash step was also implemented (DE, UQ, Q0W, Q1W, Q2W, Q3W). Uninfected HzAM1 cells were set up and processed in a similar fashion to Sf9 cells, except that the cells were propagated as 10 mL shaker tube cultures using 50 mL conical-bottom/vented tubes (single-use TubeSpin® bioreactors; TPP, Switzerland). The tube cultures were incubated in an upright position on a tube-rack that was secured onto an orbital shaker platform (220 rpm, 28 °C). Quenching and extraction solutions were added to HzAM1 cells in the same volumetric ratios as those used for Sf9 cells. The motivation for using tube cultures is the potential for enhanced efficiencies in the use of labor, time and resources, especially for large replicated experiments. Preliminary experiments showed that tube cultures were as good as shaker cultures in supporting HzAM1 cell growth, but unfortunately this was not the case for Sf9 cells (data not published). Hence tube cultures were only employed for HzAM1 experiments.

Infected experiments were set up using the following protocols. Sf9 and HzAM1 cultures were set up as 100 mL cultures in 250 mL

shaker flasks (at 1.5 and 0.75 $\times$ 10^6 cells/mL, respectively), allowed to double in cell density over 24 h (to ensure good cell condition), then diluted back to 1.5 and 0.75 $\times$ 10^6 cells/mL, respectively with virus inoculum and fresh Sf-900 II medium to a final volume of 200 mL in 1 L single-use bottles (Corning). High MOIs were then applied, being 20 PFU/cell (rβ-Gal-AcMNPV) and 17 PFU/cell (wtHaSNPV) for the Sf9 and HzAM1 cultures respectively, to ensure synchronous infections (minimal cell growth post-infection).

Once infected, the 200 mL cultures were immediately aliquoted into multiple smaller cultures (with good mixing between each aliquot), i.e. 30 mL shaker flask cultures (125 mL Erlenmeyer flasks, 120 rpm, 28 °C) for the AcMNPV-Sf9 infections, and 10 mL shaker tube cultures (50 mL TubeSpin® bioreactors, 240 rpm, 28 °C) for the HaSNPV–HzAM1 infections. These infected cultures were incubated for 24 h post-infection (h.p.i.), then processed for intracellular metabolite analysis as described for the uninfected cultures (DE, UQ, Q0W, Q1W, Q2W, Q3W).

High levels of free amino acids are present in Sf-900 II medium (according to in-house analysis), which could contribute to the intracellular amino acids content being measured if they were inadequately removed from the cell pellet's liquid residue during the washing procedure. To resolve this issue, Norvaline (Nva) was spiked into the QS (for the quenching step only), so that its presence in the intracellular fraction can be monitored, and to determine the required number of cell pellet wash steps (using Nva-free QS). Nva was chosen as the spiking agent as it is a non-standard/non-proteinogenic amino acid [38]. Nva was spiked into the QS at a concentration of 2.5 mM, which was based on the levels of three highly abundant amino acids in the medium (Asp, Asn and Glu). In addition, the extent of reduction in the intracellular amino acids content between wash steps was also used as an indicator of cell pellet washing efficiency.

All experiments in this study were conducted in three biological replicates. The cell extracts were analyzed for 11 nucleotides (up to 2 wash steps) and 20 amino acids (up to 3 wash steps) using HPLC. For the infected experiments, separate infected cultures (and uninfected controls) were set up identical to those intended for metabolomics analysis, so that the infection progress (cell density and protein production) can be monitored on a daily basis.

For both metabolomics studies, the total cell number and average cell volume of each pellet had to be determined accurately prior to the acetonitrile extraction step, so that the intracellular metabolite levels can be calculated in terms of both mol/cell and mol/cell volume. Hence the cell density/volume, cell viability and total volume of each processed sample (prior to the final centrifugation step before extraction) were measured via the Multisizer-4 coulter counter, Cell Lab Quanta flow cytometer and 5-decimal digital balance (Shimadzu, Japan), respectively. For volume measurements, the sample container (centrifuge tube) was weighed before and after sample addition to obtain the net sample weight, which was converted to sample volume by assuming that the sample had the same density as water (1 g/mL), a reasonable assumption for a dilute cell suspension/aqueous solution. For the DE case, these measurements were made 1 h prior to acetonitrile extraction, to allow sufficient time for re-equilibration of the designated shaker culture (post sampling) in the incubator.

3. Results

3.1. Efficacy of three NaCl-based quenching solutions for intracellular metabolite analysis of uninfected Sf9 cells

Quenching of uninfected Sf9 cells with ice-cold QS without cell pellet wash steps (Q0W) was most effective when the default QS (NaCl) was supplemented with PF68 (NaCl + P), or with PF68, sucrose and additional salts (NaCl + P + S), which supported intracellular ATP recoveries of 88 or 89% respectively (Fig. 1A), and high cell viabilities of 96% or 98% respectively (Fig. 1B). The ATP recovery (%) for a particular quenching/washing treatment was calculated with respect to the ATP level in the direct extracted (DE) case. Although the DE case exhibited a higher ATP concentration, it was not significantly different from the NaCl + P (Q0W) and NaCl + P + S (Q0W) cases ($P > 0.05$, one-way ANOVA, Tukey's HSD). In contrast, the default QS supported a significantly lower ATP recovery (81%) and a substantially lower cell viability (89%) when compared to the DE case (Fig. 1A and 1B).

When one or two cell pellet wash steps were implemented post quenching (Q1W or Q2W), the use of either ice-cold NaCl + P or NaCl + P + S as the washing solution resulted in insignificant declines in ATP concentration ($P > 0.05$, Fig. 1A) and minimal declines in cell viability (Fig. 1B), when compared to the corresponding cases in Q0W. In contrast, these indicators were much reduced when NaCl alone was used (62% ATP recovery and 67% viability for Q2W). Unquenched Sf9 cells (UQ, i.e. using room temperature QS) exhibited uniformly and significantly lower ATP recoveries (48–57%) for all three QSs tested ($P < 0.05$, Fig. 1A). However, the viabilities of UQ cells were high, in particular for the NaCl + P and NaCl + P + S cases (96–97%, Fig. 1B).

Hence NaCl + P and NaCl + P + S were the best performing of the three QSs tested, in terms of intracellular ATP recovery and retention of high cell viabilities after quenching and washing procedures. Since both QSs were very similar in performance, NaCl + P (being a simpler formulation) was chosen as the new default QS for subsequent studies.

3.2. Washing optimization for intracellular metabolite analysis of the Sf9–rAcMNPV system

The cell growth and β-Gal production temporal profiles of rAcMNPV-infected Sf9 cells are presented in Fig. 2A. The intracellular concentrations of selected metabolites in uninfected and rAcMNPV-infected Sf9 cells are shown in Fig. 3A and B respectively (adenosine phosphates, AdoP), and in Fig. 4A and B respectively (amino acids), to illustrate the differences between the five types of sample treatment (DE, Q0W, Q1W, Q2W, UQ). ATP and total AdoP recoveries (%) for a particular treatment were calculated with respect to the corresponding ATP and total AdoP levels in the DE case (Table 1).

Despite the application of a high MOI (20 PFU/cell), the infected culture grew from a TOI of 1.5 $\times$ 10^6 cells/mL to a peak total cell density (PTCD) of 2 $\times$ 10^6 cells/mL at 48 h.p.i. (Fig. 2A). However, this growth was minor and the cells could be considered to be synchronously infected. In contrast, the uninfected control demonstrated a 24-hour doubling time over the exponential growth phase and reached a PTCD of 17.6 $\times$ 10^6 cells/mL (data not shown), which indicated that the stock cells were in good condition, and that cell growth retardation was due only to virus infection. The β-Gal production also peaked at 48 h.p.i., demonstrating that the infection kinetics were rapid [33,34]. Hence, the Sf9–rAcMNPV infections set up in this study were optimally-infected, and were suitable for metabolomic studies.

Analysis of the intracellular AdoP content of uninfected and infected Sf9 cells (Fig. 3A and B) showed that quenching with ice-cold NaCl + P (Q0W) resulted in ATP recoveries of 85% and 81%, respectively (Table 1). However, the difference in ATP levels between the Q0W and DE cases was not significant for uninfected cells ($P > 0.05$, one-way ANOVA, Tukey's HSD), while it was significant for infected cells ($P < 0.05$). Uninfected Sf9 cells that have been washed once or twice with ice-cold NaCl + P post quenching (Q1W or Q2W) did not exhibit a significant reduction in ATP level, when compared to the DE or Q0W cases ($P > 0.05$). The ATP level of

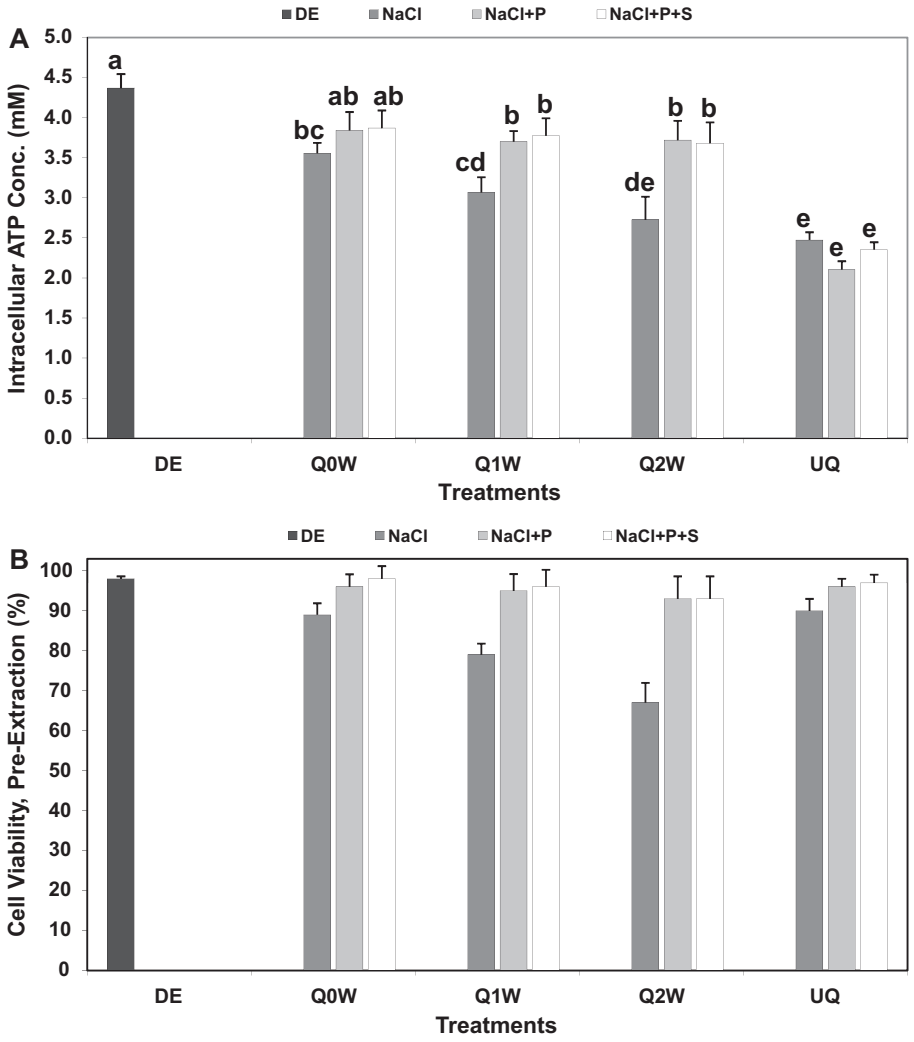

Fig. 1. Evaluation of three ice-cold (0.5–1 °C) quenching solutions (QS) for the recovery of intracellular ATP in uninfected Sf9 cells. The QSs were 1.1% w/v NaCl (NaCl), 1.1% w/v NaCl + 0.2% w/v Pluronic® F-68 (NaCl + P), and 0.8% w/v NaCl + 0.2% w/v Pluronic® F-68 + 1.65 g/L sucrose + 0.5 g/L $CaCl_2$ + 0.918 g/L $MgSO_4$ + 1.2 g/L KCl + 0.35 g/L $NaHCO_3$ + 1.16 g/L $NaH_2PO_4{\cdot}H_2O$ (NaCl + P + S). Early-exponential phase Sf9 cell cultures (1×10^6 cells/mL) were either direct extracted (DE) with 1:1 cold 100% acetonitrile (−40 °C), quenched with 1:5 QS (Q0W), quenched and washed once with 1:5 QS (Q1W), quenched and washed twice with 1:5 QS (Q2W), or unquenched by adding 1:5 room temperature QS (UQ). The quenched/washed and unquenched cell pellets were extracted with cold 50% v/v acetonitrile in deionized water (−40 °C). Cell extracts were freeze-dried and resuspended in deionized water prior to analysis using the ATPlite luminescence assay. (A) Intracellular ATP concentration. (B) Cell viability prior to the extraction step. Error bars show the standard deviation of biological triplicates. Tukey's HSD test ($\alpha = 0.05$) was used to compare the means (ATP concentration) from different treatments, means with the same letter indicate that they are not significantly different.

infected Sf9 cells did not change significantly between the Q0W and Q1W cases ($P > 0.05$), but did decline significantly between the Q1W and Q2W cases ($P < 0.05$), leading to a low ATP recovery of 61%. The lowest ATP recovery recorded was for the UQ uninfected case (37%). For both uninfected and infected Sf9 cells, ADP levels did not differ significantly between the DE, Q0W, Q1W and Q2W cases ($P > 0.05$). AMP was not detected in Sf9 cells for the DE case, but was present after quenching and washing steps. The total intracellular AdoP (ATP, ADP and AMP) content of uninfected Sf9 cells was not significantly different between the DE, Q0W, Q1W and Q2W cases ($P > 0.05$). The total AdoP of infected Sf9 cells was also unchanged for the DE, Q0W and Q1W cases ($P > 0.05$) but decreased significantly by 16% between Q1W and Q2W ($P < 0.05$). The total AdoP of unquenched Sf9 cells was better retained when infected rather than when uninfected (83% and 41% of DE, respectively).

Intracellular amino acids analysis of uninfected and infected Sf9 cells (Fig. 4A and B) showed that QS-derived Norvaline (Nva) was present at a high level (27.9 and 13.8 mM respectively) after quenching without washing (Q0W), presumably originating from the cell pellet's residual liquid fraction. Intracellular Nva levels declined dramatically (7 and 5-fold respectively for uninfected and infected cases) when quenching was followed by 1 wash step (Q1W), but further declines were minimal when additional wash steps were implemented, with Nva levels between Q1W and Q2W cases, and between Q2W and Q3W cases, being not significantly different ($P > 0.05$, one-way ANOVA, Tukey's HSD). As with Nva, there was a dramatic decline in the intracellular level of each standard (proteinogenic) amino acid between the Q0W and Q1W cases, for both uninfected and infected Sf9 cells (Fig. 4A and B). When additional wash steps (Q2W or Q3W) were implemented, further declines in intracellular amino acid levels were not significant for uninfected Sf9 cells ($P > 0.05$). However, two amino acids (Asp and Glu) experienced significant modest declines between the Q1W and Q2W cases ($P < 0.05$), and seven amino acids (Asp, Glu, Asn, Gln, Gly, Phe and Pro) experienced significant modest declines between the Q2W and Q3W cases ($P < 0.05$), for infected Sf9 cells.

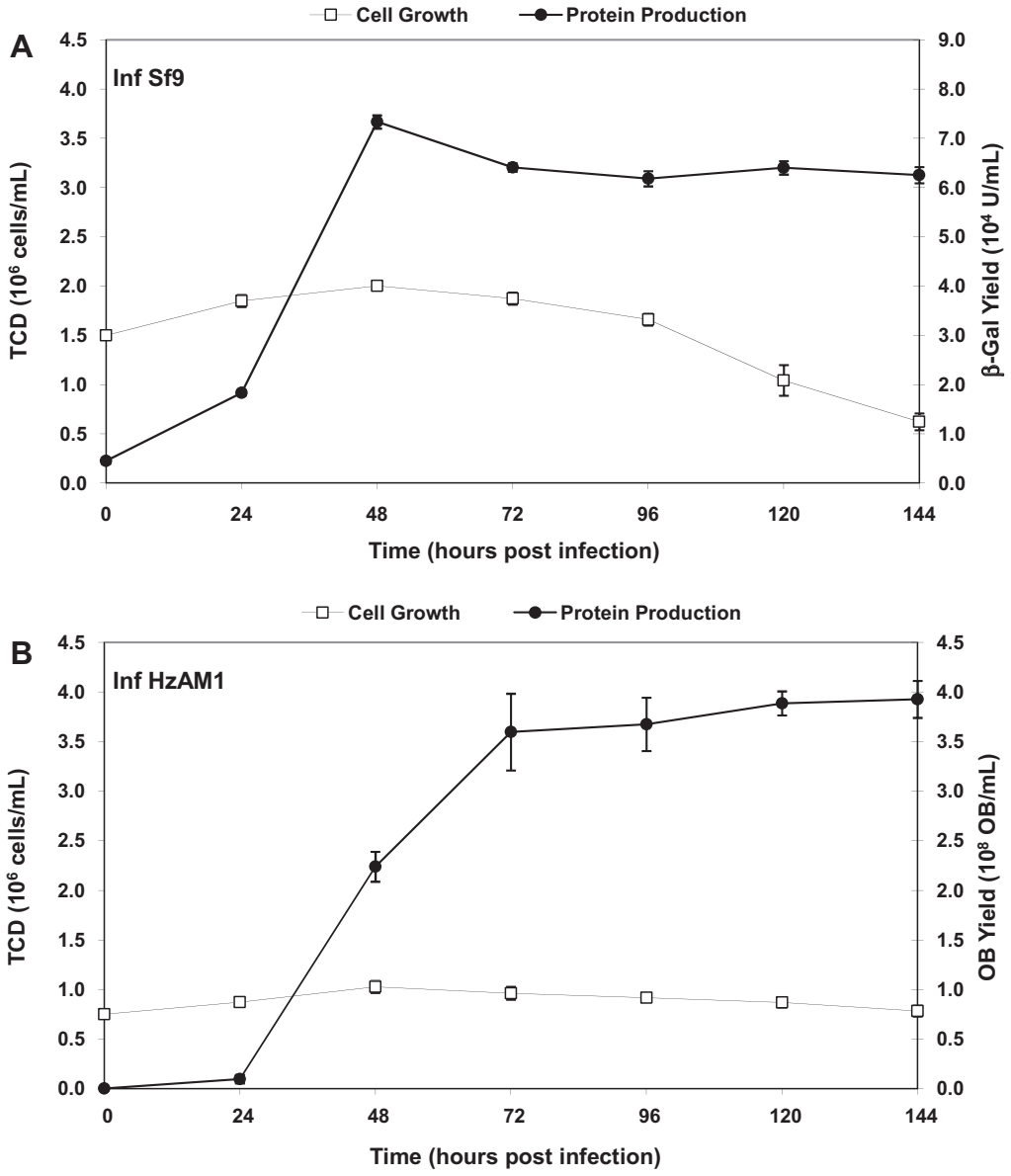

Fig. 2. Total cell density (TCD) and volumetric protein yield profiles over time for two baculovirus-infected insect cell systems used for intracellular metabolite analysis. (A) Sf9 cells infected with recombinant β-galactosidase-expressing AcMNPV at a TOI of 1.5×10^6 cells/mL and an MOI of 20 PFU/cell. (B) HzAM1 cells infected with occlusion body (OB) producing wild-type HaSNPV at a TOI of 0.75×10^6 cells/mL and an MOI of 17 PFU/cell. Error bars show the standard deviation of biological triplicates.

3.3. Washing optimization for intracellular metabolite analysis of the HzAM1–HaSNPV system

The cell growth and OB production temporal profiles of HaSNPV-infected HzAM1 cells are presented in Fig. 2B. The intracellular concentrations of selected metabolites in uninfected and HaSNPV-infected HzAM1 cells are shown in Fig. 3C and D respectively (AdoP), and in Fig. 4C and D respectively (amino acids), to illustrate the differences between the DE, Q0W, Q1W, Q2W and UQ cases. ATP and total AdoP recoveries (%) for a particular treatment were calculated with respect to the corresponding ATP and total AdoP levels in the DE case (Table 1).

The infected culture grew minimally from a TOI of 0.75×10^6 cells/mL to a PTCD of 1.0×10^6 cells/mL at 2 d.p.i., which could be considered to be synchronously-infected, and was consistent with the high MOI that was applied (17 PFU/cell) (Fig. 2B). The uninfected control doubled in cell density on a daily basis during the exponential growth phase, and reached a PTCD of 8.3×10^6 cells/mL (data not shown), indicating that the HzAM1 stock cells were in good condition. The OB production peaked at 72 h.p.i., which was consistent with the slower kinetics of HaSNPV infections when compared to AcMNPV infections [34]. A high maximum cell-specific yield of around 400 OB/cell was obtained [32]. Hence, the HzAM1–HaSNPV infections set up in this study were optimally-infected, and were suitable for metabolomic studies.

Analysis of the intracellular AdoP content of uninfected and infected HzAM1 cells (Fig. 3C and D) showed that quenching with ice-cold NaCl + P (Q0W) resulted in ATP recoveries of 95% and 85% respectively (Table 1). However, the difference in ATP levels between the Q0W and DE cases was not significant for both uninfected and infected HzAM1 cells ($P > 0.05$, one-way ANOVA, Tukey's HSD). Uninfected HzAM1 cells that have been washed once or twice with ice-cold NaCl + P post quenching (Q1W or Q2W) did not exhibit a significantly reduced ATP level compared to Q0W ($P > 0.05$), but only the Q1W case was not significantly reduced from the DE case ($P > 0.05$). For infected HzAM1 cells, both

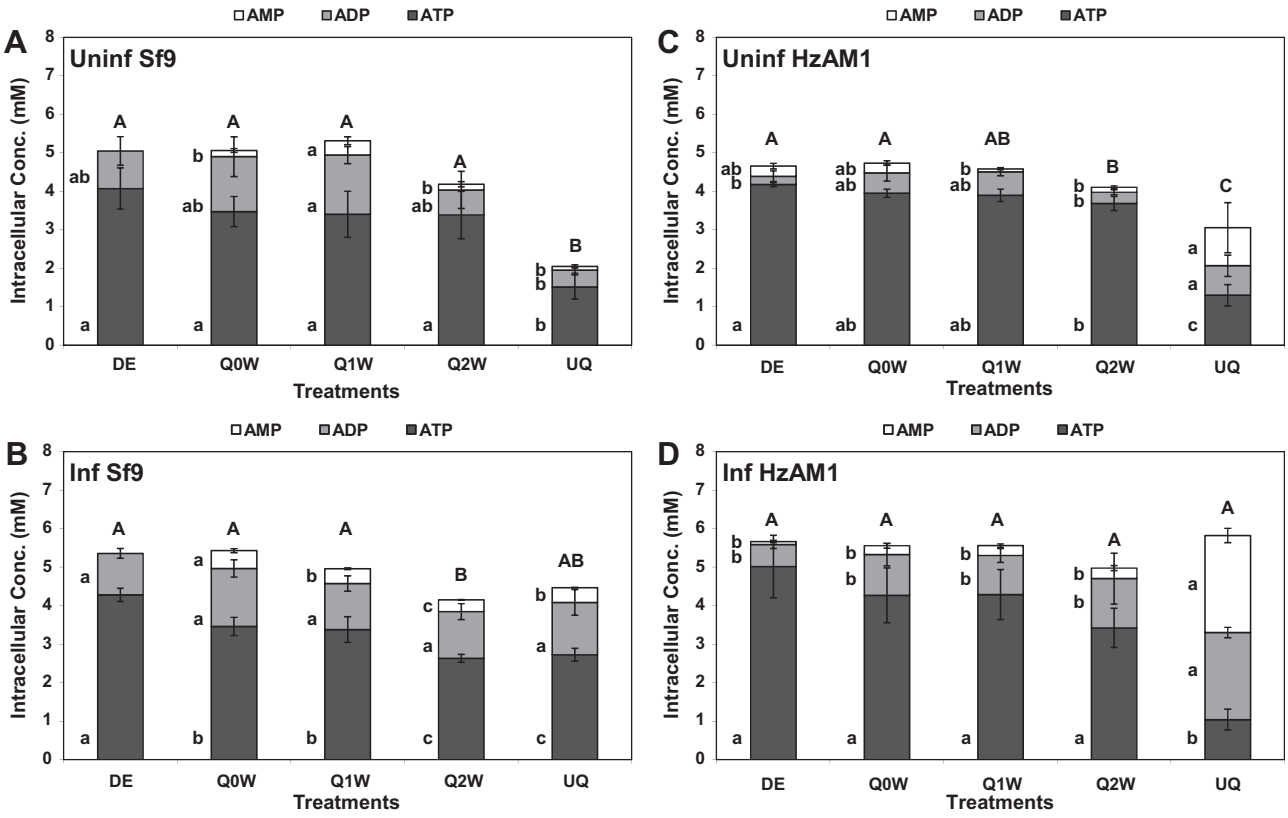

Fig. 3. Intracellular concentrations of ATP, ADP and AMP (adenosine phosphates, AdoP) from uninfected and baculovirus-infected insect cells, after being direct extracted (DE), quenched but not washed (Q0W), quenched and washed one or two times (Q1W, Q2W) and unquenched (UQ). Ice-cold NaCl + P (0.5–1 °C) was used for both quenching and washing, while room temperature NaCl + P was used for the UQ case. 100% acetonitrile (−40 °C) was used for direct extraction of cell cultures, while 50% v/v acetonitrile in deionized water (−40 °C) was used to extract quenched and unquenched cell pellets. (A) Uninfected Sf9 cells, sampled at 1×10^6 cells/mL. (B) Infected Sf9 cells, with rβ-Gal-AcMNPV at a TOI of 1.5×10^6 cells/mL and an MOI of 20 PFU/cell, sampled at 24 h.p.i. (C) Uninfected HzAM1 cells, sampled at 1×10^6 cells/mL. (D) Infected HzAM1 cells, with wtHaSNPV at a TOI of 0.75×10^6 cells/mL and an MOI of 17 PFU/cell, sampled at 24 h.p.i. Error bars show the standard deviation of biological triplicates. Tukey's HSD test ($\alpha = 0.05$) was used to compare the means from different treatments, for ATP, ADP, AMP and total AdoP concentrations separately. Means with the same letter indicate that they are not significantly different. Lower-case letters are used for ATP, ADP or AMP concentrations, while upper-case letters are used for total AdoP concentration.

the Q1W and Q2W cases did not exhibit significantly reduced ATP levels when compared to that of the Q0W or DE cases ($P > 0.05$). Uninfected and infected HzAM1 cells exhibited the lowest ATP recoveries (31% and 21%, respectively) when unquenched (UQ). For both uninfected and infected HzAM1 cells, neither ADP nor AMP levels were significantly different between the DE, Q0W, Q1W and Q2W cases ($P > 0.05$). The total intracellular AdoP (ATP, ADP and AMP) content of uninfected HzAM1 cells was not significantly different between the DE, Q0W and Q1W cases ($P > 0.05$), but declined significantly by 10% between Q1W and Q2W ($P < 0.05$). The total AdoP of infected HzAM1 cells was not significantly different between the DE, Q0W, Q1W and Q2W cases ($P > 0.05$). The total AdoP of unquenched HzAM1 cells was better retained when infected rather than when uninfected (103% and 65% of DE, respectively).

Intracellular amino acids analysis of uninfected and infected HzAM1 cells (Fig. 4C and D) illustrated that QS-derived Nva was present at a high level (13.1 and 14.3 mM respectively) for the quenched/unwashed case (Q0W). The intracellular Nva level declined dramatically (6- and 5-fold, respectively for uninfected and infected cases) when quenching was followed by 1 wash step (Q1W), but it did not decline further when a second wash step (Q2W) was conducted ($P > 0.05$, one-way ANOVA, Tukey's HSD). When a third wash step was implemented (Q3W), the Nva level declined significantly for uninfected HzAM1 cells ($P < 0.05$), but did not decline significantly for infected HzAM1 cells ($P > 0.05$). The intracellular levels of the standard amino acids also declined dramatically between the Q0W and Q1W cases, for both uninfected and infected HzAM1 cells (Fig. 4C and D). When additional wash steps (Q2W or Q3W) were implemented, further declines in intracellular amino acid levels were not significant for infected HzAM1 cells ($P > 0.05$). For uninfected HzAM1 cells, the majority of amino acids did not decline significantly between the Q1W and Q2W cases ($P > 0.05$) except for Lys ($P < 0.05$), while none of the amino acids declined significantly between the Q2W and Q3W cases ($P > 0.05$).

4. Discussion

4.1. Pluronic® F-68 supplementation improved the quenching and washing efficacy of ice-cold saline for uninfected Sf9 cells

As many metabolites such as nucleotides have rapid turnover rates [39], it is necessary to quench the cells upon sampling to terminate cellular metabolism and hence preserve the intracellular metabolite profiles at the instant of sampling. The ideal quenching protocol should meet this objective, as well as prevent the leakage of metabolites from the cells [40,41]. However, the development of quenching protocols can be challenging, especially for mammalian and insect cells which are more vulnerable to mechanical damage due to the absence of cell walls.

Buffered and non-buffered cold methanol solutions (60% v/v in water, −40 °C) have been used widely for quenching yeast and bacteria [15,39,42–46], but they have been reported to cause metabo-

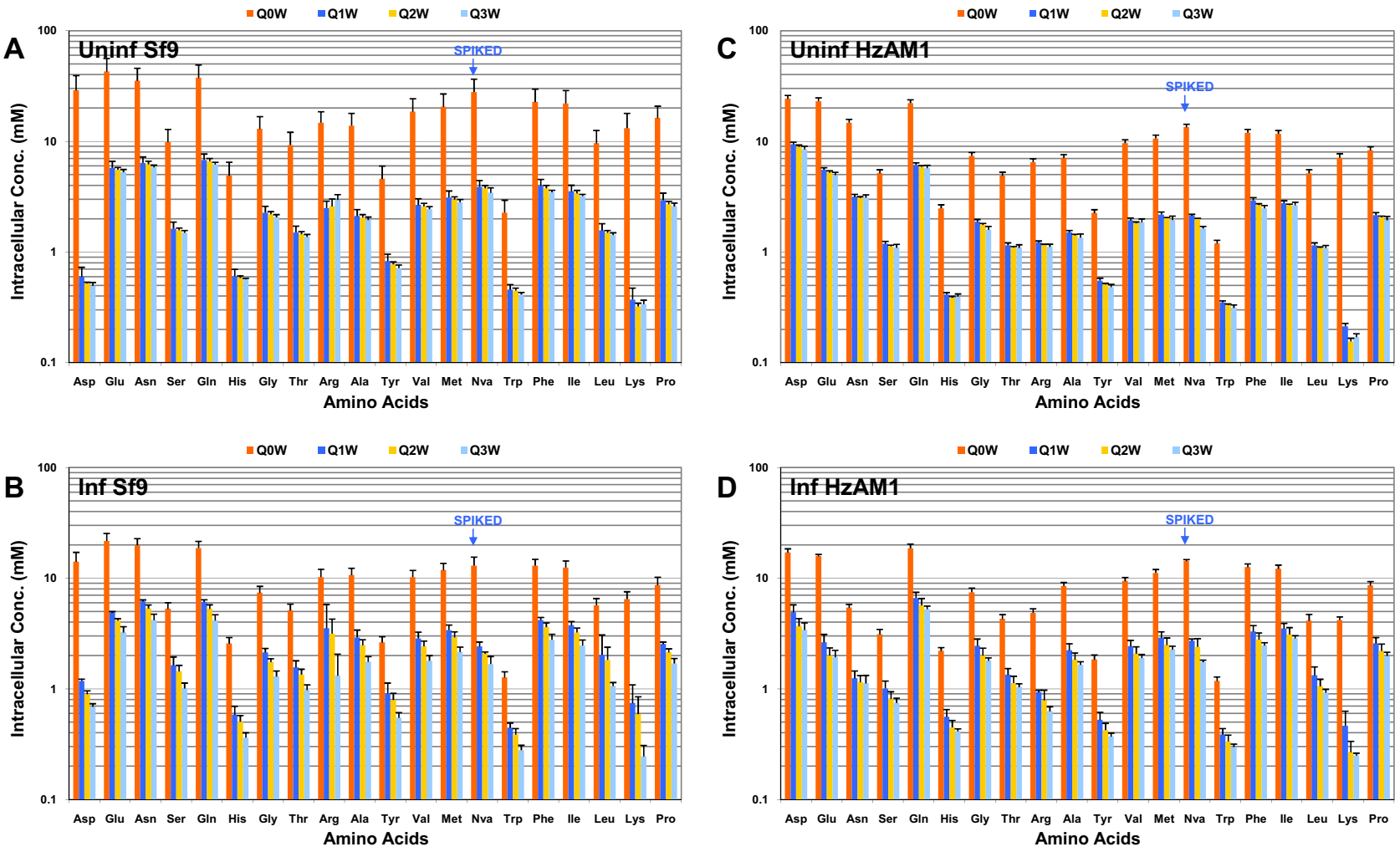

Fig. 4. Intracellular concentrations of amino acids from uninfected and baculovirus-infected insect cells after being quenched but not washed (Q0W), and quenched with one, two or three wash steps (Q1W, Q2W, Q3W), using ice-cold NaCl + P as the quenching solution (QS). Non-standard Norvaline (Nva) was spiked into the QS as a means of gauging washing efficiency. Ice-cold NaCl + P (0.5–1 °C) was used for both quenching and washing, and 50% v/v acetonitrile in deionized water (−40 °C) was used to extract the cell pellets. (A) Uninfected Sf9 cells, sampled at 1×10^6 cells/mL. (B) Infected Sf9 cells, with rβ-Gal-AcMNPV at a TOI of 1.5×10^6 cells/mL and an MOI of 20 PFU/cell, sampled at 24 h.p.i. (C) Uninfected HzAM1 cells, sampled at 1×10^6 cells/mL. (D) Infected HzAM1 cells, with wtHaSNPV at a TOI of 0.75×10^6 cells/mL and an MOI of 17 PFU/cell, sampled at 24 h.p.i. Error bars show the standard deviation of biological triplicates.

Table 1
Intracellular ATP and total adenosine phosphate (AdoP) levels in quenched but not washed (Q0W), quenched and washed one or two times (Q1W, Q2W) and unquenched (UQ) samples, expressed as a percentage of the levels in the corresponding direct extracted (DE) sample, from uninfected Sf9 and HzAM1 cells, and from rβ-Gal-AcMNPV-infected Sf9 and wtHaSNPV-infected HzAM1 cells. Ice-cold NaCl + P (0.5–1 °C) was used for both quenching and washing, while room temperature NaCl + P was used for the UQ case. One hundred percent acetonitrile (−40 °C) was used for direct extraction of cell cultures, while 50% v/v acetonitrile in deionized water (−40 °C) was used to extract quenched and unquenched cell pellets.

	AdoP recovery (% of direct extract, DE)							
	Q0W	Q1W	Q2W	UQ	Q0W	Q1W	Q2W	UQ
	Uninfected Sf9 cells				Uninfected HzAM1 cells			
ATP	85	84	83	37	95	93	88	31
Total AdoP	100	105	83	41	101	97	87	65
	Infected Sf9 cells				Infected HzAM1 cells			
ATP	81	79	61	64	85	85	69	21
Total AdoP	101	93	78	83	98	98	88	103

lite leakage from these cells [16,19,47]. The extent of intracellular metabolite leakage was worse when these QSs were used for mammalian cells [12,13]. Recently, Dietmair et al. demonstrated that ice-cold isotonic NaCl (0.9% w/v, 0.5 °C) was the most efficacious QS for Chinese Hamster Ovary (CHO) cells, which effectively minimized the conversion of intracellular ATP to ADP and AMP [12]. Since insect cells are similar physically to mammalian cells, a NaCl-based QS was anticipated to be just as effective for the former (using 1.1% w/v NaCl, which is isotonic for insect cells). However, this study showed that ice-cold NaCl (0.5–1 °C) was not outstanding for quenching uninfected Sf9 insect cells, since only about 80% of intracellular ATP was recovered after the quenching step with respect to direct extraction (DE), with a corresponding 10% decline in cell viability (Fig. 1A and B). In addition, ATP recovery and cell viability declined substantially when quenching was followed by cell pellet wash steps using the same QS, indicating that significant fluid-mechanical damage had occured (Fig. 1A and B). Cell damage was also observed in CHO cells that have been quenched and washed once in ice-cold NaCl [12]. In other studies, cell damage and metabolite leakage were reported for quenched/washed bacteria [48] and mammalian cells [13].

This outcome was disappointing, as cell pellet washing is essential for intracellular metabolite analysis of insect cells, which are grown in a complex medium containing an abundance of metabolites such as amino acids. Furthermore, if washing causes damage to uninfected insect cells, it would be even more damaging to baculovirus-infected insect cells, which have compromised cell membranes due to the lytic infection process. Hence, an alternative QS was required to minimize fluid-mechanical damage during the quenching and washing procedures. An obvious strategy involves the addition of a cell-protective agent such as Pluronic® F-68 (PF68) to the default NaCl-based QS. PF68 is a non-ionic surfactant that has been used for decades to enable animal cell cultures to be scaled-up in gas-sparged stirred-tank bioreactors [25,49–53], and is typically applied at a concentration of 0.1% v/v in insect cell cultures [54]. In this study, the alternative QS (NaCl + P) was supplemented with twice this level of PF68, which was found to be efficacious in the development of a high cell density fed-batch suspension culture process for HaSNPV biopesticides (personal communication, Leslie Chan). A second alternative QS (NaCl + P + S) was also tested, which contained 0.2% v/v PF68 as well as sucrose and the major basal salts of IPL-41 medium [54]. Preliminary studies showed that quenching with ice-cold Sf-900 II medium resulted in excellent ATP recoveries (99%) and preservation of high cell viabilities (data not reported). Hence, NaCl + P + S was formulated as a streamlined version of the commercial medium, with the rationale being that a balanced salts composition (optimal Na/K and Mg/Ca ratios) and the buffering of pH and osmolality (sucrose) could result in a better QS than one comprising only NaCl and PF68 (but this was found to be not the case).

At ice-cold temperatures, NaCl + P and NaCl + P + S were better than NaCl alone for quenching uninfected Sf9 cells, since the former two QSs supported statistically insignificant differences in ATP levels, and very similar cell viabilities, to those of the DE case (Fig. 1A and B). Most importantly, PF68 supplementation in the QS allowed high ATP recoveries and cell viabilities to be maintained when one or two cell pellet wash steps were implemented after quenching, while the unsupplemented default QS was clearly unsuccessful in this respect (Fig. 1A and B). The quenching and washing procedures involved multiple centrifugation and cell pellet resuspension steps, but since the latter was performed by gentle tube inversion the shear stresses encountered by cells were mainly from the centrifugal forces [55]. The ability of PF68 to protect animal cells from fluid-mechanical damage may derive from a fast-acting biological mechanism involving direct interaction between the surfactant molecules and the cell plasma membrane, resulting in a more rigid and shear-resistant membrane [52,56]. The cell-protective effect of PF68 was not cold temperature-dependent, as Sf9 cells processed with NaCl + P or NaCl + P + S solutions at room temperature (UQ case) also exhibited high cell viabilities (Fig. 1B). However, the efficacy of a QS is assessed by both the ability to terminate cellular metabolism and to prevent cell damage/metabolite leakage (i.e. maintain high cell viabilities), and ice-cold temperatures were clearly required to achieve both outcomes.

4.2. Optimizing the number of wash steps for intracellular metabolite analysis of uninfected and baculovirus-infected Sf9 and HzAM1 cells

Having established that ice-cold NaCl + P was an effective quenching/washing solution for uninfected Sf9 cells, in terms of preserving the intracellular content of a highly-labile metabolite (ATP), it was necessary to determine whether it was equally efficacious in this capacity for AcMNPV-infected Sf9 cells and for another insect cell–baculovirus system (HzAM1–HaSNPV). As discussed previously, cell pellet washing post quenching is not an optional step for insect cells grown in a metabolites-rich medium, yet excessive washing is likely to damage fragile plasma membranes and result in metabolite leakage. Hence this phase of the study was designed to determine an optimal number of wash steps that will remove most of the medium-derived metabolites from the intracellular fraction without compromising cell integrity (for medium-prominent metabolites represented by amino acids), while maintaining good preservation of the more labile intracellular metabolites (represented by nucleotides), for the two insect cell–baculovirus systems. Nucleotides were represented by adenosine phosphates (AdoPs) due to their rapid turnover rates, in particular ATP (1.5 mM/s) and ADP (2 mM/s) [12,39].

4.2.1. Nucleotides

For uninfected cultures, the recovery of ATP with respect to direct extraction from Sf9 (85%) or HzAM1 (95%) cells after quenching (Q0W) was similar to that obtained by Dietmair et al. for CHO cells (89%) [12], albeit such declines were not statistically significant (Fig. 3A and C, Table 1). Most importantly, ATP levels did not decline significantly when quenching was followed by one or two wash steps with ice-cold NaCl + P (Q1W or Q2W), for both types of uninfected insect cells. This outcome was not achieved in the previous CHO cell study [12], which used an unsupplemented ice-cold NaCl solution for quenching and washing steps. Furthermore, ADP or total AdoP levels were largely not significantly different between the DE, Q0W, Q1W and Q2W cases, which suggested that nucleotide degradation and cell leakage had been minimal.

Among the two types of infected insect cells, infected HzAM1 cells were best able to tolerate quenching and washing procedures, exhibiting insignificant differences in AdoP (ATP, ADP and total AdoP) levels between the DE, Q0W, Q1W and Q2W cases (Fig. 3D). In contrast, infected Sf9 cells were more vulnerable to such procedures, exhibiting significant (but moderate) declines in ATP content between the DE and Q0W cases, and between the Q1W and Q2W cases (Fig. 3B), although total AdoP and ADP levels were not changed significantly (up to 1 and 2 wash steps respectively).

AMP levels after quenching/washing steps were quite different between the two cell lines, being insignificantly changed for uninfected and infected HzAM1 cells, and significantly changed for uninfected and infected Sf9 cells (Fig. 3). For uninfected Sf9 cells, ATP, ADP or total AdoP levels were unchanged statistically up to 2 wash steps, hence it follows that the corresponding AMP levels should also be unchanged for the mass balance to close. However, AMP levels were the lowest measured among the AdoPs, hence they would be most affected by experimental error and the possibility of a 'false positive' significance difference test. For infected Sf9 cells, ATP levels declined significantly while ADP and total AdoP levels did not (up to 1 wash step), hence there appeared to be a significant net conversion of some ATP to AMP for the Q0W or Q1W cases, demonstrating that it was more challenging to preserve metabolite levels in infected Sf9 cells.

Baculovirus infection being a cell-lytic process, it would not be surprising if infected insect cells are shown to be more sensitive to quenching/washing procedures and the ensuing mechanical damage, than uninfected cells. In this study, AcMNPV-infected Sf9 cells were more sensitive than uninfected Sf9 cells, but they were also more vulnerable than HaSNPV-infected HzAM1 cells. This could be related to the much faster infection kinetics of AcMNPV (e.g. 18-fold higher binding rate and 50-fold higher budding rate), in comparison to those of HaSNPV [34], which would lead to a more advanced infection at 24 h.p.i and potentially more compromised plasma membranes. It remains to be seen whether an earlier sampling time post-infection would result in better ATP recoveries for infected Sf9 cells.

It was interesting to observe that total AdoP levels were variable for unquenched samples (treated with room temperature QS), ranging from low in uninfected Sf9 cells to high in infected HzAM1 cells, when compared to DE samples (Fig. 3). When the uninfected Sf9 cell experiment was repeated on a separate occasion, the total AdoP level of the unquenched sample was this time very close to the DE case, while those of quenched/washed samples were found to be similar to previous levels (data not reported), further demonstrating that total AdoP recoveries were variable for unquenched insect cells. The expectation was that total AdoP levels would be conserved, since high viabilities were maintained in unquenched cells, but reduced levels could be the result of ATP efflux from cells [57,58] or the degradation of AdoP into IMP, nucleosides and bases [59,60], due to continuing metabolic activity at room temperature under conditions of stress like oxygen limitation (hypoxia) and fluid-mechanical shear [57,61]. Such conditions were likely to be present during the centrifugation step prior to cell pellet extraction, and could be the source of the variability observed in unquenched samples.

This study has confirmed that ice-cold NaCl + P was largely effective in minimizing the degradation of highly-labile metabolites such as ATP and ADP, as well as minimizing cell leakage due to mechanical damage (from PF68 supplementation), during quenching and washing of uninfected and infected insect cells. However, substantial leakage (or further degradation) may occur after the second wash step (particularly for infected Sf9 cells), hence quenching followed by one wash step is the most prudent protocol going forward.

4.2.2. Amino Acids

This study has shown that the measured intracellular amino acids content would be largely free from medium-derived amino acids contamination after just one wash step post quenching with ice-cold NaCl + P, for both uninfected and infected (at 24 h.p.i.) insect cells (Sf9 and HzAM1). This finding was indicated by the steep declines in the intracellular concentration of 19 standard amino acids (and the spiked non-standard Nva) between the Q0W and Q1W cases, followed by largely insignificant declines upon one (Q2W) or two (Q3W) additional wash steps (Fig. 4). The exception was infected Sf9 cells, which experienced significant declines for many amino acids after the second wash step, but these were minor when compared to those between Q0W and Q1W. The increased sensitivity of infected Sf9 cells to quenching/washing procedures may be attributed to the faster kinetics of AcMNPV infections, as discussed previously in Section 4.2.1. In general, the minor decline (if any) in amino acids content after the second and third successive wash steps also indicated that cell integrity was largely intact, which again confirmed that PF68 was efficacious in protecting both uninfected and infected insect cells from serious mechanical damage during multiple centrifugation and pellet resuspension steps.

4.2.3. Effect of PF68 on HPLC analysis

Although PF68 supplementation of the QS was largely successful in protecting insect cells during quenching and washing procedures, resulting in the preservation of high cell viabilities and reduction in metabolite leakage, it may be argued that PF68 residues in the intracellular extract could interfere with HPLC analysis. To address this concern, 11 nucleotides and 20 amino acids (standards) were analyzed separately using HPLC, with and without the presence of 0.1% PF68 (data not shown). This level of PF68 is the estimated residual concentration in the freeze-dried cell extracts of Q0W, Q1W, Q2W and Q3W samples after resuspension with water. One-way ANOVA demonstrated that there were insignificant differences between the negative and positive PF68 cases, for the analysis of nucleotides ($P = 0.051$) and amino acids ($P = 0.503$). Hence, it appeared that the presence of a small amount of PF68 in the cell extracts would not be detrimental to metabolites analysis.

4.2.4. Intracellular ATP levels of uninfected and infected insect cells, and comparison with other cell types

Uninfected HzAM1 cells were around 70% larger than uninfected Sf9 cells (approximately 3200 and 1900 μm^3 respectively), while infected HzAM1 and Sf9 cells were around 30% larger than their uninfected counterparts (approximately 4300 and 2500 μm^3 respectively). The sizes of uninfected and infected insect cells appeared to be positively-correlated with their specific intracellular ATP yields (fmol/cell), as illustrated in Table 2. In particular, uninfected HzAM1 cells exhibited around 80% more ATP/cell than uninfected Sf9 cells, while infected HzAM1 and Sf9 cells exhibited around 30–50% more ATP/cell than their uninfected counterparts. The increased specific ATP yield of insect cells upon infection was also observed previously [62], and corresponded with a previous positive correlation between insect cell size and recombinant protein production capacity [63].

When the intracellular ATP content was expressed as a volumetric yield in terms of the cell volume (mM), the differences between HzAM1 and Sf9 cells, and between uninfected and infected cells, became much less pronounced. In fact, the volumetric ATP yield of all insect cell treatments were around 4–5 mM (DE case, Table 2). Interestingly, the volumetric ATP levels of insect cells were similar to those reported for mammalian cells (CHO, rat hepatocyte) and bacteria (*Lactobacillus*, *Eschericia coli*) (Table 2), which suggested a universality in energy metabolism on a per biomass basis.

Table 2
Comparison of intracellular ATP concentrations in insect, mammalian and microbial cells, in direct extracted (DE) and quenched-unwashed (Q0W) samples.

Cell type		DE (mM)	DE (fmol/cell)	Q0W (mM)	Q0W (fmol/cell)	Reference
Insect	Sf9 (Uninf)	4.1	7.7	3.5	6.6	This study
	Sf9 (Inf)	4.3	11.0	3.5	8.8	"
	HzAM1 (Uninf)	4.2	13.6	4.0	12.2	"
	HzAM1 (Inf)	5.0	20.8	4.3	18.1	"
Mammalian	CHO	–	4.6	–	4.1	[12]
	CHO	–	–	7.14	–	[13]
	MDCK	–	7.06	–	–	[11]
	MDCK	–	–	–	13–25	[65]
	Vero	–	4.49	–	–	[11]
	Vero	–	–	–	1.7–6.3	[66]
	Vero	–	–	–	9.6–17.8	[22]
	Rat hepatocyte	4.5	–	–	–	[67]
	Rat hepatocyte	–	–	5.08	–	[68]
Bacteria	*Lactobacillus*	5.9/4.8	–	–	–	[44]
	E. coli	–	–	4.27	–	[69]

This notion is supported by a previous study by Beis et al., who reported ATP/biomass levels in the snap-frozen muscle tissues of a variety of invertebrates and vertebrates, including insects (5–9 μmol/g, equivalent to mM), mammals (4–6 μmol/g) and birds (6–8 μmol/g) [64].

4.3. Conclusions

Insect cells are similar to mammalian cells in terms of fragility during processing for intracellular metabolite analysis, but would be even more challenging to process when subjected to baculovirus infection (a cell-lytic process). Although ice-cold saline is an ideal quenching solution for CHO cells [12], it was found to be inadequate for insect cells in this study. However, addition of the cell-protectant PF68 to ice-cold saline resulted in a successful quenching solution for both uninfected and infected Sf9 and HzAM1 insect cells, and furthermore permitted wash steps to be carried out post quenching with minimal impact on cell integrity and metabolites retention. Wash steps are important when processing insect cells, since they are usually grown in media containing high concentrations of metabolites, which have to be removed from the intracellular fraction. This study has shown that quenching following by one wash step was the ideal procedure for removing medium-derived metabolites (represented by amino acids) and for preserving the levels of labile metabolites (represented by adenosine phosphates), for both uninfected and 24 h-infected Sf9 and HzAM1 cells (using AcMNPV and HaSNPV, respectively). Having developed a suitable protocol for intracellular metabolite analysis of insect cells, future studies will be focused on more comprehensive metabolome profiling of baculovirus-infected Sf9 and HzAM1 cells, particularly via time-course studies and metabolic flux analysis, to provide insights into the mechanisms that cause lower yields of recombinant protein and occlusion body when infections are carried out at high cell densities.

Acknowledgements

The authors wish to acknowledge financial support from the Australian Research Council and a UQ Vietnam-Australia 35 Year Commemorative Research Higher Degree scholarship. The authors are grateful to Michael Wang from Metabolomics Australia (UQ-node) for his invaluable assistance in the HPLC analysis.

References

[1] D.L. Jarvis, in: R.R. Burgess, M.P. Deutscher (Eds.), Methods in Enzymology, Vol. 463, Academic Press, Burlington, 2009, pp. 191–222.
[2] T.A. Kost, J.P. Condreay, D.L. Jarvis, Nat. Biotechnol. 23 (2005) 567–575.
[3] J.A. Mena, A.A. Kamen, Expert Rev. Vaccines 10 (2011) 1063–1081.
[4] M.G. Aucoin, J.A. Mena, A.A. Kamen, Curr. Gene Ther. 10 (2010) 174–186.
[5] F. Moscardi, M.L. de Souza, M.E.B. de Castro, M.L. Moscardi, B. Szewczyk, in: I. Ahmad, F. Ahmad, J. Pitchtel (Eds.), Microbes and Microbial Technology: Agricultural and Environmental Applications, Springer, New York, 2011, pp. 415–445.
[6] B. Szewczyk, L. Rabalski, E. Krol, W. Sihler, M.L.d. Souza, J. Biopesticides 2 (2009) 209–216.
[7] C.B. Elias, A. Zeiser, C. Bedard, A.A. Kamen, Biotechnol. Bioeng. 68 (2000) 381–388.
[8] M. Cuperlovic-Culf, D.A. Barnett, A.S. Culf, I. Chute, Drug Discov. Today 15 (2010) 610–621.
[9] N. Jamshidi, B.O. Palsson, Mol. Syst. Biol. 4 (2008) 171.
[10] M. Oldiges, S. Lutz, S. Pflug, K. Schroer, N. Stein, C. Wiendahl, Appl. Microbiol. Biot. 76 (2007) 495–511.
[11] J.B. Ritter, Y. Genzel, U. Reichl, Anal. Biochem. 373 (2008) 349–369.
[12] S. Dietmair, N.E. Timmins, P.P. Gray, L.K. Nielsen, J.O. Kromer, Anal. Biochem. 404 (2010) 155–164.
[13] C.A. Sellick, R. Hansen, A.R. Maqsood, W.B. Dunn, G.M. Stephens, R. Goodacre, A.J. Dickson, Anal. Chem. 81 (2009) 174–183.
[14] J.I. Castrillo, A. Hayes, S. Mohammed, S.J. Gaskell, S.G. Oliver, Phytochemistry 62 (2003) 929–937.
[15] M.O. Loret, L. Pedersen, J. Francois, Yeast 24 (2007) 47–60.
[16] S.G. Villas-Boas, J. Hojer-Pedersen, M. Akesson, J. Smedsgaard, J. Nielsen, Yeast 22 (2005) 1155–1169.
[17] B.U. Jaki, S.G. Franzblau, S.H. Cho, G.F. Pauli, J. Pharmaceut. Biomed. 41 (2006) 196–200.
[18] C.L. Winder, W.B. Dunn, S. Schuler, D. Broadhurst, R. Jarvis, G.M. Stephens, R. Goodacre, Anal. Chem. 80 (2008) 2939–2948.
[19] C. Wittmann, J.O. Kromer, P. Kiefer, T. Binz, E. Heinzle, Anal. Biochem. 327 (2004) 135–139.
[20] X.H. Wu, H.L. Yu, Z.Y. Ba, J.Y. Chen, H.G. Sun, B.Z. Han, Biotechnol. J. 5 (2010) 75–84.
[21] C.A. Sellick, D. Knight, A.S. Croxford, A.R. Maqsood, G.M. Stephens, R. Goodacre, A.J. Dickson, Metabolomics 6 (2010) 427–438.
[22] M.K. Grob, K. O'Brien, J.J. Chu, D.D.Y. Chen, J. Chromatogr. B 788 (2003) 103–111.
[23] L.A. King, R.D. Possee, The Baculovirus Expression System: A Laboratory Guide, Chapman & Hall, London, 1992.
[24] J. Wu, G. King, A.J. Daugulis, P. Faulkner, D.H. Bone, M.F.A. Goosen, Appl. Microbiol. Biot. 32 (1989) 249–255.
[25] D.W. Murhammer, C.F. Goochee, Nat. Biotechnol. 6 (1988) 1411–1418.
[26] R. Haas, L.K. Nielsen, Biotechnol. Bioeng. 91 (2005) 768–772.
[27] S. Reid, L.H.L. Lua, Method of producing baculovirus, Patent Cooperation Treaty (PCT) International Publication Number WO/2005/045014, 2005.
[28] L.K. Nielsen, G.K. Smyth, P.F. Greenfield, Biotechnol. Progr. 7 (1991) 560–563.
[29] L.K. Nielsen, G.K. Smyth, P.F. Greenfield, Cytotechnology 8 (1992) 231–236.
[30] L.J. Reed, H. Muench, Am. J. Hyg. 27 (1938) 493–497.
[31] L.C.L. Chan, P.F. Greenfield, S. Reid, Biotechnol. Bioeng. 59 (1998) 178–188.
[32] Q. Nguyen, Y.M. Qi, Y. Wu, L.C.L. Chan, L.K. Nielsen, S. Reid, J. Virol. Methods 175 (2011) 197–205.
[33] J.F. Power, S. Reid, K.M. Radford, P.F. Greenfield, L.K. Nielsen, Biotechnol. Bioeng. 44 (1994) 710–719.
[34] M.R.S. Pedrini, S. Reid, L. Nielsen, L.C.L. Chan, Biotechnol. Progr. 27 (2011) 614–624.
[35] L.H.L. Lua, M.R.S. Pedrini, S. Reid, A. Robertson, D.E. Tribe, J. Gen. Virol. 83 (2002) 945–955.
[36] J. Zhang, N. Kalogerakis, L.A. Behie, J. Biotechnol. 33 (1994) 249–258.
[37] S.G. Villas-Boas, S. Mas, M. Akesson, J. Smedsgaard, J. Nielsen, Mass Spectrom. Rev. 24 (2005) 613–646.
[38] E.V. Sycheva, T.A. Yampol'skaya, E.S. Preobrajenskaya, A.E. Novikova, N.G. Matrosov, N.V. Stoynova, Microbiology 76 (2007) 712–718.

[39] W. Dekoning, K. Vandam, Biochemistry 204 (1992) 118–123.
[40] B. Alvarez-Sanchez, F. Priego-Capote, M.D. Luque de Castro, TrAC-Trend. Anal. Chem. 29 (2010) 120–127.
[41] M.R. Mashego, K. Rumbold, M. De Mey, E. Vandamme, W. Soetaert, J.J. Heijnen, Biotechnol. Lett. 29 (2007) 1–16.
[42] C.J. Bolten, C. Wittmann, Biotechnol. Lett. 30 (2008) 1993–2000.
[43] A.B. Canelas, C. Ras, A. ten Pierick, J.C. van Dam, J.J. Heijnen, W.M. van Gulik, Metabolomics 4 (2008) 226–239.
[44] M. Faijes, A.E. Mars, E.J. Smid, Microb. Cell Fact. 6 (2007) 88–99.
[45] B. Gonzalez, J. Francois, M. Renaud, Yeast 13 (1997) 1347–1355.
[46] M.A. Hans, E. Heinzle, C. Wittmann, Appl. Microbiol. Biot. 56 (2001) 776–779.
[47] C.J. Bolten, P. Kiefer, F. Letisse, J.C. Portais, C. Wittmann, Anal. Chem. 79 (2007) 3843–3849.
[48] J. Plassmeier, A. Barsch, M. Persicke, K. Niehaus, J. Kalinowski, J. Biotechnol. 130 (2007) 354–363.
[49] M.-F. Clincke, E. Guedon, F.T. Yen, V. Ogier, O. Roitel, J.-L. Goergen, Biotechnol. Progr. 27 (2010) 181–190.
[50] S. Goldblum, Y.K. Bae, W.F. Hink, J. Chalmers, Biotechnol. Progr. 6 (1990) 383–390.
[51] J.D. Michaels, J.F. Petersen, L.V. McIntire, E.T. Papoutsakis, Biotechnol. Bioeng. 38 (1991) 169–180.
[52] L.A. Palomares, M. Gonzalez, O.T. Ramirez, Enzyme Microb. Tech. 26 (2000) 324–331.
[53] Z. Zhang, M. Al-Rubeai, C.R. Thomas, Enzyme Microb. Tech. 14 (1992) 980–983.
[54] E.J. Schlaeger, Cytotechnology 20 (1996) 57–70.
[55] B.J. Kim, D.J. Oh, H.N. Chang, Biotechnol. Progr. 24 (2008) 166–174.
[56] J.Y. Wu, A.J. Daugulis, P. Faulkner, M.F.A. Goosen, Biotechnol. Progr. 11 (1995) 127–132.
[57] R. Beigi, E. Kobatake, M. Aizawa, G.R. Dubyak, Am. J. Physiol.-Cell Ph. 276 (1999) C267–C278.
[58] I.H. Chaudry, Yale J. Biol. Med. 55 (1982) 1–10.
[59] S.S. Matsumoto, K.O. Raivio, J.E. Seegmiller, J. Biol. Chem. 254 (1979) 8956–8962.
[60] B. Wagenknecht, M. Lieberman, Mol. Cell. Biochem. 107 (1991) 119–125.
[61] G.R. Dubyak, C. Elmoatassim, Am. J. Physiol. 265 (1993) C577–C606.
[62] A.M. Olejnik, K. Czaczyk, R. Marecik, W. Grajek, T. Jankowski, Appl. Microbiol. Biot. 65 (2004) 18–24.
[63] L.A. Palomares, J.C. Pedroza, O.T. Ramirez, Biotechnol. Lett. 23 (2001) 359–364.
[64] I. Beis, E.A. Newsholme, Biochem. J. 152 (1975) 23–32.
[65] R.W. Nash, B.S. McKay, J.M. Burke, Invest. Ophth. Vis. Sci. 35 (1994) 2850–2856.
[66] A. Burgener, K. Coombs, M. Butler, Biotechnol. Bioeng. 94 (2006) 667–679.
[67] F. Bontemps, M.F. Vincent, G. Vandenberghe, Biochem. J. 290 (1993) 671–677.
[68] L. Hue, Biochem. J. 206 (1982) 359–365.
[69] C. Chassagnole, N. Noisommit-Rizzi, J.W. Schmid, K. Mauch, M. Reuss, Biotechnol. Bioeng. 79 (2002) 53–73.

Chapter 4

Metabolic study of the cell density effect - Sf9/rAcMNPV in Sf900™III medium

4.1 Introduction

There is an ongoing interest in using the baculovirus insect cell expression system as a research tool for producing recombinant proteins (Kost et al., 2005; Mena and Kamen, 2011), human and veterinary vaccines (Mena and Kamen, 2011; van Oers, 2006), and as vectors for gene delivery (Hitchman et al., 2010; Hu, 2008). Moreover, the system is also of interest for the production of baculoviruses as biological control agents for agricultural insect pests, for use as part of integrated pest management programs (Moscardi et al., 2011; Szewczyk et al., 2006; Szewczyk et al., 2009).

To be commercially successful, baculovirus insect cell bioprocesses need to be optimized to deliver higher protein yields, and this normally involves a high cell density production process using fed-batch cultures in stirred-tank bioreactors (Elias et al., 2000). However, it has been well documented that there is a drop in cell specific yield when cells are infected at high cell densities, a phenomenon known as “the cell density effect” (Carinhas et al., 2009; Caron et al., 1990; Chakraborty et al., 1996; Chan et al., 2002; Doverskog et al., 2000; Huynh et al., 2013; Radford et al., 1997; Taticek and Shuler, 1997; Wong et al., 1996). There has been much speculation as to the cause of the cell density effect, including nutrient limitation, toxic compound accumulation as well as cell-to-cell contact inhibition but the reasons for this effect remain unidentified (Doverskog et al., 1997; Taticek and Shuler, 1997).

It has been suggested that the cause of the drop in productivity at high cell densities for baculovirus infection processes is related to nutrient limitations rather than accumulation of toxins (Drews et al., 1995; Radford et al., 1997; Wong et al., 1996). This is supported by the fact that there is an increase in the cell specific yield with an improvement of the nutrient supply through fed-batch strategies (Chan et al., 1998; Elias et al., 2000; Jardin et al., 2007). However, the process limitation for the cell density effect may not be entirely related to nutrient supply, but could be complex involving interactions between the virus infection process, cellular physiology and physico-chemical environmental effects. The reduction in recombinant protein production has been shown to be strongly correlated with limitations in the upstream processes of virus replication and transcription (Huynh et al., 2013). Other possible factors causing low productivity in high density cultures have been suggested, including oxygen limitations (Lecina et al., 2006; Palomares et al., 2004; Taticek and Shuler, 1997), the cell cycle phase at the time of infection (Calles et al., 2006; Doverskog et al., 2000) and the history of the culture (Doverskog et al., 2000).

Many attempts have been made to identify the cause of the cell density effect and to overcome this bottleneck. These include the measurement of extracellular metabolites to identify the limiting nutrients in the medium (Caron et al., 1990; Drews et al., 1995; Reuveny et al., 1993); the measurement of consumption rates and fluxomics analysis (Bernal et al., 2009); and supplementing culture media with glucose, glutamine, complex nutrient mixtures, and key intermediate metabolites (Carinhas et al., 2010; Reuveny et al., 1993). However, a possible limitation of these approaches is that the metabolite levels in the media do not necessarily reflect intracellular metabolite levels. The metabolite environment inside the cells at low and high cell densities at the time of infection may reveal the cause of the cell density effect. In particular intracellular metabolite measurements in combination with consumption rates of key metabolites may identify limitations during high cell density infections. It is possible, for example, that poor transport of key metabolites into cells at high cell densities or post-infection contribute to the cell density effect, rather than a limitation of metabolites in the medium.

It is important to note that a number of metabolism-based studies of infected insect cells have been conducted under optimal infection conditions, (i.e. infections performed at relatively low cell densities of 1-2×10^6 cells/mL). In this study, the drop in cell specific yield at a high cell density at the time of infection has been investigated using a metabolomics approach. Substrate consumption rates as well as intracellular metabolite levels of infected cells at both low and high cell densities at the time of infection have been measured and compared between these two infection conditions.

4.2 Materials and methods

4.2.1 Cell line, virus stock and medium

The *Spodoptera frugiperda* clone 9 cell line (Sf9; ATCC CRL 1711) and a recombinant *Autographa californica* multiple nucleopolyhedrovirus (rAcMNPV) expressing *E. coli* LacZ gene under the control of the polyhedrin promoter used in this study have been described previously (Chan et al., 1998; Wong et al., 1996). Working stock cells were maintained by regular passaging every 3-4 days in single-use shaker flasks (Corning, Lowell, MA) at seeding densities of 0.3-0.5×10^6 cells/mL. The shaker cultures were agitated at 120 rpm on an orbital shaker platform (Thermoline, NSW, Australia) and incubated at 28^{o}C in a refrigerated incubator (Thermoline). The preparation of virus stock has been previously described (Huynh et al., 2013; Tran et al., 2012). Virus stocks were stored at 4^{o}C, and were titered prior to use. The titers of virus stocks were 1-1.5×10^9

PFU/mL as determined by using a modified endpoint dilution method (Nielsen et al., 1992). The Sf900™III serum free medium (Gibco, Life Technologies, USA) was used in all experiments.

4.2.2. Experimental procedures

Two experiments were conducted to evaluate the extraction protocol post-infection and to investigate the difference between low and high infection cell densities (ICDs) in terms of intracellular metabolite concentrations, substrate consumption and protein production rates.

The first experiment involved evaluation of the extraction protocol for intracellular metabolites (Tran et al., 2012) for infected Sf9 cells via a time-course infection experiment. This experiment aimed to identify the latest time point post-infection at which the infected cells still maintain their membrane integrity during quenching and washing procedures. Sf9 cells were setup at the initial cell density of 0.5×10^6 cells/mL and allowed to grow for 2 doubling times (2 days) and then infected at an ICD of approximately 2.5×10^6 cells/mL and a multiplicity of infection (MOI) of 10 PFU/cell. Infection was conducted in a 1 L bottle and then aliquoted into various shaker flasks at 20 mL each for intracellular metabolite extractions at 12 hour intervals from 0-72 hours post-infection (hpi). Three shaker flasks were set up at 35 mL each as the infected control for measuring total cell density (TCD) and viability, β-Gal yield, viral DNA (vDNA) copies and extracellular metabolite measurements at the various time points mentioned above. The uninfected control (in triplicate) was set up and allowed to grow to a peak cell density of $1.8\text{-}2\times10^7$ cells/mL demonstrating the cells were in optimal condition during the experimental period.

The second experiment investigated the changes in the intra- and extra-cellular metabolome as well as the β-Gal production and metabolite consumption rates of the cells infected at low and high cell densities. The initial seeding cell density was at 0.5×10^6 cells/mL. For the low cell density infection, cells were infected at the ICD of 2×10^6 cells/mL (48 hours post-inoculation). For the high cell density infection, cells were allowed to grow to 6×10^6 cells/mL (84 hours post-inoculation) at the time of infection. All of the infections were conducted at an MOI of 10 PFU/cell (0.02 and 0.06 mL of virus stock was added into 1 mL of culture for low and high ICDs, respectively). The experiment was conducted in shaker flasks with biological triplicates at each cell density. Samples for intracellular metabolite analysis were taken at 12 hour intervals from 0-48 hpi in triplicate. Samples for extracellular metabolite analysis and for measuring TCD, viability, intracellular vDNA

copies and β-Gal yield were collected from 3 infected control shakers at 12 hour intervals from 0-72 hpi. An uninfected control was also set up and left to grow to a peak cell density in batch culture (1.8-2×10^7 cells/mL).

4.2.3 Intracellular metabolite extraction

Intracellular metabolites were extracted using the optimized protocol as described previously (Tran et al., 2012). Briefly, infected cultures were set up in 125 mL shaker flasks at a working volume of 20 mL, involving three flasks for each treatment at each time point as biological triplicates. Quenching solution (QS) (1.1% NaCl, 0.2% Pluronic F68) was prepared in 250 ml shaker flasks at 80 mL each and placed in an ice bath to ensure the temperature of the quenching solution was 0.5 to 1ºC. Taking out each flask at a time from the incubator, the culture of each flask (20 mL) was quickly poured into 80 mL of ice-cold QS. The quenched culture was then centrifuged (1000× g, 1 min) at 0ºC. The supernatant was removed and the cell pellet was washed with the sample volume of ice-cold QS. Another centrifugation step was applied (1000× g, 1 min, 0ºC) to collect the cell pellet which was then extracted with a cold 50% acetonitrile (ACN) solution at the ratio of 1 mL for 2×10^6 cells. The cell extracts were clarified by centrifugation (5000×g, 5 min, 0ºC), with the supernatants collected, frozen at -80ºC and then lyophilised in a freeze-dryer (Alpha 1-4 LSC, Martin Christ, Germany). The freeze-dried samples were then stored at -80ºC until analysed. For the direct extract, infected cultures were poured directly into the same volume of 100% ACN and then the supernatants were collected for subsequent steps as described above with the cell extract samples.

4.2.4 Assays

Total cell density (cell/mL) and cell diameter was estimated using a Multisizer^{TM}4 Coulter Counter (Beckman Coulter, Fullerton, CA, USA). Samples of various cell densities were initially diluted with medium to a TCD of around 0.5×10^6 cells/mL before proceeding with the cell enumeration process. Cell viabilities were estimated from triplicated hemocytometer counts using the 0.05 %w/v Trypan Blue exclusion method (Nielsen et al., 1991).

The β-Gal protein yield of infected whole-culture samples was quantified using a well-established colorimetric assay based on the enzymatic hydrolysis of ONPG, as described previously (Power et al., 1994; Radford et al., 1997; Wong et al., 1996). Briefly, fresh samples were initially diluted appropriately with MiliQ water, and then 50 µL of the diluted

sample was added into 950 µL Z buffer (0.06M Na_2HPO_4, 0.04 M NaH_2PO_4, 0.001 M $MgSO_4$, 0.01 M KCl and 0.035%v/v β-mercaptoethanol). The mixture was then incubated for 30 minutes at 37ºC after adding 200 µL of substrate (4 mg/mL ONPG). A stop buffer (1M Na_2CO_3) was added at 500 µL to terminate the reaction. The absorbance was measured at 420 nm using a spectrophotometer, and was accepted if it fell within the linear range (0.3-0.8) and converted to β-Gal activity units (U/mL) using Beer's Law (Chan et al., 1998). The β-Gal assay of each sample was conducted three times as technical triplicates.

Total cell protein was estimated using a BCA protein assay kit (Thermo Fisher Scientific, Rockford, IL, USA) as described previously (Huynh et al., 2012). Briefly, a volume of each culture containing 1×10^6 cells was pelleted (1000× g, 5 min) and the cell pellets were washed twice with PBS (adjusted with NaCl to a final osmolarity of 350 mOsmol/kg as in Sf900™III medium) and kept in a -20ºC freezer for subsequent analysis. The cell pellets were lysed with 1 mL of NaOH, 0.1 M, at 40ºC for 20 minutes and then diluted four fold prior to conducting total protein analysis, following the manufacturer's protocol using BSA as a standard. The BSA standard curve was fitted with a sigmoidal logistic model using SigmaPlot 11 (Systat Software Chicago, IL).

The intracellular vDNA copies were measured using a quantitative real time polymerase chain reaction assay (qRT-PCR) as described by Rosinski et al. (2002). The detail of the procedure for the preparation of the vDNA standard and for qRT-PCR has been previously described (Huynh et al. 2013). Briefly, cultures containing 1×10^6 cells/mL were pelleted (300×g, 5 min) and kept at -20 ºC until analysed. Pellets were treated with 1 mL of a digestion buffer (100 mM NaCl, 10 mM Tris.HCl, 25 mM EDTA, 0.5% SDS, 0.1 mg/mL Proteinase K) at 50 ºC for 15 hours prior to measuring the vDNA. The Eppendorf epMotion 5075 Robotics System (Eppendorf, Germany) and the ABI PRISM® 7900HT Sequence Detection System (Life Technology, USA) were used for qRT-PCR analysis. Each sample was measured using technical triplicates in the same PCR plate. The estimated genome size of 1.359×10^{-7} ng/genome (Rosinski et al., 2002) was used to convert the mass production to a genome copy number.

Intracellular nucleotides and TCA cycle intermediates were measured by LC-MS/MS as described in Dietmair et al. (2012) with the following modifications: the analytical column was equipped with a pre-column Security Guard Gemini-NX C18 4mm x 2 mm I.D. cartridge (Phenomenex, Aschaffenburg, Germany). Azidothymidine was added as an internal standard to all samples and the 12.5 µM calibrant at a final concentration of 10 µM. The samples were run with sample- and analyte-relevant calibration standards and

pooled QC samples (Hodson et al., 2009; Sangster et al., 2006) to control for reproducibility of data acquisition and to ensure data integrity. Analyte stock solutions were prepared in purified water (Veolia) and aliquots of each solution were mixed to achieve a final calibrant solution at 200 µM. This calibrant solution was serially diluted and the dilutions used as calibration standards from 200 to 0.006µM, constituting $9 \leq x \leq 20$ calibration points for all analytes to account for differential responses in the mass spectrometer. Data were processed and analysed in Analyst 1.5.2 and MultiQuant 2.1.1 (ABSciex, Canada).

A HPLC system was used to analyse extra- and intra-cellular amino acids (AAs) as described previously (Dietmair et al., 2010) with some modifications including the increase of flow rate from 1 mL/min to 2 mL/min and the decrease of the running time. The detail of the method was presented in Chapter 2 of this thesis.

Extracellular organic acids (α-ketoglutarate, pyruvate, succinate, lactate, fumarate, acetate and propionate) and sugars (sucrose, glucose and maltose) were also analyzed by HPLC (Agilent 1200 series, Agilent, Mulgrave, Victoria, Australia) using both MWD and RID detectors. The detail of the method was presented in Chapter 2 of this thesis.

The intracellular ATP in the first experiment was measured using the ATPlite luminescence ATP detection assay system (PerkinElmer Life Sciences, Boston, MA), which was described in Tran et al. (2012). This assay is based on the production of light when ATP reacts with D-Luciferin in the presence of Luciferase, and was conducted according to the manufacturer's instructions.

4.2.5 Statistical analysis

One-way analysis of variance (ANOVA), followed by Tukey's Honestly Significant Difference (HSD) test, was used to determine whether the means from two or more groups of data were significantly different at the 95% confidence level. Minitab 15 Statistical Software (Minitab, State College, PA) was used for all data analysis.

4.3 Results

4.3.1 Assessment of the extraction protocol for infected Sf9 cells post-infection

Results for the evaluation of the extraction protocol at different times post-infection are presented in Fig. 4.1. At a high MOI infection (10 PFU/cell), the cell density increase post-infection (cells/mL) of 40% was almost negligible compared with the uninfected culture that reached a peak cell density of 1.8-2×10^7 cells/mL (Fig.4.1a). Also as shown in Figure 4.1a, the increase in cell diameter post-infection was rapid for the first 24 hpi, and then gradually increased until 48 hpi, with a peak increase in cell diameter of 18% and then declined after that point. Cell viability of the infected culture remains as high as that of the uninfected one (above 90%) until 48 hpi and then dropped sharply after that (Fig. 4.1a). These results indicate that the cell integrity was affected greatly after 48 hpi when infected cells began to die and lyse. The kinetics of vDNA and β-Gal production for infected Sf9 cells were as expected for rAcMNPV infected Sf9 cells (Fig. 4.1b). As shown, vDNA production started after 6 hpi and increased rapidly from 12 until 24 hpi to a value close to the peak yield seen at 36 hpi, while β-Gal production commenced by 24 hpi and rapidly increased until 60 hpi then slightly increased to the peak yield at 72 hpi. The results of vDNA and β-Gal yield shows that the rAcMNPV infected Sf9 cells set up in this study were optimally-infected, and were suitable for endometabolome studies.

The intracellular ATP content of infected Sf9 cells and the recovery of cell extract samples compared to the direct extract over the time course post-infection (from 0 to 72 hpi) are shown in Figure. 4.1c. There was good recovery of ATP in cell extract samples until 48 hpi (recovery of at least 90% of the direct extract). In other words, the extraction protocol still works for infected Sf9 cells until 48 hpi. Intracellular ATP concentrations remained at a peak level of around 3.8 mM (Fig. 4.1c), from 0-48 hpi and started to decrease after 48 hpi, presumably due to cell lysis after that point. In addition, intracellular AA concentrations of Sf9 infected cells at various times post-infection (Fig. 4.1d) remained unchanged during the first 48 hpi for most AA and dropped significantly after that. The drop (after 48 hpi) also occurred with alanine which gradually increased during the first 48 hpi. These results indicate that 48 hpi is the latest time that the infected cells can be quenched and extracted without a significant loss of intracellular metabolites.

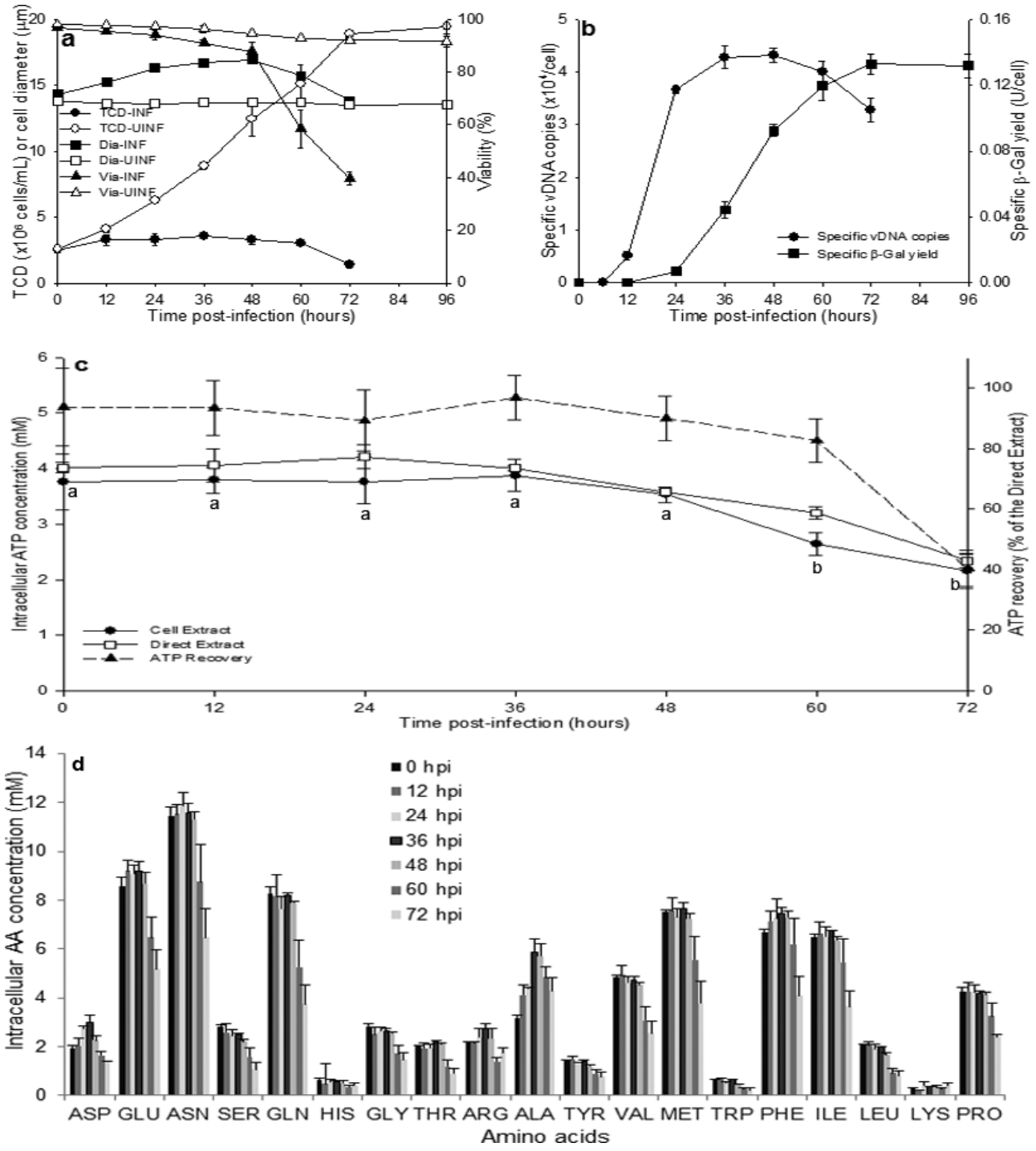

Fig. 4.1 The kinetics of cell growth, cell size expansion and viability (a), specific vDNA and β-Gal production (b), intracellular ATP levels and ATP recovery at different times post-infection (c) and intracellular amino acid levels (AAs) (d) of Sf9 cells infected with a recombinant baculovirus (rAcMNPV) at an MOI of 10 PFU/cell. Infections were conducted in Sf900™III serum free medium at an infection cell density (ICD) of 2.5×10^6 cells/mL. The experiment was conducted in shaker-flask suspension cultures. Each data point is the average from three biological replicates, and the error bars represent the standard deviation. Abbreviations, TCD: total cell density, Via: viability, Dia: cell diameter, INF: infected, UINF: uninfected.

4.3.2 Low versus high cell densities at the time of infection

Figure 4.2 represents data obtained from infected Sf9 cells with a rAcMNPV at low and high ICDs. The results confirmed the cell density effect when Sf9 cells were infected with a rAcMNPV at low (2×10^6) and high (6×10^6 cells/mL) ICDs. There was no significant difference in the cell density increase post-infection (cells/mL) when infections were conducted at low or high ICDs, with an increase of 49% and 46% for low and high ICDs, respectively (Fig. 4.2a). However, the cell diameter increase post-infection of the low ICD (21%) was significantly higher than that of the high ICD (14%) (Fig. 4.2a). Cell viabilities of the infected cultures of both ICDs were comparable with the uninfected culture until 48 hpi, and then significantly reduced after that point (Fig. 4.2a) as was also shown for the case of the previous experiment for evaluating the extraction protocol (Fig. 4.1a).

Table 4.1. Total cell protein (TCP) per cell increase post-infection (pi) and the proportion of β-Gal protein over TCP increase pi for Sf9 cells infected with a recombinant baculovirus (rAcMNPV) at either low (2×10^6) or high (6×10^6 cells/mL) ICDs

	0-24 hpi		24-60 hpi		0-60 hpi	
	Low ICD	High ICD	Low ICD	High ICD	Low ICD	High ICD
TCP increase pi (pg/cell)	65±29	72±10	151±16	66±4	217±27	139±13
β-Gal yield (pg)	-	-	88±6	31±2	-	-
β-Gal/TCP increase (%)	-	-	57±7	46±5	40±2	22±3
TCP produced 24-60 hpi/0-24 hpi	-	-	2.78±1.66	0.93±0.11	-	-

Although the early events of the virus infection and cessation of cell growth was similar between low and high ICDs (Fig. 4.2a), there was a contrast between these two ICDs in terms of cell specific yields (Fig. 4.2b). The peak specific β-Gal yield for the low and high ICDs was 0.14 and 0.05 U/cell, respectively, and the specific vDNA yield for these two ICDs was 4.4 and 3×10^4 copies/cell. However, the time frame from the starting point of vDNA and β-Gal production to the point where peak yields were achieved was similar for both ICDs (Fig. 4.2b). This indicates that the infection process follows a similar time sequence for low and high ICDs, but the vDNA and β-Gal productivities during the post-infection period are lower for the high density infection.

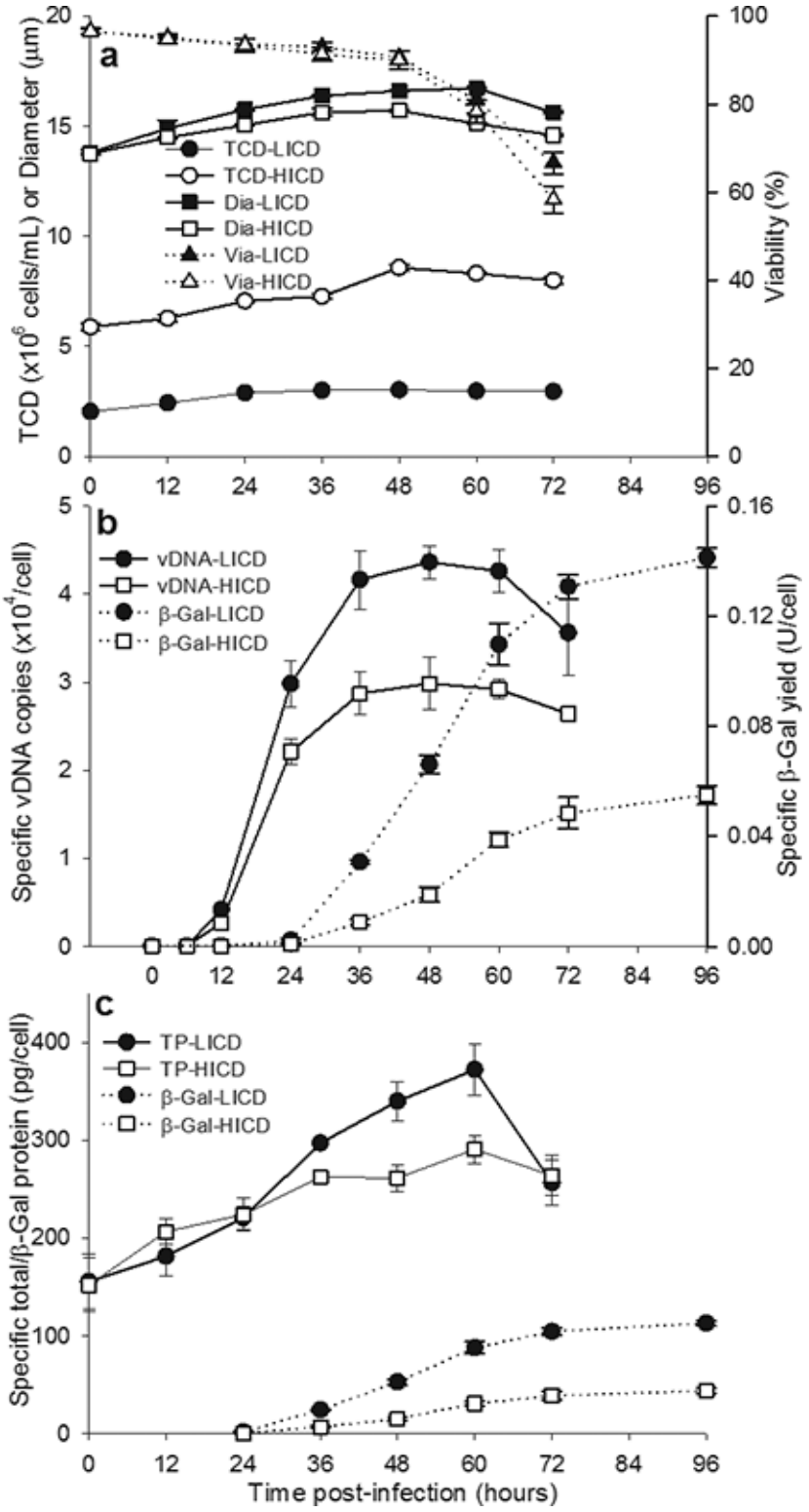

Fig. 4.2 Total cell density and cell hypertrophy (a), specific vDNA and β-Gal production (b), and total cell protein vs β-Gal (c) of Sf9 cells infected with a rAcMNPV. Infections were conducted in Sf900™III serum free medium at low (2×10^6) and high (6×10^6 cells/mL) ICDs and at an MOI of 10 PFU/cell. The experiment was conducted in shaker-flask suspension cultures. Each data point is the average from three biological replicates, and the error bars represent the standard deviation. Abbreviations, TCD: total cell density, Via: viability, Dia: cell diameter, LICD: low infection cell density, HICD: high infection cell density.

The total cell protein (TCP) content of the low and high ICDs, (Fig. 4.2c) shows that both cultures started at a similar level of TCP content at ~155 pg/cell. For the first 24 hpi, the TCP increase was similar for the low and high ICDs. The TCP increase for these two ICDs was, however, divergent after 24 hpi which coincided with the starting time of β-Gal production, with a faster rate of increase shown for the lower ICD. The TCP peaked at 60 hpi for both cultures and quickly declined after that point due to cell death and lysis, while the β-Gal protein continued to increase at a lower rate up to 96 hpi. The TCP was measured from cell pellets, while β-Gal protein was measured from whole cultures, hence, β-Gal protein increased despite the decrease in TCP after 60 hpi. The gap between the peak specific TCP of low and high ICDs (81 pg/cell) was larger than the difference in the specific β-gal protein content of cells from low and high ICDs, which at most is 57 pg/cell (calculated based on the conversion factor of 0.8 mg/10^6 U of β-gal protein (Chan et al., 1998)) (Table 4.1). These data clearly indicate that significant protein production occurs post-infection other than that accounted for by β-Gal protein. For the low ICD, the β-Gal produced accounted for 40% of the TCP produced post-infection and 57% of the TCP produced after 24 hpi. For the high ICD, the β-Gal produced accounted for only 22% of the total protein produced post infection and 46% of the total protein produced after 24 hpi (Table 4.1). The TCP increase during the late infection stage (24-60 hpi) was 2.78 and 0.93 times of the TCP increase at the early infection stage (0-24 hpi) for low and high ICDs, respectively (Table 4.1).

4.3.3 Intracellular metabolite measurements of low versus high ICDs

In the multivariate classification of numerous metabolites at different times post-infection, principle component analysis (PCA) models have been applied using the soft independent modelling of class analogy (SIMCA). The orthogonal projection to latent structure (OPLS) is a linear multivariate regression method that is used for classification and prediction of multiple parameters in biological application. OPLS is a modification of the usual partial least squares (PLS) regression method which filters out variations that not directly related to the response (Eriksson et al., 2006). The OPLS couple with the discriminant analysis (OPLS-DA) is a powerful tool for the regression prediction and classification of various components in a metabolomics study. The main benefit of using OPLS-DA lies in the ability to separate predictive from non-predictive (orthogonal) variation (Bylesjo et al., 2006). Therefore, it improves the detection limit for outliers in the scores and decreases the total number of components used.

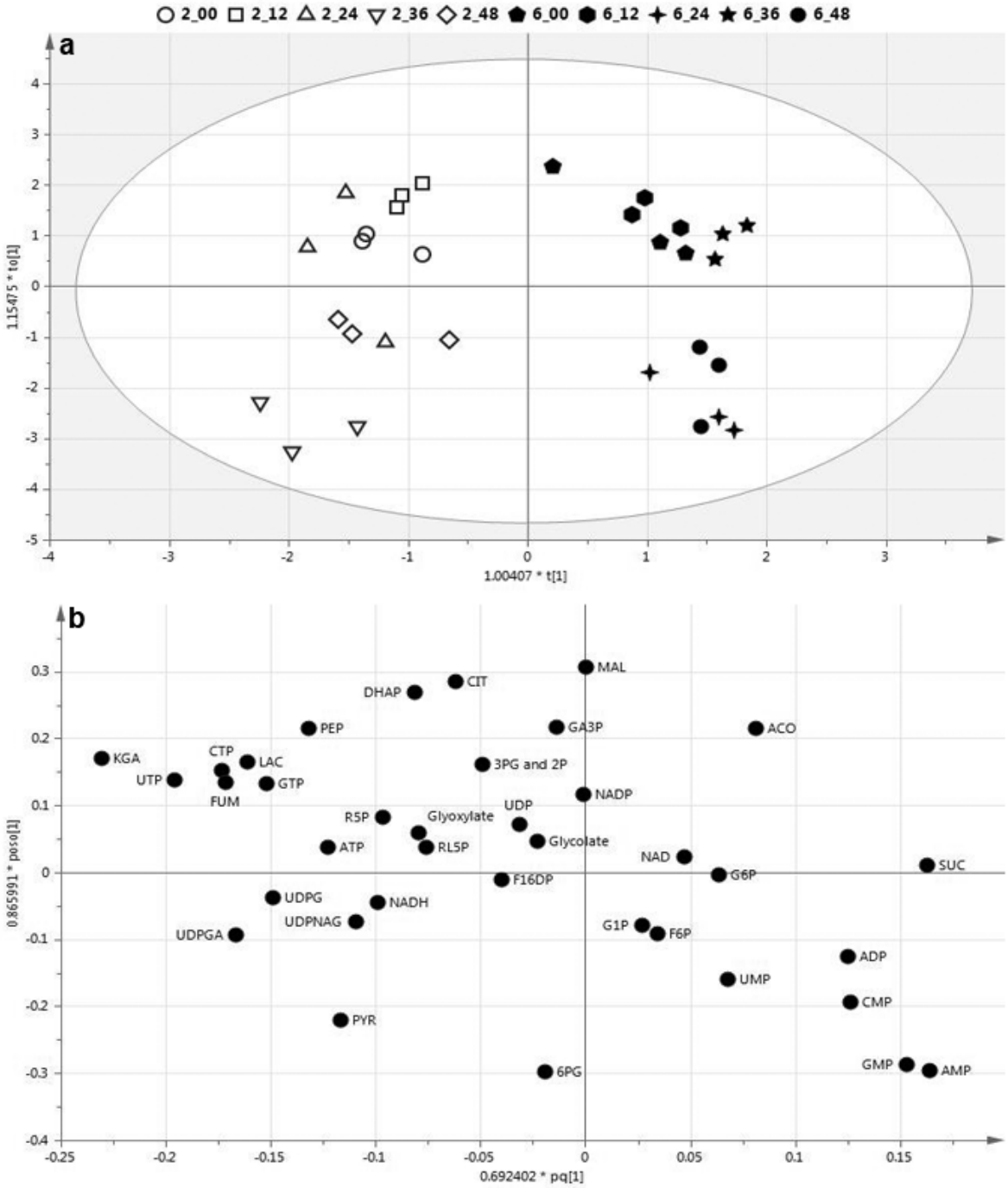

Fig. 4.3 Multivariate analysis of intracellular metabolite concentrations of Sf9 infected cells at low ($2x10^6$ cells/mL) and high ($6x10^6$ cells/mL) ICDs. Orthogonal projection to latent structures–discriminant analysis (OPLS-DA) scores (a) and loadings (b) plots of the 5 time points post-infection at low and high ICDs, classified by cell density. OPLS-DA model metrics: Predictive component R2X = 0.197; R2 = 0.913; Q2 = 0.869; R2Y = 1: Orthogonal component R2X = 0.278.

Figure 4.3 presents the intracellular concentrations of 37 metabolites (including nucleotides, nucleotide sugars and organic acids) of 5 time points post-infection (0, 12, 24, 36, 48 hpi) at low ($2×10^6$ cells/mL) and high ($6×10^6$ cells/mL) ICDs. The orthogonal projection to latent structures – discriminant analysis (OPLS-DA) of all the samples over

the time course of infection (Fig. 4.3a) showed a clear separation of low and high ICDs. Figure 4.3a also indicates that the biological replication is reliable as the scores for the three replicates indicate similar positions in biochemical space. Based on the OPLS-DA loadings (Fig. 4.3b), the metabolites most influential in the projected separation between low and high ICDs are the nucleoside tri-phosphates, nucleoside di-phosphates, nucleoside mono-phosphates, α-ketoglutarate, pyruvate, fumarate, lactate, succinate and UDP sugars (UDP-glucose, UDP-glucuronic acid, and UDP*N*-acetylglucosamine). These metabolites have a variable importance on projection (VIP) score of >1 and have been selected for further statistical analysis as detailed in Table 4.2 and Fig. 4.4. Generally, intracellular metabolite levels at the low ICD were higher than those at the high ICD with the exception of succinate (Table 4.2, Fig. 4.4).

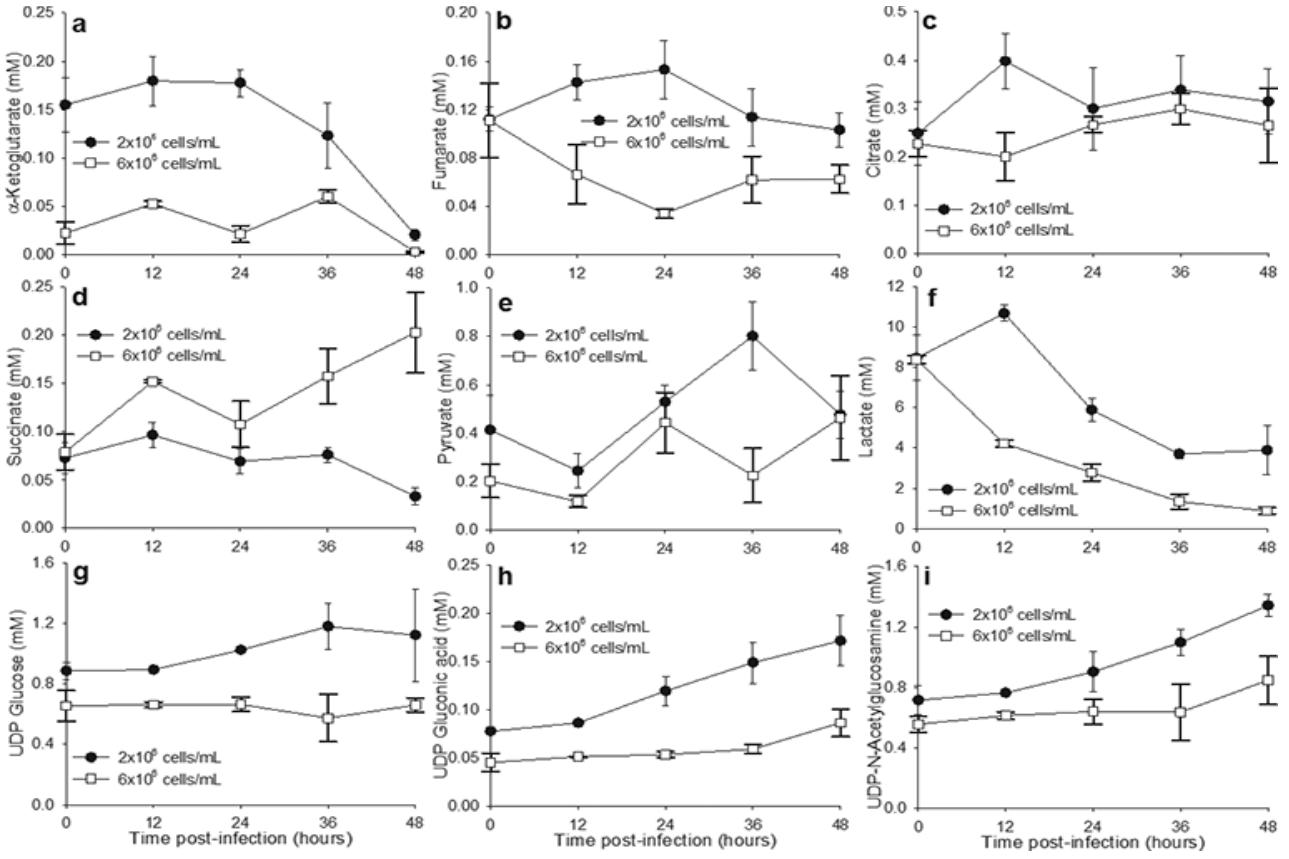

Fig. 4.4 Intracellular concentrations of organic acids and UDP sugars for infected Sf9 cells at low (2×10^6) and high (6×10^6 cells/mL) ICDs. Infections were conducted in Sf900™III serum free medium at an MOI of 10 PFU/cell in shaker-flask suspension cultures. Each data point is the average from three biological replicates, and the error bars represent the standard deviation.

The concentrations of nucleoside tri-, di-, and mono-phosphates of infected Sf9 cells at low (2×10^6) and high (6×10^6 cells/mL) ICDs over the time course of infections are presented in Fig.4.5. Intracellular ATP levels appeared to increase over time post-infection

for the low ICD, while the levels slightly decrease post-infection for the high ICD (Fig. 4.5a). There were significant differences in ATP levels between the low ICD at 24 and 36 hpi and the high ICD at 48 hpi. In contrast, ADP concentrations tended to be higher for the high ICD at all time points and for the low ICD at the late infection stage (Table 4.2, Fig. 4.5a). In general, the ADP concentration of the high ICD infection was significantly higher than that of the low ICD cases. Unlike the low ICD, there was a significant amount of AMP in the high ICD cases (Table 4.2, Fig. 4.5a). As a result, the total adenosine (ATP+ADP+ AMP) was similar between low and high ICDs except for the low ICD at 0 and 12 hpi, which were lower than the other time points. The trends for intracellular concentrations of other nucleotides (uridine, guanine and cytosine) were similar to that of adenosine with the nucleotide tri-phosphate levels during the low ICD being generally higher than those during the high ICD (Fig. 4.5 b, c, d). The trend for total uridine, guanine and cytosine concentrations over various time points post-infection for low and high ICDs were similar to that for total adenosine.

It is interesting to note that at 24 hpi towards the end of the rapid rise in vDNA for both low and high ICDs (Fig 4.2b), the UTP, CTP, GTP and ATP levels in the low ICD case are all significantly higher than the levels of these metabolites in the high ICD case (Table 4.2). Indeed the UTP level at 24 hpi is 8 times higher in the low ICD case compared to that in the high ICD case at the same time post-infection. Similarly the CTP level is 5 times higher, GTP 3 times higher and ATP 1.6 times higher at 24 hpi in the low versus high ICD case. It is possible that the supply of UTP, CTP, GTP and ATP is rate limiting for the production of vDNA during the 6-24 hpi period for high cell density infections.

The intracellular amino acid (AA) concentrations of infected Sf9 cells at low and high ICDs over the 0-48 hpi period and a comparison of this data between low and high ICDs at 0 and 36 hpi are shown in Fig. 4.6. In the case of the low ICD, the levels of most AAs inside the cells were stable over time, except for alanine, which gradually increased (Fig. 4.6a). In contrast, there is a slight decrease in intracellular levels of some AAs (asparagine, serine, methionine, isoleucine, leucine, and proline) for the high ICD case during the time post-infection, in particular the glutamine concentration dropped quickly over the period of 0-24 hpi (Fig. 4.6b). The intracellular alanine concentration continuously increased over the time post-infection for the high ICD case as found in the case of the low ICD. Comparing between the low and high ICDs in terms of intracellular AA levels, Fig. 4.6 c, d shows that the concentrations of most AA of the low ICD were significantly higher than those of the high ICD either at 0 hpi (Fig. 4.6c) or 36 hpi (Fig.4.6d). The significant

differences between intracellular AA levels of low and high ICDs were more pronounced during the latter stages of the infection (36 hpi, Fig. 4.6d).

Table 4.2 Intracellular metabolite concentrations (mM) over various times post-infection for Sf9 cells infected with a recombinant baculovirus (rAcMNPV) at either low (2×10^6) or high (6×10^6 cells/mL) infection cell densities (ICDs). Data represented as an average of biological triplicates. The metabolites listed were selected on the basis of showing significant variations in levels between different ICDs or times post infection following the analysis shown in Fig. 4.3.

	Low ICD (2×10^6 cells/mL)					High ICD (6×10^6 cells/mL)					
Metabolites	0 hpi	12 hpi	24 hpi	36 hpi	48 hpi	0 hpi	12 hpi	24 hpi	36 hpi	48 hpi	P<
KGA	0.15^{ab}	0.18^{a}	0.18^{a}	0.12^{b}	0.02^{cd}	0.02^{cd}	0.05^{cd}	0.02^{cd}	0.06^{c}	0.00^{d}	0.001
UTP	1.79^{ab}	1.86^{ab}	2.11^{a}	1.53^{abc}	1.47^{abc}	0.80^{cd}	0.99^{bcd}	0.26^{d}	1.04^{bcd}	0.71^{cd}	0.001
CTP	0.93^{a}	0.93^{a}	0.95^{a}	0.65^{b}	0.74^{ab}	0.56^{bc}	0.50^{bc}	0.19^{d}	0.52^{bc}	0.34^{cd}	0.001
UDPGA	0.08^{de}	0.09^{cd}	0.12^{bc}	0.15^{ab}	0.17^{a}	0.05^{e}	0.05^{de}	0.05^{de}	0.06^{de}	0.09^{cd}	0.001
FUM	0.11^{ab}	0.14^{a}	0.15^{a}	0.11^{ab}	0.10^{ab}	0.11^{ab}	0.07^{bc}	0.00^{c}	0.06^{bc}	0.06^{bc}	0.001
SUC	0.07^{de}	0.10^{cd}	0.07^{de}	0.08^{de}	0.03^{e}	0.08^{de}	0.15^{abc}	0.11^{bcd}	0.16^{ab}	0.20^{a}	0.001
LAC	8.47^{b}	10.69^{a}	5.90^{c}	3.71^{d}	3.89^{d}	8.39^{b}	4.23^{cd}	2.79^{de}	1.35^{ef}	0.88^{f}	0.001
GMP	0.02^{b}	0.01^{b}	0.03^{b}	0.07^{ab}	0.08^{ab}	0.07^{ab}	0.04^{b}	0.21^{a}	0.04^{b}	0.13^{ab}	0.01
UDPG	0.89^{abc}	0.90^{abc}	1.03^{ab}	1.18^{a}	1.12^{a}	0.66^{c}	0.66^{bc}	0.67^{bc}	0.58^{c}	0.66^{bc}	0.001
GTP	1.47^{a}	1.46^{a}	1.34^{ab}	1.23^{ab}	1.25^{ab}	0.95^{abc}	1.03^{abc}	0.40^{c}	0.94^{abc}	0.70^{bc}	0.001
PEP	0.03^{ab}	0.05^{a}	0.02^{ab}	0.00^{b}	0.00^{b}	0.02^{ab}	0.01^{b}	0.01^{b}	0.00^{b}	0.00^{b}	0.01
CMP	0.02^{b}	0.01^{b}	0.01^{b}	0.04^{b}	0.05^{ab}	0.04^{ab}	0.04^{ab}	0.05^{ab}	0.03^{b}	0.09^{a}	0.001
PYR	0.41^{ab}	0.24^{b}	0.53^{ab}	0.80^{a}	0.48^{ab}	0.20^{b}	0.12^{b}	0.44^{ab}	0.22^{b}	0.46^{ab}	0.001
UDPNAG	0.72^{cd}	0.76^{cd}	0.90^{bc}	1.10^{ab}	1.34^{a}	0.56^{d}	0.61^{cd}	0.64^{cd}	0.64^{cd}	0.85^{bcd}	0.001
AMP	0.07^{ab}	0.04^{b}	0.16^{ab}	0.30^{ab}	0.35^{ab}	0.33^{ab}	0.20^{ab}	0.68^{a}	0.15^{ab}	0.66^{ab}	0.05
ADP	1.20^{c}	1.00^{c}	1.40^{bc}	1.43^{abc}	1.76^{bc}	1.44^{bc}	2.09^{abc}	2.34^{ab}	1.87^{bc}	2.95^{a}	0.001
ATP	4.58^{abc}	4.63^{abc}	5.73^{a}	5.92^{a}	5.32^{ab}	4.38^{abc}	4.33^{abc}	3.63^{bc}	4.01^{abc}	2.90^{c}	0.001
Adenosine	5.84^{b}	5.66^{c}	7.30^{abc}	7.65^{a}	7.43^{ab}	6.14^{abc}	6.62^{abc}	6.65^{abc}	6.03^{abc}	6.51^{abc}	0.01

Data in the same row with different superscripts were significantly different at $P < 0.05$.

Abbreviation: KGA: α-ketoglutarate, UTP: uridine tri-phosphate, CTP: cytidine tri-phosphate, UDPGA: uridine di-phosphate gluconic acid, FUM: fumarate, SUC: succinate, LAC: lactate, GMP: guanosine mono-phosphate; UDPG: uridine di-phosphate glucose, GTP: guanosine tri-phosphate; PEP: phosphoenol pyruvate, CMP: cytidine mono-phosphate, PYR: pyruvate, UDPNAG: uridine di-phosphate N-acetylglucosamine, AMP, ADP and ATP: adenosine mono-, di- and tri-phosphate.

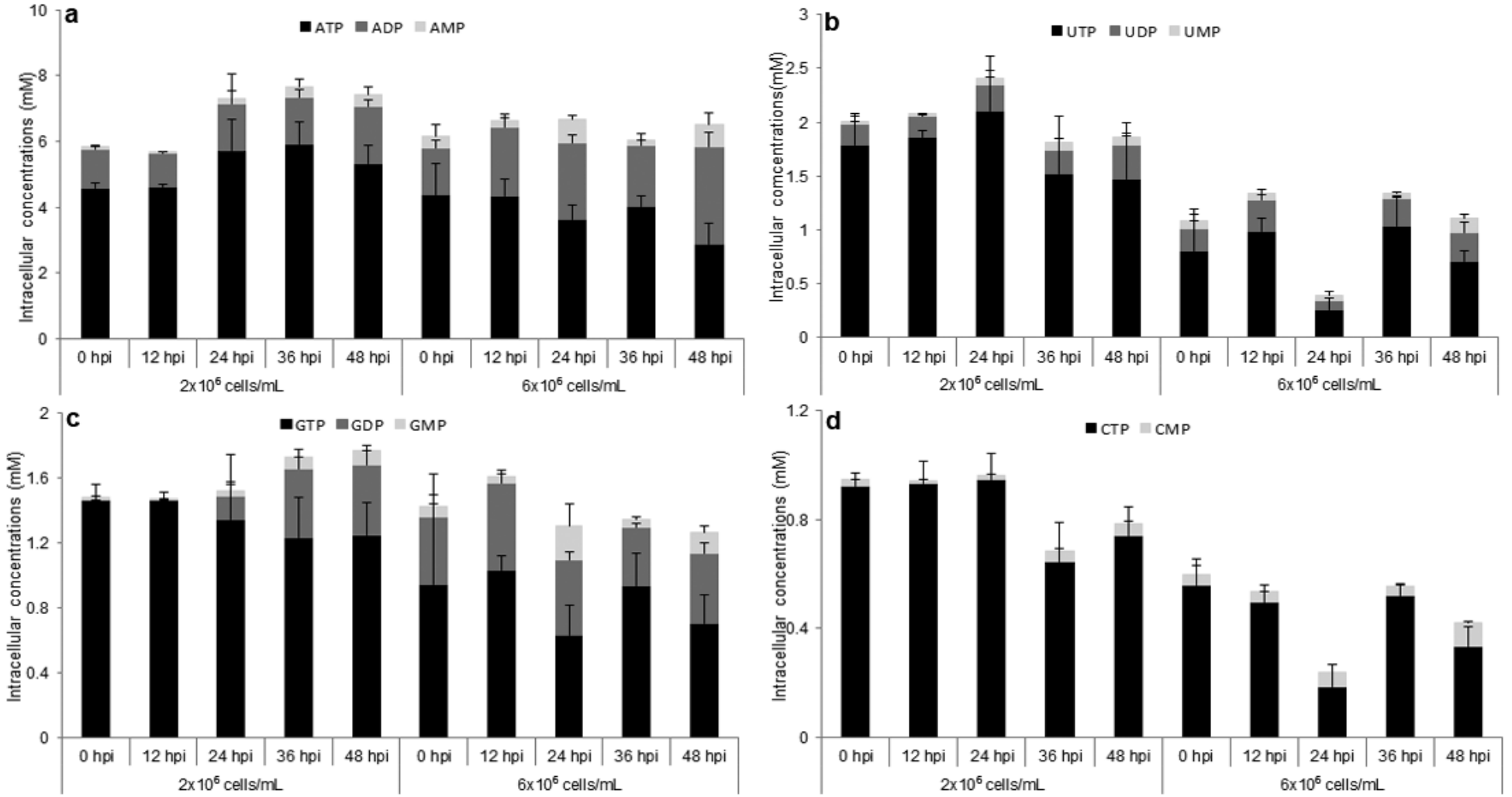

Fig. 4.5 Stacked bar charts of (a) adenosine, (b) uridine, (c) guanosine and (d) cytidine nucleotide concentrations of Sf9 infected cells over 5 time points post-infection at low ($2x10^6$ cells/mL) and high ($6x10^6$ cells/mL) ICDs. Infections were conducted in Sf900™III serum free medium at an MOI of 10 PFU/cell. The experiment was conducted in shaker-flask suspension cultures. Each data point is the average from three biological replicates, and the error bars represent the standard deviation.

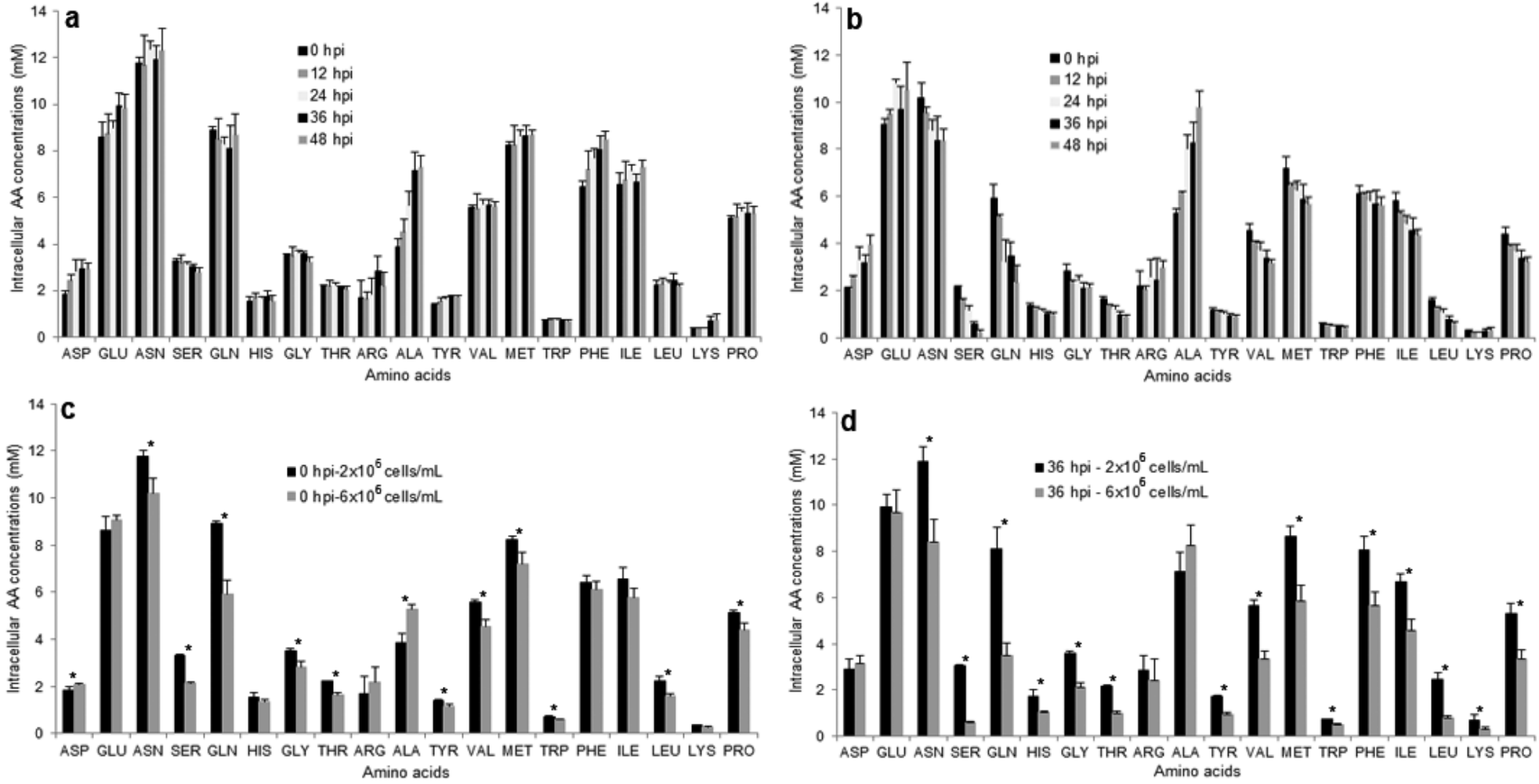

Fig. 4.6 Intracellular AA concentration of infected Sf9 cells at various times post-infection at low (a) and high (b) ICDs, and the comparison between low and high ICD for intracellular AA levels at 0hpi (c) and 36 hpi (d). Infections were conducted in Sf900™III at low (2×10^6) and high (6×10^6 cells/mL) ICDs and at an MOI of 10 PFU/cell. The experiment was conducted in shaker-flask suspension cultures. Each data point is the average from three biological replicates, and the error bars represent the standard deviation.

4.3.4 Glucose and AA consumption rates between low versus high ICDs

Glucose and AA consumption rates of uninfected and baculovirus infected Sf9 cells at low and high ICDs are shown in Table 4.3. The cell specific glucose consumption rate of infected cells at the low ICD was significantly higher than that of the uninfected cells. However, the glucose consumption rate of infected cells at the high ICD was not significantly different to either infected cells at the low ICD or to uninfected cells. However, the glucose consumption rate per unit of cell biomass was similar among uninfected and infected cultures (Table 4.4) due to the enlargement of infected cells post-infection. In this Table cell volume is assumed to reflect cell biomass.

AA consumption rates of infected cells at the low ICD were significantly higher than those at the high ICD for most of the AAs except for aspartate, glutamate, tyrosine and tryptophan (Table 4.3). Differences in AA consumption rates between low and high ICDs were less pronounced for the consumption per unit of cell volume, Table 4.4, as the lower ICD generated a larger cell volume post-infection. However, the AA consumption rates per unit of cell biomass at the low ICD were still significantly higher than those at the high ICD, except for the four AAs mentioned above plus serine, glutamine and alanine (Table 4.4). The consumption rates of AAs for uninfected Sf9 cells were somewhere in between of the values for the two infection cases (Table 4.3). Interestingly, the consumption rate of glutamine for uninfected cells was much higher than that for infected cells (both low and high ICDs). In addition, the asparagine consumption rate of uninfected cells was almost double that of the low ICD infected cells. Based on consumption per unit cell volume the AA consumption rates of uninfected cells were significantly higher than those of infected cells in many cases at both low, (9 out of 19 AAs measured), and high, (14 out of 19 AAs measured) ICDs (Table 4.4). The change of extracellular glucose, maltose and AA concentrations over the time post-infection/post-inoculation can be seen in Appendix A2.1 & A2.2.

Comparison of the AA consumption rates between early (0-24 hpi) and late stages (24-60 hpi) of the virus infection process at the same ICD or between infected Sf9 cells at low and high ICDs are shown in Fig. 4.7. For the low ICD, there was almost no difference in AA consumption rates between the early and late stages of the virus infection. In this case, significant differences in AA consumption rates were only seen for serine, glutamine and tyrosine (Fig. 4.7a). In contrast, a larger number of significant differences were found in the AA consumption rates between the early and late infection stages in the case of infected cells at the high ICD, with significant differences found for 12 out of the 19 AAs quantified (Fig. 4.7b).

Table 4.3. Glucose and AA consumption rates ($\times 10^{-12}$mmol/cell/hour) of uninfected and rAcMNPV infected Sf9 cells at low and high ICDs. Uninfected and infected cultures were set up at 0.5×10^6 cells/mL. For uninfected cultures no infection was made and sampling was conducted at every 24 hours until the total cell density reached 6×10^6 cells/mL. For infected cells, cultures were infected with a baculovirus at an MOI of 10 PFU/cell when the cell density reached 2×10^6 cells/mL (48 hours) or 6×10^6 cells/mL (84 hours) and sampling was conducted every 12 hours until 60 hours post-infection. Data is the average of biological triplicates.

	Uninfected	2×10^6 cells/mL†	6×10^6 cells/mL†	P<
Glucose	-25.58^{b}	-40.90^{a}	-27.86^{ab}	0.05
Glucose, 0-24 hpi	-	-34.34	-46.67	NS
Glucose, 24-60 hpi	-	-48.42^{a}	-15.15^{b}	0.05
Maltose	-5.62	-5.68	-8.22	NS
Amino acids				
Aspartate	-4.50	-5.02	-2.98	NS
Glutamate	-5.96	-4.72	-4.54	NS
Asparagine	-8.66^{a}	-4.97^{b}	-0.62^{c}	0.001
Serine	-5.81^{a}	-5.48^{ab}	-4.89^{b}	0.05
Glutamine	-43.65^{a}	-14.91^{b}	-6.64^{c}	0.001
Histidine	-0.82^{b}	-1.36^{a}	-0.59^{b}	0.001
Glycine	-2.37^{a}	-2.50^{a}	-1.07^{b}	0.01
Threonine	-2.41^{ab}	-3.49^{a}	-1.70^{b}	0.05
Arginine	-2.39^{b}	-4.71^{a}	-1.65^{b}	0.01
Alanine	23.05^{a}	26.25^{a}	18.37^{b}	0.01
Tyrosine	-1.62	-0.72	-1.12	NS
Valine	-1.87^{b}	-4.06^{a}	-1.63^{b}	0.001
Methionine	-0.43^{b}	-4.02^{a}	-0.64^{b}	0.001
Tryptophan	-1.92	-1.29	-0.40	NS
Phenylalanine	-0.40^{b}	-3.43^{a}	-0.71^{b}	0.001
Isoleucine	-2.33^{ab}	-3.68^{a}	-1.35^{b}	0.01
Leucine	-3.55^{ab}	-5.21^{a}	-2.75^{b}	0.05
Lysine	-1.92^{b}	-3.74^{a}	-1.32^{b}	0.01
Proline	-6.04^{a}	-4.53^{a}	-0.98^{b}	0001

† Infected cultures at low (2×10^6 cells/mL) and high (6×10^6 cells/mL) ICDs

Consumption rates in the same row with different superscripts were significantly different at P<0.05

NS: Not significant

Table 4.4. Comparison of sugar and AA consumption rates ($\times 10^{-6}$mmol/mm^3 cell volume/ hour) between uninfected and infected cells at low (2×10^6) and high (6×10^6 cells/mL) ICDs. Detailed description is presented in Table 4.3.

	Uninfected	2×10^6 cells/mL†	6×10^6 cells/mL†	P<
Glucose	-19.73	-19.47	-14.85	NS
Maltose	-2.80^a	-2.62^b	-4.51^a	0.05
Amino acids				
Aspartate	-3.31	-2.32	-1.64	NS
Glutamate	-4.33^a	-2.18^b	-2.49^b	0.05
Asparagine	-6.33^a	-2.29^b	-0.34^c	0.001
Serine	-4.24^a	-2.53^b	-2.69^b	0.001
Glutamine	-71.53^a	-6.88^b	-3.65^b	0.001
Histidine	-0.60^a	-0.63^a	-0.32^b	0.01
Glycine	-1.73^a	-1.15^b	-0.59^c	0.01
Threonine	-1.76^a	-1.61^a	-0.93^b	0.05
Arginine	-1.75^a	-2.17^a	-0.91^b	0.01
Alanine	16.86^a	12.11^b	10.09^b	0.001
Tyrosine	-1.19^a	-0.33^b	-0.61^{ab}	0.05
Valine	-1.36^b	-1.87^a	-0.89^c	0.001
Methionine	-0.31^b	-1.86^a	-0.35^b	0.01
Tryptophan	-1.40	-0.60	-0.22	NS
Phenylalanine	-0.29^b	-1.58^a	-0.39^b	0.01
Isoleucine	-1.70^a	-1.70^a	-0.74^b	0.05
Leucine	-2.60^a	-2.40^a	-1.51^b	0.05
Lysine	-1.40^{ab}	-1.73^a	-0.73^b	0.05
Proline	-4.41^a	-2.09^b	-0.54^c	0001

† Infected cultures at low (2×10^6 cells/mL) and high (6×10^6 cells/mL) ICDs

Consumption rates in the same row with different superscripts were significantly different at P<0.05

NS: Not significant

Comparing between the low and high ICDs, AA consumption rates at the early infection stage (0-24 hpi) of infected cells at low ICDs was higher than those at the high ICD in most of the AAs with significant differences observed in 10 out of 19 AAs measured (Fig. 4.7c). At the late infection stage the significant differences were expanded in terms of the level of difference as well as the number of AAs involved, with significant differences

found in 11 out of 19 AAs measured (Fig. 4.7d). The difference in AA consumption rates calculated based on a cell biomass basis between early and late infection stages as well as between low and high ICDs (Fig. 4.8) followed the same pattern as found when calculated based on a per cell basis. This result indicates that infected cells at the low ICD consume AAs at higher rates than those at the high ICD and the consumption of AAs by infected cells at high ICDs were poorer at the late stage of the baculovirus infection process.

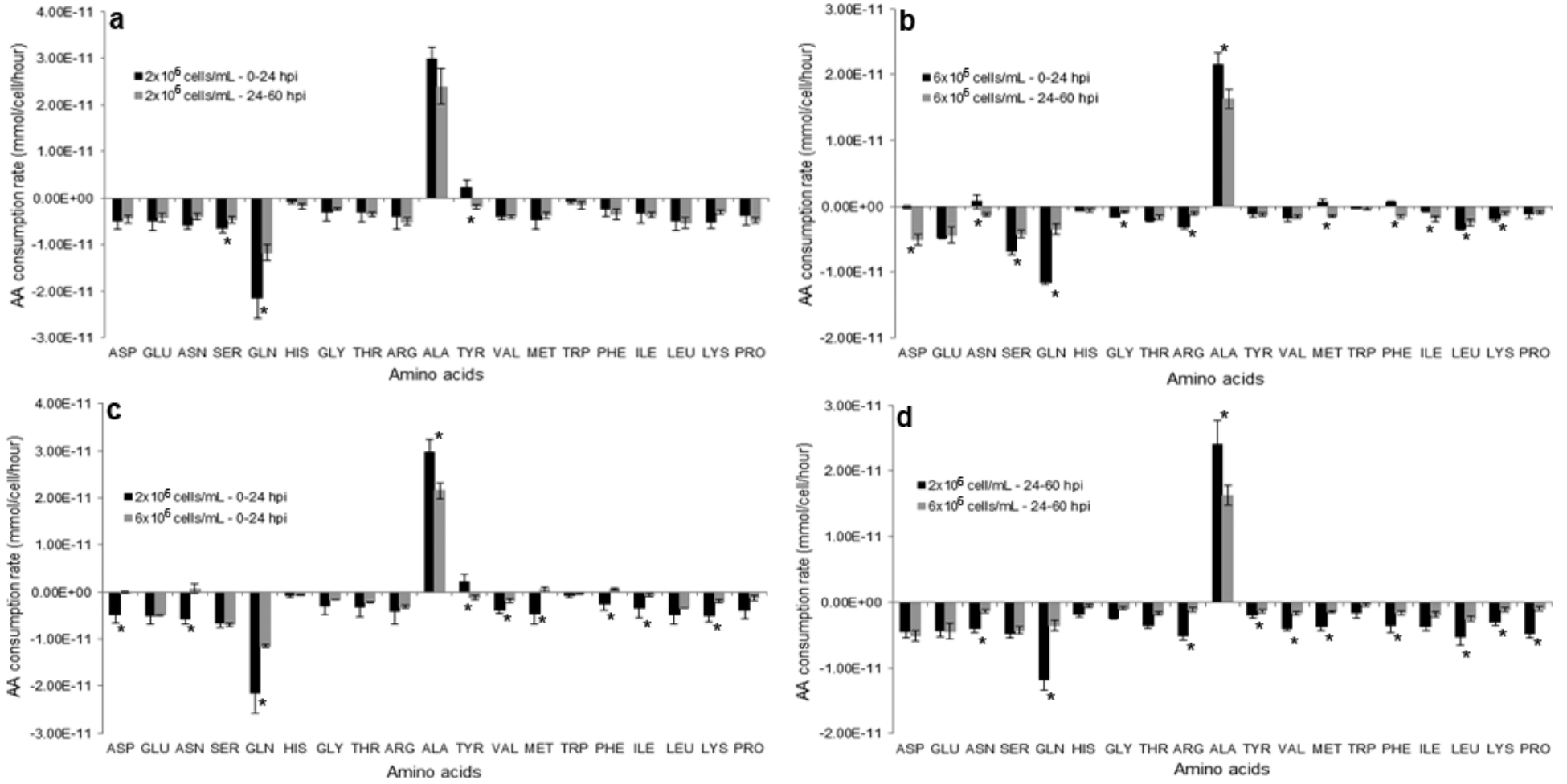

Fig. 4.7 AA consumption rates (mmol/cell/hour) between early (0-24 hpi) and late (24-60 hpi) infection stages for low (a) and high ICD (b) and between low and high ICDs for early (c) and late infection (d) of Sf9 cells infected with a rAcMNPV. Infections were conducted in Sf900™III at low (2×10^6) and high (6×10^6 cells/mL) ICDs and at an MOI of 10 PFU/cell. The experiment was conducted in shaker-flask suspension cultures. Each data point is the average from three biological replicates, and the error bars represent the standard deviation.

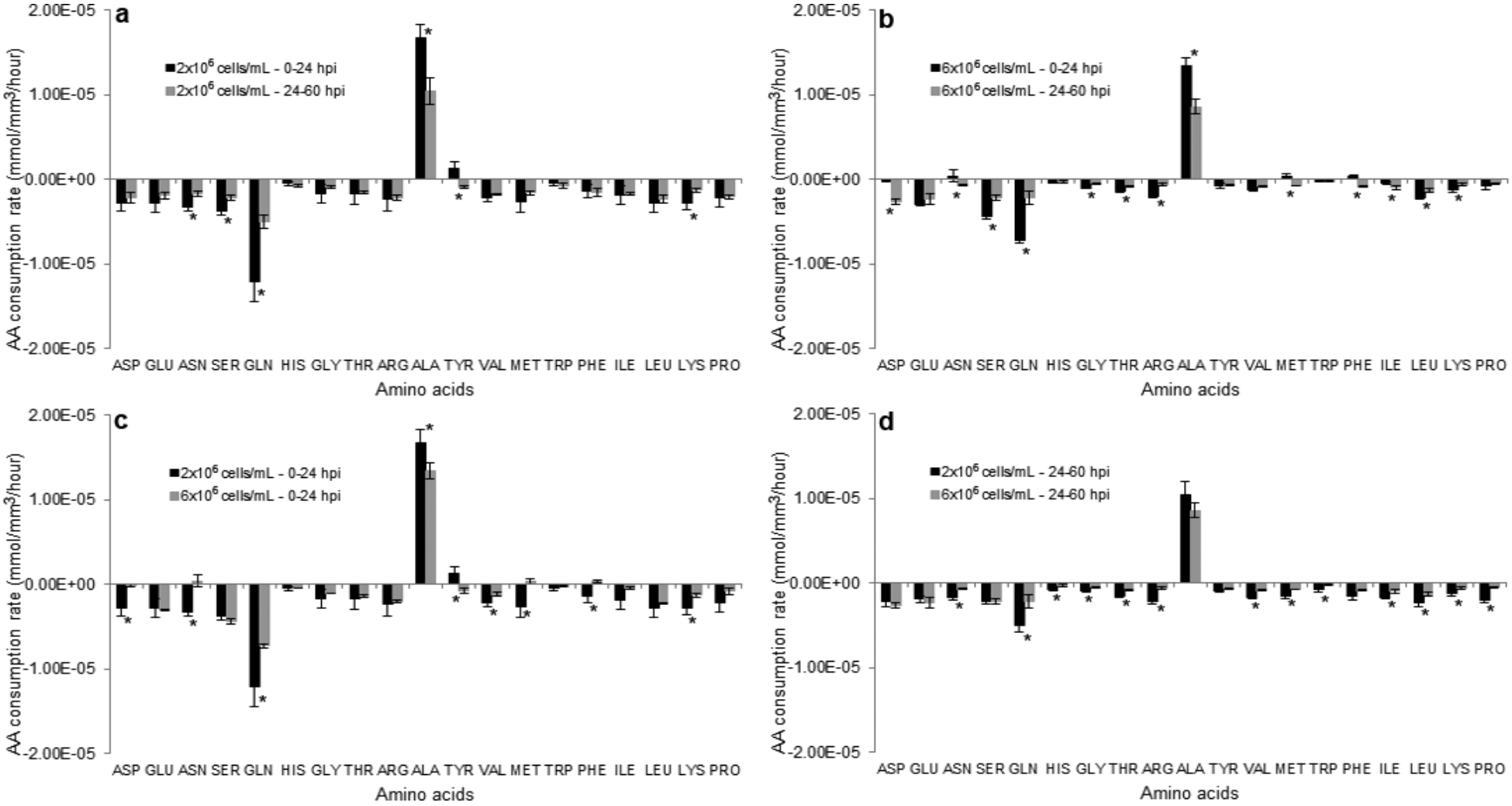

Fig. 4.8 AA consumption rates (mmol/mm^3 cell biomass/hour) between early (0-24 hpi) and late (24-60 hpi) infection stages for low (a) and high ICD (b) and between low and high ICDs for early (c) and late infection (d) of Sf9 cells infected with a rAcMNPV. Infections were conducted in Sf900™III at low (2×10^6) and high (6×10^6 cells/mL) ICDs and at an MOI of 10 PFU/cell. The experiment was conducted in shaker-flask suspension cultures. Each data point is the average from three biological replicates, and the error bars represent the standard deviation.

4.3.5 Ratios between high and low ICDs and between intra- and extracellular AAs

When comparing AA concentrations between high and low ICDs, Fig. 4.9 a, b shows that extra- and intra-cellular AA levels of infected cells at the high ICD were generally lower than those for the low ICD, as indicated by the ratios of high/low ICD AA values being less than 1 for the majority of the AAs. At 0 hpi, the ratios of high/low ICDs for extracellular AA levels were mostly similar to those for intracellular AA levels (Fig. 4.9a). At the late infection stage (36 hpi), ratios were almost maintained for extracellular AA levels, while those for intra-cellular AA levels were reduced significantly. Therefore, ratios of high/low ICDs for extracellular AA levels, at 36 hpi were significantly higher than those for intracellular AA levels for the majority of AAs (14 out of 19 AAs) (Fig. 4.9b). This result indicates a possibly poorer AA uptake into the cells at the late stage of virus infection for infected cells at the high ICD compared with those at the low ICD. Serine, glutamine, threonine, tyrosine, leucine and lysine are among the AAs that have low intracellular levels at the high ICD compared with the low ICD, (ratio of AAs between high/low ICDs less than 0.5).

When comparing the ratios of intra-/extra-cellular AA levels for low and high ICDs, these two ratios were also similar among the majority of AAs at 0 hpi (Fig. 4.9c). It is of interest that the intra-/extra-cellular ratios for most AAs for both low and high ICDs are close to one (16 out of 19 AAs). This suggests that the AA uptake by cells in culture before and after infection reaches an equilibrium of the AAs in the cell with the level in the external medium or alternatively that the external AA level dictates the extent of AA uptake. This in turn suggests the only way to keep intracellular AA levels high is to have high AA levels in the external media. At 36 hpi, these ratios increased in the case of the low ICD (more AAs had a ratio above 1), but they decreased significantly in the case of the high ICD (Fig. 4.9d). As a result, ratios of intra-/extra-cellular AA levels for the low ICD were significantly higher than those for the high ICD in many of the AAs (12 out of 19 AAs investigated). Again this result indicates low intracellular AA levels of infected cells for the high ICD in comparison with the low ICD.

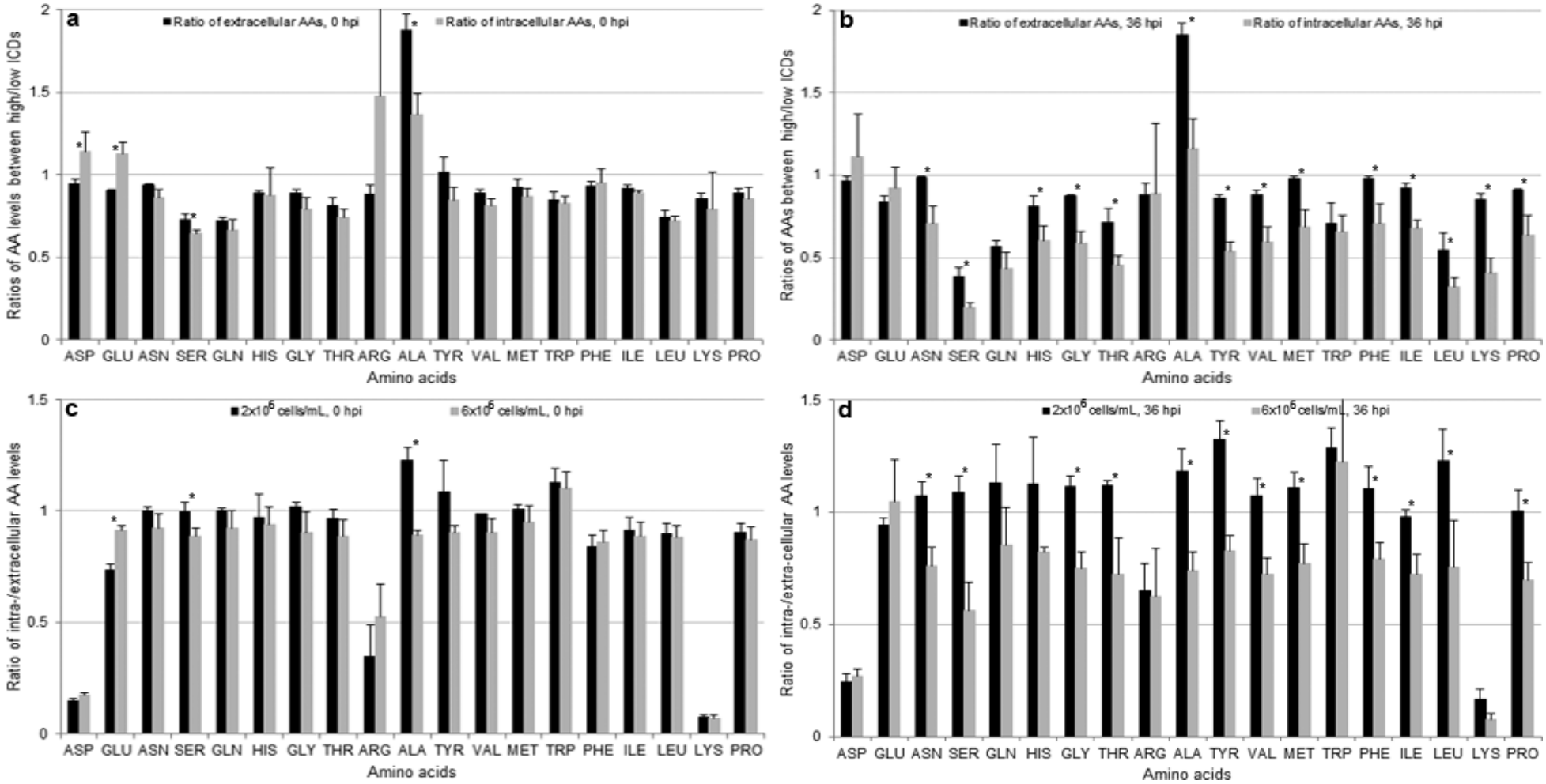

Fig. 4.9 Ratios of AA levels between high versus low ICDs for extra- and intra-cellular AAs at 0 hpi (a) and 36 hpi (b) and ratios between intra- versus extra-cellular AA levels for low and high ICDs at 0 hpi (c) and 36 hpi (d) of Sf9 cells infected with a recombinant baculovirus (rAcMNPV). Infections were conducted in Sf900™III at low (2×10^6) and high (6×10^6 cells/mL) ICDs and at an MOI of 10 PFU/cell. The experiment was conducted in shaker-flask suspension cultures. Each data point is the average from three biological replicates, and the error bars represent the standard deviation.

4.4 Discussion

A quantitative and reproducible intracellular metabolite extraction protocol for infected Sf9 cells has been developed previously (Tran et al., 2012). However, this previous report only evaluated the one time point post-infection of 24 hpi. Since baculovirus infections ultimately kill the cells, accurate profiling of intracellular metabolite levels is likely to be restricted to a relatively short timeframe post-infection, prior to significant cell lysis. Therefore, it was necessary to investigate the extent of this timeframe, which is important for determining the dynamics of the endometabolome post-infection before designing subsequent studies to explore whether limitations in the endometabolome are implicated in the decline in productivity when insect cells are infected at high cell densities.

At a high MOI infection (e.g ≥ 5 PFU/cell), rAcMNPV infected Sf9 cells exhibit a synchronous infection pattern leading to a minimal increase in cell density post-infection (O'Reilly et al., 1994; Wong et al., 1996). With an MOI of 10 PFU/cell, the cell density increase post-infection of the two experiments in this report was less than half of a cell doubling (Fig. 4.1 a, 4.2 a). The cell growth post-infection together with the cell diameter enlargement post-infection (Fig. 4.1 a, 4.2 a) as well as the timing of virus replication, β-Gal production and the peak virus yields (Fig. 4.1 b, 4.2 b) were typical for rAcMNPV infected Sf9 cells and were similar to those reported previously for these ICDs (Huynh et al., 2013). In addition to a reduction in cell diameter after 48 hpi, the cell viability also significantly declined after that point (Fig. 4.1 a, 4.2 a). The decrease in cell diameter and viability after 48 hpi means that the membrane integrity was affected and hence, the accuracy of intracellular metabolite measurements would be impacted when infected cells are processed through the quenching and washing steps prior to extracting intracellular metabolites. These results indicate that these infected cultures were suitable for further investigation of extra- and intra-cellular metabolite patterns, as they display typical behaviour for infected cultures for this cell line/virus system.

As reported previously (Tran et al., 2012), the recovery of ATP in the cell extract compared to direct extract controls is one of the key indicators for evaluating the efficiency of the extraction protocol for intracellular metabolite studies. This is because ATP has a rapid turnover rate of 1.5 mM/s (de Koning and van Dam, 1992; Theobald et al., 1997; Weibel et al., 1974) and it is present in the cell at high levels given its role of energy supply for the cell. The ATP recovery reduced after 48 hpi and the intracellular ATP level of the cell extract samples also significantly decreased after that point (Fig 4.1c). The drop in intracellular ATP after 48 hpi has previously been reported (Olejnik et al., 2004). In addition, the intracellular AA levels of the cell extract also showed a significant reduction at

60 and 72 hpi (Fig. 4.1 d). All together, these results indicate that the extraction protocol was effective for infected Sf9 cells up to 48 hpi.

It is known that the cell specific yield of foreign proteins expressed by recombinant baculoviruses drops when the cell density at the time of infection increases. The phenomenon has been widely reported in the literature (Carinhas et al., 2009; Caron et al., 1990; Chakraborty et al., 1996; Chan et al., 2002; Doverskog et al., 2000; Huynh et al., 2013; Radford et al., 1997; Taticek and Shuler, 1997; Wong et al., 1996). A recent study for Sf9 cells infected with a rAcMNPV (Huynh et al., 2013) indicated that the reduction in cell specific protein yield for infections at high cell densities was related to a reduction in the upstream processes of vDNA replication and lacZ mRNA transcription. However, there is still limited information on the differences in intracellular metabolite levels as well as the uptake rates of metabolites from culture medium between cells at low and high ICDs. Thus there is a need to investigate whether there are any differences in uptake rates of key nutrients and the intracellular metabolite levels between low and high ICDs during the time-course of such infections.

As reported previously (Huynh et al., 2013), the specific β-Gal yield (expressed under control of the polyhedral promoter by a rAcMNPV as used in this study), reduced linearly with the increasing ICD, commencing at 1×10^6 cells/mL. In the current study, the ICD of 2×10^6 cells/mL was chosen instead of 1×10^6 cells/mL to represent a low cell density infection since the cell specific β-Gal yield of the former was comparable to the latter (~80%) (Huynh et al., 2013) and it is more accurate to calculate the consumption rates (glucose and AAs) for a culture infected at 2×10^6 cells/mL instead of 1×10^6 cells/mL. For the high cell density case, the ICD of 6×10^6 cells/mL was selected as it still provided a reasonable specific β-Gal yield (~0.05U/cell) and there was a good contrast in specific β-Gal yield between the low (2×10^6 cells/mL) and high (6×10^6 cells/mL) ICDs of approximately 3-fold based on the data of Huynh et al. (2013). Therefore, these two ICDs represented the low and high ICDs for the process of investigating the difference in intra- and extracellular metabolite due to variations in the ICD for this report.

At 0 hpi, the TCP (total cell protein) level was in the range of 130-180 pg/cell (Fig. 4.2 c), which was similar to the TCP of uninfected cultures for the cell density range of 0.5-8×10^6 cells/mL (data not shown) and was also comparable with that reported by (Wickham et al., 1992) for Sf9 cells of 204 pg/cell. The TCP was similar between the low and high ICDs until 24 hpi, the time β-Gal production commenced. After that the TCP of infected cells at the low ICD increased faster than that of the high ICD case. At 60 hpi the gap in

TCP between these two ICDs was 81 pg/cell, while the gap in β-Gal protein yield between these ICDs was 57 pg/cell. A difference of 24 pg/cell indicates that apart from higher β-Gal production, low ICD cells also produced more non-β-Gal protein compared to the high ICD cells. It would be expected that the cells need to produce other proteins to support β-Gal protein production and the more β-Gal produced, the more supporting protein that would be required. Another possible explanation is that the conversion factor of 800 pg of protein/U β-Gal may be an under estimation. Due to cell lysis after 60 hpi, it is difficult to measure total cell protein accurately at the time of the peak β-Gal yield (72-96 hpi).

Generally, the intracellular metabolite levels at the low ICD were higher than those at the high ICD (Fig 4.3 a). The multivariate analysis (Fig. 4.3 b) highlighted the metabolites that showed the most significant differences between low and high ICDs and among the various time points post-infection (Table 4.2).

The concentrations of nucleotide tri-phosphates (ATP, UTP, GTP and CTP) at the low ICD tended to be higher than those at the high ICD (Fig 4.5 a-d).This suggests a possible limitation in building blocks for vDNA and mRNA production at the high ICD. Low levels of intracellular nucleotide tri-phosphates with increasing ICD may lead to the limitation of deoxyribose nucleotide tri-phosphates that are required for DNA synthesis. As a result, vDNA and mRNA levels decrease with increasing ICD (Huynh et al., 2013). The nucleotide di- and mono-phosphates are higher in concentration at the high ICD and at later stages of infection, especially adenosine and guanosine (Fig. 4.5 a-d), most likely indicating that more energy was used in the case of the high ICD or late infection stage, or the cell struggled to maintain energy levels in these cases. This may be the result of deterioration of the glycolytic and TCA energy production pathways at the late infection stages.

Among the intracellular organic acids, the TCA cycle intermediates including α-ketoglutarate (KGA), fumarate (FUM), citrate (CIT), succinate (SUC) and pyruvate (PYR) were found to be significantly different between the low and high ICDs (Fig 4.4 a-e). In particular, the KGA levels at 0, 12, 24 and 36 hpi for the low ICD were significantly higher than those for the high ICD. The intracellular concentrations of PYR and FUM at the low ICD also tended to be higher than those at the high ICD, whereas intracellular SUC concentrations were higher post-infection for the high ICD case compared to those for the low ICD case and they tended to increase during the later stages of the infection for the high ICD case (Fig. 4.4). KGA and PYR were found to be limiting at high cell density infections and the supplement of either PYR or KGA at the time of infection has been

previously shown to result in an improvement of budded virus yields by 6-7 fold (Carinhas et al., 2010). It is possible that the lower level of KGA in the high ICD case may contribute to the lower yield at the high ICD as it is a key metabolite that can be supplied into the TCA cycle through glutamine and glutamate. However, low intracellular concentrations of KGA and PYR at the high ICD case may not link directly to the extracellular levels of these metabolites as no differences were found in the extracellular levels of KGA and PYR between low and high ICDs (Fig. 4.10). The low intracellular KGA concentration at the high ICD may derive from the low intracellular glutamine concentration (Fig. 4.6 c, d) and low glutamine consumption rate (Fig. 4.7) for the high ICD in comparison with that for the low ICD cases.

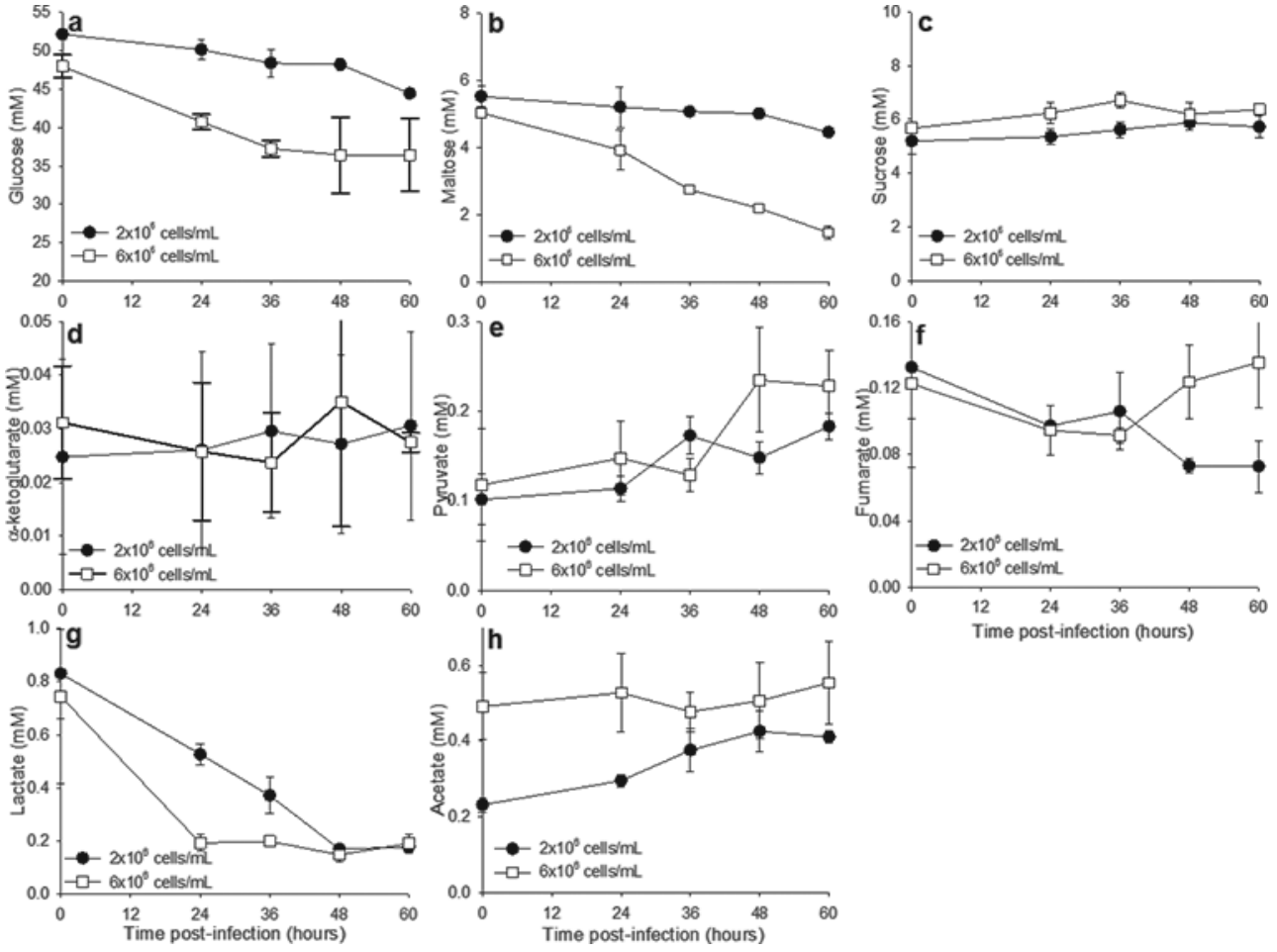

Fig. 4.10 Extracellular concentrations of sugars and organic acids for infected Sf9 cells at low (2×10^6) and high (6×10^6 cells/mL) ICDs over various times post-infection. Infections were conducted in Sf900™III serum free medium at an MOI of 10 PFU/cell in shaker-flask suspension cultures. Each data point is the average from three biological replicates, and the error bars represent the standard deviation

Glucose consumption rates for uninfected and baculovirus infected Sf9 cells have been extensively reported in the literature (Benslimane et al., 2005; Bernal et al., 2009;

Kamen et al., 1996; Radford et al., 1997; Raghunand and Dale, 1999; Rhiel et al., 1997; Wong et al., 1994), but the values vary considerably, possibly due to cell size differences reported for the Sf9 cell line used. The consumption rate varied in the range of 4.52-12×10^{-11} and 2.07-24.2×10^{-11} mmol/cell/hour for uninfected and infected Sf9 cells propagated in Sf900™II medium, respectively. Raghunand and Dale (1999) reported that there is an increase in glucose consumption rate after infection, while others showed a reduction in the consumption rate post-infection (Bernal et al., 2009; Rhiel et al., 1997; Wong et al., 1994). In the current study, the glucose consumption rate/cell was the highest for infected cells at the low ICD followed by infected cells at the high ICD and then the uninfected cells (Table 4.3). For infected cultures, the glucose consumption rate was similar between the low and high ICDs during the first 24 hpi. However, the consumption rate of infected cells at the low ICD was significantly higher than that at the high ICD at the later stage of infection, 24-60hpi (Table 4.3). The consumption rate of infected Sf9 cells in the current study was similar to that reported by Bernal et al. (2009), and Wong et al. (1994), whereas, the glucose consumption rate for uninfected Sf9 cells (25.6×10^{-12}mmol/cell/hour) was lower than most values reported in the literature. The discrepancy in the glucose consumption rate on a per cell basis among the literature may result from the differences in cell size. Calculations based on the unit of cell biomass show that the glucose consumption rate was not significantly different among uninfected and infected cells at low and high ICDs (Table 4.4). In addition, the glucose consumption rate of cells in culture may be influenced by the presence of other carbohydrate sources (maltose) and AAs used as an energy source (glutamine, asparagine) as well as other elements available in the medium. The interdependence of glucose and glutamine uptake for Sf9 insect cells has been reported elsewhere (Bedard et al., 1993; Drews et al., 2000; Neermann and Wagner, 1996; Raghunand and Dale, 1999).

Although the AA consumption rates varied from the literature (Bernal et al., 2009; Radford et al., 1997) probably due to the differences in cell size, the reduction in consumption rates with increasing ICDs has been found for most of the AAs (Bernal et al., 2009). Generally, AA consumption rates of infected cells at the low ICD were higher than those at the high ICD, whereas consumption rates of the uninfected Sf9 cells were intermediate but in general closer to the high ICD consumption rates for most of the AAs (Table 4.3). However, AA consumption rates of uninfected cells were the highest for most of the AAs and AA consumption rates for the low ICD were significantly higher than those for the high ICD when calculated on a unit of cell biomass basis (Table 4.4). This means that the AA consumption rate per cell biomass was reduced for infected cells in

comparison with uninfected cells and the reduction was more severe for the high cell density infection. Over the post-infection period, consumption rates of most AAs at the early stage were generally higher than those of the late infection stage (Fig. 4.7 a, b), indicating a possible limitation for protein production post-infection as compared to uninfected cells. The limitation post-infection was more severe for high cell density infections (Fig. 4.7 b, c, d). These results indicate that the efficiency of AA uptake reduced post-infection as well as with an increase of the ICDs. This may contribute to the reduction in β-Gal yield with increasing ICD regardless of the fact that the uninfected culture is still doubling as normal after that high cell density (6×10^6 cells/mL) to the peak cell density of $1.8\text{-}2\times10^7$ cells/mL.

Although intracellular AA levels do not necessarily reflect the flux of AA into the cell and subsequent utilisation for protein synthesis, the measurement of intracellular AA levels at various times post-infection reveals whether there is a change in intracellular AA concentrations post-infection. As the result of possible poorer AA uptake rates at the late infection stage as well as at high cell densities at the time of infection, intracellular AA levels in mM were found to be stable or to reduce post-infection, especially for the case of the high ICD (Fig. 4.6 a, b). The intracellular AA levels that were found to be reduced post-infection were glutamine and to a lesser extent asparagine, valine, isoleucine and proline for the high ICD case since these AA are not only used as building blocks for protein synthesis but also as a possible energy source (Drews et al., 1995), and so these AAs may be utilized at a much higher rate than would be the case if they were consumed for protein synthesis alone (Ferrance et al., 1993). The only case of an increase in intracellular concentration post-infection was for alanine. Alanine is the main by-product of nitrogen metabolism by Sf9 cells (Bedard et al., 1993; Benslimane et al., 2005; Drews et al., 2000; Ohman et al., 1995). As a result of possible poor AA uptake rates post-infection, as well as with the increasing ICD, the intracellular AA levels of the low ICD were significantly higher than those of the high ICD for the majority of AAs at both 0 and 36 hpi (Fig. 4.6 c, d). The differences in intracellular AAs levels between low and high ICDs were more significant at the later stage in the virus infection process (36 hpi), with a significant difference being found for 15 out of 19 AAs investigated (Fig. 4.6 d). Poorer uptake rates for AA, resulting in lower intracellular AA levels, particularly during the late stage of baculovirus infections at high cell densities could be partially responsible for the reduction in cell specific yields with increasing ICDs.

The poorer uptake efficiency for the high ICD compared with the low ICD found above was clearly indicated through the ratios between high and low ICDs for extra- and

intra-cellular AA levels at 0 and 36 hpi (Fig. 4.9 a, b). Extra- and intra-cellular AA level ratios of high over low ICDs were <1 in most cases. The ratios of high over low ICDs for intra-cellular AA levels were significantly lower than those for extra-cellular AA ratios at 36 hpi but less significant at 0 hpi, indicating that the AA uptake efficiency reduced significantly in combination with the increase in ICD and the time post-infection. In addition, the active uptake of AAs seemed to increase over the time post-infection for the low ICD (compare intra/extra cellular ratios for 2×10^6 cells/mL at 36 hpi in Fig 4.9 d, versus the corresponding ratios at 0 hpi in Fig 4.9 c), but significantly decreased for the high ICD (compare intra/extra cellular ratios for 6×10^6 cells/mL at 36 hpi in Fig 4.9 d versus the corresponding ratios at 0 hpi in Fig 4.9 c). These Figures also indicate that the uptake efficiencies for aspartate, arginine and lysine were very poor compared to the other AAs. These AAs may be the first ones to become limiting for recombinant protein production, especially arginine and lysine as they are both essential AAs.

4.5 Conclusion

The cell density effect in baculovirus infected insect cells is a complex phenomenon that relates to many factors and the interaction among them. Of these factors, nutrient limitation is an important consideration as the cell specific yield is often recovered when fresh medium or fed-batch approaches are used for high density infections (Chan et al., 1998; Huynh et al., 2013). However, nutrient limitation may not only be related to the depletion of particular nutrients in the medium but may be also related to the uptake efficiency of nutrients into the cells at the late infection stage in the case of high infection cell densities. Results from the current study shows that there was a reduction in intracellular nucleotide tri phosphate concentrations when the infection cell densities increased. As a result, there may be a limitation in the availability of substrates for nucleic acid synthesis that may account for the low vDNA and mRNA production levels previously reported for high density infections (Huynh et al., 2013). In addition, infected Sf9 cells at a high ICD had lower intracellular AA levels as well as possible lower AA uptake efficiencies at the late infection stage in comparison with those at the low ICD. The lower AA uptake rates with increasing ICD may be the result of cell regulation due to lower AA requirements for protein synthesis, which was affected from the reduction in vDNA and mRNA levels at the high ICD. Lower AA consumption rates with increasing ICD may be also the result of the poor active transport of AAs by infected cells at the high ICD during the late stage of protein production. Serine, glutamine and leucine are among possible limiting AAs at high

ICDs, while aspartate, lysine and, to a lesser extent, arginine are among AAs showing a poor uptake efficiency. Furthermore, intracellular organic acid concentrations and in particular, TCA cycle intermediates, were also found to be reduced for high ICDs. Overall the data shows a reduction in the cell metabolism capacity with increasing cell density which may lead to a reduction in the cell specific yield at high cell densities.

Chapter 5

Metabolic study of the cell density effect -Sf9/rAcMNPV in chemically defined medium

5.1 Introduction

The media used for culturing insect cells currently in this thesis is serum free, whereby the growth factors, lipids and shear protectants normally provided by serum are supplied alternatively by protein hydrolysates and a manufactured lipid emulsion which contains the shear protectant Pluronic F-68. The use of hydrolysates in insect cell culture medium is considered as a revolution in serum free medium (SFM) development. However, the reliance on hydrolysates for supplying amino acids and growth factors has disadvantages in terms of the lot to lot variability of these undefined components (Reid et al., 2013). The variations of materials and processes for hydrolysate production lead to the variations of the medium and ultimately the cell culture process (Pasupuleti and Braun, 2010). Although ultrafiltration processes may help to improve the consistency, the underlining variability in chemical composition is still present (Reid et al., 2013). In addition, hydrolysates also provide an amount of undesirable components together with desirable ones. Desirable components include amino acids, peptides and low molecular weight growth factors while undesirable components include high levels of inorganic salts, leading to high osmolarities (Pasupuleti and Braun, 2010), and possibly some undefined components imparting cellular toxicity (Lu et al., 2007). Other problems associated with protein hydrolysates include a wide divergence in aqueous solubility that limits their inclusion at high levels, especially in concentrated feeds.

The problems associated with hydrolysates may be addressed by the development of a chemically defined medium (CDM). CDM are also useful for metabolomics and fluxomics studies as all the ingredients are chemically defined. Although it is feasible to gain some metabolic insights using insect cells propagated in hydrolysate containing media, the replacement of hydrolysates by chemically defined substitutions would enhance the range and scope of metabolic studies (Bhatia et al., 1997). Currently, CDM formulations are well established for mammalian cell culture, but are not yet available for insect cell culture (Reid et al., 2013). However, it should be feasible to have a CDM for insect cell culture as insects have generally similar nutritional requirements to that of vertebrates, and there are high levels of similarities in the chemical composition between insect and mammalian basal media (Schlaeger, 1996). Fortunately, a CDM was made available for testing by Life Technologies for inclusion in the studies of this thesis.

This chapter aims to investigate the adaptation of Sf9 insect cells to the CDM provided and to study such adapted cells during cell growth and baculovirus infections in relation to the cell density effect. The intracellular metabolite concentrations and the

consumption rates of substrates of infected Sf9 cells in CDM at low (1×10^6 cells/mL) versus high (5×10^6 cells/mL) infection cell densities (ICDs) are investigated. The chapter also examines differences in the intracellular metabolite levels of the Sf9 cells in a fully chemically defined medium compared to that for cells in Sf900™III, especially for high cell density infections. The CDM contains no peptides, and the free amino acid levels of most amino acids (except for glutamine and alanine) are higher than that in Sf900™III (Fig. 5.1). The difference in amino acid (AA) concentrations between these two media vary from 4% for glycine to 108% for leucine, but generally they are within the range of 30-60% higher for most of the AAs in the CDM compared to Sf900™III. In addition, substrate consumption rates and intracellular metabolite levels of infected cells at low and high ICDs were measured and compared between these two infection conditions using the available CDM as a comparison to the results obtained in Chapter 4 using the commercially available Sf900™III medium.

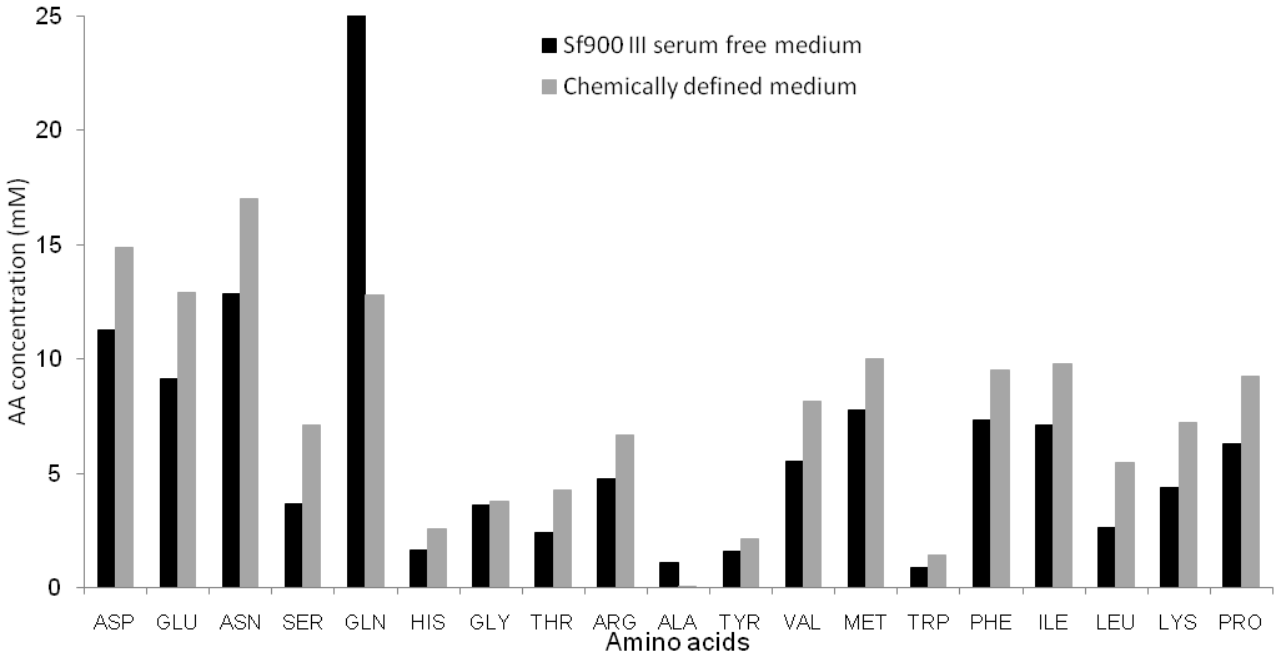

Fig. 5.1 Free AA concentrations of Sf900™III and CDM media. Sf900™III would be expected to contain other AAs in the form of small peptides from the yeast hydrolysate present in the medium. However the AA levels shown for the CDM are expected to represent the total AA concentration present in the medium.

5.2 Materials and methods

5.2.1 Cell line, virus stock and medium

The *Spodoptera frugiperda* clone 9 cell-line (Sf9; ATCC CRL 1711) and a recombinant *Autographa californica* multiple nucleopolyhedrovirus (rAcMNPV) expressing

an *E. coli* LacZ gene under the control of the polyhedrin promoter used in this study have been described previously (Chan et al., 1998; Wong et al., 1996). Working stock cells were maintained by regular passaging every 3-4 days in single-use shaker flasks (Corning, Lowell, MA) at seeding densities of 4-5×10^5 cells/mL. The shaker cultures were agitated at 120 rpm on an orbital shaker platform (Thermoline, NSW, Australia) and incubated at 28^{o}C in a refrigerated incubator (Thermoline). The preparation of virus stock was described in previous publications (Huynh et al., 2013; Tran et al., 2012). Virus stocks were stored at 4^{o}C, and were titered prior to use. The titers of virus stocks were around 1-1.5×10^9PFU/mL as determined by using a modified endpoint dilution method (Nielsen et al., 1992). The prototype chemically defined medium (CDM) (Life Technologies, USA) was used in all of the experiments. Sf9 cells propagated in Sf900™III medium were used as a control.

5.2.2 Experimental procedures

Sf9 cells in Sf900™III medium were first adapted into the CDM. Cells were then passaged in CDM for 5 passages prior to cryo-preserving in liquid nitrogen. Sf9 cells used in the current study were from frozen stocks stored in liquid nitrogen which had previously been adapted to the CDM. The stability of cell growth in the CDM was recorded over 14 passages of 3-4 days each at the seeding cell density of 0.4-0.5×10^6 cells/mL. Sf9 cells in Sf900™III were routinely passaged in parallel with Sf9 cells in CDM as a control. A growth curve was conducted of uninfected Sf9 cells propagated in either Sf900™III or CDM using biological triplicates. Cultures in shaker flasks were seeded at 0.5×10^6 cells/mL and left to grow over 7 days. Total cell density (TCD) and viability were recorded everyday over the above period. The ability to support a baculovirus infection of the Sf9 cells in the CDM was also investigated at both a low (1×10^6) and a high (5×10^6 cells/mL) ICD in triplicate. Infections were conducted with a rAcMNPV virus stock prepared in Sf900™III at a multiplicity of infection (MOI) of 10 PFU/cell.

The experiment investigating the changes in the intra- and extra-cellular environment as well as the β-Gal production and metabolite consumption rates of infected Sf9 cells in CDM at a low and a high infection cell density (ICD) was as follows. The initial seeding cell density was at 0.5×10^6 cells/mL after which they were left to grow to 1×10^6 cells/mL (about 24 hours post-inoculation), and then the cells were infected with the virus. This case represented the low cell density infection. For the case of a high cell density infection, cells were allowed to grow to around 5×10^6 cells/mL (72 hours post-inoculation) prior to infection with the virus inoculum. All of the infections were conducted at an MOI of 10

PFU/cell. The experiment was conducted in shaker flasks with biological triplicates at each cell density. Samples for intracellular metabolite analysis were taken at 12 hour intervals from 0-48 hpi in duplicate. Samples for extracellular metabolite analysis and for measuring TCD, viability and β-Gal yield were collected from 3 infected control shakers at 12 hour intervals from 0-96 hpi. An uninfected control was also set up and left to grow to a peak cell density in batch culture (1-1.2×10^7 cells/mL).

5.2.3 Intracellular metabolite extraction

Intracellular metabolites were extracted using the optimized protocol as described previously (Tran et al., 2012). Briefly, infected cultures were set up in 125 mL shaker flasks at a working volume of 20 mL, involving three flasks for each treatment at each time point as biological triplicates. Quenching solution (QS) (1.1% NaCl, 0.2% Pluronic F68) was prepared in 250 ml shaker flasks at 80 mL each and placed in an ice bath to make sure the temperature of the quenching solution was around 0.5 to 1^{o}C. The culture of each flask (20 mL) was quickly poured into 80 mL of ice-cold QS straightaway after taking out from the incubator. The quenched culture was then centrifuged (1000× g, 1 min) at 0^{o}C. The supernatant was removed and the cell pellet was washed with the sample volume of ice-cold QS. Another centrifugation step was applied (1000× g, 1 min, 0^{o}C) to collect the cell pellet which was then extracted with a cold 50% acetonitrile (ACN) solution at the ratio of 1 mL for 2×10^6 cells. The cell extracts were clarified by centrifugation (5000×g, 5 min, 0^{o}C), with the supernatants collected, frozen at -80^{0}C and then dried in a freeze-dryer (Alpha 1-4 LSC, Martin Christ, Germany). The freeze-dried samples were then stored at -80^{0}C until analysed. For the direct extract, infected cultures were poured directly into the same volume of 100% ACN and then the supernatants were collected for subsequent steps as described above with the cell extract samples.

5.2.4 Assays

Total cell density (cell/mL) and cell diameter was estimated using a Multisizer^{TM}4 Coulter Counter (Beckman Coulter, Fullerton, CA, USA). Samples of various cell densities were initially diluted with medium to a TCD of around 0.5×10^6 cells/mL before proceeding with the cell enumeration process. Cell viabilities were estimated from triplicated hemocytometer counts using the 0.05 %w/v Trypan Blue exclusion method (Nielsen et al., 1991).

The β-Gal protein yield of infected whole-culture samples was quantified using a well-established colorimetric assay based on the enzymatic hydrolysis of ONPG, as described previously (Power et al., 1994; Radford et al., 1997; Wong et al., 1996). Briefly, fresh samples were initially diluted appropriately with MiliQ water, and then 50 µL of the diluted sample was added into 950 µL Z buffer (0.06M Na_2HPO_4, 0.04 M NaH_2PO_4, 0.001 M $MgSO_4$, 0.01 M KCl and 0.035%v/v β-mercaptoethanol). The mixture was then incubated for 30 minutes at 37^oC after adding 200 µL of substrate (4 mg/mL ONPG). A stop buffer (1M Na_2CO_3) was added at 500 µL to terminate the reaction. The absorbance was measured at 420 nm using a spectrophotometer, and was accepted if it fell within the linear range (0.3-0.8) and converted to β-Gal activity units (U/mL) using Beer's Law (Chan et al., 1998).The β-gal assay of each sample was conducted three times as technical triplicates.

Intracellular nucleotides and TCA cycle intermediates were measured by LC-MS/MS as described in Dietmair et al. (2012) with the following modifications: the analytical column was equipped with a pre-column Security Guard Gemini-NX C18 4mm x 2 mm I.D. cartridge (Phenomenex, Aschaffenburg, Germany). The samples were run with sample- and analyte-relevant calibration standards and pooled QC samples (Hodson et al., 2009; Sangster et al., 2006) to control for reproducibility of data acquisition and to ensure data integrity. Analyte stock solutions were prepared in purified water (Veolia) and aliquots of each solution were mixed to achieve a final calibrant solution at 200 µM. This calibrant solution was serially diluted and the dilutions used as calibration standards from 200 to 0.006µM, constituting $9 \leq x \leq 20$ calibration points for all analytes to account for differential responses in the mass spectrometer. Data were processed and analysed in Analyst 1.5.2 and MultiQuant 2.1.1 (ABSciex, Canada).

A HPLC system was used to analyze extra- and intra-cellular amino acids (AAs) as described previously (Dietmair et al., 2010). Extracellular sugars (sucrose, glucose, maltose) were also analyzed by HPLC after samples had been hydrolyzed using 6M HCl (Radford, 1995). The HPLC analysis for AAs and sugars is described in detail in Chapter 2 of this thesis.

5.2.5 Statistical analysis

One-way analysis of variance (ANOVA), followed by Tukey's Honestly Significant Difference (HSD) test, was used to determine whether the means from two or more groups

of data were significantly different at the 95% confidence level. Minitab 15 Statistical Software (Minitab, State College, PA) was used for all data analysis.

5.3 Results

5.3.1 Adaptation of Sf9 cells into chemically defined medium (CDM)

Sf9 cells in Sf900™III serum free medium were adapted into a chemically defined medium for insect cell culture. The results show that Sf9 cells adapted well into the CDM within 7 days. Passaging of stock cells in CDM and Sf900™III as a control over 50 days (14 passages) is shown in Fig. 5.2 a. Over 14 passages, Sf9 cells propagated in CDM showed a reasonable growth rate with close to a 24 hour doubling time that was comparable to Sf9 cells propagated in Sf900™III medium. The viability of Sf9 cells in CDM was high within the range of 95-98% and was similar to that found in Sf900™III (Fig. 5.2a).

Figure 5.2 b shows the growth curve and viability of Sf9 cells propagated in either Sf900™III or CDM over 7 days post-inoculation. In CDM, uninfected Sf9 cells doubled almost every 24 hours during the first 3 days from 0.5 to 4×10^6 cells/mL and then slowed down and reached a peak cell density of around 1.2×10^7 cells/mL at 6 days and declined after that point. Whereas in Sf900™III medium, Sf9 cells grew faster to the peak uninfected cell density of 1.9-2×10^7 cells/mL at 5 days and slightly reduced in cell density after that time (Fig. 5.2 b). The cell viability remained at a high level (around 90% or higher) over 7 days post-inoculation for Sf9 cells propagated in both Sf900™III and CDM medium. This result indicates that Sf9 cells can adapt and grow well in CDM although the peak cell density achieved in CDM was much lower than that in Sf900™III medium.

For infected cultures, Fig. 5.2 c shows that CDM also supported good infected cultures in comparison with Sf900™III medium. At a high MOI of 10 PFU/cell, good infections were found (inhibition of cell growth post-infection in a similar time frame) for infected Sf9 cells in CDM and Sf900™III media at both low (1×10^6 cells/mL) and high ICDs (5×10^6 cells/mLfor CDM, and 6×10^6 cells/mL for Sf900III) (data not shown). β-Gal yields of infected cultures in CDM at a low ICD (1×10^6 cells/mL) was even higher than that in Sf900™III medium (0.23 vs 0.19 U/cell) (Fig. 5.2 c). The cell specific yield reduced with increasing ICD as was observed for Sf9 cells propagated in both media. At a high ICD, the peak specific β-Gal yield was about 0.08 and 0.06 U/cell for infected Sf9 cells in CDM and Sf900™III, respectively. Generally, the timing of β-Gal production was similar between infected Sf9 cells in Sf900™III and CDM media.

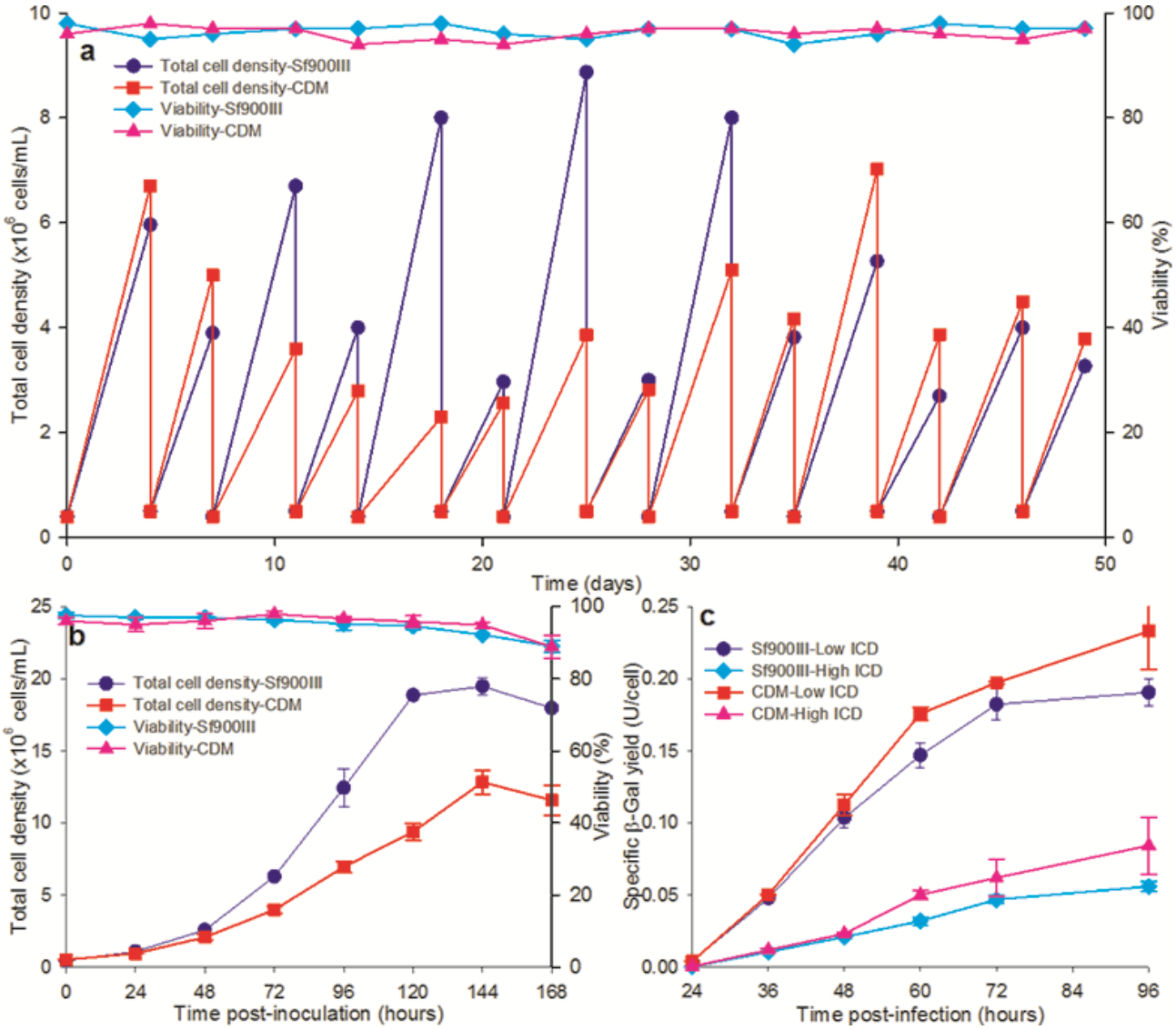

Fig. 5.2 Stock cell maintenance of Sf9 cells propagated either in Sf900™III (blue) or CDM (red) over 50 days (a). Cells were passaged every 3-4 days at a seeding cell density of 4-5×10^5 cells/mL. The growth curve of Sf9 cells propagated either in Sf900™III (blue) or CDM (red) over 168 hours post-inoculation (b). Cell specific β-Gal yield of Sf9 cells infected at an MOI of 10 PFU/cell either in Sf900™III or CDM at low (1×10^6 cells/mL) and high (6×10^6 or 5×10^6 cells/mL for Sf900™III or CDM, respectively) ICDs, (c). Cell cultures were maintained in shaker flasks with three biological replicates and the error bars are the standard deviation of the triplicates.

5.3.2 Investigation of intra- and extra-cellular metabolites for infected Sf9 cells in CDM at low and high ICDs

Total cell density, cell diameter increase post-infection and β-Gal yield of low vs high ICDs

The total cell density and viability, cell diameter and β-Gal yield post-infection for Sf9 cells propagated in CDM at low (1×10^6) and high (5×10^6 cells/mL) ICDs are presented in Fig. 5.3.

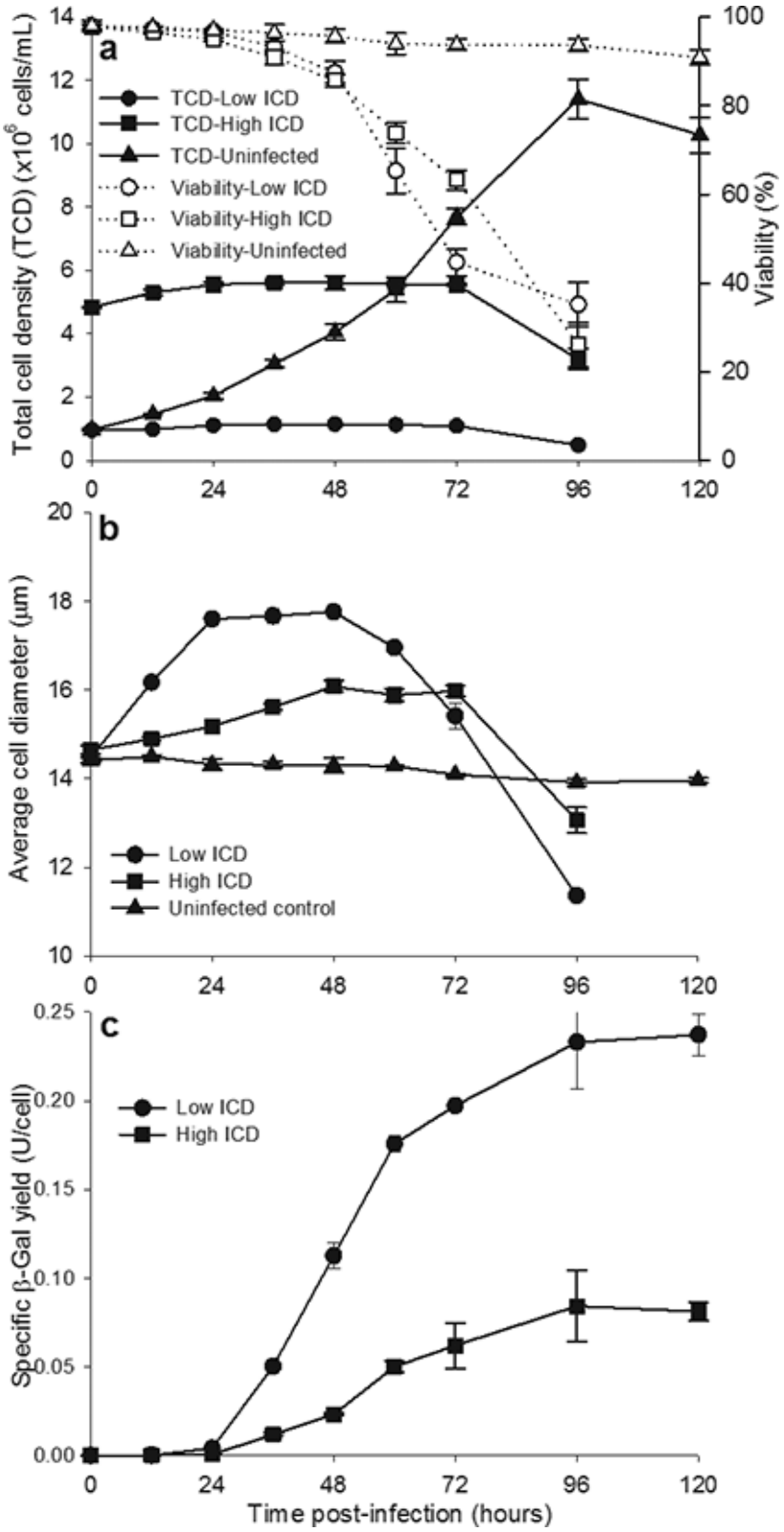

Fig. 5.3 The kinetics of cell growth and cell viability (a), cell size expansion (b) and specific β-Gal yield (c) of infected Sf9 cells propagated in CDM at low (1×10^6 cells/mL) and high (5×10^6 cells/mL) ICDs. Infections were conducted at a multiplicity of infection (MOI) of 10 PFU/cell in shaker-flask suspension cultures. Each data point is the average from three biological replicates, and the error bars represent the standard deviation.

There was no significant difference in cell density increase post-infection when infections were conducted at low or high ICDs, with an increase of 20% and 16% for low and high ICDs, respectively (Fig. 5.3 a). Whereas, the total cell density of the uninfected control increased as normal from the initial cell density of 1×10^6cells/mL up to the peak cell density of 1.2×10^7 cells/mL. The cell viability of infected cultures of both low and high ICDs remained at a high level (>80%) until 48 hpi and then declined significantly after that (Fig. 5.3 a). For the uninfected control, the viability remained as high as 90% beyond the point where the peak cell density was achieved. Although the cell density increase post-infection was similar between low and high ICDs, the cell diameter increase post-infection of the low ICD (23%) was significantly higher than that of the high ICD (10%) (Fig. 5.3 b).The cell diameter of the uninfected control was almost unchanged or slightly declined over the time post-inoculation. It is interesting to note that the size of the Sf9 cells in CDM and Sf900™III are similar (compare Fig. 5.3 b to Fig. 4.1 a and 4.2 a as presented in Chapter4).

Although the early events of the virus infection and cessation of cell growth were similar between low and high ICDs (Fig. 5.3 a), there was a contrast between these two ICDs in terms of cell specific yields (Fig. 5.3 c). The peak specific β-Gal yield for the low and high ICDs was 0.23 and 0.08 U/cell, respectively. However, the time frame from the starting point of β-Gal production to the point where peak yields were achieved was similar for both ICDs (Fig. 5.3 c). This indicates that the infection process follows a similar time sequence for low and high ICDs, but the β-Gal productivity during the post-infection period is lower for the high density infection.

Intracellular metabolite concentration of low versus high ICDs

Figure 5.4 presents the intracellular concentration of 34 metabolites (including nucleotides, nucleotide sugars and organic acids) of 4 time points post-infection (0, 24, 36 and 48 hpi) at low (1×10^6 cells/mL) and high (5×10^6 cells/mL) ICDs. The orthogonal projection to latent structures – discriminant analysis (OPLS-DA) of all the samples over the time course of infection (Fig. 5.4 a) showed a clear separation of low and high ICDs. Fig. 5.4a also indicates that the biological replication is reliable as the scores for the two replicates indicate similar positions in biochemical space. Based on the OPLS-DA loadings (Fig. 5.4 b), the metabolites most influential in the projected separation between low and high ICDs are the nucleoside triphosphates, nucleoside diphosphates, nucleoside monophosphates, UDP sugars (UDP-glucose, UDP-glucuronic acid, and UDP *N*-acetylglucosamine), α-ketoglutarate, fumarate, nicotinamide adenine dinucleotide

andnicotinamide adenine dinucleotide phosphate. These metabolites have a variable importance on projection (VIP) score of >1 and have been selected for further statistical analysis as detailed in Table 5.1. Generally, intracellular metabolite levels at the low ICD were higher than that at the high ICD (Table 5.1).

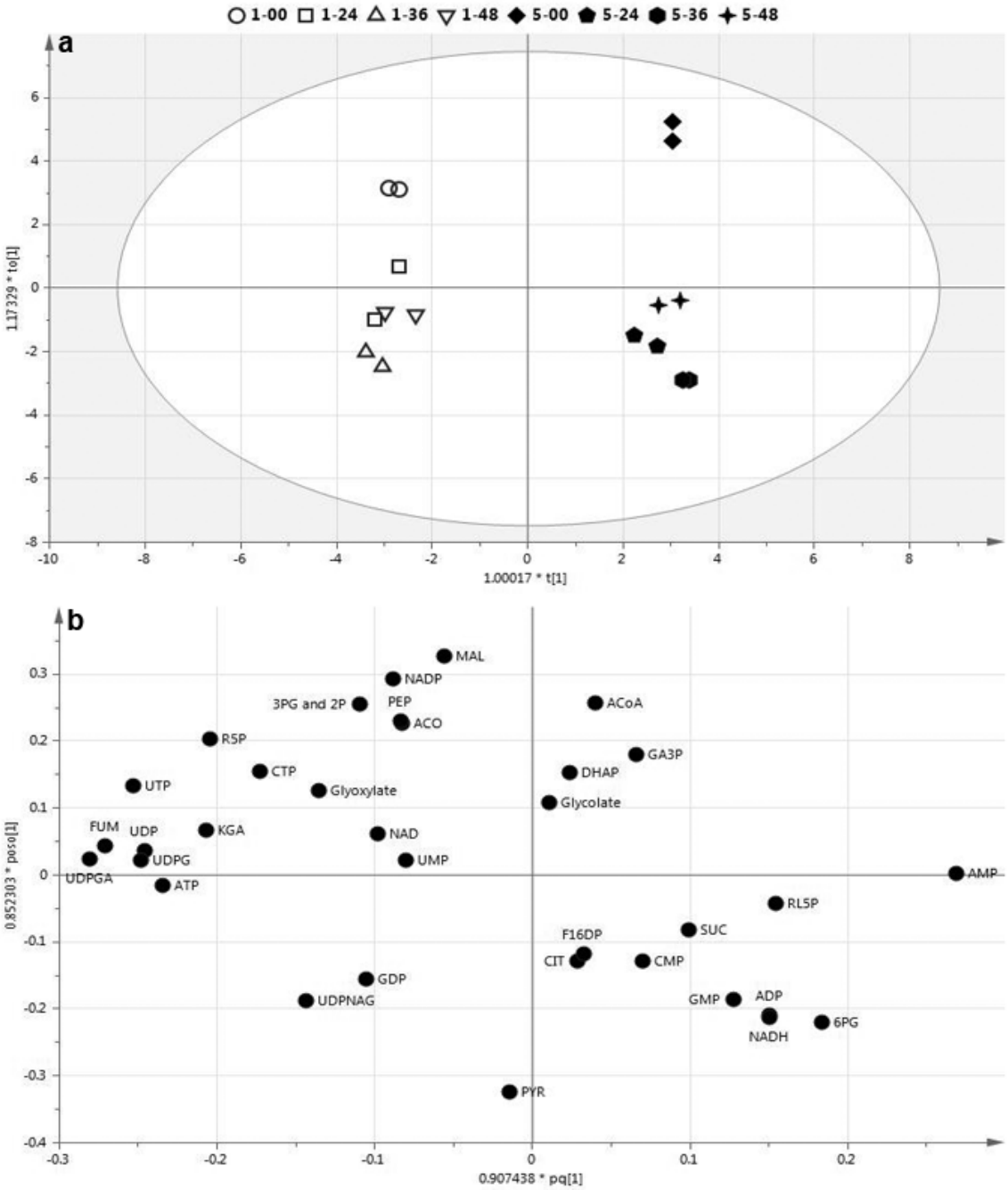

Fig. 5.4 Multivariate analysis of intracellular metabolite concentrations of infected Sf9 cells propagated in CDM at low (1×10^6 cells/mL) and high (5×10^6 cells/mL) ICDs. Orthogonal projection to latent structures–discriminant analysis (OPLS-DA) scores (a) and loadings (b) plots of the 4 time points post-infection at low and high ICDs, classified by cell density. OPLS-DA model metrics: Predictive component R2X = 0.279; R2 = 0.987; Q2 = 0.907; R2Y = 1: Orthogonal component R2X = 0.203. Infections were conducted at a multiplicity of infection (MOI) of 10 PFU/cell in shaker-flask suspension cultures.

Table 5.1. Intracellular metabolite concentrations (mM) over various times post-infection for Sf9 cells infected with a recombinant baculovirus (rAcMNPV) in a chemically defined medium at either low (1×10^6) or high (5×10^6 cells/mL) infection cell densities (ICDs). Data represented as an average of biological duplicates. The metabolites listed were selected on the basis of showing significant variations in levels between different ICDs or times post infection following the analysis shown in Fig. 5.4

Metabolites	Low ICD (1×10^6 cells/mL)				High ICD (5×10^6 cells/mL)				P<
	0 hpi	24 hpi	36 hpi	48 hpi	0 hpi	24 hpi	36 hpi	48 hpi	
Adenosine	8.882	9.64	9.78	9.53	9.39	9.59	9.69	9.66	NS
ATP	5.54^{abc}	6.83^{ab}	6.88^{a}	6.48^{abc}	5.25^{bc}	4.98^{c}	4.91^{c}	5.08^{c}	0.01
ADP	2.66	2.58	2.56	2.82	2.46	2.56	2.78	2.94	NS
AMP	0.61^{b}	0.23^{b}	0.34^{b}	0.23^{b}	1.68^{a}	2.04^{a}	2.00^{a}	1.63^{a}	0.001
UTP	1.79^{ab}	1.90^{a}	1.37^{bc}	1.26^{c}	0.64^{d}	0.66^{d}	0.38^{d}	0.76^{d}	0.001
UDP	0.43^{a}	0.38^{ab}	0.35^{ab}	0.27^{b}	0.07^{c}	0.11^{c}	0.03^{c}	0.27^{b}	0.001
UMP	0.27^{a}	0.11^{b}	0.09^{b}	0.06^{b}	0.02^{b}	0.15^{ab}	0.07^{b}	0.10^{b}	0.01
CTP	1.07^{c}	2.03^{a}	1.91^{ab}	1.23^{bc}	0.65^{c}	0.67^{c}	0.66^{c}	0.73^{c}	0.001
CMP	0.13	0.05	0.06	0.04	0.09	0.13	0.15	0.05	NS
GDP	0.48^{a}	0.31^{ab}	0.38^{ab}	0.28^{ab}	0.12^{b}	0.23^{ab}	0.42^{ab}	0.32^{ab}	0.05
GMP	0.14	0.05	0.07	0.04	0.19	0.13	0.29	0.08	NS
UDPG	2.38^{a}	2.56^{a}	2.28^{ab}	1.98^{bc}	1.56^{d}	1.89^{c}	1.88^{c}	1.54^{d}	0.001
UDPGA	0.54^{a}	0.46^{a}	0.51^{a}	0.45^{a}	0.14^{b}	0.22^{b}	0.23^{b}	0.26^{b}	0.001
UDPNAG	1.38^{ef}	2.12^{ab}	2.18^{a}	1.94^{abc}	1.24^{f}	1.74^{cd}	1.86^{bcd}	1.56^{de}	0.001
FUM	0.16^{a}	0.16^{a}	0.12^{ab}	0.12^{ab}	0.03^{c}	0.07^{bc}	0.05^{c}	0.05^{c}	0.001
KGA	0.13^{b}	0.22^{a}	0.05^{c}	0.05^{c}	0.02^{c}	0.02^{c}	0.01^{c}	0.02^{c}	0.001
NAD	1.48^{a}	1.27^{bc}	1.18^{bcd}	1.11^{cd}	1.02^{d}	1.27^{bc}	1.32^{ab}	1.05^{d}	0.001
NADP	0.11^{a}	0.06^{ab}	0.05^{ab}	0.05^{ab}	0.08^{ab}	0.06^{ab}	0.04^{b}	0.04^{b}	0.05

Data in the same row with different superscripts were significantly different at $P < 0.05$

Abbreviation: AMP, ADP and ATP: adenosine mono-, di- and tri-phosphate; UMP, UDP and UTP: uridine mono-, di- and tri-phosphate; CMP and CTP: cytidine mono- and tri-phosphate; GMP and GDP: guanosine mono- and di-phosphate; UDPG: uridine di-phosphate glucose; UDPGA: uridine di-phosphate gluconic acid; UDPNAG: uridine di- phosphate N-acetylglucosamine, FUM: fumarate; KGA: α-ketoglutarate; NAD: nucotinamideadenine dinucleotide; NADP: NAD phosphate

The concentrations of adenosine, uridine and cytosine tri-, di-, and mono-phosphates of infected Sf9 cells at low (1×10^6 cells/mL) and high (5×10^6 cells/mL) ICDs over the time course of infections are presented in Fig. 5.5 and Table 5.1. Intracellular ATP levels were not significantly different over the time course post-infection for both low and high ICDs (Fig. 5.5 a). However, ATP concentrations for the low ICD at 24 and 36 hpi were statistically higher than those for the high ICD at 24, 36 and 48 hpi (Table 5.1). In contrast, AMP concentrations at various times post-infection for the low ICD were significantly lower than those for the high ICD. Intracellular ADP concentrations were not different among treatments (Table 5.1, Fig. 5.5 a). As a result, the total adenosine (ATP+ADP+AMP) was similar among treatments (Table 5.1).

The trends for intracellular concentrations of uridine and cytidine tri phosphates were similar in that they reduced over the 24-36 h post-infection period, (Fig. 5.5 b, c). In addition, the nucleoside triphosphate (UTP and CTP) levels at the low ICD were statistically higher than those at the high ICD throughout the infection period, (Table 5.1). Uridine di- and mono-phosphate levels for the low ICD tended to be higher than those for the high ICD (Fig. 5.5 b, Table 5.1), while no difference among treatments was found in terms of intracellular CMP concentrations (Table 5.1).

It is interesting to note that at 24 hpi, presumably the time of the rapid rise in vDNA towards the peak yield for both low and high ICDs for infected Sf9 cells the UTP, CTP and ATP levels in the low ICD case are all significantly higher than the levels of these metabolites in the high ICD case (Table 5.1). In fact, at 24 hpi the UTP, CTP and ATP level in the low ICD case were 2.9, 3.0 and 1.4 times higher than those in the high ICD case, respectively. It is possible that the supply of UTP, CTP and ATP is rate limiting for the production of vDNA during the 6-24 hpi period for high cell density infections.

It is presumed that the rise in vDNA for CDM infections shows similar timing to that seen for infections in Sf900™III given the similarities in the timing of the B-Gal yields seen in both media (compare B-Gal increase of Fig. 5.3 c to Fig.4.1 b, 4.2 b). UTP in particular may be limiting the rate of vDNA synthesis when it is considered that UTP is ultimately the source of dTTP (deoxythymidine tri-phosphate) required for DNA synthesis (Table 5.1, Fig. 5.5 b).

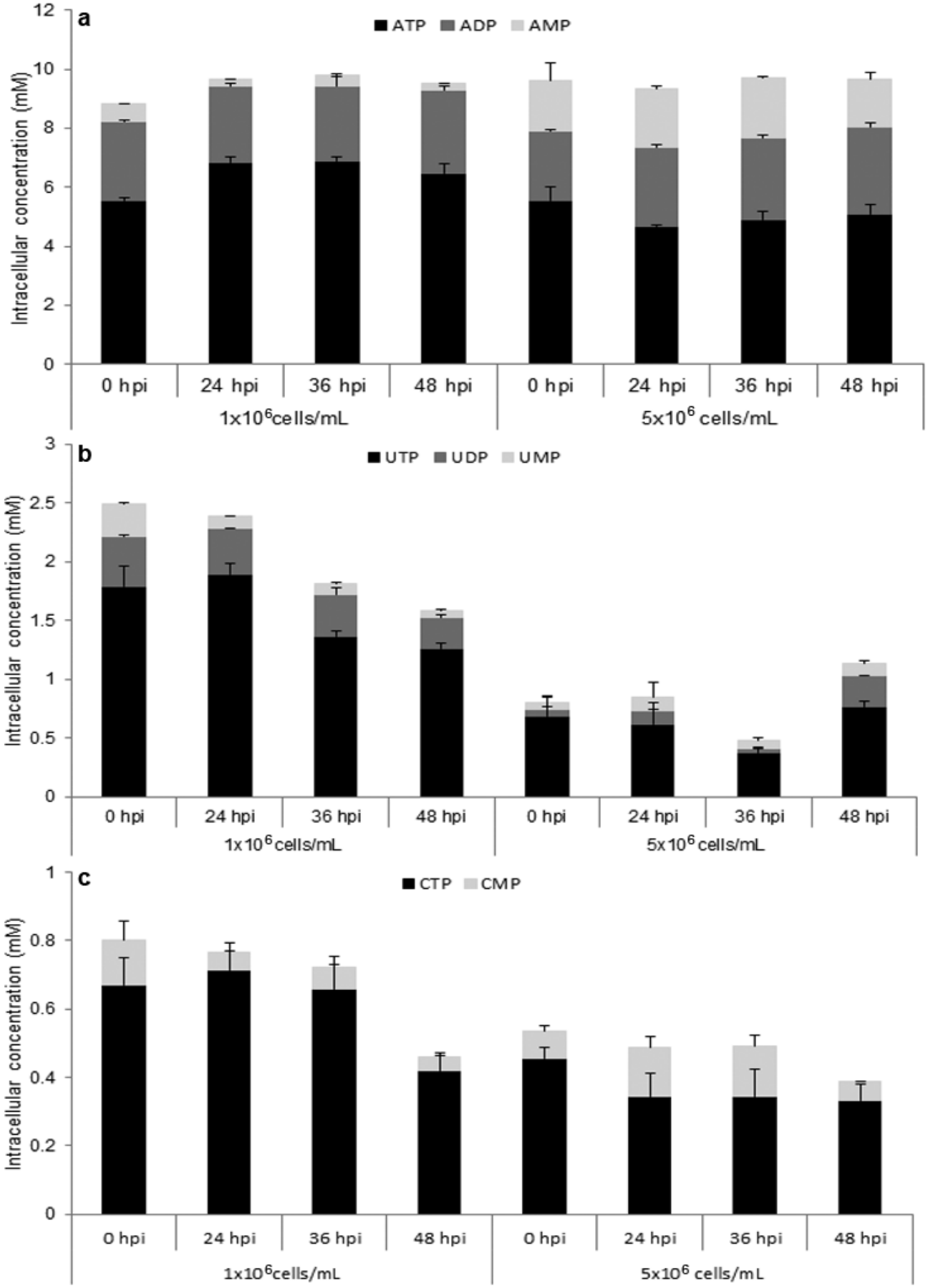

Fig. 5.5 Stacked bar charts of (a) adenosine, (b) uridine, and (c) cytidine nucleotide concentrations for four time points post-infection of infected Sf9 cells propagated in CDM at low (1×10^6 cells/mL)

and high (5×10^6 cells/mL) ICDs. Infections were conducted at an MOI of 10 PFU/cell in shaker-flask suspension cultures. Each data point is the average from two biological replicates, and the error bars represent the standard deviation.

Apart from nucleotides, other metabolites were found to be significantly different between low and high ICDs including TCA cycle intermediates (α-ketoglutarate (KGA), fumarate (FUM)), UDP sugars (UDP-glucose (UDPG), UDP-glucuronic acid (UDPGA), and UDP *N*-acetylglucosamine (UDPNAG)), nicotinamide adenine dinucleotide (NAD) and NAD phosphate (NADP) as presented in Table 5.1. Generally, intracellular concentrations of these metabolites at the low ICD were significantly higher than those at the high ICD. These differences may contribute to the higher yields for the low ICD in comparison with those for the high ICD. KGA is of particular interest in that it is at a low level throughout the high density infection (0.02 mM or lower) and drops to 0.05 mM at 36-48 hpi from a peak value of 0.22 mM at 24 hpi for the low density infection.

Intracellular AA concentrations of infected Sf9 cells at low and high ICDs over the time course of 0-48 hpi and a comparison of this data between low and high ICDs at 0 and 36 hpi are shown in Fig. 5.6. Generally, the levels of most AAs inside the cells were stable over the time course post-infection, except for glutamate, asparagine and glutamine that decreased at 48 hpi, while alanine and arginine gradually increased for both low and high ICD cases (Fig. 5.6 a, b). The relatively large drop in levels of some of the AAs from 36-48 hpi may be partially explained by cell lysis of some of the cells during the quenching and washing procedures during this late infection period.

Comparison between the low and high ICDs in terms of intracellular amino acid levels, Fig. 5.6 c, d, shows that the concentrations of most amino acids for the low ICD were higher than those for the high ICD either at 0 hpi (Fig. 5.6c) and 36 hpi (Fig. 5.6d), (except for glutamate, arginine and alanine), with a significant difference being found for 11 out of 19 AAs at 0 hpi and for 10 out of 19 AAs at 36 hpi. The significant differences between intracellular AA levels of low and high ICDs were similar for the early (0 hpi) and late (36 hpi) stages of the infection process (Fig. 5.6 c, d).

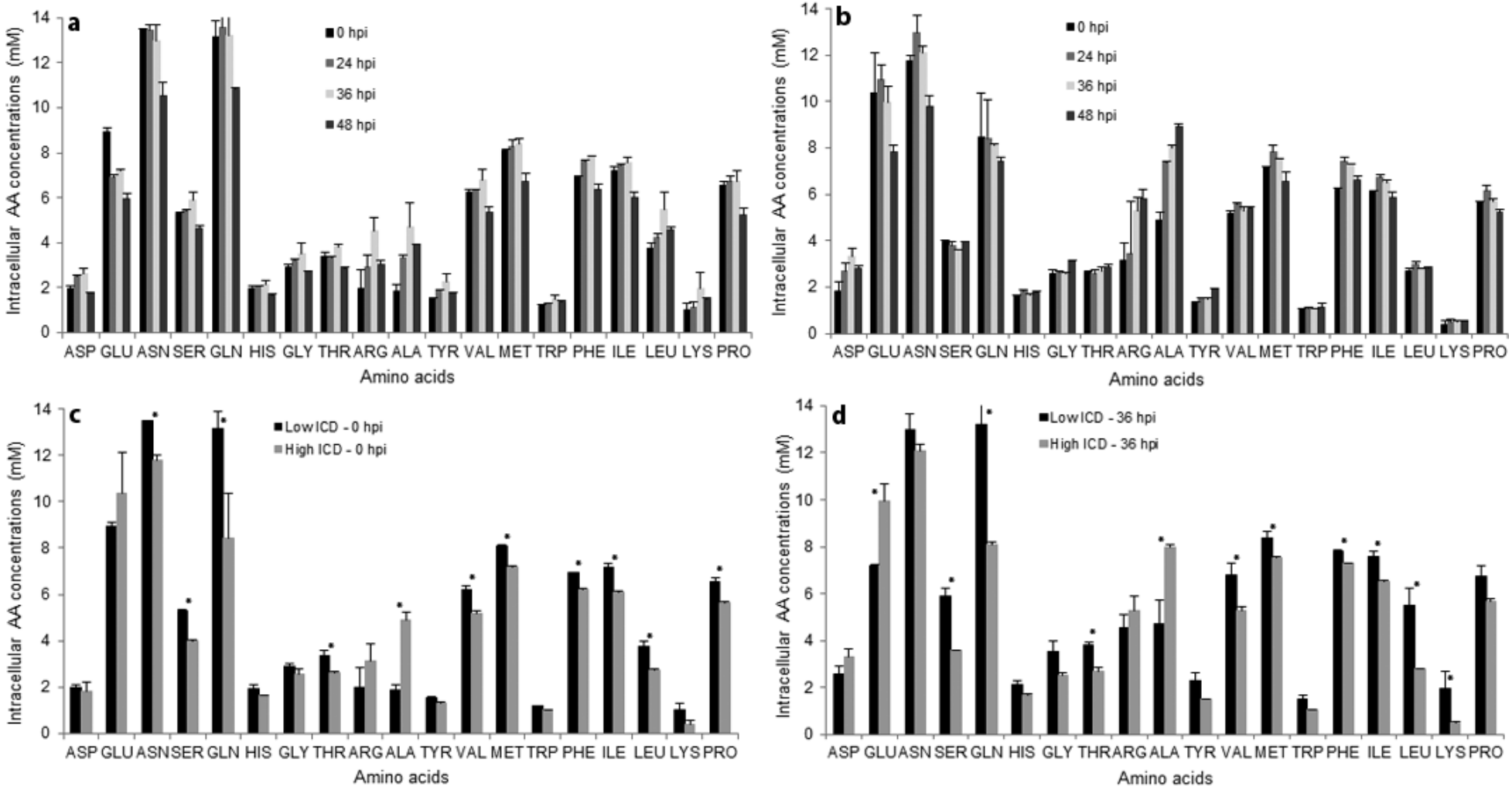

Fig. 5.6 Intracellular AA concentrations of infected Sf9 cells at four times post-infection for low (a) and high (b) ICDs, and the comparison between low and high ICDs for intracellular AA levels at 0hpi (c) and 36 hpi (d). Infections were conducted in CDM at low (1×10^6 cells/mL) and high (5×10^6 cells/mL) ICDs and at an MOI of 10 PFU/cell. The experiment was conducted in shaker-flask suspension cultures. Each data point is the average from two biological replicates, and the error bars represent the standard deviation. *indicates significant differences in the levels observed.

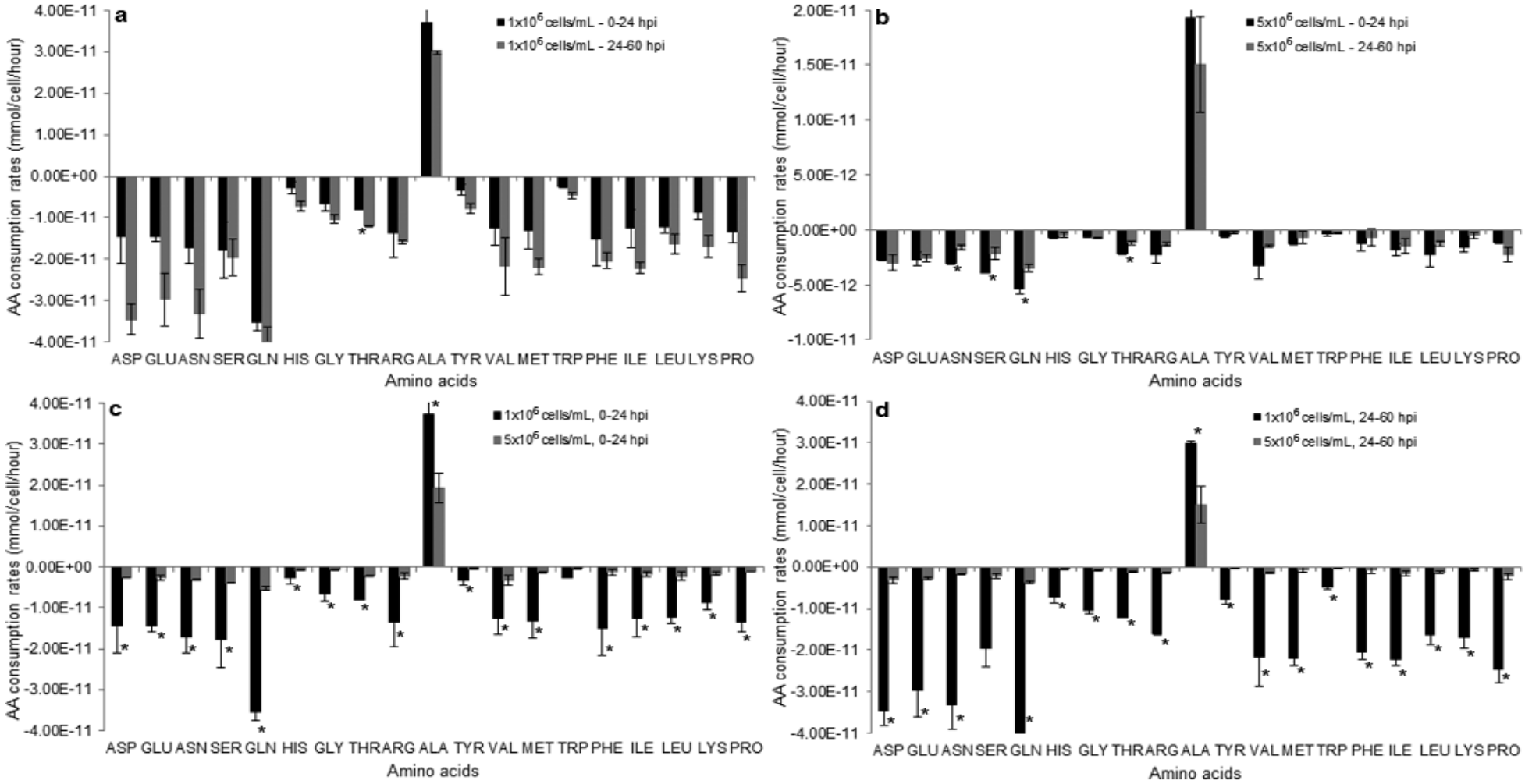

Fig. 5.7 Comparison of AA consumption rates (mmol/cell/hour) between early (0-24 hpi) and late (24-60 hpi) infection stages for low (a) and high ICDs (b) and between low and high ICDs for early (c) and late infection stages (d) of Sf9 cells infected with a rAcMNPV. Infections were conducted in CDM at low (1×10^6 cells/mL) and high (5×10^6 cells/mL) ICDs and at an MOI of 10 PFU/cell. The experiment was conducted in shaker-flask suspension cultures. Each data point is the average from two biological replicates, and the error bars represent the standard deviation. *indicates significant differences in the levels observed

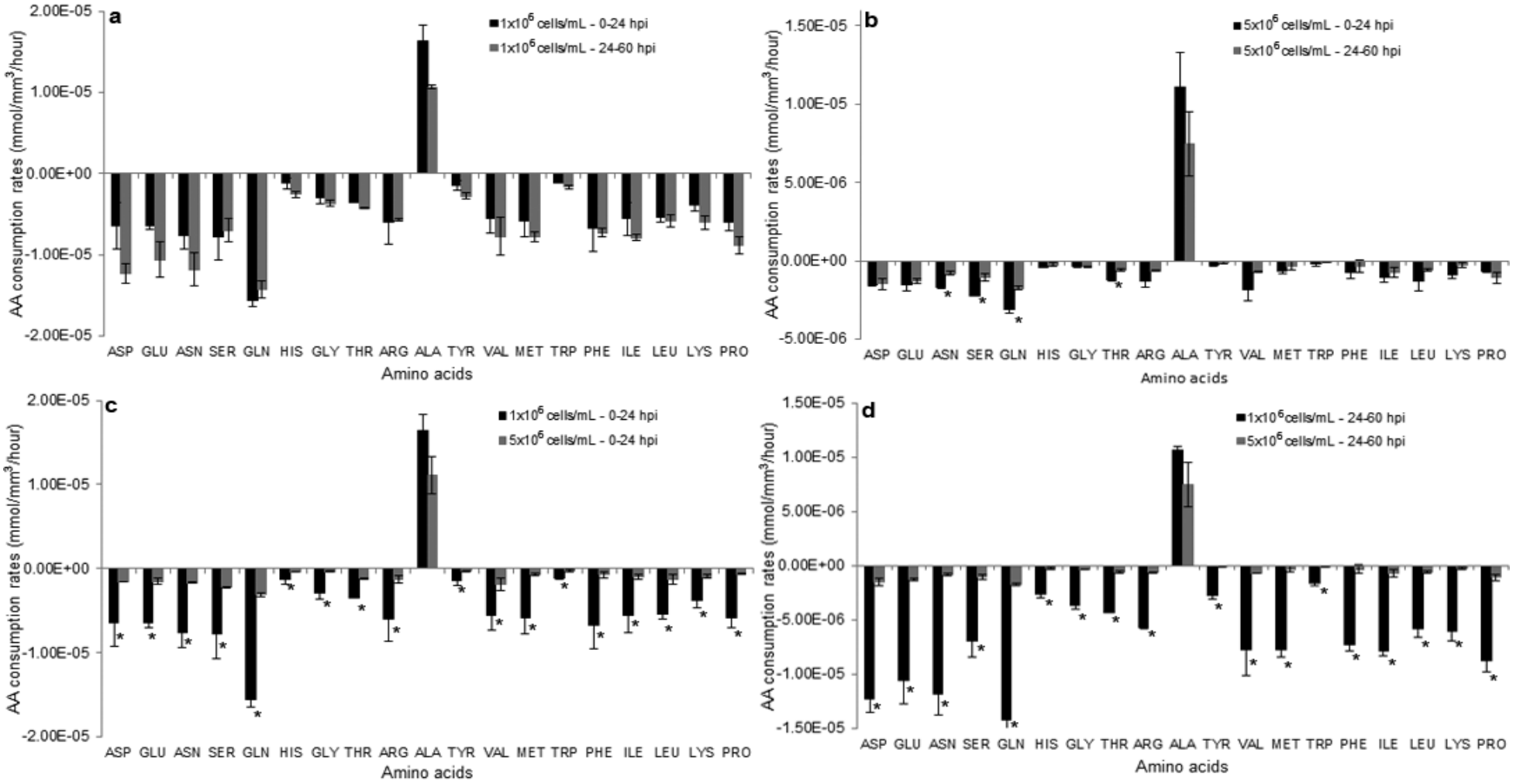

Fig. 5.8 Comparison of AA consumption rates (mmol/mm^3 of cell volume/hour) between early (0-24 hpi) and late (24-60 hpi) infection stages for low (a) and high ICDs (b) and between low and high ICDs for early (c) and late infection stages (d) of Sf9 cells infected with a rAcMNPV. Infections were conducted in CDM at low (1×10^6 cells/mL) and high (5×10^6 cells/mL) ICDs and at an MOI of 10 PFU/cell. The experiment was conducted in shaker-flask suspension cultures. Each data point is the average from two biological replicates, and the error bars represent the standard deviation. *indicates significant differences in the levels observed.

Glucose and AA consumption rates

Table 5.2. Glucose and amino acid consumption rates ($\times 10^{-12}$ mmol/cell/hour) of uninfected and infected Sf9 cells infected with a rAcMNPVat low (1×10^6) and high (5×10^6 cells/mL) ICDs in a chemically defined medium (CDM). Uninfected and infected cultures were set up at 0.5×10^6 cells/mL. For the case of uninfected cultures no infection was made and sampling was conducted at every 24 hours during the 24-hour doubling time period. For infected cases, cultures were infected with a baculovirus at an MOI of 10 PFU/cell at 1×10^6 and 5×10^6 cells/mL and sampling was conducted every 12 hours until 60 hours post-infection. Data is the average of biological duplicates.

	Uninfected	Low ICD infection	High ICD infection	P<
Glucose	-45.12^{a}	-33.29^{b}	-22.01^{c}	0.01
Maltose	-6.20^{ab}	-8.57^{a}	-5.12^{b}	0.05
Amino acids				
Aspatate	-3.03^{b}	-27.38^{a}	-2.83^{b}	0.05
Glutamate	-1.49^{b}	-22.82^{a}	-2.29^{b}	0.05
Asparagine	-2.03^{b}	-27.35^{a}	-2.34^{b}	0.05
Serine	-5.75^{b}	-18.12^{a}	-2.80^{b}	0.01
Glutamine	-21.80^{b}	-39.87^{a}	-3.99^{c}	0.01
Histidine	-1.00^{b}	-5.40^{a}	-0.58^{b}	0.01
Glycine	-1.73^{b}	-8.61^{a}	-0.71^{b}	0.001
Threonine	-2.25^{b}	-10.18^{a}	-1.43^{b}	0.001
Arginine	-2.27^{b}	-14.13^{a}	-1.73^{b}	0.01
Alanine	27.78^{ab}	34.24^{a}	16.92^{b}	0.05
Tyrosine	-0.77^{b}	-6.40^{a}	-0.35^{b}	0.01
Valine	-2.89^{b}	-17.64^{a}	-2.18^{b}	0.05
Methionine	-1.89^{b}	-17.69^{a}	-1.32^{b}	0.01
Tryptophan	-0.52^{b}	-3.76^{a}	-0.35^{b}	0.05
Phenylalanine	-1.55^{b}	-17.21^{a}	-1.39^{b}	0.05
Isoleucine	-2.27^{b}	-17.55^{a}	-1.68^{b}	0.01
Leucine	-3.24^{b}	-14.06^{a}	-1.52^{b}	0.01
Lysine	-3.05^{b}	-13.32^{a}	-1.01^{b}	0.05
Proline	-3.15^{b}	-20.01^{a}	-1.89^{b}	0.001

Consumption rates in the same row with different superscripts were significantly different ($P<0.05$)

NS: Not significant

Table 5.3. Comparison of AA consumption rates ($\times 10^{-6}$ mmol/mm^3 cell volume/hour) between uninfected and infected Sf9 cells infected with a rAcMNPV at low (1×10^6cells/mL) and high (5×10^6 cells/mL) ICDs in a chemically defined medium (CDM). Further description details are as shown in Table 2.

	Uninfected	Low ICD infection	High ICD infection	P<
Glucose	-27.57^a	-13.00^b	-11.44^b	0001
Maltose	-3.79	-3.35	-2.66	NS
Amino acids				
Aspatate	-1.99^b	-10.54^a	-1.44^b	0.05
Glutamate	-0.99^b	-8.78^a	-1.17^b	0.05
Asparagine	-1.34^b	-10.52^a	-1.19^b	0.05
Serine	-3.78^b	-6.98^a	-1.43^b	0.01
Glutamine	-14.25^b	-15.32^a	-2.04^c	0.01
Histidine	-0.65^b	-2.08^a	-0.30^b	0.01
Glycine	-1.14^b	-3.32^a	-0.36^c	0.001
Threonine	-1.48^b	-3.92^a	-0.73^b	0.001
Arginine	-1.49^b	-5.44^a	-0.88^b	0.01
Alanine	18.15^a	13.19^{ab}	8.64^b	0.05
Tyrosine	-0.49^b	-2.46^a	-0.18^b	0.01
Valine	-1.88^b	-6.79^a	-1.11^b	0.05
Methionine	-1.24^b	-6.81^a	-0.68^b	0.01
Tryptophan	-0.35^b	-1.45^a	-0.18^b	0.01
Phenylalanine	-1.05^b	-6.62^a	-0.71^b	0.05
Isoleucine	-1.49^b	-6.76^a	-0.86^b	0.01
Leucine	-2.12^b	-5.41^a	-0.78^b	0.01
Lysine	-2.00^b	-5.13^a	-0.52^b	0.01
Proline	-2.07^b	-7.71^a	-0.97^b	0.001

Consumption rates in the same row with different superscripts were significantly different ($P<0.05$)
NS: Not significant

Tables 5.2 and 5.3 represent consumption rates of glucose and AAs between uninfected and baculovirus infected Sf9 cells at low and high ICDs in CDM based on a per cell or per unit of cell volume basis, respectively. The cell specific glucose consumption rate of uninfected Sf9 cells propagated in CDM was the highest followed by that of the infected cells at the low ICD and the consumption rate of infected cells at the high ICD was

the lowest, and there was a significant difference in glucose consumption rate among them (Table 5.2). Based on a per cell basis, the maltose consumption rate of infected cells at the low ICD was significantly higher than that of the high ICD case, while the maltose consumption rate of uninfected cells was not significantly different in comparison to both the infected cases. However, the maltose consumption rate per unit of cell volume was similar among uninfected and infected cultures (Table 5.3). In addition, no significant difference between infected cultures at low and high ICDs was found in terms of the glucose consumption rate per unit of cell volume (Table 5.3). However the glucose consumption/unit volume of non-infected cells was higher than that seen for the infected cultures.

Table 5.2 shows that infected cells at the low ICD consumed AAs at significantly higher rates than those at the high ICD for all of the common AAs investigated, except for alanine which showed an increase at both ICDs. Significantly higher AA consumption rates for infected cells at the low ICD in comparison with those at the high ICD were also found for the consumption on a per unit of cell volume basis (Table 5.3), although the peak cell volume post-infection for the low ICD was much larger than that for the high ICD case (Fig. 5.3 b). The AA consumption rates for uninfected Sf9 cells were close to the high ICD for the majority of the AAs (16 out of 19 AAs) for both consumption rates on a per cell and a per volume basis (Table 5.2, 5.3).

Comparison of the AA consumption rates between early (0-24 hpi) and late stages (24-60 hpi) of the virus infection process at the same ICD or between infected Sf9 cells at low and high ICDs are shown in Fig. 5.7. Although consumption rates at the late infection stage appeared to be higher than those at the early infection stage for all of the AAs, there was no significant difference in AA consumption rates between the early and late stages of the virus infection for the low ICD case for all of the AAs, except for threonine (Fig. 5.7 a). In contrast, the AA consumption rates at the early infection stage appeared higher than those at the late infection stage for most of the AAs in the case of the high ICD (Fig. 5.7 b). However, significant differences in AA consumption rates between the early and late infection stages for the high ICD case were only found for asparagine, serine, glutamine and threonine. Comparison between early and late infection stages within the same ICD in the case of the consumption rate per unit of cell volume (Fig. 5.8 a, b) also showed similar trends as above.

Comparing low and high ICDs, the AA consumption rates on a per cell basis at the low ICD were significantly higher than those at the high ICD for all of the AAs measured for both the early and late infection stages, except for alanine (Fig. 5.7 c, d). Similar trends

were found for the consumption rates calculated based on a cell volume basis (Fig. 5.8). This result indicates that infected cells at the low ICD consume AAs at much higher rates than those at the high ICD and the consumption of AAs by infected cells at the high ICD were poorer at the late stage of the baculovirus infection process.

Ratios between intra- and extracellular AAs and between AA levels for low and high ICDs

Figure 5.9 shows the ratios of extra- and intra-cellular AA concentrations between high and low ICDs and the ratios between intra- and extracellular AA concentrations for low and high ICDs. When comparing AA concentrations between high and low ICDs, Fig. 5.9a, b shows that extra- and intra-cellular AA levels of infected cells at the high ICD were generally lower than those for the low ICD, as indicated by the ratios of high/low ICD AA values being less than 1 for the majority of the AAs. At 0 hpi, the ratios between low and high ICDs of extracellular AA levels were mostly similar to those for intracellular AA levels (Fig. 5.9a), except for arginine and lysine. However, at 36 hpi, ratios between high and low ICDs for extracellular AA levels seemed to increase, while those for intra-cellular AA levels reduced significantly. As a result, ratios between high and low ICDs for extracellular AA levels, at 36 hpi were significantly higher than those for intracellular AA levels for the majority of the AAs (12 out of 19 AAs) (Fig. 5.9b). This result indicates a possibly poorer AA uptake into the cells at the late stage of virus infection for infected cells at the high ICD compared with those at the low ICD. Serine, glutamine, leucine and lysine are among the AAs that have low intracellular levels at the high ICD compared with the low ICD, (ratio of AAs between high/low ICDs around 0.5 or lower).

When comparing the ratios between intra- and extra-cellular AA levels for low and high ICDs, these two ratios were also similar among the majority of AAs at 0 hpi (Fig. 5.9 c). Intracellular AA levels of the majority of AAs were in the range of 70-90% of the extracellular ones for both low and high ICDs, except for glutamine and alanine, low ICD case, where the intracellular AA levels were higher than the extracellular levels. This suggests that the AA uptake by cells in culture before and after infection reaches an equilibrium of the AAs in the cell with the level in the external medium or alternatively that the external AA level dictates the extent of AA uptake. This in turn suggests the only way to keep intracellular AA levels high is to have high AA levels in the external media. At 36 hpi, these ratios increased in the case of the low ICD (more AAs had a ratio above 1), but remained at similar levels in the case of the high ICD (Fig. 5.9 d).

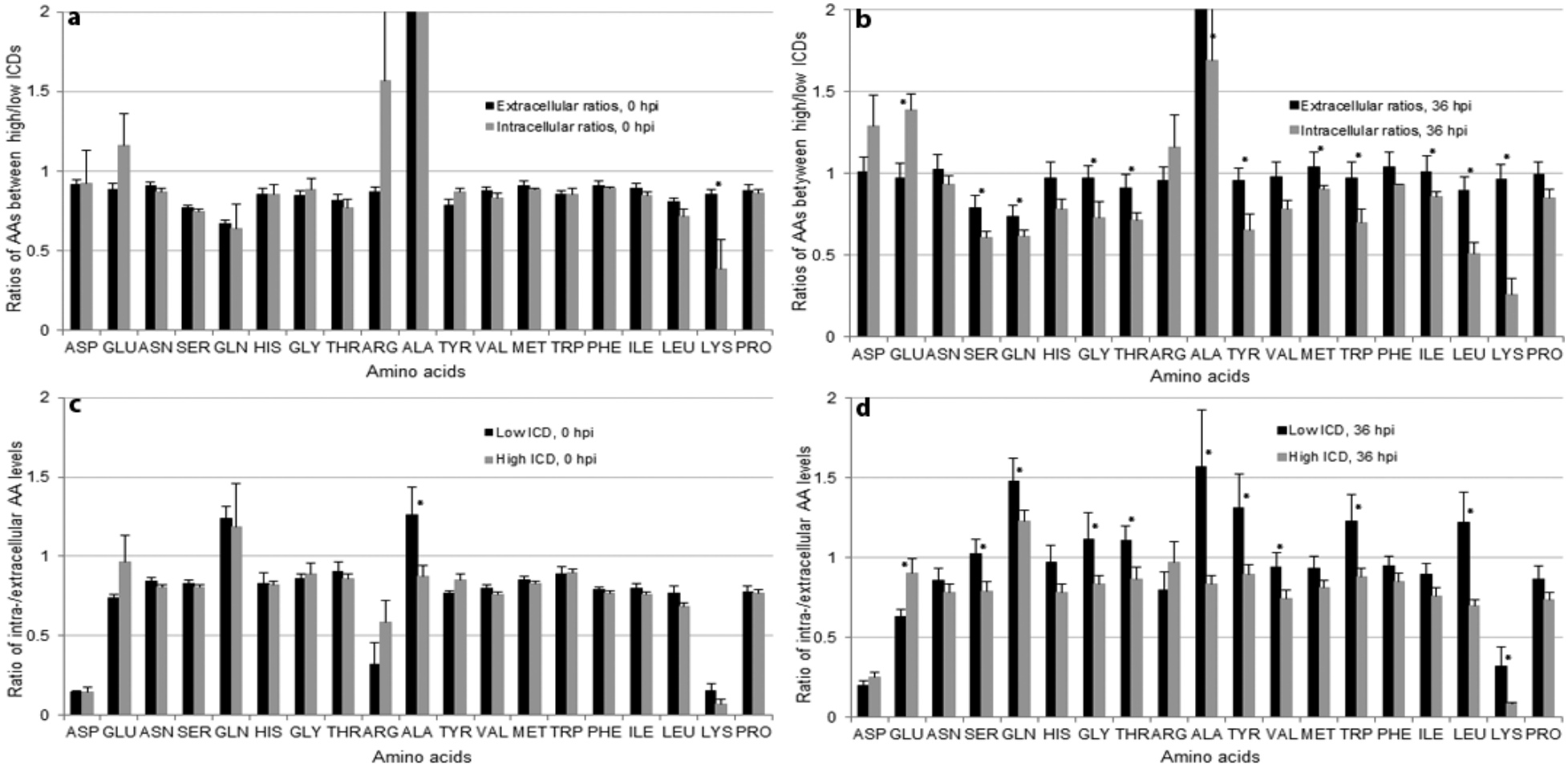

Fig. 5.9 Ratios of AA levels between high versus low ICDs for extra- and intra-cellular AAs at 0 hpi (a) and 36 hpi (b), and ratios between intra- versus extra-cellular AA levels for low and high ICDs at 0 hpi (c) and 36 hpi (d) of Sf9 cells infected with a recombinant baculovirus (rAcMNPV). Infections were conducted in CDM at low (1×10^6 cells/mL) and high (5×10^6 cells/mL) ICDs, at an MOI of 10 PFU/cell. The experiment was conducted in shaker-flask suspension cultures. Each data point is the average from two biological replicates, and the error bars represent the standard deviation. *indicates significant differences in the levels observed. The ratios of alanine are off scale in some cases in the above figure and so are listed here: 3.7, 2.6 and 3.2 for extra and intracellular at 0hpi and extracellular at 36 hpi, respectively

It is of interest that the intra-/extra-cellular ratios for aspartate and lysine were very low (0.07 to 0.32) for both low and high ICDs (Fig. 5.9 c, d). This result indicates that it might be difficult for these AAs to get into the cell regardless of the extracellular concentrations, or that they are consumed at a high rate and unable to form an equilibrium with the external level present.

5.3.3 Comparison between the two media of Sf900™III and CDM

In this section, the data for infected Sf9 cells propagated in Sf900™III medium are calculated from the dataset described in Chapter 4. As the ICDs represented for low and high ICDs in the case of infected cells in Sf900™III (2×10^6 vs 6×10^6 cells/mL) differ from the case ofthe CDM (1×10^6 vs 5×10^6 cells/mL), the comparison between these two media in terms of the cell density effect was made through comparing the ratios of recorded parameters between high and low ICDs for these two media.

When comparing the β-Gal yield between low and high ICDs at various times post infection for Sf9 cells propagated in either Sf900™III or CDM media, Fig. 5.10, shows that the ratios in β-Gal yield between low and high ICDs were comparable between the two media (within the range of 0.29 to 0.39 for Sf900™III and 0.15 to 0.36 for CDM). It is of interest to note that the largest difference between the media was at 24 hpi where the ratio of the β-Gal yield for the high ICD compared to the low ICD was much lower for the CDM case. This suggests that in the CDM, infections at high cell densities are delayed compared to those in Sf900™III but the β-Gal production level catches up by 36-48 hpi.

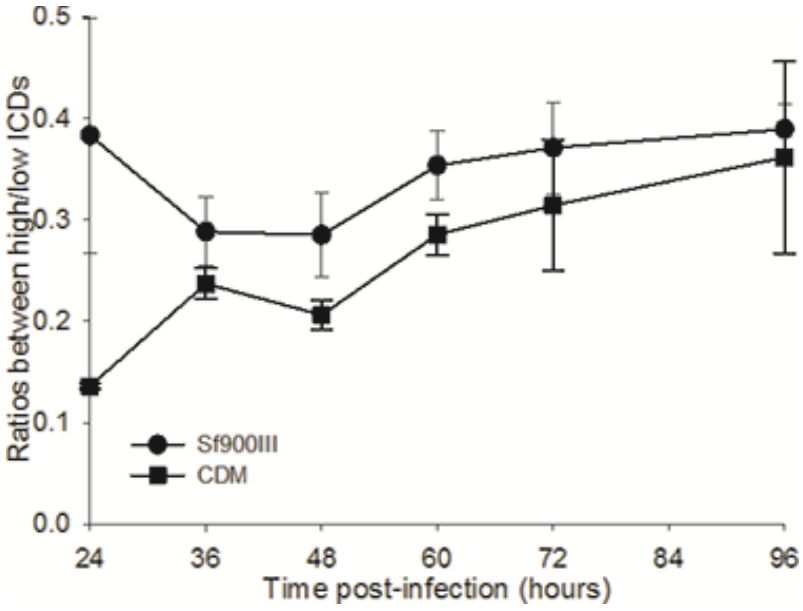

Fig. 5.10 Ratios of specific β-Gal yield between high and low ICDs for infected Sf9 cells in Sf900™III and CDM media. The ratio was calculated from the average values (from biological triplicates) for high and low ICDs and the error bar is the standard deviation calculated from standard deviations of the dividend and divisor. Data for infected Sf9 cells in Sf900™III medium was from the dataset in Chapter 4.

The question of interest here is whether the ratios between high and low ICDs for other parameters (intracellular metabolite concentrations, AA consumption rates) for these two media were also similar to each other as was found for the β-Gal yield at various times post infection.

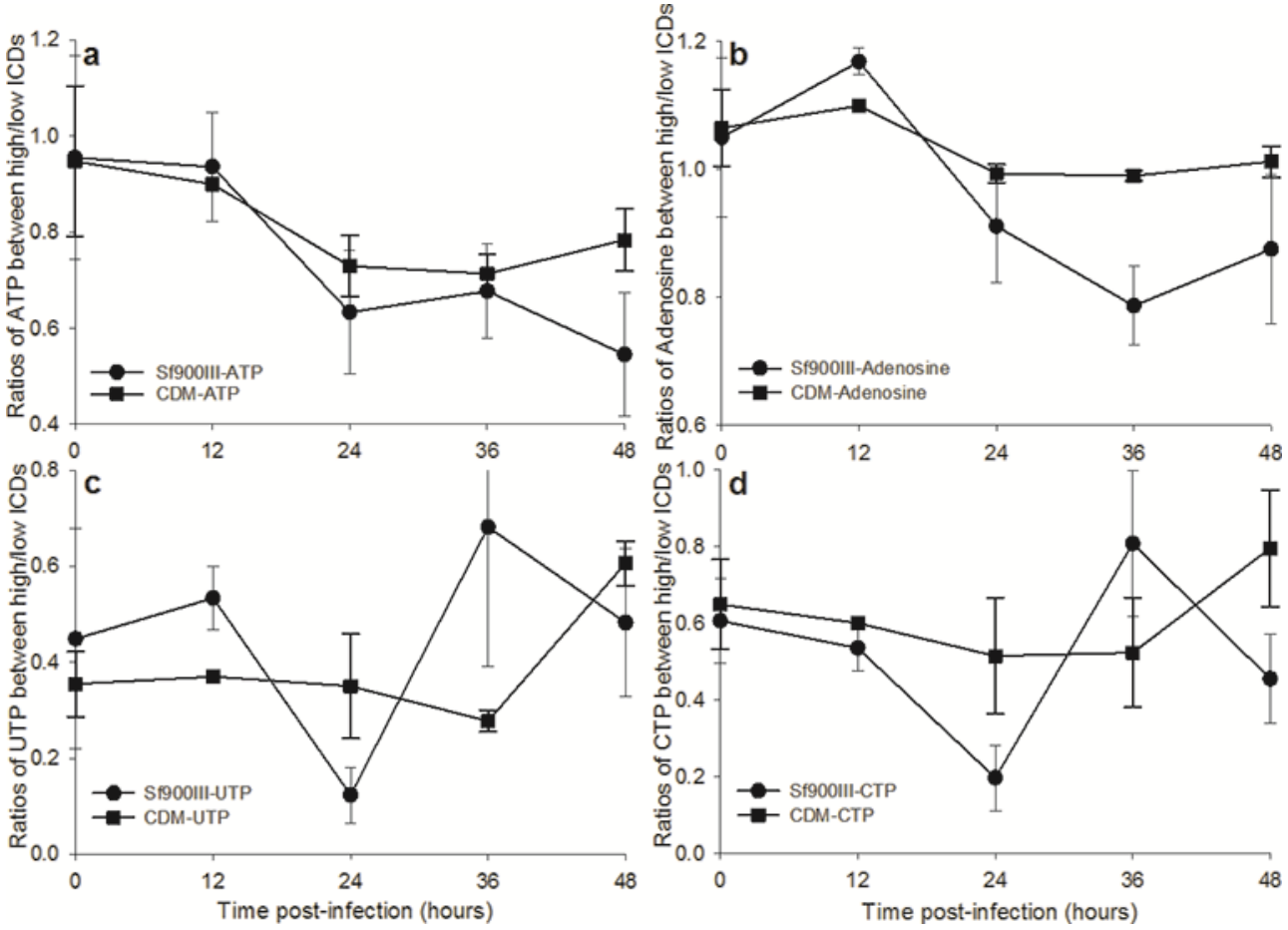

Fig. 5.11 Ratios of intracellular ATP (a), total adenosine (b), UTP (c) and CTP (d) between high and low ICDs for infected Sf9 cells in Sf900™III and CDM media. The ratio was calculated from the average values (from biological triplicates) for high and low ICDs and the error bar is the standard deviation calculated from standard deviations of the dividend and divisor. Data for infected Sf9 cells in Sf900™III medium was from the dataset in Chapter 4.

As found for the β-Gal yield, there was no significant difference in the ratios of high/low ICDs between two media for ATP, total Adenosine, UTP and CTP (Fig. 5.11).The ratios between high/low ICDs for Sf900™III and CDM media respectively were in the range of 0.55 to 0.96 and 0.78 to 0.95 for ATP (Fig. 5.11a), 0.88 to 1.17 and 0.99 to 1.07 for total adenosine (Fig. 5.11b), 0.12 to 0.68 and 0.28 to 0.61 for UTP (Fig. 5.11 c) and 0.2 to 0.81 and 0.51 to 0.80 for CTP (Fig. 5.11 d). Limitations of these nucleotides at high ICDs in comparison with low ICDs were not as much as those seen for the β-Gal yield. Generally, there were large variations among different times post-infection and among

replicates within one time point resulting in large error bars in many cases. As shown in Fig. 5.11, the ratios displayed less variation at different times post infection for CDM in comparison with Sf900™III.

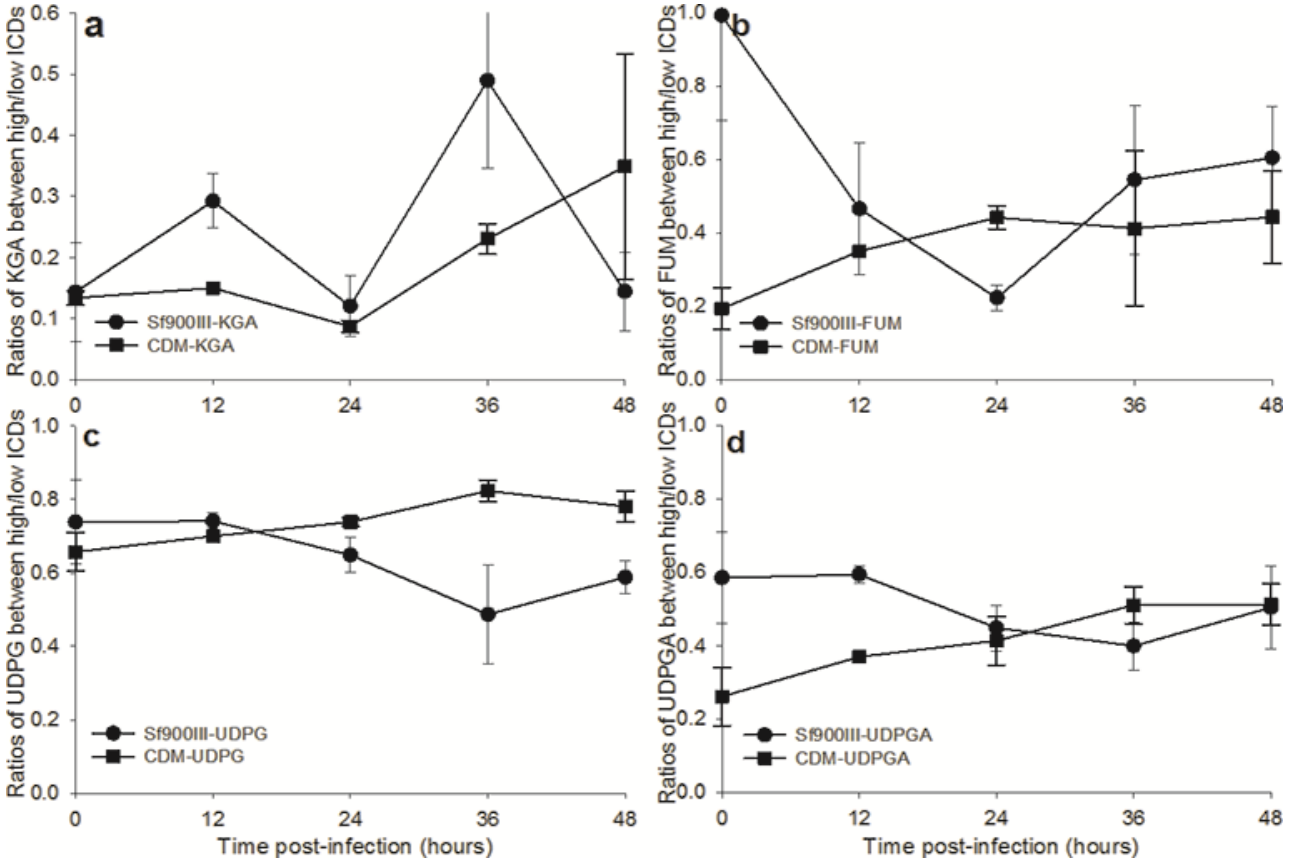

Fig. 5.12 Ratios of intracellular KGA (a), FUM (b), UDPG (c) and UDPGA (d) between high and low ICDs for infected Sf9 cells in Sf900™III and CDM media. The ratio was calculated from the average values (from biological triplicates) for high and low ICDs and the error bar is the standard deviation calculated from standard deviations of the dividend and divisor. Data for infected Sf9 cells in Sf900™III medium was from the dataset in Chapter 4.

Other metabolites plotted in this regard include α-ketoglutarate (KGA), fumarate (FUM), UDP glucose (UDPG) and UDP gluconic acid (UDPGA) and they followed similar patterns to those found for the nucleotides above (Fig. 5.12). The ratios between high/low ICDs respectively for Sf900™III and CDM media were in the range of 0.12 to 0.49 and 0.09 to 0.35 for KGA (Fig. 5.12 a), 0.22 to 0.99 and 0.19 to 0.44 for FUM (Fig. 5.12 b), 0.49 to 0.74 and 0.66 to 0.82 for UDPG (Fig. 5.12 c) and 0.40 to 0.59 and 0.26 to 0.51 for UDPGA (Fig. 5.12 d). Ratios of the TCA cycle intermediate (KGA) at the high ICD in comparison with the low ICD were similar to those found for the β-Gal yield. Therefore, there might be a direct link between the limitation in intracellular KGA and the reduction in recombinant protein yield with increasing ICD for infected Sf9 cells propagated in different media, but this is speculative.

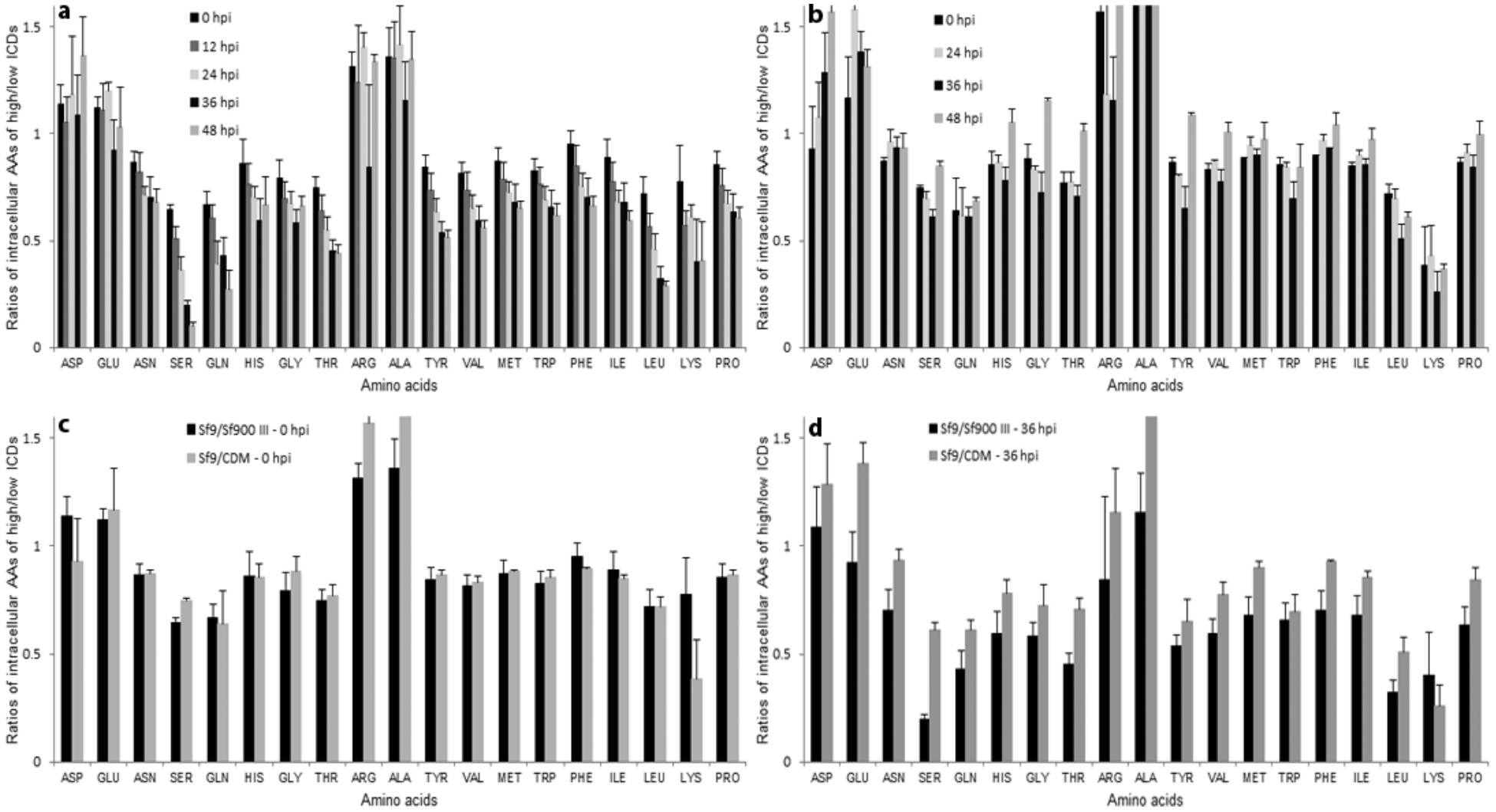

Fig. 5.13 Ratios between high/low ICDs for intracellular AAs at various time post-infection of infected Sf9 cells in Sf900™III (a) and CDM (b), and the comparison of these ratios for infected Sf9 cells in Sf900™III and CDM at 0 hpi (c) and 36 hpi (d). The ratio was calculated from the average values (from biological triplicates) for high and low ICDs and the error bar is the standard deviation calculated from standard deviations of the dividend and divisor. Data for infected Sf9 cells in Sf900™III medium was from the dataset in Chapter 4.

A comparison of the ratios of high/low ICDs between Sf900™III and CDM media for intracellular AAs, Fig. 5.13, shows that intracellular AA levels at the low ICD were higher than those at high ICD for the majority of AAs, except for the cases of aspartate, glutamate, arginine and alanine for both media. Serine, leucine and lysine are among the AAs that have the lowest ratios between the high/low ICDs (Fig. 5.13 a, b), especially at the late infection stage (36 hpi), and may become limiting for protein production at the high ICD. The ratios between high/low ICDs for intracellular AAs of infected Sf9 cells propagated in Sf900™III declined post-infection for many AAs, while these ratios of infected Sf9 cells propagated in CDM seemed to be maintained over the time course post-infection (Fig. 5.13 a, b).

Comparing between the two media, the ratios of intracellular AAs between high/low ICDs were similar at 0 hpi for most of the AAs, except for lysine (Fig. 5.13 c). At the late infection stage (36 hpi), the ratios of intracellular AAs between high/low ICDs declined for both media for many of the AAs. However, these declines were higher for the case of infected cells in Sf900™III medium. As a result, the ratios of intracellular AAs between high/low ICDs for the case of the CDM were higher than those for the case of the Sf900™III medium for all of the AAs except for lysine (Fig. 5.13 d). However, given the size of the error bars, most differences were not significant.

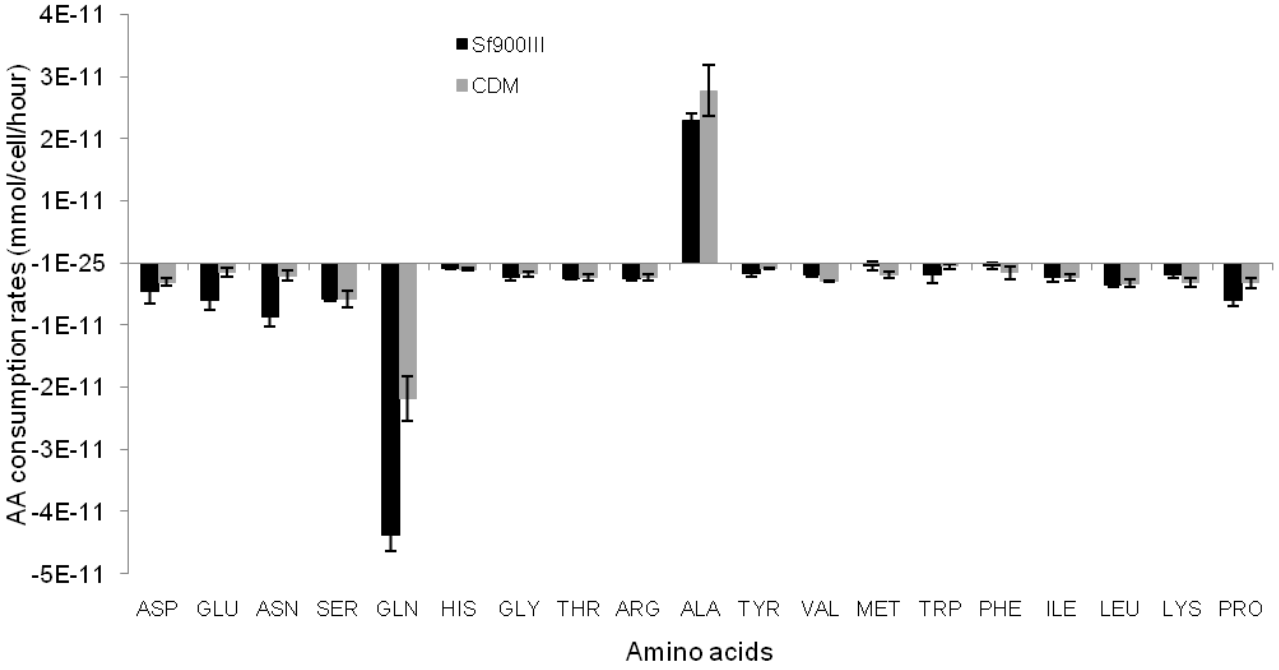

Fig. 5.14 Comparison of AA consumption rates of uninfected cultures between Sf9 cells propagated in Sf900™III and CDM over the exponential period of 0-72 hours post-inoculation. The values were the average of biological triplicates and the error bar is the standard deviation of the triplicates. Data for infected Sf9 cells in Sf900™III medium was from the dataset in Chapter 4.

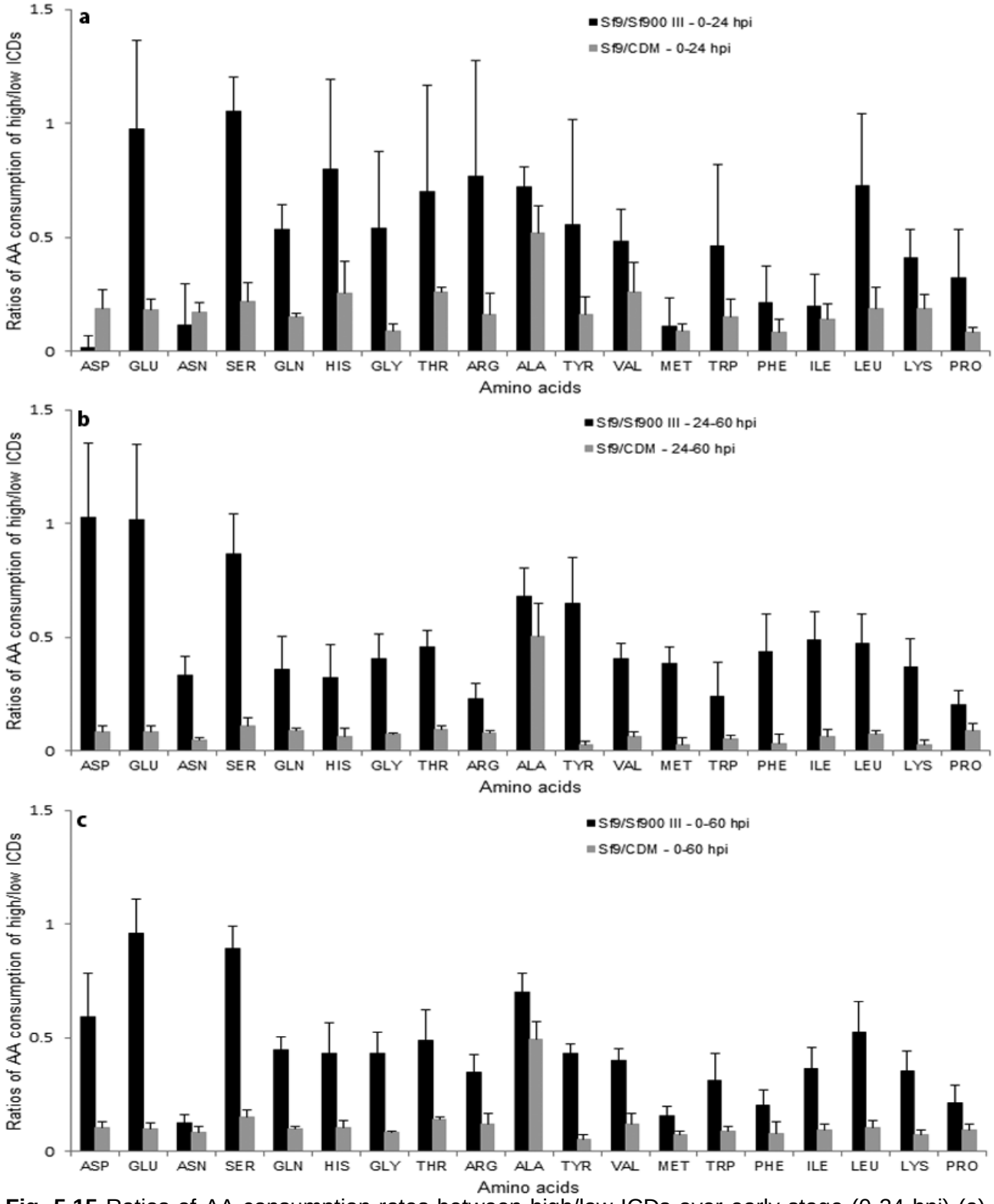

Fig. 5.15 Ratios of AA consumption rates between high/low ICDs over early stage (0-24 hpi) (a), late stage (24-60 hpi) (b) and the whole infection stage (0-60 hpi) (c) for infected Sf9 cells in Sf900™III and CDM. The ratio was calculated from the average values (from biological triplicates) for high and low ICDs and the error bar is the standard deviation calculated from standard deviations of the dividend and divisor. Data for infected Sf9 cells in Sf900™III medium was from the dataset in Chapter 4.

The AA consumption rates of uninfected Sf9 cells propagated in Sf900™III and CDM were similar for most of the AAs, except for glutamate, asparagine and glutamine, in which, the AA consumption rates of uninfected cells in Sf900™III were significantly higher than those in CDM (Fig. 5.14). Interestingly, the ratios of AA consumption rates between high/low ICDs for infected cells in CDM were much lower than those for Sf900™III medium (Fig. 5.15). The ratios of AA consumption rates between high/low ICDs for infected cells in Sf900™III medium were in the range of 0.13 to 0.96 with an average of 0.44, while for infected cells in CDM they were in the range of 0.06 to 0.49 with an average of 0.12 (Fig. 5.15 c). It is not clear what leads to this difference in AA consumption given the similar levels of β-Gal/cell produced at the high ICD in both media.

5.4 Discussion

Insect cell culture media was first developed based on the analysed chemical composition of hemolymph, or insect blood, from chemically defined components. Heat treated hemolymph was included into the culture medium for supplying unknown but essential substrates to improve the performance of insect cell culture. Insect hemolymph was then successfully replaced by animal serum, most commonly fetal calf (bovine) serum (FCS) (Gardiner and Stockdale, 1975; Hink, 1970) as serum was cheaper and was available in large quantities compared with insect hemolymph (Schlaeger, 1996). Due to several limitations associated with serum (Reid et al., 2013; Schlaeger, 1996), serum free and protein free media were subsequently developed with the use of lipid emulsions and protein hydrolysates (Goodwin, 1991).

Serum free medium has successfully supported insect cell culture to high cell densities in batch culture and allows good baculovirus infections (e.g. Sf900™III medium). However, the undefined nature of the hydrolysate containing medium may interfere with some down-stream processes as well as interfere with systems biology studies such as transcriptomics, metabolomics and fluxomics. Therefore, limitations due to the undefined nature of hydrolysates have been addressed through the development of a chemically defined medium (CDM). Although it is possible to gain some metabolic insights using insect cells propagated in hydrolysate containing media, its substitution with chemically defined components will greatly enhance the range and scope of such studies (Bhatia et al., 1997). In addition, CDM also ensures reproducibility of optimized process conditions (Bhatia et al., 1997) because of the minimal effect from lot-to-lot variation caused by the presence of hydrolysates.

It should be feasible to develop a CDM for insect cell culture as originally, insect culture medium was developed from defined components to form a basal medium, and then undefined components (serum, hydrolysates) were added into the basal medium to get higher cell growth rates. Currently, CDM formulations are well established for mammalian cell culture, but are not yet commercially available for insect cell culture (Reid et al., 2013). A prototype CDM for insect cell culture has been developed by Life Technologies and has been trialed for insect cell culture in our laboratory. As it is a hydrolysate free medium, the concentrations of free AAs in the CDM are slightly higher than those in Sf900™III medium except for glutamine (Fig. 5.1).

Sf9 insect cells propagated in Sf900™III adapted well into the CDM within 7 days. They grew well in CDM under the routine stock cell maintenance process used for cells propagated in Sf900™III (Fig. 5.2 a), although the peak uninfected cell density of Sf9 cells in CDM was much lower than that of Sf9 cells in Sf900™III medium (1.2×10^7 vs 2×10^7 cells/mL, respectively) (Fig. 5.2 b). The presence of undefined growth promoters in the protein hydrolysate (yeast extract) together with other essential substrates including peptides, carbohydrates, vitamins and minerals in the Sf900™III medium (Ikonomou et al., 2001; Siemensma et al., 2010; Sommer, 1996; Zhang et al., 2003) possibly explain the extra cell growth of the Sf900™III medium. The viability of Sf9 cells propagated in CDM was similar to that in Sf900™III (Fig. 5.2 a, b) indicating that the CDM can support Sf9 insect cell growth as well as one of the best commercial medium for insect cell culture. In addition, the CDM supports good baculovirus infections with the peak specific β-Gal yield being slightly higher than that for Sf900™III (Fig. 5.2 c). The timing of β-Gal production post-infection was similar to that found for Sf900™III, which is typical for recombinant AcMNPV infected Sf9 cells. As the peak uninfected cell density of Sf9 cells in CDM was lower than that in Sf900™III, the reduction in specific β-Gal yield with increasing ICD for Sf9 cells in CDM would be expected to appear at a lower cell density than that for Sf9 cells in Sf-900™III. However this may not be the case as the specific β-Gal yield of infected Sf9 cells in CDM at 5×10^6 cells/mL was slightly higher than that in Sf900™III at 6×10^6 cells/mL (Fig. 5.2 c).

Typically for Sf9 cells infected with a recombinant baculovirus (rAcMNPV) at a high MOI (e.g. ≥5 PFU/cell) cell division is inhibited rapidly as a result of a synchronous infection (O'Reilly et al., 1994). In CDM, a minimal increase in cell density post-infection of Sf9 cells infected with a rAcMNPV at an MOI of 10 PFU/cell was also found for both low and high ICDs (Fig. 5.3a). In addition, the cell viability and cell diameter increase post-infection for both low and high ICDs (Fig. 5.3 a, b) were also similar to those found for

infected Sf9 cells in Sf900™III at low and high ICDs. This result indicates that the infection process of Sf9 cells in CDM follows a similar pattern to that of Sf9 cells in Sf900™III. The peak specific β-Gal yield of infected Sf9 cells in CDM was slightly higher than that in Sf900™III and infected Sf9 cells in CDM were also influenced by the cell density effect (as discussed in Chapter 4) with the reduction in specific yield with increasing ICD appearing at a similar density for the case of infected cells in Sf900™III, based on the limited studies in this regard in this thesis.

As found previously for infected Sf9 cells in Sf900™III (Chapter 4), the intracellular nucleotide concentrations for a low ICD were significantly higher than those for a high ICD, especially for the nucleotide tri-phosphates (Fig. 5.5, Table 5.1). These forms of nucleotides are used for nucleic acid synthesis. Therefore, the reduction in vDNA and mRNA production with increasing ICD as found previously (Huynh et al., 2013) may be explained by the limitation in intracellular nucleotide tri-phosphates when the ICD increases. In addition, intracellular levels of TCA cycle intermediates such as KGA and FUM for infected cells at a low ICD were significantly higher than those at a high ICD (Table 5.1) as found for infected cells in Sf900™III (Chapter 4). A reduction in intracellular KGA levels with increasing ICD is a possible contributor to the cell density effect. Carinhas et al. (2010) reported an improvement in cell specific yields at a high ICD with the supplement of KGA to the medium used for infections. Other metabolites were found to reduce significantly with the increasing ICD including UDP sugars (UDPG, UDPGA and UDPNAG) (Table 5.1) as was found for infected Sf9 cells in Sf900™III (Chapter 4).

The low intracellular KGA concentration at the high ICD may be the result of the lower intracellular glutamine level at the high ICD in comparison with that of the low ICD (Fig. 5.6). However, the intracellular glutamate level at the high ICD was higher than that at the low ICD. Bernal et al. (2009) provides an extensive discussion of the role glutamate and glutamine play in the energy metabolism of Sf9 cells and shows how the levels of these AAs may influence KGA levels.

Generally, intracellular AA concentrations for infected Sf9 cells in CDM followed a similar pattern to that found for infected Sf9 cells in Sf900™III, although the intracellular concentrations of many AAs in CDM (Fig. 5.6) were slightly higher than the levels observed in Sf900™III (Fig. 4.6). For the AAs that showed a lower intracellular AA concentration for infected Sf9 cells in CDM in comparison with those in Sf900™III, especially at the late stage of the infection (36 hpi) (Fig. 5.6 c, d) suggests that they may limit protein production at the high ICD (lysine, tryptophan) but the fact that these AAs

remain at reasonable levels in the outside medium (Fig A3.2) suggest they are unlikely to be limiting.

Low intracellular AA concentrations at high ICDs in comparison with those at low ICDs may be the result of poorer uptake rates of AAs at high ICD, especially at the late infection stage (Fig. 5.9). However the intra/extracellular ratio for the AAs at the high ICD at 36 hpi are not much lower than for the low ICD at this stage of the infection, except perhaps for lysine (Fig 5.9 d). It is noted that there were huge differences in AA consumption rates between low and high ICDs for infected cells in CDM with significant differences being found for all of the AAs during the early and late infection stages (Fig. 5.7c, d). All of the AA supply in the CDM comes from free AAs, while peptides in Sf900™III may contribute to part of the AAs required by the cells grown in that medium. Therefore, AA consumption rates measured in infected cells propagated in CDM may be closer to the real values in comparison with those in Sf900™III. The less significant differences in AA consumption rates between the low and high ICDs for infected Sf9 cells in Sf900™III (Chapter 4) may be the result of the role peptide consumption plays as a source of AAs by the infected cells at low ICDs in the Sf900™III medium.

AA consumption rates obtained in this work with the CDM medium varied greatly from the literature (Bernal et al., 2009; Radford et al., 1997) which may be the result of the discrepancy in the size of infected cells as well as the presence of peptides in the culture media used by others and the proportions of the peptides used by the cells as a source of AAs.

Use of a CDM is the most suitable medium for measuring AA consumption rates as the AA supply comes from free AAs only. Although the CDM does not contain peptides as for Sf900™III, the AA consumption rate of uninfected Sf9 cells in CDM were similar to those in Sf900™III for most of the AAs, except for glutamate, asparagine and glutamine with the AA consumption rates for these AAs in CDM being significantly lower than those in Sf900™III (Fig. 5.14). AA consumption rates on a per cell basis (Table 5.2) or on a per unit of biomass (cell volume) basis (Table 5.3) for infected Sf9 cells at a low ICD were significantly higher than those at a high ICD for most of the AAs. This result most likely reflects the decline in cell specific yield with increasing ICD due to a drop in vDNA and LacZ mRNA levels as discussed in Chapter 4 rather than reflecting an AA substrate limitation for protein production.

As discussed in Chapter 4 of this thesis, the glucose consumption rate for uninfected and baculovirus infected Sf9 cells have been reported with a vast difference among investigators (Benslimane et al., 2005; Bernal et al., 2009; Kamen et al., 1996; Radford et

al., 1997; Raghunand and Dale, 1999; Rhiel et al., 1997; Wong et al., 1994). The values reported fall within a range of 4.5-12×10^{-11} and 2.1-24.2×10^{-11} mmol/cell/hour for uninfected and infected Sf9 cells propagated in Sf900™II medium, respectively. Raghunand et al., (1999) reported that there is an increase in glucose consumption rate after infection, while others showed a reduction in the glucose consumption rate for infected cells in comparison with uninfected cells (Bernal et al., 2009; Rhiel et al., 1997; Wong et al., 1994).

The current study for Sf9 cells in CDM found that the glucose consumption rate of uninfected cells was the highest, followed by infected cells at a low ICD and the lowest glucose consumption rate was found for infected cells at a high ICD (Table 5.2). The glucose consumption rate for uninfected cultures of the current study (4.5×10^{-11} mmol/ cell/hour) was similar to that reported by Kamen et al. (1996) and Wong et al. (1994), but was lower than others (Benslimane et al., 2005; Bernal et al., 2009; Radford et al., 1997; Raghunand and Dale, 1999; Rhiel et al., 1997). The glucose consumption rate of infected Sf9 cells in the current study was lower than that reported by Bernal et al. (2009) and Wong et al. (1994). The discrepancy in glucose consumption rate on a per cell basis among the literature may result from the differences in cell size and medium used by the various groups. In addition, the glucose consumption rate of cells in culture was influenced by the presence of other carbohydrate sources (maltose) and AAs used as an energy source (glutamine, asparagine) as well as other elements available in the medium. Many investigators (Bedard et al., 1993; Drews et al., 2000; Neermann and Wagner, 1996; Raghunand and Dale, 1999) pointed out that there is an interrelationship in the glucose and glutamine uptake rates for Sf9 insect cells.

The prototype CDM used in these studies is a promising medium for metabolomics and fluxomics studies, especially in terms of AA uptake and protein production rates as it does not contain undefined peptides from hydrolysates that the cells can be used in parallel with free AAs. Therefore, the measurement of AA consumption rates for cells in CDM has the advantage of eliminating the effect of AAs originating from peptides. As a result, AA consumption rates for cells in CDM are expected to be higher than those in hydrolysate containing medium (Sf900™III) if cells require the same amount of AAs. Unfortunately, the total cell density for low and high ICD of cells in CDM and Sf900™III were not the same (2×10^6 and 6×10^6 cells/mL for Sf900™III and 1×10^6 and 5×10^6 cells/mL for CDM). Therefore, it is difficult to compare AA consumption rates (as well as other parameters) directly between these two media in this study. Fortunately, the ratios between high/low ICDs for the β-Gal yield of infected Sf9 cells in these two media were

comparable. A question of interest is whether the ratios between high/low ICDs for other parameters (intracellular metabolites, AA consumption rates) were also similar between these two media.

It is interesting to note that the ratios between high/low ICDs for AA consumption rates of infected Sf9 cells in CDM were much lower than those in Sf900™III (Fig. 5.15) despite the ratios for β-Gal yield of infected Sf9 cells in these two media being similar (Fig. 5.10). This result may be explained by a high level of peptides consumed by infected Sf9 cells in Sf900™III at the low ICD. There is evidence that very small peptides contribute to the nutritional value of a medium as a source of AAs (Heidemann et al., 2000; Nyberg et al., 1999) and so it is possible that the use of small oligo-peptides as an AA source is preferable than the use of free AAs in some situations. Di-peptides and tri-peptides are taken up more readily in the intestine than corresponding free amino acids (Grimble et al., 1987; Silk et al., 1985). In addition, the uptake of peptides seems to be independent of free amino acid uptake and their transport can be affected by other peptides but not by free amino acids (Brandsch et al., 1995a; Brandsch et al., 1995b). As a result, Sf9 cells in Sf900™III at the low ICD likely consumed small peptides as a source of AAs which is not accounted for in the AA consumption calculation, while less peptides would be available for consumption at the high ICD and hence, more free AAs are required in this case. Consequently, the ratio of AA consumption rates between high/low ICD for the case of infected Sf9 cells in Sf900™III were much higher than those for CDM, which does not contain peptides from hydrolysates. The ratios between high and low ICDs for other parameters including intracellular nucleotides, nucleotide sugars, organic acids and AAs of infected cells in either Sf900™III or CDM were not significantly different (Fig. 5.11-5.12).

5. 5 Conclusion

A Chemically Defined Medium (CDM) is a useful medium for metabolic studies as well as for avoiding some downstream process problems of recombinant protein production. This initial study using a prototype CDM for Sf9 insect cells from Life Technologies showed cells can be easily adapted into this medium. Although the peak cell density of the uninfected culture in the CDM was much lower than that in Sf900™III, the peak β-Gal yield at a low ICD in CDM was slightly higher than that in Sf900™III. Infected Sf9 cells in CDM were also subject to the cell density effect with the cell specific recombinant protein yield being reduced significantly with an increasing ICD. As found for infected Sf9 cells in Sf900™III, nutrient limitations remain as a possible cause of the cell

density effect. Results from the current study show that infected Sf9 cells in the CDM at a high ICD had a lower intracellular concentration of nucleotides, TCA cycle intermediates and AAs than those at a low ICD. The poorer AA uptake rates at the high ICD in comparison with those at the low ICD may partially explain the lower recombinant protein yield at the high ICD versus the low ICD. Although the ratios of the β-Gal yield between the high/low ICDs of infected Sf9 cells in CDM were similar to that in Sf900™III, the ratios of AA consumption rates of infected cells in CDM for high versus low ICDs was much lower than those in Sf900™III. This is a major difference between the two medium that presumably comes from the presence or absence of peptides originating from hydrolysates, which are available in Sf900™III but not in the CDM. As found for infected Sf9 cells in Sf900™III, aspartate, lysine and, to a lesser extent, arginine are among the AAs that show a poor uptake efficiency, although they do not appear to be limiting in the culture medium.

Based on data from Chapter 4 and Huynh et al. (2013), the most likely cause of the drop in yield at higher ICDs for CDM infections is an earlier drop in vDNA and recombinant protein mRNA levels possibly caused by a substrate limitation related to the supply of nucleotides. This chapter along with Chapter 4 supplies some data to support this possibility (low UTP levels at the high ICD versus the low ICD for example). However, this chapter does supply new data to suggest that peptides are an important source of amino acids post-infection and if vDNA/recombinant protein mRNA levels can be maintained for high cell density infections, the supply of sufficient amino acids to support correspondingly high protein production levels will become a challenge.

Chapter 6

Metabolic study of the cell density effect of HzAM1/HearNPV system in Sf900™III medium

6.1 Introduction

The baculovirus-insect cell expression systems have been widely used as a research tool for producing recombinant proteins (Kost et al., 2005; Mena and Kamen, 2011), human and veterinary vaccines (Mena and Kamen, 2011; van Oers, 2006), and as vectors for gene delivery (Hitchman et al., 2010; Hu, 2008). Besides being a valuable commercial tool for recombinant protein production, the baculovirus insect cell systems have been studied for the production of baculoviruses which can be developed as effective biopesticides to control various types of insect pests (Chakraborty et al., 1996; Chakraborty et al., 1999; Pedrini et al., 2006), especially as part of an integrated pest management program (Moscardi et al., 2011; Szewczyk et al., 2009).

Helicoverpa spp. are the major pests of field crops worldwide and it becomes difficult to control them because of the development of resistance to existing methods of chemical and biological control. In addition to the resistance to existing chemical pesticides, the increasing concern about the environment and food safety issues, and the desire of farmers to use safer pesticides are all reasons for the interest in biopesticides (Franzmann et al., 2008; Jacobson et al., 2009). Hence, the development of a viral biopesticide, as alternatives to the use of chemical pesticides, to control Helicoverpa pest species is potentially of great benefit for agriculture.

Baculoviruses, among other insect viruses, are regarded as safe and selective bioinsecticides, restricted to invertebrates (Moscardi, 1999). Baculoviruses are one of the most promising biocontrol agents, with a low chance of resistance development and proven high safety levels (Szewczyk et al., 2006). More than 50 baculovirus based pesticides have been registered and used worldwide (Moscardi et al., 2011). In fact, baculoviruses have been used to control caterpillar pests that affect major crops such as soybean, sorghum, maize, tomato, cotton, pigeon pea, and pepper in many counties including Brazil, China, India, America, and Australia (Buerger et al., 2007; Szewczyk et al., 2009). It is considered as an ideal tool for Integrated Pest Management (IPM) programs (Buerger et al., 2007; Moscardi et al., 2011).The market share for baculovirus biopesticides was estimated at about 5-10% of the potential market for biopesticides with a 14% annual increment (Glare et al., 2012).

Traditionally, baculovirus biopesticides have been widely produced *in vivo* from infected larvae raised in insectaries. A number of successful production processes of baculovirus biopesticides using infected larvae have been documented (Buerger et al., 2007; Harrison and Hoover, 2012; Moscardi et al., 2011). However, this production method is also associated with several limitations including high cost of production, requirement for

specific facilities for insect rearing, quality control problems in relation to the purity of products and contamination of insect rearing facilities by other viruses, bacteria or fungi. *In vitro* baculovirus biopesticide production in insect cell culture overcomes disadvantages associated with *in vivo* production (Harrison and Hoover, 2012; Moscardi et al., 2011). *In vitro* production is more promising in terms of process scalability and reliability (Moscardi, 1999). The production of wild-type NPVs using insect cell culture for use as biopesticides is thought to be a promising strategy (Murhammer, 1996).

In vitro production is a key focus of industry for producing baculovirus biopesticides. In fact, it has been indicated as a key element in making biopesticides more desirable in the market (Szewczyk et al., 2006). However, there are several technical limitations that need to be solved in order to successfully commercialize baculovirus biopesticide production *in vitro.* At the present, none of the *in vitro* production systems reported for baculoviruses have achieved economically viable yields for commercial use because of high production costs even with the use of fed-batch cultures. One of the bottlenecks is the reduction in cell specific yield at high cell density infections regardless of the ability to grow cells to a very high cell density as uninfected cultures. The so called 'cell density effect' has been reported thoroughly for the *Spodoptera frugiperda* (Sf9/Sf21) cell line (Carinhas et al., 2009; Caron et al., 1990; Doverskog et al., 2000; Huynh et al., 2013; Jesionowski and Ataai, 1997; Radford et al., 1997; Reuveny et al., 1993; Taticek and Shuler, 1997; Wong et al., 1996; Yamaji et al., 1999). There are also a few papers that have investigated the reduction in cell specific yield for wild-type baculovirus infected *Heliothis zea* (HzAM1) cells (Chakraborty et al., 1996) and *Antacarsia gemmatilis* cells (Micheloud et al., 2009). This issue is a key drawback for improving the yield of the baculovirus infected insect cell systems while there is a critical need to reduce production costs given the low margin nature of biopesticide products.

It has been suggested that the cause of the drop in productivity at high cell densities for baculovirus infection processes is related to nutrient limitations rather than accumulation of toxins (Drews et al., 1995; Radford et al., 1997; Wong et al., 1996). Many attempts have been made to identify the cause of the cell density effect including the measurement of extracellular metabolites to identify the limiting nutrients in the medium (Caron et al., 1990; Drews et al., 1995; Reuveny et al., 1993); the measurement of consumption rates and fluxomics analysis (Bernal et al., 2009); and supplementing culture media with glucose, glutamine, complex nutrient mixtures, and key intermediate metabolites (Carinhas et al., 2010; Reuveny et al., 1993). However, the limitation of these approaches is that the metabolite levels in the media might not reflect intracellular

metabolite levels. For many reasons, some metabolites may not get into the cells even if they are available in the culture medium at reasonable levels. Therefore, intracellular metabolite measurements can provide a better understanding of what happens inside the cells and consequently, appropriate actions may be taken to improve yields.

The limitations related to the reduction in cell specific yield at high cell density infections have been investigated in the Sf9/rAcMNPV system, as a control system, using a metabolomics approach (Chapter 4). In particular, intracellular metabolite concentration and consumption rates of key metabolites were measured in order to possibly identify limitations during high cell density infections. For the HzAM1 cell line infected with a wild-type baculovirus, the question addressed in this chapter is whether or not potential intracellular limitations identified in the Sf9/rAcMNPV system also apply to the HzAM1/HearNPV? Therefore, in this study, substrate consumption rates as well as intracellular metabolite levels of infected cells at both low and high cell densities at the time of infection have been measured and compared between these two infection conditions.

6.2 Materials and methods

6.2.1 Cell line, virus and medium

The *Helicoverpa zea* cell line (BCIRL-HZAM1) and wild-type *Helicoverpa armigera*single nucleopolyhedrovirus (HearNPV, Strain H25EA1) have been described previously in the PCT patent WO/2005/045014 by Reid and Lua (2005). Working stock cells were maintained in 25 ml suspension cultures in 125ml Erlenmeyer flasks (Corning Incorporation, Corning, USA) and routinely passaged every 3-4 days in single-use shaker flasks (Corning, Lowell, MA) at seeding densities of $0.3\text{-}0.5\times10^5$ cells/mL. The shaker cultures were agitated at 120 rpm on an orbital shaker platform (Thermoline, NSW, Australia) and incubated at 28^oC in a refrigerated incubator (Thermoline). Cells were propagated in Sf900^{TM}III serum-free medium (Life Technologies, Carlsbad, USA).

The virus stock was prepared as described previously (Tran et al., 2012). Virus stocks were stored at -80^oC, and were titered prior to use. The titers of the HearNPV virus stock used in the experiments were around $4\text{-}6\times10^7$ PFU/ml as determined by a suspension culture assay (Matindoost et al., 2012). Due to the low titer of the HearNPV virus stocks, this necessitated the use of high volumes of virus to achieve high MOI infections. This was not a problem for the Sf9/rAcMNPV system as very high titer stocks are readily prepared for AcMNPV.

6.2.2 Experimental procedures

There were two experiments conducted to assess the efficiency of the extraction protocol for infected HZAM1cells at different times post-infection, and to investigate the difference between low and high infection cell densities (ICDs) in terms of intracellular metabolite concentrations, substrate consumption rates and occlusion body (OB) yield.

The first experiment involved evaluation of the extraction protocol for intracellular metabolites (Tran et al., 2012) for infected HzAM1cells via a time-course infection experiment. This experiment identified the latest time point post-infection at which the infected cells still maintain their membrane integrity during quenching and washing procedures. The cells were setup at the initial cell density of 1×10^6 cells/mL and allowed to grow to 2×10^6 cells/mL (after 1 day post inoculation) and then diluted back to 1×10^6 cells/mL for infection at an ICD of approximately 1×10^6 cells/mL with a multiplicity of infection (MOI) of 5 PFU/cell. The infection was conducted in a 1 L bottle and then aliquoted into various shaker flasks at 20 mL each for intracellular metabolite extractions at 12 hour intervals from 0-96 hours post-infection (hpi). Three shaker flasks were set up at 35 mL each as infected controls for measuring the total cell density (TCD) and viability, OB yield, and viral DNA (vDNA) copies at the various time points mentioned above. The uninfected control (in triplicate) was set up and grown to a peak cell density of 1×10^7 cells/mL demonstrating that the cells were in optimal condition during the experimental period.

The second experiment investigates the changes in the intra- and extra-cellular environment as well as the production and consumption rate of various metabolites by the cells infected at low (0.5×10^6 cells/mL) and moderately high (2×10^6 cells/mL) cell densities. In addition, this experiment also aims to investigate the difference in cell condition before infection among different cell densities at the time of infection (with a wide range from 0.5×10^6 up to 8×10^6 cells/mL). For the case of a low cell density infection, the culture was set up at 0.55×10^6 cells/mL but the ICD after adding the virus was 0.5×10^6 cells/mL. For the case of a moderate high cell density infection, the initial seeding cell density was at 0.5×10^6 cells/mL and the cells were allowed to grow to about 2.7×10^6 cells/mL and the ICD after adding the virus was 2×10^6 cells/mL. For the case of the other ICDs, the initial seeding cell density was at 0.5×10^6 cells/mL and the cells were allowed to grow to different cell densities at the time of infection in order to get the cell densities after adding virus, of around 1, 1.5, 3 and 4×10^6 cells/mL, corresponding to the cell density before infection of 1.2, 2, 5 and 8×10^6 cells/mL, respectively. All of the infections were conducted at an MOI

of 5 PFU/cell. The experiment was conducted in shaker flasks with biological triplicates at each ICD. Samples for intracellular metabolite analysis were taken at 12 hour intervals from 0-60hpi in triplicate for both the low (0.5×10^6 cells/mL) and the moderately high (2×10^6 cells/mL) ICDs. For the other infection cell densities (1, 1.5, 3 and 4×10^6 cells/mL), samples for intracellular metabolite analysis were taken at 0 hpi only. The additional 0 hpi samples were taken in order to assess whether, as cells grow in culture prior to infection, there is a consistent change in intracellular levels of certain key metabolites. Such changes are likely to affect the yield post-infection. While ideally samples would have been taken post-infection for all cell densities investigated this would have greatly increased the cost of the experiment.

Samples for extracellular metabolite analysis and for measuring the TCD, viability, intracellular vDNA copies and OB yield were collected from 3 infected control shakers at 12 hour intervals from 0-72 hpi (each infection cell density had 3 infected control shakers). An uninfected control was also set up and left to grow to a peak cell density in batch culture (around 1×10^7 cells/mL).

6.2.3 Intracellular metabolite extraction

Intracellular metabolites were extracted using the optimized protocol as described previously (Tran et al., 2012). Briefly, infected cultures were set up in 125 mL shaker flasks at a working volume of 20 mL, involving three flasks for each treatment at each time point as biological triplicates. Quenching solution (QS) (1.1% NaCl, 0.2% Pluronic F68) was prepared in 250 ml shaker flasks at 80 mL each and placed in an ice bath to make sure the temperature of the quenching solution was around 0.5 to 1^oC. Taking out each flask at a time from the incubator, the culture of each flask (20 mL) was quickly poured into 80 mL of ice-cold QS. The quenched culture was then centrifuged (1000×g, 1 min) at 0^oC. The supernatant was removed and the cell pellet was washed with the sample volume of ice-cold QS. Another centrifugation step was applied (1000×g, 1 min, 0^oC) to collect the cell pellet which was then extracted with a cold 50% acetonitrile (ACN) solution at the ratio of 1 mL for 2×10^6 cells. The cell extracts were clarified by centrifugation (5000×g, 5 min, 0^oC), with the supernatants collected, frozen at -80^0C and then dried in a freeze-dryer (Alpha 1-4 LSC, Martin Christ, Germany). The freeze-dried samples were then stored at -80^0C until analysed. For the direct extract, infected cultures were poured directly into the same volume of 100% ACN and then the supernatants were collected for subsequent steps as described above with the cell extract samples.

6.2.4 Assays

Total cell density (cell/mL) and cell diameter data was obtained using a Multisizer^{TM}4 Coulter Counter (Beckman Coulter, Fullerton, CA, USA). Samples of various cell densities were initially diluted with medium to a TCD of around 0.5×10^6 cells/mL before proceeding with the cell enumeration process. Cell viabilities were estimated from triplicated hemocytometer counts using the 0.05 % (w/v) Trypan Blue exclusion method (Nielsen et al., 1991).

Baculovirus occlusion bodies (OBs) were extracted from infected cells using SDS digestion, and were enumerated via microscopy using a hemocytometer, as described previously (Pedrini et al., 2005). The OB count for each sample was conducted in technical triplicates.

The number of vDNA copies was quantified using the quantitative real time polymerase chain reaction (qRT-PCR) as described previously (Pedrini et al., 2011; Rosinski et al., 2002). Briefly, the vDNA standard was prepared from budded virus and purified using mini kit genomic tips (Qiagen, Venlo, Netherlands), and then quantified using a Quant-iT picoGreen dsDNA assay kit (Life Technologies). The vDNA standard curve was generated from 6 dilutions ranging from 3×10^{-1} to 3×10^{-6} ng/µL. Samples (1×10^6 cells/mL) were pelleted (300×g, 5 min) and kept in -20^0C for later analysis. Supernatants from the same samples were also kept for measuring extra-cellular vDNA. Prior to measuring intra-cellular vDNA, pellets were treated with 1 mL of digestion buffer (100 mM NaCl, 10 mM Tris.HCl, 25 mM EDTA, 0.5% SDS, 0.1 mg/mL Proteinase K) at 50^oC for 15 hours. Supernatant samples were also treated in the same way with the same volume of a 2X digestion buffer. Alkaline saline (25 mM Na_2CO_3, 50 mM NaCl) was used to release ODV from the cell lysate samples. The Eppendorf epMotion 5075 Robotics System (Eppendorf, Germany) and the ABI PRISM® 7900HT Sequence Detection System (Life Technology, USA) were used for qRT-PCR analysis. Each sample was measured using technical triplicates in the same PCR plate. The estimated genome size of 1.4×10^{-7} ng/genome (Pedrini et al., 2011) was used to convert the mass production into the genome copy number basis.

Intracellular nucleotides and TCA cycle intermediates were measured by LC-MS/MS as described in Dietmair et al. (2012) with the following modifications: the analytical column was equipped with a pre-column Security Guard Gemini-NX C18 4mm x 2 mm I.D. cartridge (Phenomenex, Aschaffenburg, Germany). The samples were run with sample- and analyte-relevant calibration standards and pooled QC samples (Hodson et al., 2009;

Sangster et al., 2006) to control for reproducibility of data acquisition and to ensure data integrity. Analyte stock solutions were prepared in purified water (Veolia) and aliquots of each solution were mixed to achieve a final calibrant solution at 200 µM. This calibrant solution was serially diluted and the dilutions used as calibration standards from 200 to 0.006 µM, constituting $9 \leq x \leq 20$ calibration points for all analytes to account for differential responses in the mass spectrometer. Data were processed and analysed in Analyst 1.5.2 and MultiQuant 2.1.1 (ABSciex, Canada).

A HPLC system was used to analyse extra- and intra-cellular amino acids (AAs) as described previously (Dietmair et al., 2010) with some modifications including the increase of flow rate from 1 mL/min to 2 mL/min which resulted in a time reduction for each run. In brief, derivatised amino acids were analysed by RP-HPLC. Derivatisation was performed in a high-performance autosampler (Agilent HiP-ALS SL, G1367C). First, 0.5 uL of sample containing 250 uM of internal standards, sarcosine and 2-aminobutanoic acid, was added into 2.5 uL of borate buffer (0.4 N, pH 10.2, Agilent PN: 5061-3339), mixed and incubated for 20 s at 4^{o}C. Then 1 uL of OPA reagent (10 mg *o*-pthalaldehyde/mL in 3-mercaptopropionic acid, Agilent PN: 5061-3335) was added to initially derivatise primary amino acids. The reaction was mixed and incubated for 20 s at 4^{o}C. After that 0.4 uL of FMOC reagent (2.5 mg 9-fluorenylmethyl chloroformate /mL in acetonitrile, Agilent PN: 5061-3337) was added, mixed and incubated for 20 s at 4^{o}C, to derivatise other amino acids. 45.6 uL of Buffer A (40 mM Na_2HPO_4, 0.02% NaN_3, pH 7.8) was added to lower the pH of the reaction prior to injecting the 50 uL reaction onto an Agilent Zorbax Extend C-18 column (3.5 um, 4.6×150 mm, Agilent PN: 763953-902) with a guard column (Security Guard Gemini C18, Phenomenex PN: AJO-7597). Column temperature was kept at 37^{o}C in a thermostatted column compartment (Agilent TCC, G1316B). Chromatography was performed using an Agilent 1200-SL HPLC system, equipped with an active seal wash and a degasser (Agilent Degasser, G1379B). The HPLC gradient was 2-45% B from 0-18 min, 50-60% B from 18.1-20 min, 100% B from 20.1-24 min, and 2% B from 24.1-27 min – using a binary pump (Agilent Bin Pump SL, G1312B). Buffer B was 45% acetonitrile, 45% methanol and 10% water. Flow rate was 2 mL/min. Derivatised amino acids were monitored using a fluorescence detector (Agilent FLD, G1321A). OPA-derivatised amino acids were detected at 340_{ex} and 450_{em} nm from 1-18 min, and FMOC-derivatised amino acids at 266_{ex} and 305_{em} nm from 18-27 min. Chromatograms were integrated using ChemStation (Rev B.03.02[341]).

Extracellular organic acids (α-ketoglutarate, pyruvate, succinate, lactate, fumarate, acetate and propionate) and sugars (sucrose, glucose and maltose) were also analyzed by

HPLC (Agilent 1200 series, Agilent, Mulgrave, Victoria, Australia) using both MWD and RID detectors. The detail of the method is presented in chapter 2 of this thesis.

The intracellular ATP in the first experiment was measured using the ATPlite luminescence ATP detection assay system (PerkinElmer Life Sciences, Boston, MA, USA), which was described in Tran et al. (2012). This assay is based on the production of light when ATP reacts with D-Luciferin in the presence of Luciferase, and was conducted according to the manufacturer's instructions.

6.2.5 Statistical analysis

One-way analysis of variance (ANOVA) was used to determine whether the means from two or more groups of data were significantly different at the 95% confidence level. Minitab 15 Statistical Software (Minitab, State College, PA, USA) was used for all data analysis. Treatment mean differences were tested using the Tukey's HSD test.

6.3 Results

6.3.1 Assessment of the extraction protocol for infected HzAM1 cells post-infection

Figure 6.1 presents results for the evaluation of the extraction protocol at different times post-infection. For an infection at a high MOI (5 PFU/cell), the cell density (cells/mL) increase post-infection was minimal (about 41%) that was almost negligible compared with the uninfected culture that reached a peak cell density of around 1×10^7 cells/mL (data not shown). In addition, the cell diameter post-infection quickly increased for the first 24 hpi, and then increased slowly until 60 hpi, with a peak increase in cell diameter of about 9% and then declined quickly after 60 hpi (Fig. 6.1 a). Also as shown in Fig. 6.1a, the cell viability of infected cultures is very high (more than 90%) for the first 48 hpi; after which it started to decrease to around 80% at 60 hpi and then dropped sharply after that (Fig. 6.1 a). These results indicate that the cell integrity was slightly affected after 48 hpi, and more badly after 60 hpi when infected cells began to die and lyse.

Figure 6.1 b shows the kinetics of vDNA and OB production for infected HzAM1 cells being as expected for wild-type HearNPV infected HzAM1 cells in Sf900™III serum free medium. The vDNA production started at 6 hpi and showed a rapid increase from 12 until 24 hpi to a value of about 83% of the peak yield (2.5×10^5 copies/cell) seen at 36 hpi. The OB production commenced later (around 24 hpi) and sharply increased until 60 hpi, and then slowly increased to the peak yield between 72-168 hpi. The peak OB yield may be achieved as early as 72 hpi. However, an OB count using a microscope is subject to a

high level of error, especially for immature OB at early stages. Therefore, OB yields estimated at the later stage of 168 hpi (7 days post infection) is more accurate and is normally used for estimating the OB yield of an infected culture. The peak specific OB yield achieved was 354 OB/cell for the current experiment. The results of the vDNA and OB yields indicated that the HearNPV infected HzAM1 cells set up in this study were optimally-infected, and were suitable for evaluation of the extraction protocol for endometabolite studies.

The intracellular ATP concentration of infected HzAM1 cells and the ATP recovery of cell extract samples compared to the direct extract over the time course post-infection (from 0 to 96 hpi) are shown in Fig. 6.1 c. The recovery of ATP in the cell extract samples was very high (recovery of over 93% of the direct extract) for the first 48 hpi. The ATP recovery was reasonable until 60 hpi (about 85% of the direct extract) but reduced quickly after that point. This indicates that the extraction protocol works well for infected HzAM1 cells propagated in Sf900™III medium until 48 hpi and possibility until 60 hpi. The peak intracellular ATP level of the cell extract was around 4 mM obtained during the first 48 hpi. There was no significant difference among intracellular ATP levels up to 60 hpi (Fig. 6.1 c) although the ATP level at 60 hpi was about 85% of the peak value. This result indicates that 48 hpi and possibly 60 hpi is the latest time that the infected cells can be extracted without a significant loss of intracellular metabolites.

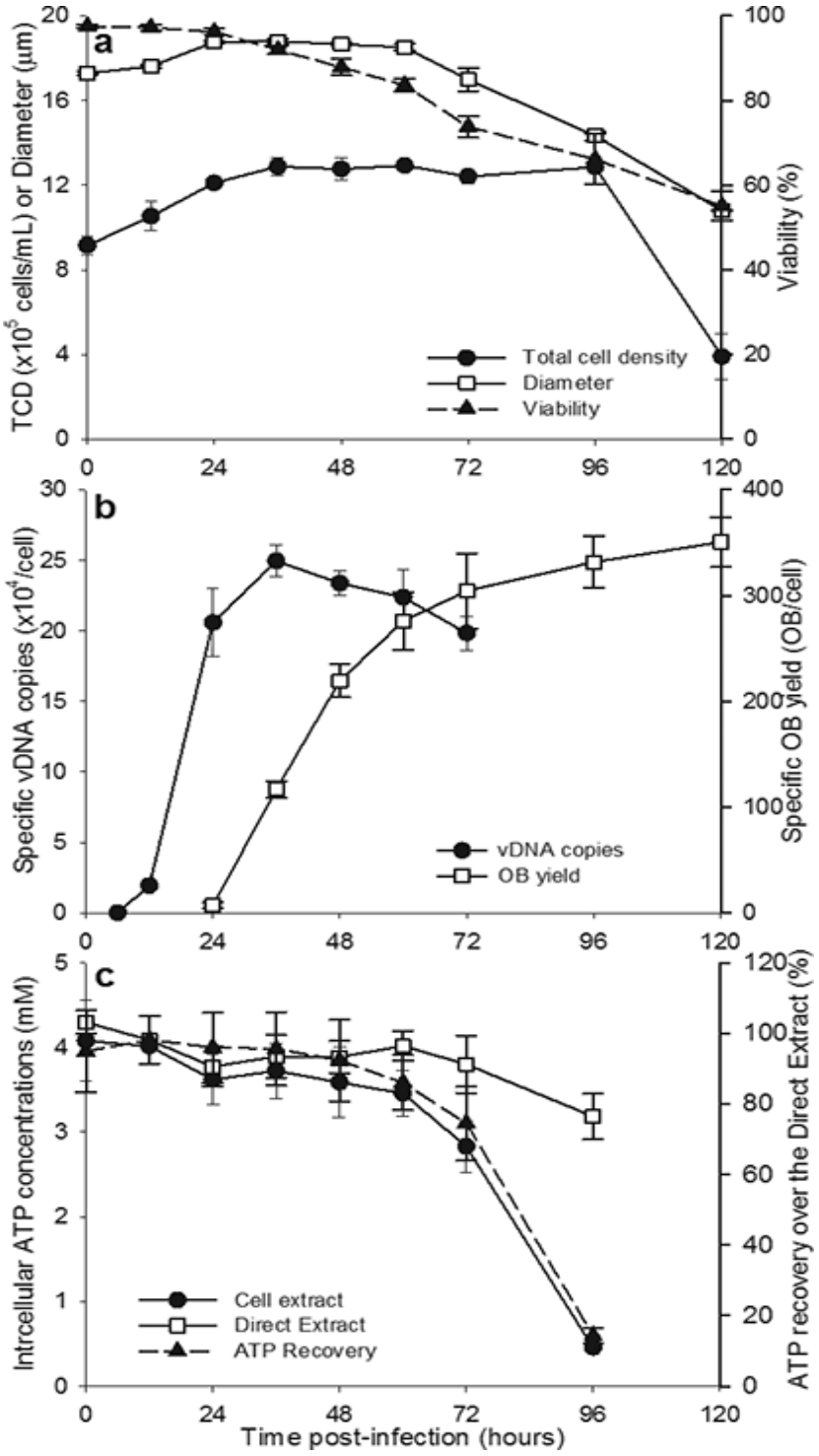

Fig. 6.1 The kinetics of cell growth, cell size expansion and viability (a), specific vDNA and OB yields (b) and intracellular ATP levels and ATP recovery over various times post-infection (c) of HzAM1 cells infected with a wide-type baculovirus (HearNPV) at a multiplicity of infection (MOI) of 5 PFU/cell. Infections were conducted in Sf900™III medium at infection cell densities (ICD) of 1×10^6 cells/mL. The experiment was conducted in shaker-flask suspension cultures. Each data point is the average from three biological replicates, and the error bars represent the standard deviation.

6.3.2 Kinetics of cell growth post-infection and yields of various ICDs

Figure 6.2 shows the results of cell growth (cells/mL) and cell size increase post-infection and the virus yields for various ICDs of 0.5-4×10^6 cells/mL for wild-type baculovirus infected HzAM1 insect cells. The cell density increase post-infection was in the range of 25-48% when infections were conducted at the different ICDs indicated above, and there was no significant difference among different ICDs (Fig. 6.2a). The total cell density peaked around 48-60 hpi for most of the ICDs. The early infection events of virus getting into the cell and inhibiting cell growth were similar for the different ICDs and showed a typical pattern for a baculovirus infection process. The total cell density of the control uninfected cultures continued to double almost every 24 hours to the peak cell density expected for HzAM1 insect cells propagated in Sf900™III of around 1×10^7 cells/mL (Fig. 6.2 a).

In all infected cultures, the average cell diameter increased rapidly within the first 24 hpi followed by a further slow increase to a peak value by 48 hpi and reduced after that point for most of the cases, except for the high ICDs (3 and 4×10^6 cells/mL), in which cases the cell diameter started to reduce after 24 hpi (Fig. 6.2 b). Unlike the increase in cell density post-infection, the enlargement of the cell diameter post-infection reduced with the increase of the ICD. The highest increase of cell volume post-infection of 50% was obtained at the ICD of 0.5×10^6 cells/mL. The cell size increase post-infection reduced to 33% at the ICD of 2×10^6 cells/mL and 20% for the highest ICD investigated of 4×10^6 cells/mL. The difference in cell volume increase post-infection is a good indicator of the difference in cell specific yields among the various ICDs.

As shown in Fig. 6.2 c, the timing for vDNA production was in general similar among the various ICDs. The vDNA production commenced at 6 hpi, rapidly increased in the period of 12-24 hpi, and achieved a peak value at 36 hpi. Higher ICDs seemed to reach the peak vDNA yield earlier than that of the lower ICDs. In general, the time frame from the starting point of vDNA production to the point where peak yields were achieved was similar for different ICDs (Fig. 6.2 c). This indicates that the infection process follows a similar time sequence for low and high ICDs, at least in terms of the time at which vDNA synthesis commences, but the vDNA productivity during the post-infection period and the period of vDNA production is lower for the high density infections. For OB production, the timing of OB production post-infection was not available due to the inaccuracy and time required for counting of immature OBs at the early infection periods. Therefore, only the peak yield at 168 hpi is presented and this shows a rapid reduction in specific OB yields as

the ICD increased (Fig. 6.2 d). Although there was no difference among ICDs in terms of cell density increase post-infection (Fig. 6.2 a), the cell specific yields (vDNA, OB) significantly reduced with increasing ICD (Fig. 6.2 c, d).

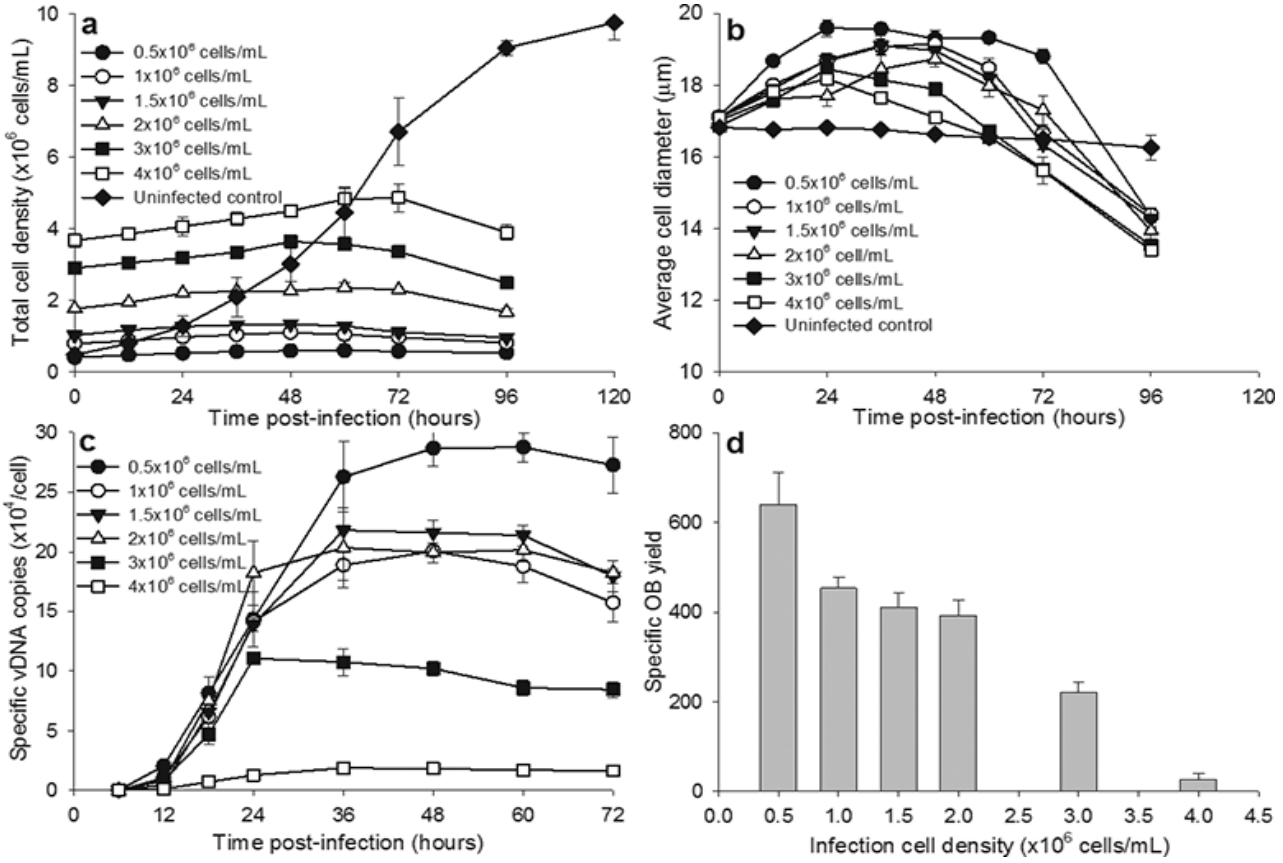

Fig. 6.2 Total cell density (a), cell hypertrophy (b), specific vDNA (c) and OB production (d) of HzAM1 cells infected with a wild-type HearNPV. Infections were conducted in Sf900™III serum free medium at various ICDs from 0.5-4×10^6 cells/mL at an MOI of 5 PFU/cell. The experiment was conducted in shaker-flask suspension cultures. Each data point is the average from three biological replicates, and the error bars represent the standard deviation. For OB yield, measurement was conducted only once at 168 hpi due to the low accuracy of OB counts at earlier stages.

The data presented previously can be summarized by plotting the peak yields of each infection against its associated peak cell density (PCD) for both volumetric and specific yields (Fig. 6.3). The volumetric production of vDNA (Fig. 6.3 a) or OB (Fig. 6.3 c) initially increased linearly with increasing PCD until the peak values were obtained at the PCD of 2.4×10^6 cells/mL for both cases with peak volumetric yields of 4.5×10^{11} copies/mL and 9.2×10^8 OB/mL for vDNA and OB yields, respectively. Volumetric yields of vDNA and OB significantly reduced when the PCD increased above the optimal PCD for the media used. The cell-specific production of vDNA (Fig. 6.3 b) and OB (Fig. 6.3 d) declined quickly with increasing PCD from 0.6×10^6 cells/mL until 4.9×10^6 cells/mL. Specific yields declined from

2.88×10^5 copies/cell to 0.19×10^5 copies/cell for vDNA and from 640 OB/cell to 27 OB/cell for OB production. There were significant differences in specific vDNA and OB yields among various PCDs investigated, except for those at PCDs in the range of $1.1\text{-}2.4\times10^6$ cells/mL, which were statistically similar for both specific vDNA and OB yields (Fig. 6.3 b, d).

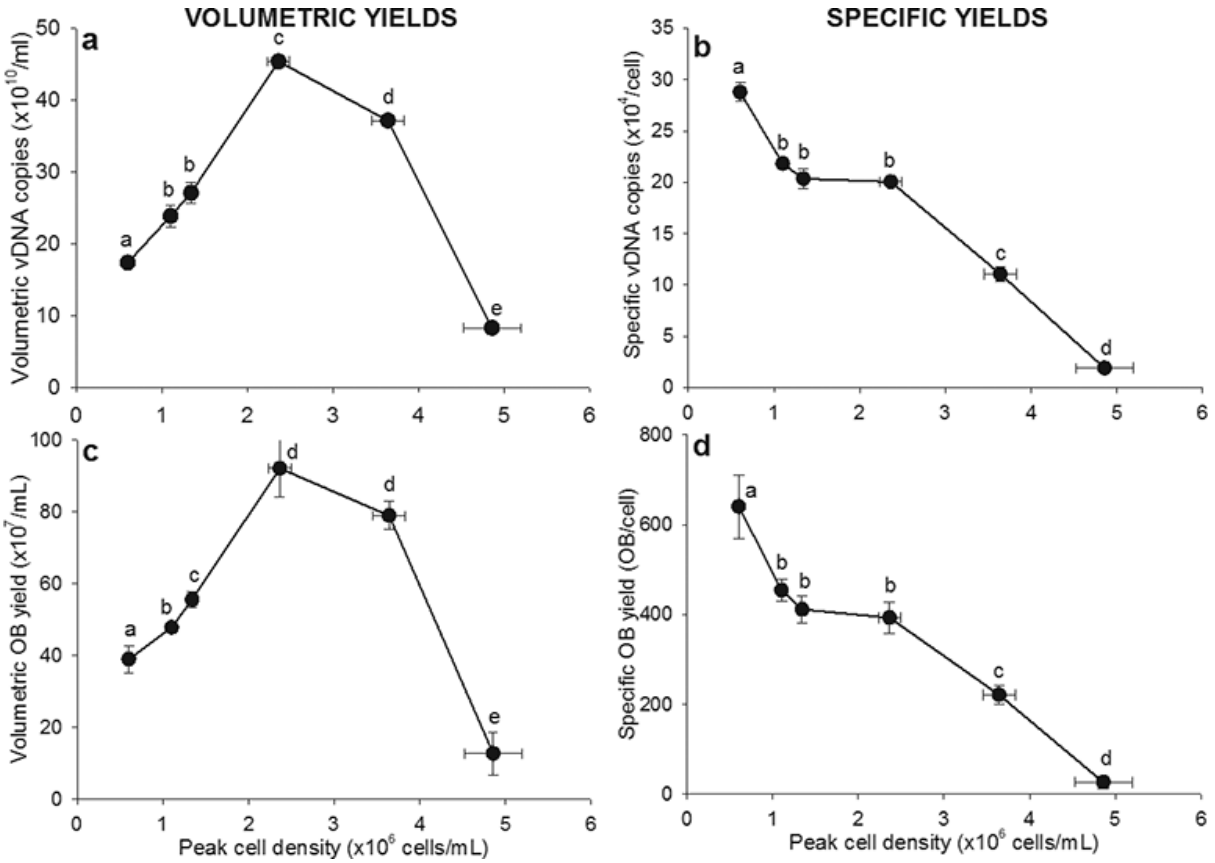

Fig. 6.3 Correlations between the peak yields (volumetric or specific) of vDNA (a, b) or OB(c, d) and the peak cell density (PCD) from HzAM1 cell cultures infected with a wild-type baculovirus (HearNPV) at various ICDs of 0.5 to 4×10^6 cells/mL, and a MOI of 5 PFU/cell. The experiment was conducted in shaker-flask suspension cultures. Each data point is the average from three biological replicates, and the error bars represent the standard deviation. Significance testing was performed separately for each experimental set of data points with different letters indicating values that are significantly different according to Tukey's HSD (α=0.05).

6.3.3 Intracellular nucleotide and amino acid concentrations of uninfected cultures

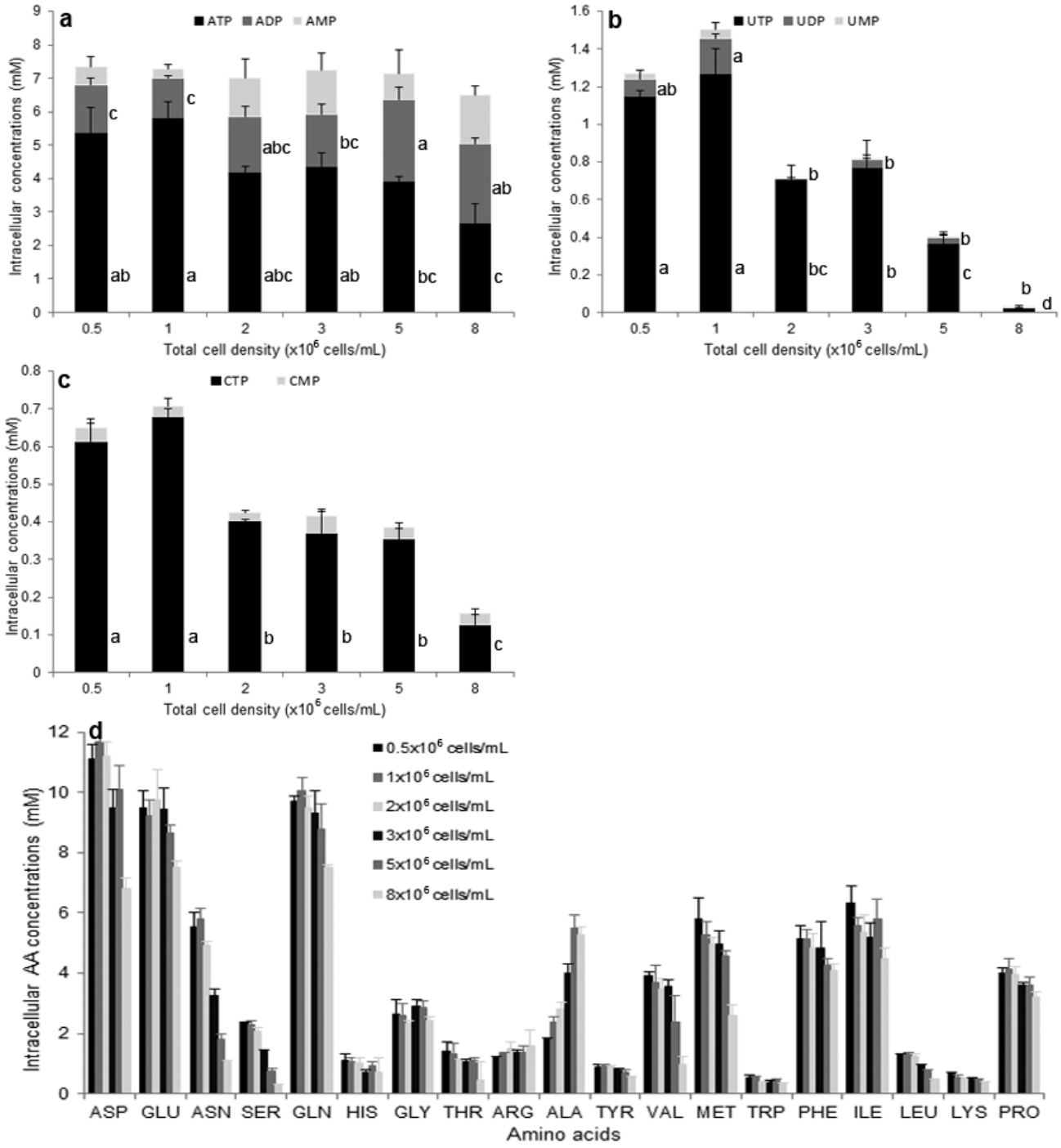

Fig. 6.4 Intracellular concentrations of adenosine (a), uridine (b) and cytidine (c) nucleotides and amino acids of uninfected HzAM1 cell cultures at various cell densities from 0.5 to 8×10^6 cells/mL. Cultures were propagated in Sf900™III serum free medium. The experiment was conducted in shaker-flask suspension cultures. Each data point is the average from three biological replicates, and the error bars represent the standard deviation. Significance testing was performed separately for each experimental set of data points with different letters indicating cases that are significantly different according to Tukey's HSD (α=0.05).

Figure 6.4 represents the intracellular nucleotide and amino acid (AA) concentrations of uninfected HzAM1 insect cells at various cell densities (0.5-8×10^6 cells/mL). Intracellular nucleotide tri phosphates (ATP, UTP and CTP) reduced significantly with the increase of total cell density of the uninfected cultures (Fig. 6.4 a, b, c). In all cases, there was no significant difference in the levels of nucleotide tri-phosphates between the two lowest cell densities of 0.5 and 1×10^6 cells/mL, but then the levels reduced when the cell density increased further (2-8×10^6 cells/mL). In particular, at the cell density of 8×10^6 cells/mL, the concentrations of UTP and CTP dropped to very low levels in comparison with those at the cell density of 1×10^6 cells/mL, about 2% and 19%, respectively. The ATP level at the cell density of 8×10^6 cells/mL also decreases compared to that for the cells at 1×10^6 cells/mL (50%), but the levels of total adenosine generally remain at a similar level for all cell densities. In addition, the intracellular concentrations of most amino acids (AA) decreased with the increase of the total cell density, especially for the case of the very high cell density of 8×10^6 cells/mL, where the intracellular AA concentrations were significantly reduced in most cases (Fig. 6.4 d). These results indicate that substrate limitations for nucleic acid and protein production are already potentially appearing inside the cells at high cell densities in cultures even before infections are initiated.

6.3.4 Intracellular metabolites of infected cultures at low and moderately high ICDs

Intracellular concentrations of 33 metabolites (including nucleotides, nucleotide sugars and organic acids) at 6 time points post-infection (0, 18, 24, 36, 48 and 60 hpi) of low (0.5×10^6 cells/mL) and high (2×10^6 cells/mL) ICDs have been analysed and results are presented in Fig. 6.5. The orthogonal projection to latent structures – discriminant analysis (OPLS-DA) of all the samples over the time course of the infections (Fig. 6.5 a) showed a clear separation of low and high ICD data. The biological replication is reliable as the scores for the three replicates indicate similar positions in the biochemical space (Fig. 6.5 a). Based on the OPLS-DA loadings (Fig. 6.5 b), the metabolites that are most influential in the projected separation between low and high ICDs are the nucleoside tri-phosphates (ATP, CTP, UTP), nucleoside di-phosphates (ADP, GDP, UDP), nucleoside mono-phosphates (AMP, GMP, CMP, UMP), fumarate (FUM), malate (MAL), ribose-5-phosphate (R5P), nicotinamide adenine dinucleotide (NAD), nicotinamide adenine dinucleotide phosphate (NADP) and UDP glucose (UDPG). These metabolites have a variable importance on projection (VIP) score of more than 1 and have been selected for further

statistical analysis as detailed in Table 6.1. Generally, intracellular metabolite concentrations at the low ICD were higher than those at the high ICD (Table 6.1).

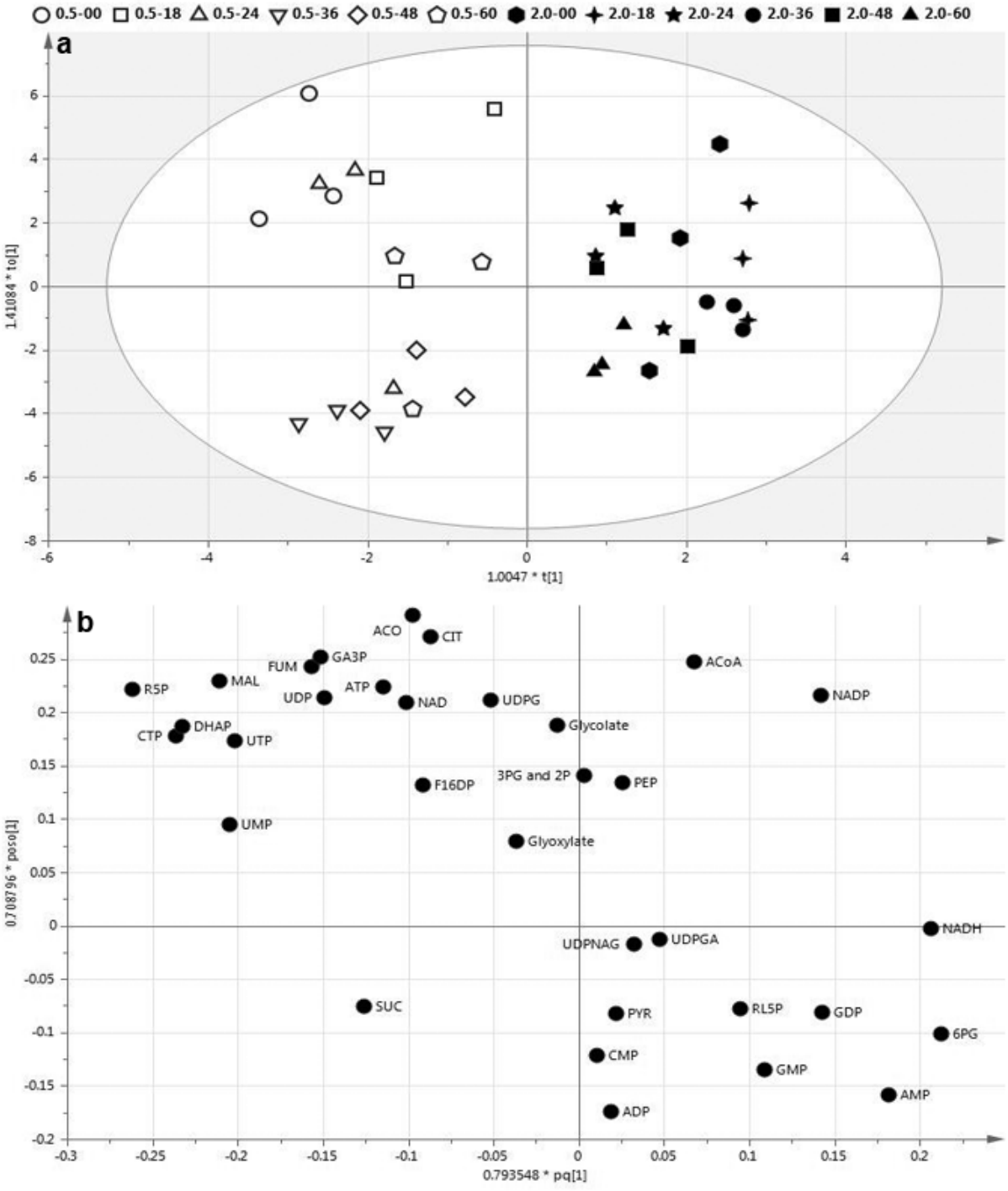

Fig. 6.5 Multivariate analysis of intracellular metabolite concentrations of infected HzAM1 at low ($0.5x10^6$ cells/mL) and moderately high ($2x10^6$ cells/mL) ICDs. Orthogonal projection to latent structures–discriminant analysis (OPLS-DA) scores (a) and loadings (b) plots of the 6 time points post-infection at low and high ICDs, classified by cell density. OPLS-DA model metrics: Predictive component R2X = 0.124; R2 = 0.857; Q2 = 0.685; R2Y = 1: Orthogonal component R2X = 0.26. Infections were conducted in Sf900™III serum free medium at an MOI of 5 PFU/cell. The experiment was conducted in shaker-flask suspension cultures.

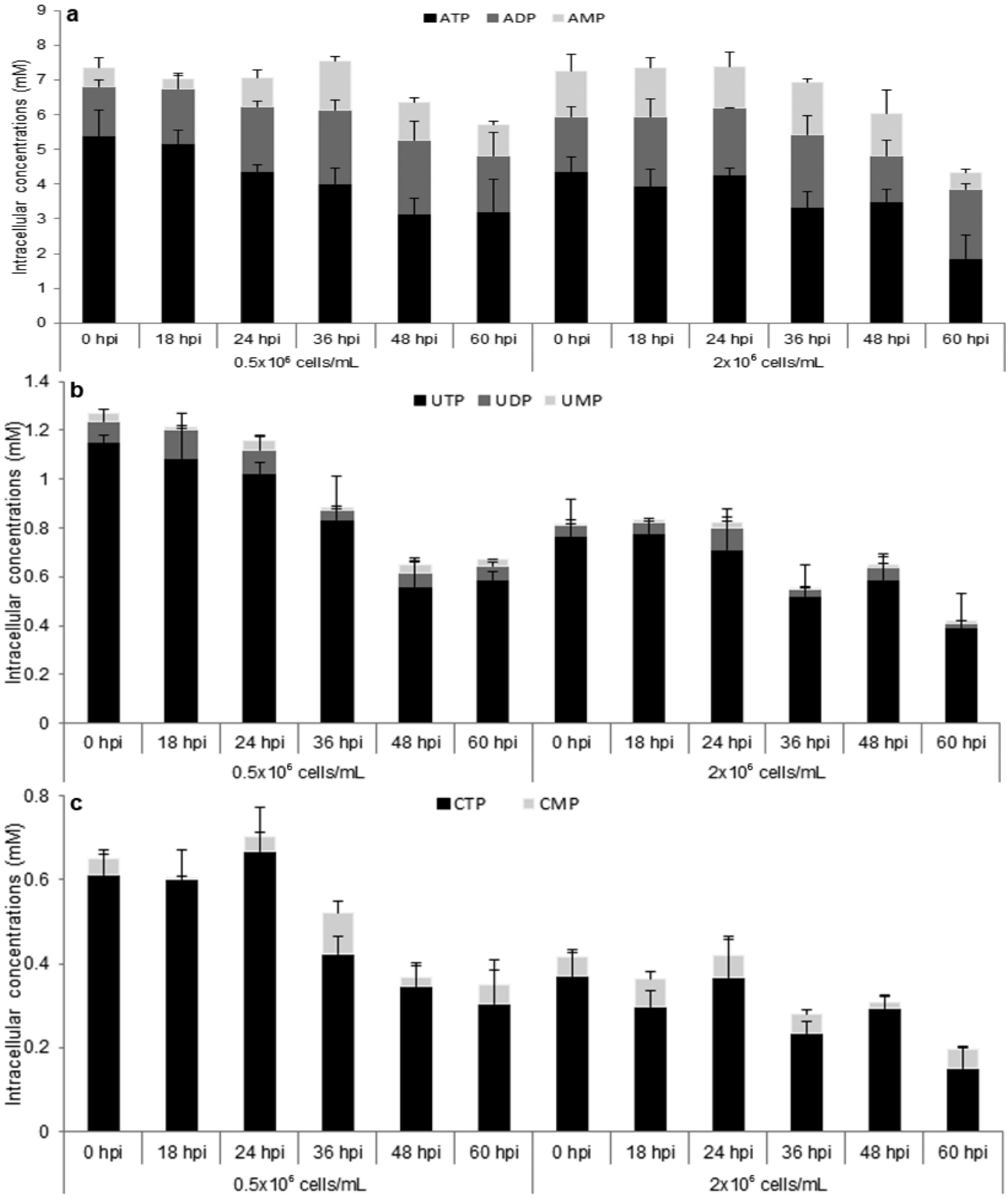

Fig. 6.6 Stacked bar charts of (a) adenosine, (b) uridine, and (c) cytidine nucleotide concentrations of 6 time points post-infection of infected HzAM1 cells at low($0.5x10^6$ cells/mL) and moderately high ($2x10^6$ cells/mL) ICDs. Infections were conducted in Sf900™III medium at an MOI of 5 PFU/cell (HearNPV). The experiment was conducted in shaker-flask suspension cultures. Each data point is the average from three biological replicates, and the error bars represent the standard deviation.

The concentrations of nucleotide tri-, di-, and mono-phosphates of infected HzAM1 cells at low (0.5×10^6) and moderately high (2×10^6 cells/mL) ICDs over the time course of infections are presented in Figure 6.6. Intracellular nucleotide tri-phosphate levels seemed to reduce over time post-infection and when the ICD increased (Fig. 6.6 a, b, c). However, statistical analysis only showed significant differences between early and late infection stages of the same ICD, but no significant difference was found between low and high ICDs at the same time points post-infection for the case of ATP (Table 6.1). For the total Adenosine (ATP+ADP+AMP), there was no statistical difference between low and high ICDs. Also, no significant difference among treatments was found for ADP, UDP, UMP and GMP. In contrast, the intracellular concentrations of UTP and CTP at the early infection stages of the low ICD were significantly higher than those at the late infection stages and at the high ICD of the same infection stage (Fig. 6.6 b, c and Table 6.1).

Figure 6.7 represents the intracellular AA concentrations of infected HzAM1 cells with a wild-type HearNPV at low and moderately high ICDs over the period of 0-60 hpi and a comparison of the data between low and moderately high ICDs at 0 and 36 hpi. Intracellular AA concentrations (in mM) tended to reduce over the time course post-infection, especially at 60 hpi where values were significantly lower than other time points for most of the AAs (Fig. 6.7 a, b). The significant reduction in intracellular AA concentrations at 60 hpi might indicate a leakage of intracellular metabolites at this late infection stage when infected cells underwent quenching and washing procedures. Comparing between low and high ICDs, intracellular AA concentrations were not significantly different for most of the AAs, except for aspartate, asparagine and serine at 0 hpi and asparagine, serine and leucine at 36 hpi, in which cases the AA concentrations for the low ICD were significantly higher than those for the high ICD (Fig. 6.7 c, d). Interestingly, intracellular alanine concentrations of the moderately high ICD were significantly higher than that of the low ICD either at 0 and 36 hpi.

Table 6.1. Intracellular metabolite concentrations (mM) for HzAM1cells infected with a wild-type baculovirus (HearNPV) at either low (0.5×10^6) or moderately high (2×10^6 cells/mL) infection cell densities (ICDs) over various times post-infection. Data represented as an average of biological triplicates. The metabolites listed were selected on the basis of showing significant variations in levels between different ICDs or times post infection following the analysis shown in Fig. 6.5.

Metabolites	Low ICD (0.5×10^6 cells/mL)						High ICD (2×10^6 cells/mL)						P<
	0 hpi	18 hpi	24 hpi	36 hpi	48 hpi	60 hpi	0 hpi	18 hpi	24 hpi	36 hpi	48 hpi	60 hpi	
Adenosine	7.34^{ab}	7.04^{ab}	7.07^{ab}	7.54^{a}	6.34^{ab}	5.70^{bc}	7.25^{ab}	7.35^{ab}	7.40^{a}	6.93^{ab}	6.04^{ab}	4.34^{c}	0.001
ATP	5.39^{a}	5.17^{a}	4.36^{ab}	4.01^{ab}	3.16^{bc}	3.21^{bc}	4.36^{ab}	3.95^{ab}	4.28^{ab}	3.34^{bc}	3.49^{b}	1.86^{c}	0.001
ADP	1.41	1.57	1.85	2.11	2.12	1.59	1.57	1.99	1.91	2.10	1.34	1.98	NS
AMP	0.54^{bcd}	0.30^{d}	0.86^{abcd}	1.41^{ab}	1.06^{abcd}	0.90^{abcd}	1.32^{abc}	1.41^{abc}	1.21^{abcd}	1.49^{a}	1.21^{abcd}	0.49^{cd}	0001
UTP	1.15^{a}	1.08^{ab}	1.03^{abc}	0.84^{abcd}	0.56^{de}	0.89^{de}	0.77^{bcd}	0.78^{bcd}	0.71^{cde}	0.52^{de}	0.59^{de}	039^{e}	0.001
UDP	0.09	0.12	0.10	0.03	0.05	0.06	0.04	0.04	0.09	0.03	0.05	0.01	NS
UMP	0.03	0.01	0.04	0.01	0.03	0.03	0.00	0.01	0.02	0.01	0.01	0.01	NS
CTP	0.61^{ab}	0.60^{ab}	0.67^{a}	0.42^{bc}	0.35^{c}	0.30^{cd}	0.37^{c}	0.30^{cd}	0.37^{c}	0.24^{cd}	0.30^{cd}	0.15^{d}	0.001
CMP	004^{ab}	0.01^{b}	0.03^{ab}	0.10^{a}	0.02^{b}	0.05^{ab}	0.04^{ab}	0.07^{ab}	0.05^{ab}	0.04^{ab}	0.01^{b}	0.05^{ab}	0.05
GDP	0.30^{ab}	0.08^{b}	0.21^{ab}	0.38^{ab}	0.10^{b}	0.09^{b}	0.33^{ab}	0.55^{a}	0.24^{ab}	0.30^{ab}	0.20^{b}	0.19^{b}	001
GMP	0.13	0.06	0.14	0.22	0.05	0.01	0.31	0.29	0.07	0.09	0.12	0.05	NS
R5P	0.05^{ab}	0.04^{a}	0.04^{a}	0.02^{bc}	0.01^{bc}	0.02^{b}	0.01^{bc}	0.02^{bc}	0.02^{bc}	0.01^{c}	0.01^{bc}	0.01^{bc}	0.001
MAL	1.28^{a}	1.20^{ab}	1.23^{a}	0.65^{ab}	0.80^{ab}	0.77^{ab}	0.75^{ab}	0.67^{ab}	0.63^{ab}	0.46^{ab}	0.58^{ab}	0.29^{b}	0.05
FUM	0.37^{a}	0.18^{bc}	0.22^{b}	0.13^{bc}	0.12^{bc}	0.12^{bc}	0.15^{bc}	0.11^{bc}	0.13^{bc}	0.08^{c}	0.09^{c}	0.07^{c}	0.001
NAD	1.62^{a}	1.25^{abc}	1.17^{abcd}	1.04^{bcde}	0.73^{de}	0.79^{de}	1.33^{ab}	1.13^{bcd}	1.01^{bcde}	0.84^{cde}	0.94^{bcde}	0.63^{e}	0.001
NADP	0.10^{ab}	0.07^{bc}	0.08^{abc}	0.06^{bc}	0.02^{c}	0.06^{bc}	0.10^{ab}	0.14^{a}	0.08^{bc}	0.07^{bc}	0.08^{abc}	0.05^{bc}	0.001
UDPG	2.10^{a}	1.64^{ab}	1.49^{bc}	1.19^{bcde}	0.76^{de}	0.81^{de}	1.71^{ab}	1.69^{ab}	1.26^{bcd}	0.95^{cde}	1.09^{cde}	0.70^{e}	0.001

Data in the same row with different superscripts were significantly different at P <0.05

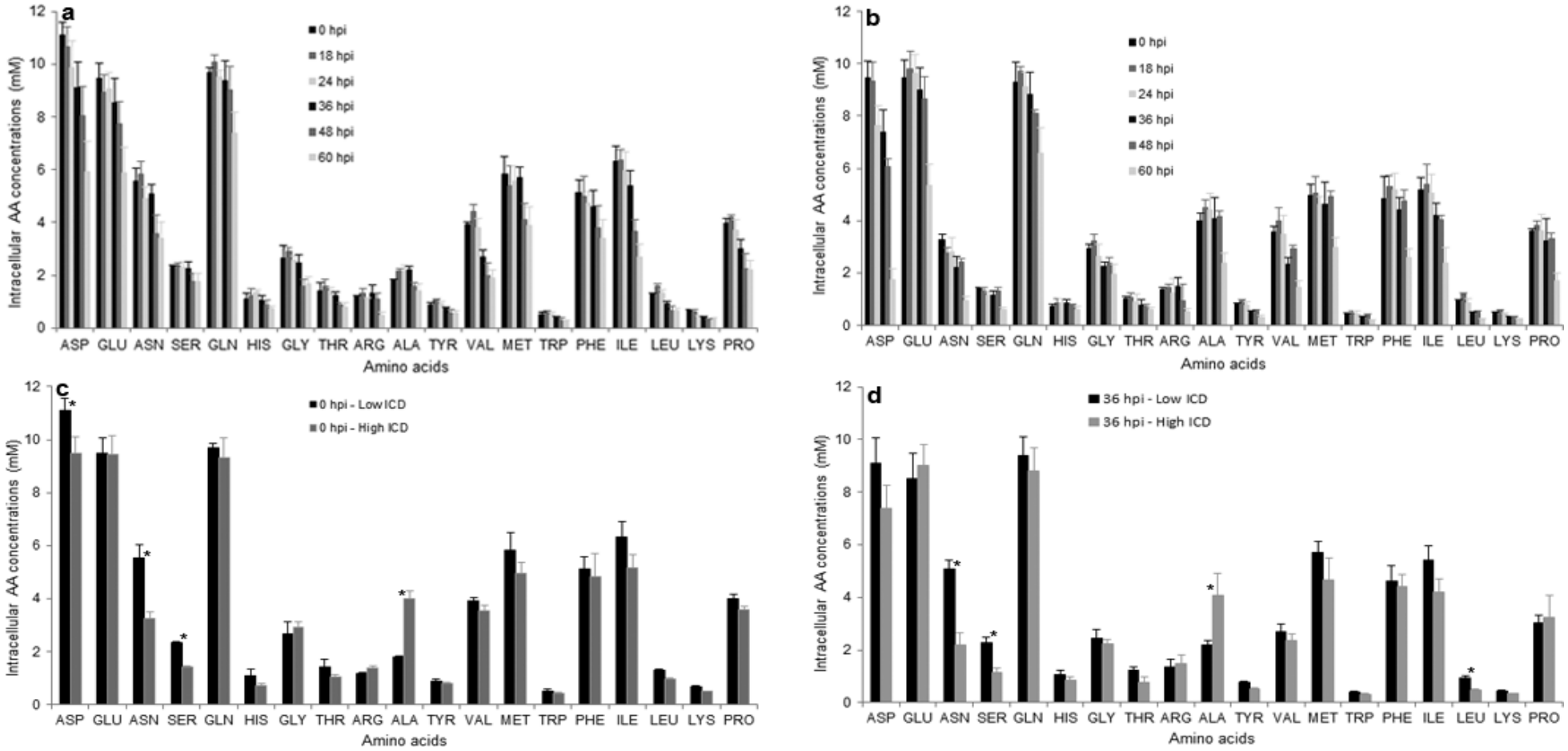

Fig. 6.7 Intracellular AA concentrations at 6 times post-infection at low (a) and high (b) ICDs , and the comparison between low and high ICDs for intracellular AA levels at 0 (c) and 36 hpi (d) of infected HzAM1 cells. Infections were conducted in Sf900™III at low ($0.5x10^6$ cells/mL) and high ($2x10^6$ cells/mL) ICDs and at an MOI of 5 PFU/cell (HearNPV). The experiment was conducted in shaker-flask suspension cultures. Each data point is the average from three biological replicates, and the error bars represent the standard deviation. Data for the same AA with an (*) was significantly different according to Tukey's HSD test (α=0.05), for high versus low ICDs at the indicated times post infection.

6.3.5 Consumption rates of glucose, maltose, and AAs

Glucose and AA consumption rates of uninfected and infected HzAM1 cells at three ICDs of 0.5, 2 and 4×10^6 cells/mL are shown in Table 6.2. The cell specific glucose consumption rates were within the range of 43.4-71.6×10^{-12} mmol/cell/hour for uninfected and infected HzAM1 cells at the various ICDs indicated above. Although glucose consumption rates of uninfected cells appeared lower than those of infected cells, especially at the low ICD of 0.5×10^6 cells/mL (43.4×10^{-12} compared to 71.6×10^{-12} mmol/ cell/hour), there was no statistical difference in glucose consumption rates among uninfected and infected HzAM1 cells at the various ICDs (Table 6.2). Also as shown in Table 6.2, no significant difference was found in the glucose consumption rates among treatments at early (0-18 hpi) and late (18-72 hpi) stages of infections. The maltose consumption rates, however, significantly reduced with the increasing ICD and there were significant differences in maltose consumption rates among the ICDs (Table 6.2). The maltose consumption rate of uninfected cultures was statistically similar to that of the infected cultures at an ICD of 2×10^6 cells/mL. The low maltose consumption rate at the high ICD (4×10^6 cells/mL) did not mean poor maltose consumption but was due to the exhaustion of maltose at this high cell density in culture. In terms of consumption rate per unit of cell biomass, Table 6.3 shows that there was no significant difference in the glucose consumption rate among the treatments as shown for the consumption rates on a per cell basis. The differences among treatments in terms of maltose consumption rate per mm^3 of cell biomass were also similar to those based on a per cell basis (Table 6.3).

Table 6.2 also shows AA consumption rates on a per cell basis for uninfected and infected HzAM1 cells at various ICDs of 0.5, 2 and 4×10^6 cells/mL. AA consumption rates for the low ICD (0.5×10^6 cells/mL) were significantly higher than those of the moderately high (2×10^6) and the high (4×10^6 cells/mL) ICDs for most of the AAs, except for glutamate, histidine and phenylalanine. Generally, AA consumption rates of the ICD of 2×10^6 cells/mL were higher than those of the high ICD (4×10^6 cells/mL), in which, significant differences were found for 7 out of 19 AAs. AA consumption rates of uninfected cultures were statistically similar to those of infected cultures at an ICD of 2×10^6 cells/mL for most of the AAs (15 out of 19 AAs) (Table 6.2).

Table 6.2. Glucose and amino acid consumption rates ($\times 10^{-12}$mmol/cell/hour) of uninfected and infected HzAM1 cells infected with a wild-type HearNPV at various ICDs. Uninfected and infected cultures were set up at 0.5×10^6 cells/mL. For the case of uninfected cultures no infection was made and sampling was conducted every 24 hours during the period that the culture maintained a 24-hour doubling time. For infected cultures, cultures were infected with an MOI of 5 PFU/cell at 0.5, 2 and 4×10^6 cells/mL and sampling was conducted every 12 hours until 60 hours post-infection. Data is the average of biological triplicates.

	Uninfected	$0.5\times10^{6\dagger}$	$2\times10^{6\dagger}$	$4\times10^{6\dagger}$	P<
Glucose	-43.38	-71.60	-51.05	-59.39	NS
Glucose, 0-18 hpi		-59.43	-44.95	-60.57	NS
Glucose, 18-60 hpi		-48.01	-48.27	-54.70	NS
Maltose	-9.61^{b}	-66.21^{a}	-14.21^{b}	-2.09^{c}	0.001
Amino acids					
Aspatate	0.15^{b}	17.95^{a}	-2.87^{c}	-5.78^{c}	0.001
Glutamate	-3.47	-3.97	-2.75	-2.87	NS
Asparagine	-30.58^{b}	-79.91^{a}	-23.96^{c}	-3.27^{d}	0.001
Serine	-9.91^{b}	-11.95^{a}	-7.78^{c}	-1.21^{d}	0.001
Glutamine	-29.57^{a}	-9.67^{b}	-7.16^{b}	-7.47^{b}	0.001
Histidine	-1.52	-1.95	-1.20	-0.42	NS
Glycine	-2.63^{b}	-4.99^{a}	-1.13^{b}	-1.12^{b}	0.001
Threonine	-3.91^{b}	-5.93^{a}	-3.73^{b}	-1.68^{c}	0.001
Arginine	-4.43^{b}	-6.88^{a}	-3.73^{b}	-0.55^{c}	0.001
Alanine	18.05^{b}	45.03^{a}	14.99^{bc}	-11.42^{c}	0.001
Tyrosine	-1.88^{bc}	-4.64^{a}	-3.22^{ab}	-0.70^{c}	0.001
Valine	-5.29^{b}	-9.30^{a}	-4.77^{b}	-1.73^{c}	0.001
Methionine	-4.47^{b}	-7.99^{a}	-3.36^{b}	-6.14^{ab}	0.001
Tryptophan	-0.89^{b}	-2.02^{a}	-0.69^{b}	-0.87^{b}	0.001
Phenylalanine	-2.09	-6.49	-3.94	-3.44	NS
Isoleucine	-3.49^{b}	-7.96^{a}	-3.87^{b}	-1.90^{b}	0.01
Leucine	-5.54^{b}	-10.83^{a}	-6.05^{b}	-2.27^{c}	0.001
Lysine	-4.55^{b}	-10.54^{a}	-3.68^{b}	-1.83^{b}	0.001
Proline	-3.85^{a}	-3.86^{a}	-3.16^{ab}	-1.05^{b}	0.05

† Infected cultures at ICDs of 0.5, 2 and 4×10^6 cells/mL

Consumption rates in the same row with different superscripts were significantly different (P<0.05)

NS: Not significantly different

Table 6.3. Comparison of AA consumption rates (x10^{-6} mmol/mm^3 cell volume/hour) of uninfected and infected HzAM1 cells infected with a wild-type HearNPV at various ICDs. Further details are as described in Table 6.2.

	Uninfected	0.5×10^6†	2×10^6†	4×10^6†	P<
Glucose	-18.85	-19.80	-16.91	-22.40	NS
Glucose, 0-18 hpi	-	-19.46	-16.47	-21.77	NS
Glucose, 18-60 hpi	-	-12.76	-15.67	-20.55	NS
Maltose	-4.19^{b}	-18.22^{a}	-4.67^{b}	-0.79^{c}	0.001
Amino acids					
Aspartate	0.32^{b}	5.14^{a}	-0.98^{bc}	-2.08^{c}	0.001
Glutamate	-1.31	-1.13	-0.95	-1.05	NS
Asparagine	-12.86^{b}	-22.80^{a}	-8.30^{c}	-1.21^{d}	0.001
Serine	-4.15^{a}	-3.41^{b}	-2.69^{c}	-0.45^{d}	0.001
Glutamine	-11.81^{a}	-2.77^{b}	-2.52^{b}	-2.74^{b}	0.001
Histidine	-0.63	-0.55	-0.42	-0.16	NS
Glycine	-1.06^{ab}	-1.42^{a}	-0.39^{c}	-0.40^{bc}	0.01
Threonine	-1.63^{ab}	-1.69^{a}	-1.28^{b}	-0.62^{c}	0.001
Arginine	-1.84^{ab}	-1.96^{a}	-1.29^{b}	-0.20^{c}	0.001
Alanine	7.72^{b}	12.86^{a}	5.15^{c}	4.14^{c}	0.001
Tyrosine	-0.78^{a}	-1.33^{a}	-1.10^{a}	-0.26^{b}	0.01
Valine	-2.19^{ab}	-2.65^{a}	-1.64^{b}	-0.64^{c}	0.001
Methionine	-1.77^{ab}	-2.28^{a}	-1.17^{b}	-2.24^{a}	0.05
Tryptophan	-0.36^{b}	-0.58^{a}	-0.24^{b}	-0.32^{b}	0.01
Phenylalanine	-0.68	-1.87	-1.36	-1.26	NS
Isoleucine	-1.39^{ab}	-2.25^{a}	-1.33^{ab}	-0.69^{b}	0.05
Leucine	-2.36^{b}	-3.09^{a}	-2.08^{b}	-0.83^{c}	0.001
Lysine	-1.96^{ab}	-3.02^{a}	-1.27^{b}	-0.68^{b}	0.01
Proline	-1.52^{a}	-1.10^{ab}	-1.08^{ab}	-0.39^{b}	0.01

† Infected cultures at ICDs of 0.5, 2 and 4×10^6 cells/mL

Consumption rates in the same row with different superscripts were significantly different (P<0.05)

NS: Not significantly different

As the cell volume of uninfected cultures was almost unchanged throughout the culture (Fig. 6.2b), AA consumption rates on a per cell basis for uninfected cultures were

relatively low in comparison with those for cultures infected at a low ICD, where the cell volume increases significantly post infection. Consequently, AA consumption rates per mm^3 of cell volume for uninfected cultures were statistically similar to those of infected cultures at the low ICD (0.5×10^6 cells/mL) in 12 out of 19 AAs in comparison with only 4 out of 19 AAs in the case of AA consumption rates on a per cell basis (Table 6.2, 6.3). In this work cell volume is assumed to equate to cell biomass. The significant differences in AA consumption rates per unit of cell volume among infected cultures at various ICDs followed a similar trend as found for the consumption rates on a per cell basis. It is important to note that infected cells at a low ICD consumed a significant amount of asparagine compared with the consumption of glutamine, while uninfected cultures consumed similar levels of these two AAs. Consumption of these two AAs significantly reduced with an increase of the ICD (Table 6.2). The change of extracellular glucose, maltose and AA concentrations over the time post-infection/post-inoculation can be seen in Appendix A4.1 & A4.2.

AA consumption rates of different infection stages of the virus infection process at early (0-18 hpi) and late (18-72 hpi) periods for the same ICD or between infected HzAM1 cells at various ICDs are shown in Fig. 6.8 and 6.9. Within the same ICD, AA consumption rates at the early infection stage (0-18 hpi) were generally higher than those at the late infection stage (18-72 hpi) at least for the higher ICDs, (Fig. 6.8). For the low ICD (0.5×10^6 cells/mL), there was almost no difference in AA consumption rates between the early and late stages of the virus infection (significant differences in AA consumption rates were only seen for aspartate, alanine and tyrosine, Fig. 6.8 a). Whereas, more significant differences were found in the AA consumption rates between the early and late infection stages with increasing ICDs. In the case of infected cells at the moderately high ICD (2×10^6 cells/mL), significant differences between early and late infection stages were found for 8 out of the 19 AAs quantified (Fig. 6.8 b). Significant differences in AA consumption rates between early and late infection stages in the case of the high ICD (4×10^6 cells/mL) were found for 14 out of the 19 AAs quantified (Fig. 6.8 c).

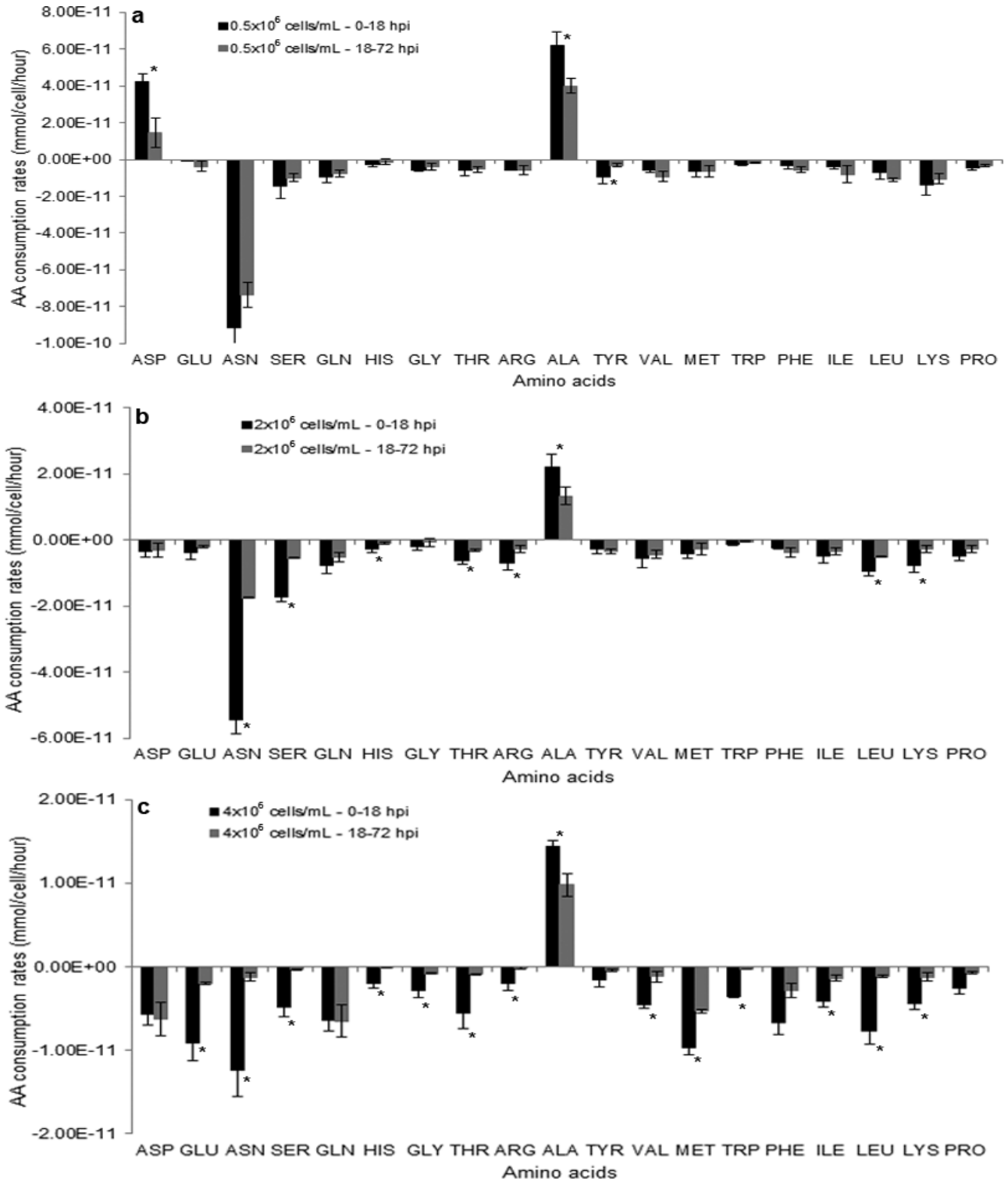

Fig. 6.8 Comparison of AA consumption rates (mmol/cell/hour) between early (0-18 hpi) and late (18-72hpi) infection stages for 3 different infection cell densities of 0.5×10^6 (a) 2×10^6 (b), and 4×10^6 cells/mL (c) of infected HzAM1 cells. Infections were conducted in Sf900™III at an MOI of 5 PFU/cell (HearNPV). The experiment was conducted in shaker-flask suspension cultures. Each data point is the average from three biological replicates, and the error bars represent the standard deviation. Data from the same AA with an (*) was significant difference according to Tukey's HSD test (α=0.05).

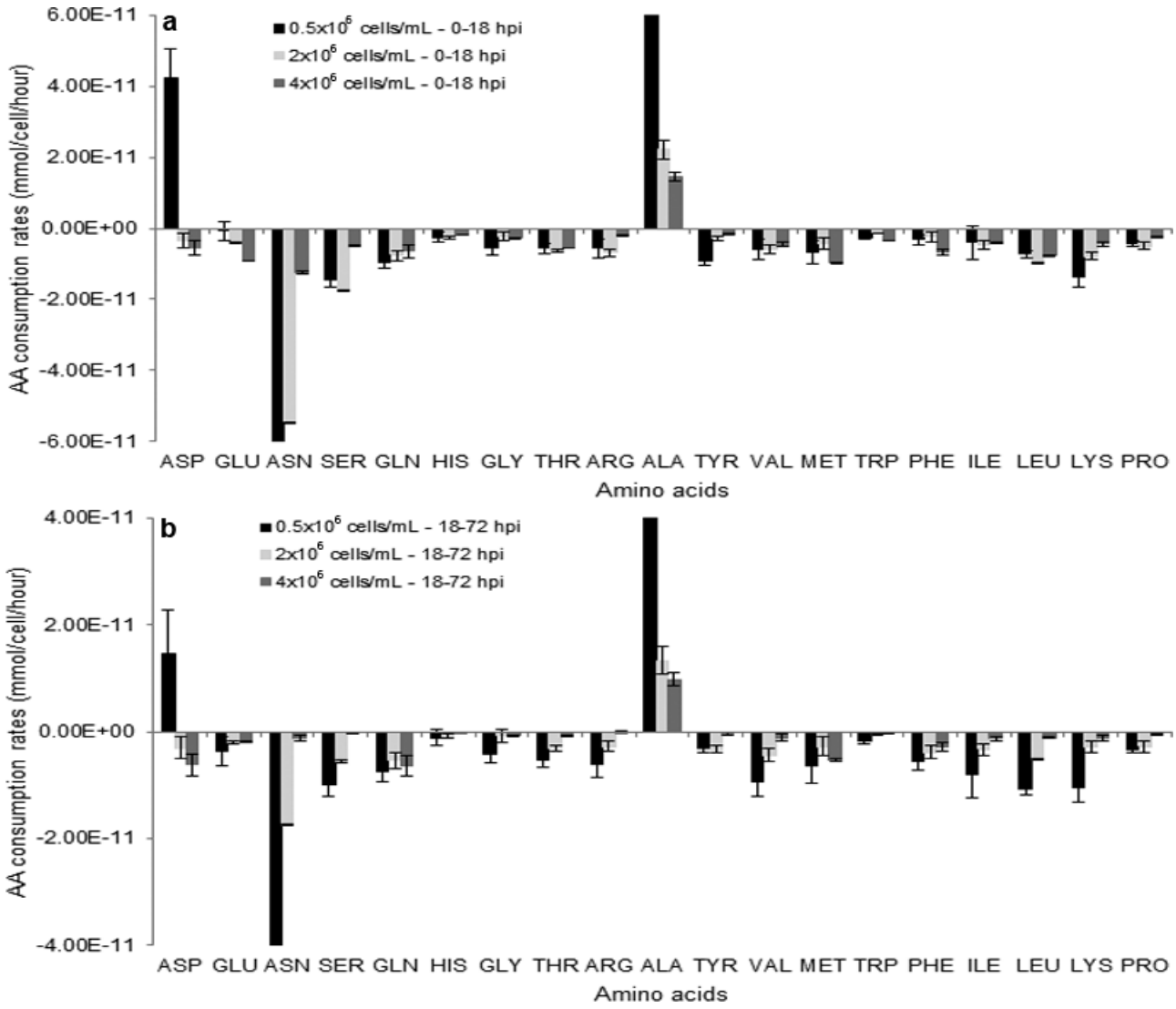

Fig. 6.9 Comparison of AA consumption rates (mmol/cell/hour) among 3 infection cell densities of 0.5×10^6, 2×10^6, and 4×10^6 cells/mL at either early (0-18 hpi) (a) or late (18-72hpi) (b) infection stages of infected HzAM1. Infections were conducted in Sf900™III at an MOI of 5 PFU/cell (HearNPV). The experiment was conducted in shaker-flask suspension cultures. Each data point is the average from three biological replicates, and the error bars represent the standard deviation.

Comparing among various ICDs, the AA consumption rates of infected cells at a low ICD were generally higher than those at moderately high or high ICDs and the differences in AA consumption rates among ICDs were more pronounced at the late infection stage (18-72hpi) (Fig. 6.9). Significant differences among various ICDs were found in 8 out of 19 AAs at the early infection stage (Fig. 6.9a), while 12 out of 19 AAs were found to have significant differences in consumption rates among ICDs at the late infection stage (Fig 6.9b). Generally, AA consumption rates reduced with an increase of the ICD, especially for the case of the late stage of the infection. Based on a cell volume basis, the differences in AA consumption rates among various ICDs at early and late infection stages (Fig. 6.10)

generally followed the same pattern as found when calculated based on a per cell basis. This result indicates that infected cells at the low ICD consumed AAs at higher rates than those at the high ICD and the consumption of AAs by infected cells at high ICDs were poorer at the late stage of the baculoivirus infection process. These observations are consistent with the reduced OB yields observed for infections at higher cell densities particularly bearing in mind that the polyhedral protein is expressed in the latter infection period.

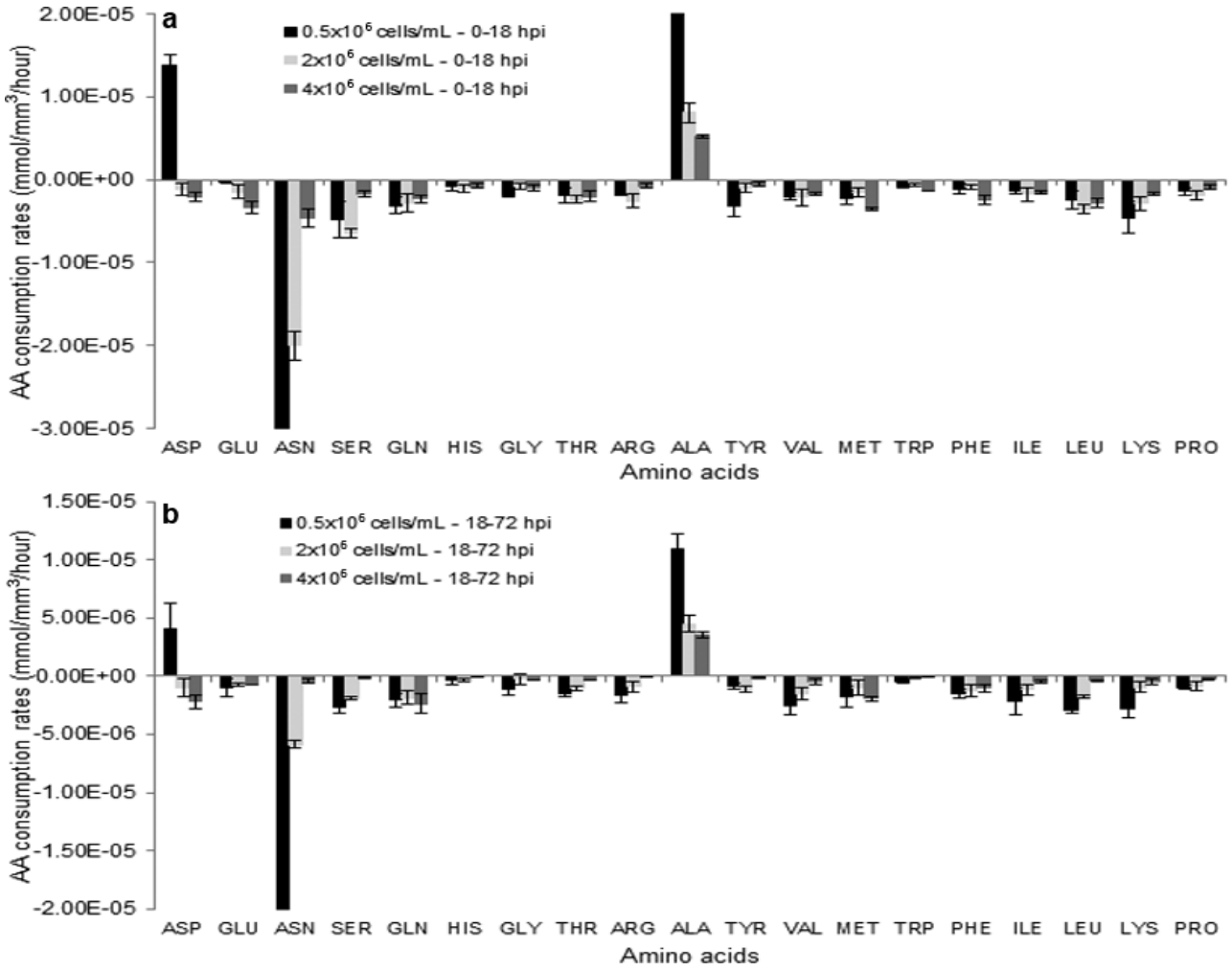

Fig. 6.10 Comparison of AA consumption rates (mmol/mm^3 of cell biomass/hour) among 3 infection cell densities of 0.5×10^6 cells/mL, 2×10^6 cells/mL, and 4×10^6 cells/mL at either early (0-18 hpi) (a) or late (18-72hpi) (b) infection stages of infected HzAM1 cells. Infections were conducted in Sf900™III at an MOI of 5 PFU/cell (HearNPV). The experiment was conducted in shaker-flask suspension cultures. Each data point is the average from three biological replicates, and the error bars represent the standard deviation.

6.3.6 Ratios of AA levels between moderately high and low ICDs, and between intra- and extracellular AAs

Figure 6.11 represents the ratios of AA levels between moderately high and low ICDs for both extra- and intracellular AA concentrations, and the ratios between intra-and extra-cellular AA concentrations of low and moderately high ICD samples at 0 and 36 hpi. When comparing AA concentrations between moderately high and low ICDs, Figure 11a and 11b show that extra- and intra-cellular AA levels of infected cells at the moderately high ICD were lower than those for the low ICD as indicated by the ratios of moderately high/low ICD AA values being less than 1 for the majority of the AAs. Generally, the ratios between moderately high and low ICDs of extracellular AAs were similar with the ratios for intracellular AAs either at early (0 hpi) or late (36 hpi) infection times. These results indicate that the intracellular AA concentrations were determined by the extracellular AA levels and that there was no difference in the capability of AA transport into the cell between low and moderately high ICDs at early or late infection stages. Low AA concentrations for the moderately high ICD in comparison with the low ICD (based on the ratio of AAs between high/low ICDs) were found for asparagine, serine and leucine; especially at the late infection stage (36 hpi), with the ratio of AAs between moderately high/low ICDs being less than 0.5 for these three AAs at 36 hpi (Fig. 6.11b).

When comparing the ratios between intra- and extra-cellular AA levels for low and high ICDs, these two ratios were similar between low and high ICDs for the majority of the AAs at 0 and 36 hpi (Fig. 6.11c, d), except for glutamine (at 0 and 36 hpi), and asparagine and serine (at 36 hpi) where the ratios between intra- and extra-cellular AAs for the high ICD were higher than those for the low ICD. It is of interest that the intra-/extra-cellular ratios for most AAs for both low and high ICDs at 0 and 36 hpi were much lower than one. On average, intracellular AA levels were about two thirds of the extracellular levels. These results suggest that the AA uptake by cells in culture before and after infection reaches an equilibrium of the AAs in the cell with the level in the external medium or alternatively that the external AA level dictates the extent of AA uptake. This in turn suggests the only way to keep intracellular AA levels high is to have high AA levels in the external media. It is also noted that intracellular levels of arginine and lysine were very low compared with extracellular levels, especially for lysine, where the intracellular level is only about 10% of the extracellular level. This may indicate poor transport rates for these AAs into the cells, or a high consumption rate of these AAs in relation to their transport rate.

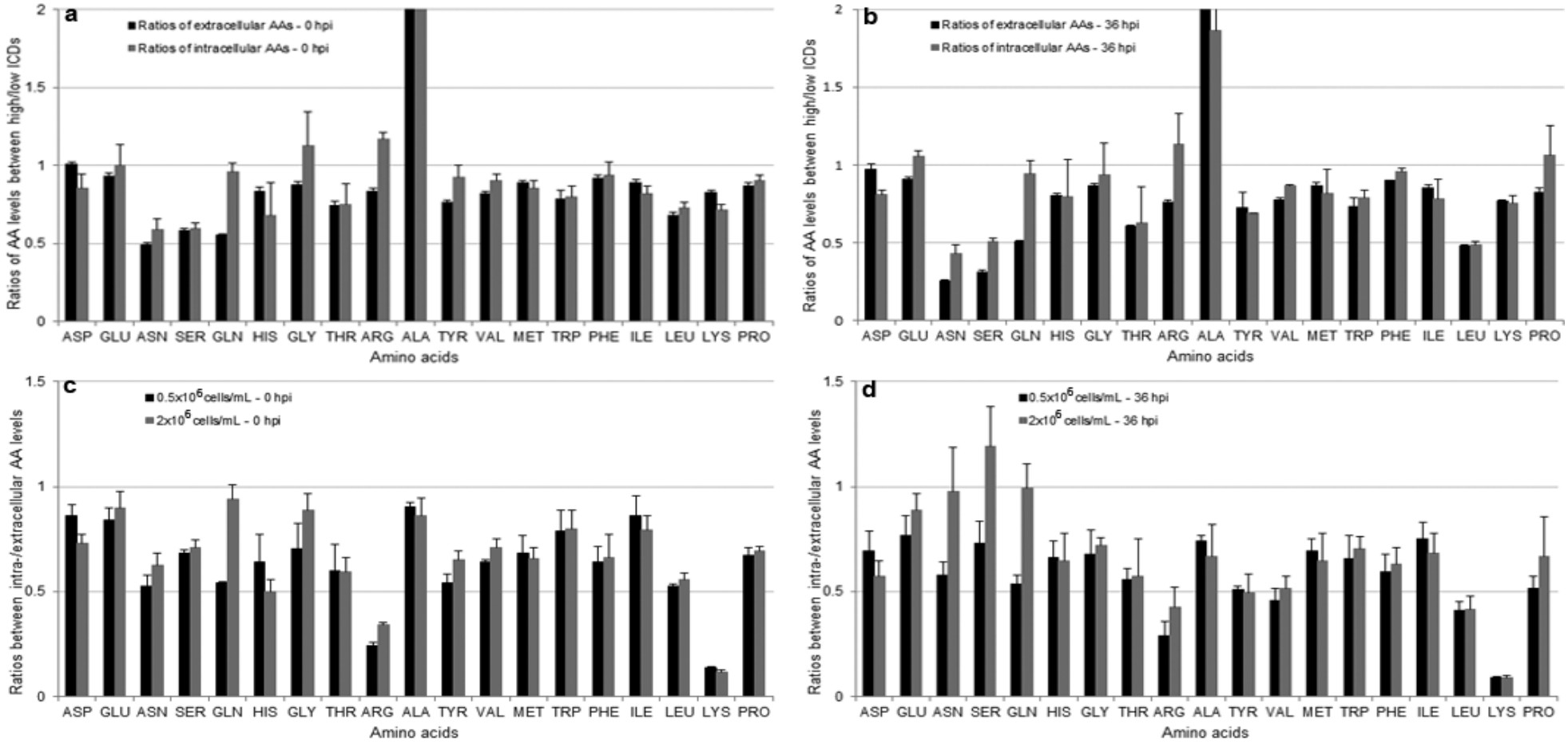

Fig. 6.11 Ratios of AA levels between high versus low ICDs for extra- and intra-cellular AAs at 0 hpi (a) and 36 hpi (b) and ratios between intra- versus extra-cellular AA levels for low and high ICDs at 0 hpi (c) and 36 hpi (d) of infected HzAM1 cells. Infections were conducted in Sf900™III at low (0.5×10^6 cells/mL) and high (2×10^6 cells/mL) ICDs and at an MOI of 5 PFU/cell (HearNPV). The experiment was conducted in shaker-flask suspension cultures. Each data point is the average from three biological replicates, and the error bars represent the standard deviation.

6.4 Discussion

The intracellular metabolite extraction protocol has been optimized for infected HzAM1 cells with a wild-type HearNPV (Tran et al., 2012). However, the previous study only evaluated the protocol at the one time point post-infection of 24 hpi, while the cell integrity changes greatly post-infection due to cell death and lysis after being infected with a baculovirus at a high MOI (e.g ≥ 5 PFU/cell). It is possible after 24 hpi that the cell integrity deteriorates such that the extraction protocol is no longer adequate. Therefore, it was necessary to investigate the extent of the time frame post-infection for which the extraction protocol works. This will be important for designing experiments to determine the dynamics of the endometabolome post-infection to explore whether limitations in the endometabolome are implicated in the decline in productivity when insect cells are infected at high cell densities.

Once a baculovirus infects insect cells at a high MOI (e.g. ≥ 5 PFU/cell), the virus rapidly takes over the cell metabolism and inhibits cell division at least for group I baculoviruses (O'Reilly et al., 1994). The virus quickly replicates inside the cells and shuts down many of the cells metabolic pathways and ultimately, the virus kills the cell as early as about 48 hpi (Slack and Arif, 2007). For group II baculovirus infections (HearNPV infected HzAM1 cells as used in the current study) using Sf900™II medium, it was reported that the virus infection process was delayed by about 24 hours or even longer in comparison with Sf9 cells infected with an AcMNPV (Lua and Reid, 2000; Pedrini et al., 2011). Therefore, for a synchronous infection with a high MOI as in the current study, it is expected that the cell integrity would be maintained for up to 72 hpi or later compared with 48 hpi for the Sf9/AcMNPV system (Chapter 4). However, the timing of the HearNPV infection in the current study using Sf900™III medium was comparable to that of the group I AcMNPV baculovirus with a rapid production between 12-24 hpi for vDNA and 24-72 hpi for OB (Fig. 6.1b). This means that the cell integrity may be maintained only until 48-60 hpi at the latest. Indeed this is what was observed in the current study, with the intracellular ATP level and the ATP recovery over the direct extract dropping quickly after 60 hpi (Fig. 6.1c) while the intracellular AA levels were reduced significantly at 60 hpi (Fig., 6.7a, b) compared to that observed at 48 hpi (most noticeable for aspartate, glutamate and glutamine, particularly for the high cell density infection). The drop of intracellular ATP after 48 hpi was also found for the Sf9/AcMNPV system (Chapter 4) and has been reported previously in the literature (Olejnik et al., 2004).

It is well known from the literature that for baculovirus insect cell systems, the cell specific protein yield drops when the cell density at the time of infection increases. The phenomenon, often called the cell density effect has been widely reported in the literature; mainly for recombinant baculovirus AcMNPV infected Sf9 or Hi5 cells (Carinhas et al., 2009; Caron et al., 1990; Chan et al., 2002; Doverskog et al., 2000; Huynh et al., 2013; Radford et al., 1997; Taticek and Shuler, 1997; Wong et al., 1996; Yamaji et al., 1999; Yang et al., 1996). There were also limited reports about the cell density effect for HzAM1 cells infected with a wild-type HearNPV (Chakraborty et al., 1996; Huynh et al., unpublished data). This bottleneck is common to different biological systems, especially for animal cells (Ferreira et al., 2005; Henry et al., 2005). In a recent study for HzAM1 cells infected with a wild-type HearNPV (Huynh et al., unpublished data) it was shown that the reduction in cell specific OB yield with increasing ICD was related to a reduction in the upstream processes of vDNA replication and polyhedron mRNA transcription. In this chapter, the differences in intracellular metabolites as well as the uptake rates of key nutrients between low and moderately high ICDs for infected HzAM1 cells has been investigated to search for evidence of intracellular metabolic changes that might help explain the cell density effect for this cell line/virus system.

As reported previously (Huynh et al., unpublished data), the specific OB yield reduced significantly with the increasing ICD, commencing for infections conducted at cell densities above 0.5×10^6 cells/mL. Therefore, 0.5×10^6 cells/mL was used as the low ICD in the current study. In this study, the specific OB yield also reduced significantly with increasing peak cell density (Fig. 6.3). In this case, the ICD of 2×10^6 cells/mL was chosen as the moderately high ICD as the specific OB yield was about 60% of the peak yield at 0.5×10^6 cells/mL. Higher ICDs (3 or 4×10^6 cells/mL) were not chosen as a contrast comparison with the low ICD because of the need to add significant amounts of budded virus stock at the time of infection (e.g. 50% v/v is required to infect a culture at 8×10^6 cells/mL to give a final ICD of 4×10^6 cells/mL) due to the low titer of HearNPV budded virus stocks (typically 2-4×10^7 PFU/mL at most).

Prior to investigating changes in intracellular metabolites of infected cultures at low and high ICDs, the intracellular nucleotide and AA levels of uninfected cultures at various cell densities were investigated. Generally, intracellular nucleotide tri-phosphates (ATP, UTP and CTP) decreased significantly with increasing cell density after 1×10^6 cells/mL (Fig 6.4a, b, c). Lower UTP and CTP levels at the high cell density, especially at 8×10^6 cells/mL compared to that of 1×10^6 cells/mL, possibly leads to limitation in supplying substrates for nucleic acid synthesis and then protein production, which are already

appearing inside the cells at high cell densities in cultures, even before infections are initiated. Intracellular AA concentrations also reduced with increasing cell density. These results indicate that the cell condition prior to infection differs for cells infected at low and high cell densities and this may affect their ability to support high virus yields, especially as nucleotide tri-phosphates are the substrates for vDNA and mRNA production. As a result, the reduction in the cell specific yield with increasing ICD not only occurs in relation to the late stage of protein production but also during virus replication and mRNA transcription as described previously for Sf9 cells (Huynh et al., 2013) and HzAM1 cells (Huynh et al., unpublished data and this work).

For infected cultures, the levels of nucleoside tri-phosphates (ATP, UTP and CTP) significantly reduced during the post-infection period as well as with the increasing cell density (Fig 6.6 a-c), especially for the case of UTP and CTP (Table 6.1). For example, at the time of infection, the levels of intracellular ATP, UTP and CTP for the high ICD were 80, 67 and 61% of those for the low ICD, respectively. The UTP and CTP levels for the high ICD dropped to 60-70% of the corresponding levels at the low cell density at 0 hpi and the specific vDNA/OB yields also declined by a similar amount for the infection at the high cell density compared to that at the low cell density (Fig. 6.3). CTP and UTP are precursors for dCTP and dTTP, so the drop in nucleotide concentrations could lead to the vDNA and OB drops. This suggests a possible limitation in building blocks for vDNA and mRNA production during the time post-infection and when the ICD increases. This result was also in agreement with that for infected Sf9 cells where the intracellular nucleoside tri-phosphates trended to reduce during the time post-infection and with increasing ICD (Chapter 4). The nucleoside di- and mono-phosphates were not significantly different or tended to increase for high ICDs and at later stages of infection, especially for the case of Adenosine (Fig. 6.3a-c) indicating that more energy was used in the case of the high ICD or late infection stage, or the cell struggled to maintain energy levels in these cases. This may be the result of deterioration of the glycolytic and TCA energy production pathways at the late infection stages. It should be noted that the nucleoside di- and mono-phosphates were much lower than that for the corresponding tri-phospates (10% or lower in many cases), so the accuracy of the quantification of these metabolites will likely be lower (Table 6.1).

A similar trend of reduction in concentrations during the time post-infection and with increasing ICD was found for other metabolites, especially the TCA cycle intermediates including malate (MAL) and fumarate (FUM) (Table 6.1). At the time of infection (0 hpi) the intracellular levels of MAL and FUM for the high ICD were only 59 and 40% of those for

the low ICD, respectively. α-ketoglutarate (KGA) was found to be significantly higher at the low ICD compared with the high ICD investigated for infected Sf9 cells (Chapter 4). In addition, Carinhas et al. (2010) claimed that KGA was found to be limiting at high cell density infections and the supplement of KGA at the time of infection resulted in an improvement of budded virus yields by 6-7 fold. In this study, however, comparison between low and high ICDs for the intracellular KGA concentration was not possible due to a failure to get accurate data for this metabolite at some time points. The intracellular concentrations of pyruvate (PYR) were not different between low and moderately high ICDs. It is possible that the lower level of TCA cycle intermediates may contribute to the lower yield at the high ICD.

Generally, the intracellular AA patterns over various times post-infection for low and moderately high ICDs of infected HzAM1 cells (Fig. 6.7a, b) were similar to that for infected Sf9 cells (Chapter 4). This result was in agreement with previous findings for intracellular AA concentrations of infected Sf9 and HzAM1 cells at 24 hpi (Tran et al., 2012). Comparing intracellular AA concentrations between infected Sf9 and HzAM1 cells, the aspatate level of infected Sf9 cells was much lower (about 1/3) than that of infected HzAM1 cells. Lysine, an AA required at a relatively high proportion for protein production in general (King and Jukes, 1969) and for polyhedrin protein in particular (Cheng et al., 1998), was found at a very low concentration inside of both infected Sf9 and HzAM1 cells although extracellular lysine concentrations remained at relatively high levels (see Appendix A4.2). This suggests that there is a difficulty for lysine to get into the cells, or this AA is being consumed at a high rate compared to its uptake rate. This may be the first limiting AA inside the cells for protein production at both low and high ICDs.

Although intracellular AA concentrations at the low ICD were higher than those at the moderately high ICD, the gaps were narrow and significant differences were only found in a few AAs (Fig. 6.7c, d). As a result, there was not a big contrast in OB yield (about 60%) between moderately high and low ICDs in this experiment. In contrast, there were significant differences in intracellular AA concentrations for most of the AAs between moderately high and low ICDs and a large contrast in protein yield between moderately high and low ICDs for the case of infected Sf9 cells (Chapter 4). This data overall indicates that there may be a link between intracellular AA concentrations and the protein yield of infected insect cells. As discussed previously, limitation of intracellular nucleotides with increasing ICD might lead to the reduction of vDNA and mRNA levels that were found in a previous study for this cell line/virus system (Huynh et al., unpublished data). The reduction in intracellular AAs and AA consumption rates with increasing ICD could be the

result of poorer AA transport associated with the increasing ICD or it could be the result of cell regulation as it is not necessary to have such a high level of AAs inside the cell while the capacity for protein synthesis (mRNA level) is limiting. Therefore, the key limiting element here is possibly the nucleotides as they are not available in the external medium for the cells to take up, and they have to be synthesized inside the cells.

Unlike intracellular metabolite information that is limited from the literature, the measurement of extracellular substrates of uninfected and infected insect cell cultures, especially glucose and AAs has been investigated by many research groups. The glucose consumption rate for uninfected and baculovirus infected insect cells has been reported widely with the majority of the reports relating to Sf9 cell cultures (Bernal et al., 2009; Kamen et al., 1996; Radford et al., 1997; Raghunand and Dale, 1999; Rhiel et al., 1997; Wong et al., 1994). For HzAM1 insect cells, there have been limited publications investigating cell metabolism and substrate consumption rates apart from Lua and Reid (2003). The glucose consumption rate for uninfected cultures from the above study in Sf900™II medium (12×10^{-11} mmol/cell/hour) was almost 3 times higher than the current study for uninfected cultures propagated in Sf900™III medium (4.34×10^{-11} mmol/cell/hour) (Table 6.2). Discrepancies in cell size, medium (Sf900™II vs Sf900™III) and peak cell density obtained (5×10^{6} cells/mL vs 1×10^{7} cells/mL in the current study) are possible explanations for the variation in the glucose consumption rates observed. The maltose consumption rate of the current study (0.96×10^{-11}mmol/cell/hour) (Table 6.2) was comparable with that reported by Lua and Reid (2003) of 1.08×10^{-11} mmol/cell/hour. Calculations based on the cell biomass; glucose consumption rates of uninfected and infected HzAM1 cells (Table 6.3) were comparable with those of uninfected and infected Sf9 cells (Chapter 4). HzAM1 consumed maltose faster than Sf9 cells (4.19×10^{-6} mmol/ mm^3/hour vs 2.80×10^{-6} mmol/mm^3/hour) for uninfected cultures. Therefore, the maltose consumption rate at the high ICD (4×10^{6} cells/mL) was minimal (0.79×10^{-6} mmol/ mm^3/hour) due to the very low level of maltose available in the medium during the high cell density infection (see appendix A4.1 & 4.2). In media containing both glucose and maltose, maltose consumption may occur during the early growth phase as evidenced from an initial rise in the glucose level and a decline in the maltose concentration by Bedard et al. (1993) and Ferrance et al. (1993).

In comparison with the recombinant AcMNPV infected Sf9 cell system, the HearNPV infected HzAM1 cell system has only a limited application as a biopesticide product and hence, research on the metabolism for this system is limited in the literature. An initial investigation on the metabolism for uninfected HzAM1 cells was conducted previously

(Lua and Reid, 2003). Consumption rates of asparagine, glutamate, and glutamine for uninfected HzAM1 cells of the current study were comparable with the results reported by the above authors. However, the production rate of alanine in the current study was about double of that previously reported. Interestingly, HzAM1 cells consumed asparagine at a comparable rate to that seen for glutamine for uninfected cultures but at a much higher rate for infected cultures at the low ICD but consumption of this AA dramatically reduced with increasing ICD (Table 6.2) due to the significant reduction of asparagine concentration in the culture medium (see Appendix A4). In contrast, Sf9 cells consumed glutamine at a much higher rate than asparagine for both uninfected and infected cultures (Chapter 4). Lua and Reid (2003) concluded that HzAM1 cell metabolism is closer to that of Hi5 cells than to Sf9 cells. In Hi5 cell cultures, asparagine is rapidly consumed in comparison with glutamine (Rhiel et al., 1997; Yang et al., 1996).

As found for infected Sf9 cells (Chapter 4), within the same ICD, AA consumption rates reduced at the late infection stage (18-72 hpi). The reduction in AA consumption rates at the late infection stage compared with the early infection stage (0-18 hpi) was more severe at higher ICDs (Fig. 6.8). In fact, the gap in AA consumption rates between early and late infection stages became larger when the ICD increased from 0.5 to 2 and then 4×10^6 cells/mL. This result possibly indicates that the ability for absorbing substrates into the cell reduces with increasing time post-infection and this effect becomes worse in combination with an increased ICD. Another explanation is that the reduction in the protein production rate at the late infection stage simply requires a lower AA uptake. As a result, the reduction in AA consumption rates with increasing ICD were more significant at the late infection stage (18-72 hpi) compared with those at the early infection stage (0-18 hpi) on both a consumption per cell basis (Fig. 6.9) and on a per biomass basis (Fig. 6.10).

Unlike infected Sf9 cells (Chapter 4), there was no evidence for a reduction in AA uptake efficiency with increasing ICD for infected HzAM1 cells, despite the result of the reduction in extracellular AA levels at the high ICD (Fig 6.11). The AA uptake efficiencies were comparable between low and moderately high ICDs for infected HzAM1 cells (Fig. 6.11c, d).

6.5 Conclusion

There could be multiple factors involved in the cell density effect phenomenon and it seems to be a general behaviour of baculovirus infected insect cell cultures. Among these factors, nutrient limitation is believed to be the most important element affecting the cell

specific yield when the infection cell densities increase. However, nutrient limitations were not related to the exhaustion of macro nutrients in the medium as they are still present at high amounts in the used medium and the uninfected cells can grow to a cell density of 2-3 times higher than at the cell density that displays a significant reduction in cell specific yield. Results from the current study show that intracellular nucleotides reduced with an increase in cell density for both uninfected and baculovirus infected HzAM1 cells. The key issue here might relate to the limitation in intracellular nucleotide levels for high cell density infections which may account for the low vDNA and mRNA production levels previously reported for high density infections (Huynh et al., 2013). Intracellular nucleoside tri-phosphates significantly reduced with increasing cell density in uninfected cultures, especially for the case of UTP. The reduction of intracellular nucleoside tri-phosphates was also found for infected cultures over the time course post-infection. In addition to nucleotides intracellular, organic acid levels, TCA cycle intermediates in particular, were also found to be lower for high ICDs.

Chapter 7

General discussion and conclusions

The improvement of the yield of the baculovirus-insect cell expression system is a major task for commercial viability of the products produced from this system. The challenge is that the specific protein yield (per cell basis) drops when cells are infected at a high cell density, which is known as “the cell density effect”. Many studies have been conducted to identify the limitations that result in the reduction in specific yield at high infection cell densities (ICDs), including the measurement of extracellular metabolites to identify the limiting nutrients in the medium (Caron et al., 1990; Drews et al., 1995; Reuveny et al., 1993), the measurement of consumption rates and fluxomics analysis (Bernal et al., 2009). However, the limitation of these approaches is that the metabolite levels in the media might not necessarily reflect intracellular metabolite levels. For many reasons, some metabolites may not get into the cells at high cell densities post-infection, although they are available at reasonable level in the culture medium. Therefore, the metabolite environment inside the cells at low and high cell densities at the time of infection provides a better understanding of what happens inside the cells and may reveal the cause of the cell density effect. In particular, intracellular metabolite measurements in combination with consumption rates of key metabolites may identify limitations during high cell density infections. Especially, at the very late phase of infection which involves a high level of protein production, it is likely that a high demand for energy and amino acids is placed upon the cell, but the cell is entering a death phase at this time and so the uptake of nutrients may be compromised.

In this thesis, we aimed to investigate the intracellular levels of some key metabolites at high ICDs in comparison with infections conducted at low ICDs. The analysis of intracellular metabolite levels is a potentially useful approach for understanding host cell and virus interactions, as well as the response of cells to their environment.

In order to address the issue regarding possible intracellular limitations during high cell density infections, key metabolites involved in the supply of energy and substrates for DNA, RNA, and protein synthesis such as intracellular nucleotides and amino acids were measured. However, there was no sample preparation protocol for quantitative intracellular metabolite analysis available for insect cells at the start of this work. Thus, a methodology for quantitative intracellular metabolite analysis of insect cells (for both uninfected and infected cases) was developed and optimized (Chapter 3). With this extraction protocol, subsequent studies could be designed to investigate whether limitations in the endometabolome are implicated in the decline in productivity when insect cells are infected at high cell densities. The limitations related to the drop in specific yield for a high cell density infection of Sf9 cells in SF900III medium was investigated using a metabolomics

approach (Chapter 4). In this chapter, substrate consumption rates as well as intracellular metabolite levels of infected cells at low and high cell densities at the time of infection were measured and compared between these two infection conditions.

Ideally, the cells should be cultured using a fully chemically defined medium (CDM) for the investigation of extra- and intra-cellular environments. However, a CDM for insect cells is not commercially available yet, and the development of such a CDM is beyond the scope of a research laboratory. Fortunately, a prototype CDM for insect cell culture was made available for testing by Life Technologies. This CDM contains no peptides, and the free amino acid levels are higher than those in Sf900™III for most of the amino acids. It is interesting to investigate any differences in intracellular metabolite levels of the Sf9 cells in the CDM compared to that for cells in Sf900™III, especially for high cell density infections. Substrate consumption rates and intracellular metabolite levels of infected cells at low and high ICDs were measured and compared between these two infection conditions using the available CDM, (Chapter 5), as a comparison to the results obtained in Chapter 4 using the commercially available Sf900™III medium.

Following the investigation of limitations related to the drop in specific yields for high cell density infections of Sf9 cells in Sf900™III and CDM media (Chapters 4 & 5), it was of interest to investigate limitations related to the decline in cell specific yield with increasing ICD for another cell line/virus system, such as the wild-type HearNPV infected HzAM1 system (Chapter 6). It is interesting to explore whether there are any differences in terms of limitations related to the cell density effect between different cell lines infected with different viruses when using the same medium for both cell lines.

In this Chapter, a further discussion of the results, brief summary of the main findings of this thesis or conclusions, and recommendations for further studies will be mentioned.

7.1 Intracellular metabolites extraction procedure for insect cells

Protocols for intracellular metabolite extraction and measurement have been reported widely for bacteria (Jaki et al., 2006; Winder et al., 2008; Wittmann et al., 2004; Wu et al., 2010), yeast (Castrillo et al., 2003; Loret et al., 2007; Villas-Boas et al., 2005a) and mammalian cells (Dietmair et al., 2010; Grob et al., 2003; Ritter et al., 2008; Sellick et al., 2009; Sellick et al., 2010). To our knowledge, however, no such protocol has been validated for insect cell cultures, especially baculovirus infected insect cells. This study aimed to develope and validates the extraction protocol for quantitative intracellular metabolite analysis of uninfected and baculovirus infected insect cells. Two particular

baculovirus applications were tested, representing recombinant protein production (β-Gal-rAcMNPV in Sf9 cells) and biopesticide production (HearNPV in HzAM1 cells).

Based on the protocol developed for mammalian cells (Dietmair et al., 2010), this extraction procedure has been optimized and validated for insect cells, particularly for infected insect cells. As insect cells are propagated in a very rich culture medium, especially amino acids (AAs) based on the high AA concentrations of hemolymph (Schlaeger, 1996), washing is a critical step in the intracellular metabolite extraction procedure for insect cell cultures. The washing step, however, increases the chance of intracellular metabolite leakage, especially for infected insect cells, which possess a more fragile cell plasma membrane than uninfected ones since the baculovirus infection is a cell lytic process (King and Possee, 1992). Therefore, an extra protection needs to be included during the quenching and washing procedure. In the current study, the cell protectant, Pluronic® F-68 was added into the default saline quenching solution to protect cell membranes from leakage of intracellular metabolites. The addition of 0.2% Pluronic® F-68 into the cold saline quenching solution successfully protected uninfected and infected insect cells and minimized the intracellular metabolite leakage during quenching and washing steps. The ice-cold saline quenching solution (without Pluronic® F-68) brought about only 70% of ATP recovery after one wash step, while the addition of Pluronic® F-68 into the ice-cold saline quenching solution improved ATP recovery significantly (86%).

As mentioned above, washing is a critical step in the intracellular metabolite extraction protocol because of the rich medium used for insect cell culture, especially for AAs. However, the more washing steps, the more chance of intracellular metabolite leakage as the cell plasma membrane is exposed to damage through the washing, and this is expected to be more severe for the case of infected insect cells. Therefore, a compromise is considered between the gain in removal of extracellular metabolites attached to the cell membrane and the loss of intracellular metabolites through leakage. With a range of washing steps after quenching (0, 1, 2 and 3) investigated in the current study, the result shows that one wash post quenching is the most suitable for intracellular metabolite extraction of uninfected and baculovirus infected insect cells.

The intracellular metabolite extraction protocol developed and validated in this study has been used successfully for intracellular metabolite analysis of infected Sf9 and HzAM1 cells at low versus high ICDs.

7.2 The role of intracellular metabolite levels on the cell density effect of Sf9/ rAcMNPV in SF900™III

In this study, Sf9 cells infected with a recombinant AcMNPV was first investigated as it is an important system for recombinant protein applications. Prior to studying intra- and extra-cellular metabolites of low versus high ICDs, a preliminary study was conducted at an ICD of 2.5×10^6 cells/mL to investigate how late post-infection the extraction protocol developed above remained efficient for. As a baculovirus infection is a cell lytic process, the cell membrane integrity only remains to a certain time post-infection. The result shows that for Sf9 cells infected with a rAcMNPV, the intracellular extraction protocol works until 48 hpi. It means that 48 hpi is the latest time point one can get intracellular metabolite concentrations reliably. For Sf9 cells infected with AcMNPV, cell death and lysis commences around 48 hpi (O'Reilly et al., 1994; Slack and Arif, 2007).

Extracellular and intracellular metabolite measurements were conducted in infected Sf9 cells at low (2×10^6) and high (6×10^6 cells/mL) ICDs. Although previous studies indicated that the reduction in protein yield with increasing ICD started as early as 1×10^6 cells/mL (Huynh et al., 2013), the ICD of 2×10^6 cells/mL was selected as a low ICD since it is a reasonable cell density for measuring substrate consumption rates and it allows the cells to undergo two doubling times prior to infection (seeding cell density at 0.5×10^6 cells/mL). Results from the current study confirmed the reduction in cell specific yields with increasing ICD not only for protein production but also for viral DNA replication. This finding agrees with the study reported previously (Huynh et al., 2013). The reduction in protein productivity, when the cell densities at the time of infection increase, might result from the upstream limitation of vDNA, which leads to poor mRNA expression (Huynh et al., 2013). The lower vDNA copy number of the high ICDs compared to that of the low ICDs is possibly because of the reduction in intracellular nucleotide concentrations with increasing ICD, especially for nucleoside tri-phosphates. This reduction with increasing ICDs was not obvious for ATP, but they were clearer for the cases of GTP, CTP and especially for UTP. The lower UTP/dUTP levels of the high ICDs compared to the low ICDs might lead to a limitation of the dTTP level that would be required for DNA synthesis. As a result, a reduction in specific vDNA copies with increasing ICD will result. Although the uninfected culture still doubles at such high cell densities, vDNA production reduces significantly at the high ICD in comparison with that at the low ICD. This is reasonable as vDNA production by infected cells can exceed that required to duplicate the DNA of the cell genome (Huynh et al., 2013; Nguyen et al., 2013). Furthermore, limitations associated with

high ICDs were found for the intracellular concentrations of TCA cycle intermediates, particularly for KGA and PYR. Through flux balance analysis, Carinhas et al. (2010) found that KGA and PYR were limited for high ICDs and a supplement of these substrates into the culture medium increased the budded virus yield significantly. However, extra-cellular levels of these metabolites were not different between low and high ICDs in the current study. In addition, the lower intra-cellular AA concentrations as well as the lower AA uptake rates with increasing ICD may reduce protein production rates. However, low protein production at high ICDs is most likely determined by low mRNA levels (in turn due to low vDNA levels), and not by poor AA uptake rates. AA consumption drops at high ICD's due mainly to less demand for AAs by the cells, not due to a lack of external AAs or poor transport of AAs.

7.3 The role of intracellular metabolite levels on the cell density effect of Sf9/ rAcMNPV in CDM

One of the obvious advantages of using a CDM for metabolomic studies is for measuring AA consumption rates as a CDM does not contain peptides that can be used by the cells together with free AAs. Therefore, measurements of AA consumption rates for cells in a CDM will be more accurate than for cells in a hydrolysate containing medium.

The prototype CDM used in the current study was developed by Life Technologies and was available for trials in the laboratory. Sf9 insect cells grew well in the CDM provided (displaying a 24-hour doubling time during the exponential phase) compared to their growth in Sf900™III, although the peak cell density of uninfected cultures in the CDM was much lower than that in Sf900™III. At a low ICD (1×10^6 cells/mL) the cell specific β-Gal yield of infected Sf9 cells in the CDM was slightly better than that in Sf900™III. However, with an increasing ICD the cell specific yield reduced for the CDM as seen for the Sf900™III medium.

It seems that the cell metabolism remains stable irrespective of the media used as long as they are rich media that support high cell and virus yields. Differences in yield and intra-cellular metabolites between low and high ICDs followed similar trends for both cells in CDM and Sf900™III media. The main difference between these two media is in the case of AA consumption rates. The presence/absence of peptides in the culture media is the likely cause for this difference. As the current free AA detection method is unable to quantify the consumption of peptides by the cells, it will likely underestimate AA consumption rates for cells propagated in peptide containing medium (Sf900™III).

7.4 The role of intracellular metabolite levels on the cell density effect of HzAM1/ HearNPV in SF900™III

As found for Sf9 insect cells infected with a recombinant baculovirus (rAcMNPV), the HzAM1 insect cells infected with a wild-type baculovirus (HearNPV), which is used for biopesticide production, also displayed a reduction in cell specific yields with increasing ICD. It is important to investigate the intra and extracellular metabolite patterns between low and high ICDs for the HzAM1/HearNPV system to see whether similar metabolic patterns are found for different baculovirus/insect cell systems. Prior to conducting intracellular metabolite extractions and measurements for low and high ICDs, it was again necessary for this cell/virus system to investigate at which time point post-infection the extraction protocol developed above remained efficient for. Previous studies showed that the timing post-infection for HzAM1 cells infected with a wild-type HearNPV was delayed by about 24 hours or even longer in comparison with Sf9 cells infected with a rAcMNPV (Lua and Reid, 2000; Pedrini et al., 2011). Therefore, it was expected that the cell membrane integrity of infected HzAM1 cells post-infection would be maintained for at least 24 hours later than that of infected Sf9 cells. However, results from current study as well as some recent studies showed that the timing post-infection for infected HzAM1 cells in Sf900™III medium was comparable with that for infected Sf9 cells. Consequently, the extraction protocol is efficient only until 60 hpi for the case of ATP, and only up to 48 hpi for the case of AA measurements for the HzAM1 cell/HearNPV system.

The reduction in cell specific yield with increasing ICD for infected HzAM1 cells commenced as early as the ICD of 0.5×10^6 cells/mL and at a higher rate than that for infected Sf9 cells due to the peak cell density of uninfected HzAM1 in Sf900™III being only about half of that for uninfected Sf9 cells in the same medium. Therefore, for infected HzAM1 cells, intra- and extra-cellular metabolite studies were conducted at the ICDs of 0.5×10^6 and 2×10^6 cells/mL to represent the low and moderately high ICDs, respectively. In addition, being a group II virus with a low virus titer in comparison with the group I AcMNPV virus, the ICD of 2×10^6 cells/mL required a large volume of virus stock to be added. Infections at higher cell densities for this system would not be ideal for metabolomics studies due to the excessive volume of used media that would be added along with the virus inoculum at the time of infection.

As found for infected Sf9 cells, a reduction in the intracellular nucleoside tri-phosphates with increasing ICD of the HzAM1cells coincided with the decline in vDNA production at the higher ICDs. This potentially then leads to lower mRNA expression levels

as the ICD increased, and consequently a reduction in polyhedrin protein yields. The substrate limitations for nucleic acid and protein production are already potentially appearing inside the cells at high cell densities in cultures, even before infections are initiated. Indeed, at the high cell density in culture (8×10^6 cells/mL), the concentrations of UTP and CTP dropped to very low levels in comparison with those at the low cell density(1×10^6 cells/mL), about 2% and 19%, respectively. After infection, the nucleoside tri-phosphates (ATP, UTP and CTP) levels of the high ICD significantly reduced compared to the low ICD, especially for the case of UTP and CTP. The UTP and CTP levels for the high ICD dropped to 60-70% of the corresponding levels at the low cell density at 0 hpi and the specific vDNA/OB yields also declined by a similar amount for the infection at the high cell density compared to that at the low cell density. CTP and UTP are precursors for dCTP and dTTP, so the drop in nucleotide concentrations probably leads to the vDNA and OB reduction. This suggests a possible limitation in building blocks for vDNA and mRNA production during the time post-infection and when the ICD increases. This result was also in agreement with that for infected Sf9 cells where the intracellular nucleoside tri-phosphates trended to reduce during the time post-infection and with increasing ICD (Chapter 4). Moreover, there were signs of a reduction in some TCA cycle intermediates with increasing ICDs. These reductions with increasing ICD might contribute to the reduction in specific protein/OB yield at the high ICD. There was no significant difference in the intracellular AA or ATP/total adenosine levels between the low and moderately high ICDs for this system. In addition, there was no evidence for a reduction in AA uptake efficiency with increasing ICD for infected HzAM1 cells. Generally then, it can be concluded that the AA and energy supply is not limiting at high ICDs for the HzAM1 cell/HearNPV system.

7.5 Summary of the main findings or conclusions

The main findings of the thesis are summarized as follows. Firstly, an intracellular metabolite extraction protocol has been optimized and validated for insect cell cultures, especially for infected insect cells. In the method development process, an ice-cold saline quenching solution used for mammalian cells was shown to be inefficient for insect cell cultures, especially infected insect cells. The addition of Pluronic F-68 helped to protect cells during the quenching and washing procedure and improved the extraction efficiency. In addition, one washing step after quenching was found to be optimal for the intracellular metabolite extraction of insect cell cultures, which are propagated in a rich media

(containing high AA levels). Once the extraction protocol had been validated, the protocol was then used for the analysis of intracellular metabolite concentrations at low versus high ICDs in order to investigate discrepancies related to the cell density effect.

The extraction protocol developed above was only initially investigated for infected insect cells (both Sf9 and HzAM1 cell lines) up until 24 hpi. Therefore, the extraction protocol was investigated over the time course post-infection prior to measuring intracellular metabolite concentrations of low vs. high ICDs as infected insect cells undergo a cell lytic process and start to die at a certain time period after infection. It was then confirmed that it is possible to extract intracellular metabolites of infected insect cells (both Sf9 and HzAM1) up to 48-60 hpi using the one washing protocol developed above.

Reductions in intracellular metabolites and consumption rates were found with increasing ICDs. A limitation in intracellular nucleotides, especially the tri-phosphate forms may be a key factor in the reduction of vDNA and mRNA production with increasing ICDs which was found recently (Huynh et al., 2013). This might in turn lead to the reduction in protein yield with increasing ICDs. The reduction in intracellular AA concentrations and AA consumption rates with increasing ICDs likely result from the reduction in protein production at the high ICDs since there is no clear sign of AA limitations from the extracellular environment. In addition, the supply of energy seems to be not limiting at high ICDs as the level of ATP/total adenosine does not significantly decrease compared to that at low ICDs.

Two insect cell lines, Sf9 cells infected with a recombinant AcMNPV and HzAM1 cells infected with a wild-type HearNPV, behave in the same way with the increase in ICD in terms of reduction in protein/OB yield, reduction in intracellular metabolites (nucleotide tri phosphates, AAs) and reduction in AA consumption rates. Reduction in these parameters with increasing ICDs is the result of a combination of the reduction at the time of infection and reduction during the infection process. In addition, the use of a CDM is valuable for measuring the AA consumption rates as the consumption of peptides is not taken into account when a peptide containing medium is used.

7.6 Recommendations and remarks for future works

7.6.1 Investigation of the limitation in intracellular nucleotides of uninfected Sf9 cells at high cell densities

It would be useful to investigate whether there is a drop in intracellular nucleotide tri-phosphate levels of the Sf9 cells in culture with increasing cell densities as found for the

HzAM1 cells in this study. For example it would be useful to know if UTP drops to very low levels as the cells approach their peak cell density as seen for HzAM1 cells in Fig. 6.4b.

7.6.2 Development/optimization of a method for measuring the dNTPs in insect cells

It would be useful to develop/optimize a method to measure deoxyribonucleotides (dRNs), especially dNTP levels in infected insect cells at low and high cell densities and also in uninfected cells as they reach their peak cell density. These levels would be useful to understand the role of nucleotide supply in limiting baculovirus vDNA yields.

It is known that the deoxyribonucleotides (dRNs) are generally essential metabolites that play an important role in a broad range of key cellular functions. There is a limitation of studies done to determine the intracellular dRN pools because of the relatively low levels of dRNs present in most cells. In addition, it is not easy to separate them from the more abundant ribonucleotides (Zhang et al., 2011). Many research groups have tried to develop a method for quantifying endogenous nucleotides generally or deoxy-ribonucleotide triphosphates (dNTPs) in particular (Hennere et al., 2003; Shewach, 1992). However, there are some limitations related to these approaches including a complexity of sample preparations.

7.6.3 Supply of nucleotides to the culture medium

If it is confirmed by some additional work that nucleotide supply is the bottle neck leading to the cell density effect, it is worth supplying these substrates to the culture medium in order to investigate whether they are able to improve the yield during high density infections.

References

Agathos, S. N. 1991. Mass production of viral insecticides. *In:* Maramorosch, K. (ed.) *Biotechnology for Biological Control of Pests and Vectors.* Boca Raton: CRC Press, pp. 217-235

Airenne, K. J., Mahonen, A. J., Laitinen, O. H. and Yla-Herttuala, S. 2009. Baculovirus mediated gene transfer: An emerging universal concept. *In:* Templeton, N. S. (ed.) *Gene and cell therapy: Therapeutic mechanisms and strategies.* Boca Raton, FL: CRC Press, pp. 263-291

Airenne, K. J., Makkonen, K.-E., Mahonen, A. J. and Yla-Herttuala, S. 2010. *In Vivo* Application and Tracking of Baculovirus. *Current Gene Therapy,* 10**,** 187-194.

Allen, J., Davey, H. M., Broadhurst, D., Heald, J. K., Rowland, J. J., Oliver, S. G. and Kell, D. B. 2003. High-throughput classification of yeast mutants for functional genomics using metabolic footprinting. *Nature Biotechnology,* 21**,** 692-696.

Alvarez-Sanchez, B., Priego-Capote, F., and Luque de Castro, M. D. 2010. Metabolomics analysis II. Preparation of biological samples prior to detection. *Trends in Analytical Chemistry,* 29**,** 120-127.

Aucoin, M. G., Mena, J. A. and Kamen, A. A. 2010. Bioprocessing of Baculovirus Vectors: A Review. *Current Gene Therapy,* 10**,** 174-186.

Bajad, S. U., Lu, W. Y., Kimball, E. H., Yuan, J., Peterson, C. and Rabinowitz, J. D. 2006. Separation and quantitation of water soluble cellular metabolites by hydrophilic interaction chromatography-tandem mass spectrometry. *Journal of Chromatography A,* 1125**,** 76-88.

Bedard, C., Tom, R. and Kamen, A. 1993. Growth, nutrient consumption, and end-product accumulation in Sf-9 and BTI-EAA insect cell cultures: insights into growth limitation and metabolism. *Biotechnology Progress,* 9**,** 615-24.

Bennett, B. D., Yuan, J., Kimball, E. H. and Rabinowitz, J. D. 2008. Absolute quantitation of intracellular metabolite concentrations by an isotope ratio-based approach. *Nature Protocols,* 3**,** 1299-1311.

Benslimane, C., Elias, C. B., Hawari, J. and Kamen, A. 2005. Insights into the central metabolism of *Spodoptera frugiperda* (Sf-9) and *Trichoplusia ni* BTI-Tn-5B1-4 (Tn-5) insect cells by radiolabeling studies. *Biotechnology Progress,* 21**,** 78-86.

Bernal, V., Carinhas, N., Yokomizo, A. Y., Carrondo, M. J. T. and Alves, P. M. 2009. Cell Density Effect in the Baculovirus-insect Cells System: A Quantitative Analysis of Energetic Metabolism. *Biotechnology and Bioengineering,* 104**,** 162-180.

Betts, J.I. and Baganz, F. 2006. Miniature bioreactors: current practices and future opportunities. *Microbial Cell Factories,* 5, 21.

Bhatia, R., Jesionowski, G., Ferrance, J. and Ataai, M. M. 1997. Insect cell physiology. *Cytotechnology,* 24**,** 1-9.

Bhattacharya, M., Fuhrman, L., Ingram, A., Nickerson, K. W. and Conway, T. 1995. Single-run separation and detection of multiple metabolic intermediates by anion-exchange high-performance liquid-chromatography and application to cell pool extracts prepared from *Escherichia coli*. *Analytical Biochemistry,* 232**,** 98-106.

Black, B. C., Brennan, L. A. and Dierks, P. M. G., I., E. 1997. Commercialisation of baculoviral insecticides. *In:* Miller, L. K. (ed.) *The Baculoviruses.* New York: Plenum Press, pp. 341-388.

Blissard, G. W. 1996. Baculovirus-insect cell interactions. *Cytotechnology,* 20**,** 73-93.

Bolten, C. J., Kiefer, P., Letisse, F., Portais, J. C. and Wittmann, C. 2007. Sampling for metabolome analysis of microorganisms. *Analytical Chemistry,* 79**,** 3843-3849.

Bolten, C. J. and Wittmann, C. 2008. Appropriate sampling for intracellular amino acid analysis in five phylogenetically different yeasts. *Biotechnology Letters,* 30**,** 1993-2000.

Boyce, F. M. and Bucher, N. L. R. 1996. Baculovirus-mediated gene transfer into mammalian cells. *Proceedings of the National Academy of Sciences of the United States of America,* 93**,** 2348-2352.

Brandsch, M., Brandsch, C., Prasad, P. D., Ganapathy, V., Hopfer, U. and Leibach, F. H. 1995a. Identification of a renal cell line that constitutively express the kidney specific high affinity H+/Peptide cotransporter. *Faseb Journal,* 9**,** 1489-1496.

Brandsch, M., Ganapathy, V. and Leibach, F. 1995b. H+-peptide cotransport in Madin-Darby canine kidney cells: expression and calmodulin-dependent regulation. *American Journal of Physiology,* 268**,** F391–F397.

Buchholz, A., Takors, R. and Wandrey, C. 2001. Quantification of intracellular metabolites in *Escherichia coli* K12 using liquid chromatographic-electrospray ionization tandem mass spectrometric techniques. *Analytical Biochemistry,* 295**,** 129-137.

Buchholz, A., Hurlebaus, J., Wandrey, C. and Takors, R. 2002. Metabolomics: quantification of intracellular metabolite dynamics. *Biomolecular Engineering,* 19**,** 5-15.

Buerger, P., Hauxwell, C. and Murray, D. 2007. Nucleopolyhedrovirus introduction in Australia. . *Virologica Sinica,* 22**,** 173-179.

Burges, H. D., Croizier, G. and Huber, J. 1980. A review of safety tests on baculoviruses *Entomophaga,* 25**,** 329-339.

Bylesjo, M., Rantalainen, M., Cloarec, O., Nicholson, J. K., Holmes, E. and Trygg, J. 2006. OPLS discriminant analysis: combining the strengths of PLS-DA and SIMCA classification. *Journal of Chemometrics,* 20**,** 341-351.

Calles, K., Svensson, I., Lindskog, E. and Haggstrom, L. 2006. Effects of conditioned medium factors and passage number on Sf9 cell physiology and productivity. *Biotechnology Progress,* 22**,** 394-400.

Canelas, A. B., Ras, C., ten Pierick, A., van Dam, J. C., Heijnen, J. J. and Van Gulik, W. M. 2008. Leakage-free rapid quenching technique for yeast metabolomics. *Metabolomics,* 4**,** 226-239.

Canelas, A. B., ten Pierick, A., Ras, C., Seifar, R. M., van Dam, J. C., van Gulik, W. M. and Heijnen, J. J. 2009. Quantitative Evaluation of Intracellular Metabolite Extraction Techniques for Yeast Metabolomics. *Analytical Chemistry,* 81**,** 7379-7389.

Carinhas, N., Bernal, V., Yokomizo, A. Y., Carrondo, M. J. T., Oliveira, R. and Alves, P. M. 2009. Baculovirus production for gene therapy: the role of cell density, multiplicity of infection and medium exchange. *Applied Microbiology and Biotechnology,* 81**,** 1041-1049.

Carinhas, N., Bernal, V., Monteiro, F., Carrondo, M. J. T., Oliveira, R. and Alves, P. M. 2010. Improving baculovirus production at high cell density through manipulation of energy metabolism. *Metabolic Engineering,* 12**,** 39-52.

Caron, A. W., Archambault, J. and Massie, B. 1990. High-level recombinant protein-production in bioreactors using the baculovirus insect cell expression system *Biotechnology and Bioengineering,* 36**,** 1133-1140.

Castrillo, J. I., Hayes, A., Mohammed, S., Gaskell, S. J. and Oliver, S. G. 2003. An optimized protocol for metabolome analysis in yeast using direct infusion electrospray mass spectrometry. *Phytochemistry,* 62**,** 929-937.

Castro, P. M. L., Hayter, P. M., Ison, A. P. and Bull, A. T. 1992. Application of a statistical design to the optimization of culture-medium for recombinant interferon-gamma production by chinese-hamster ovary cells. *Applied Microbiology and Biotechnology,* 38**,** 84-90.

Chakraborty, S., Greenfield, P. and Reid, S. 1996. In vitro production studies with a wild-type Helicoverpa baculovirus. *Cytotechnology,* 22**,** 217-224.

Chakraborty, S., Monsour, C., Teakle, R. and Reid, S. 1999. Yield, biological activity, and field performance of a wild-type Helicoverpa nucleopolyhedrovirus produced in *H. zea* cell cultures. *Journal of Invertebrate Pathology,* 73**,** 199-205.

Chan, L. C. L., Greenfield, P. F. and Reid, S. 1998. Optimising fed-batch production of recombinant proteins using the baculovirus expression vector system. *Biotechnology and Bioengineering,* 59**,** 178-188.

Chan, L. C. L., Young, P. R., Bletchly, C. and Reid, S. 2002. Production of the baculovirus-expressed dengue virus glycoprotein NS1 can be improved dramatically with optimised regimes for fed-batch cultures and the addition of the insect moulting hormone, 20-Hydroxyecdysone. *Journal of Virological Methods,* 105**,** 87-98.

Chassagnole, C., Noisommit-Rizzi, N., Schmid, J. W., Mauch, K. and Reuss, M. 2002. Dynamic modeling of the central carbon metabolism of *Escherichia coli*. *Biotechnology and Bioengineering,* 79**,** 53-73.

Chen, A., Chitta, R., Chang, D. and Anianullah, A. 2009. Twenty four well plate miniature bioreactor system as a scale down model for cell culture process development. *Biotechnology and Bioengineering,* 102, 148-160.

Cheng, X. W., Carner, G. R. and Fescemyer, H. W. 1998. Polyhedrin sequence determines the tetrahedral shape of occlusion bodies in *Thysanoplusia orichalcea* single-nucleocapsid nucleopolyhedrovirus. *Journal of General Virology,* 79**,** 2549-2556.

Chico, E. and Jager, V. 2000. Perfusion culture of baculovirus-infected BTI-Tn-5B1-4 insect cells: A method to restore cell-specific beta-trace glycoprotein productivity at high cell density. *Biotechnology and Bioengineering,* 70**,** 574-586.

de Jesus, M.J., Girard, P., Bourgeois, M., Baumgartner, G., Jacko, B., Amstutz, H. and Wurm, F.M. 2004. TubeSpin satellites: a fast track approach for process development with animal cells using shaking technology. *Biochemical Engineering Journal,* 17, 217-223.

de Jesus, M.J. and Wurm, F.M. 2009. Medium and process optimization for high yield, high density suspension cultures: from low throughput spinner flasks to high throughput millilitre reactors. *Bioprocess International,* 7, 12-17.

de Koning, W. and van Dam, K. 1992. A method for the determination of changes of glycolytic metabolites in yeast on a subsecond time scale using extraction at neutral pH *Analytical Biochemistry,* 204**,** 118-123.

de Rezende, S., Castro, M. E. B. and Souza, M. L. 2009. Accumulation of few-polyhedra mutants upon serial passage of *Anticarsia gemmatalis* multiple nucleopolyhedrovirus in cell culture. *Journal of Invertebrate Pathology,* 100**,** 153-159.

Dettmer, K., Aronov, P. A. and Hammock, B. D. 2007. Mass spectrometry-based metabolomics. *Mass Spectrometry Reviews,* 26**,** 51-78.

Dietmair, S., Timmins, N. E., Gray, P. P., Nielsen, L. K. and Kromer, J. O. 2010. Towards quantitative metabolomics of mammalian cells: Development of a metabolite extraction protocol. *Analytical Biochemistry,* 404**,** 155-164.

Dietmair, S., Hodson, M. P., Quek, L.-E., Timmins, N. E., Gray, P. and Nielsen, L. K. 2012. A Multi-Omics Analysis of Recombinant Protein Production in Hek293 Cells. *Plos One,* 7.

Doig, S.D., Baganz, F. and Lye, G.L. 2006. High throughput screeing and process optimization. In Ratledge, C. and Kristiansen, B. (Eds.) *Basic Biotechnology.* 3rd ed. Cambridge University Press, Cambridge, pp.289-306.

Doverskog, M., Ljunggren, J., Ohman, L. and Haggstrom, L. 1997. Physiology of cultured animal cells. *Journal of Biotechnology,* 59**,** 103-115.

Doverskog, M., Bertram, E., Ljunggren, J., Ohman, L., Sennerstam, R. and Haggstrom, L. 2000. Cell cycle progression in serum-free cultures of Sf9 insect cells: Modulation by conditioned medium factors and implications for proliferation and productivity. *Biotechnology Progress,* 16**,** 837-846.

Drews, M., Paalme, T. and Vilu, R. 1995. The growth and nutrient utilization of the insect cell line Spodoptera frugiperda Sf9 in batch and continuous culture. *Journal of Biotechnology,* 40**,** 187-198.

Drews, M., Doverskog, M., Ohman, L., Chapman, B. E., Jacobsson, U., Kuchel, P. W. and Haggstrom, L. 2000. Pathways of glutamine metabolism in *Spodoptera frugiperda* (Sf9) insect cells: evidence for the presence of the nitrogen assimilation system, and a metabolic switch by H-1/N-15 NMR. *Journal of Biotechnology,* 78**,** 23-37.

Dunn, W. B. and Ellis, D. I. 2005. Metabolomics: Current analytical platforms and methodologies. *Trac-Trends in Analytical Chemistry,* 24**,** 285-294.

Dunn, W. B. 2008. Current trends and future requirements for the mass spectrometric investigation of microbial, mammalian and plant metabolomes. *Physical Biology,* 5.

Elias, C. B., Zeiser, A., Bedard, C. and Kamen, A. A. 2000. Enhanced growth of Sf9 cells to a maximum density of 5.2×10^7 cells per mL and production of beta-galactosidase at high cell density by fed batch culture. *Biotechnology and Bioengineering,* 68**,** 381-388.

Eriksson, L., Johansson, E., Kettaneh-Wold, N., Trygg, J., Wikstrom, C. and Wold, S. 2006. *Multi- and megavariate data analysis. Part 2: Advanced applications and method extensions*. 2nd Edition, Umetrics AB, Umea, Sweden.

Faijes, M., Mars, A. E. and Smid, E. J. 2007. Comparison of quenching and extraction methodologies for metabolome analysis of Lactobacillus plantarum. *Microbial Cell Factories,* 6.

Faulkner, P. and Carstens, E. B. 1986. An overview of the structure and replication of baculoviruses *Current Topics in Microbiology and Immunology,* 131**,** 1-19.

Ferrance, J. P., Goel, A. and Ataai, M. M. 1993. Utilization of glucose and amino acids in insect cell cultures: Quantifying the metabolic flows within the primary pathways and medium development. *Biotechnology and Bioengineering,* 42**,** 697-707.

Ferreira, T. B., Ferreira, A. L., Carrondo, M. J. T. and Alves, P. M. 2005. Effect of refeed strategies and non-ammoniagenic medium on adenovirus production at high cell densities. *Journal of Biotechnology,* 119**,** 272-280.

Ferreira, V., Fernandez, P., Melendez, J. and Cacho, J. 1995. Analytical characteristics of sample evaporation with the micro-kuderna danish concentrator *Journal of Chromatography A,* 695**,** 41-55.

Fiehn, O. 2001. Combining genomics, metabolome analysis, and biochemical modelling to understand metabolic networks. *Comparative and Functional Genomics,* 2**,** 155-168.

Fiehn, O. 2002. Metabolomics - the link between genotypes and phenotypes. *Plant Molecular Biology,* 48**,** 155-171.

Franzmann, B. A., Hardy, A. T., Murray, D. A. H. and Henzell, R. G. 2008. Host-plant resistance and biopesticides: ingredients for successful integrated pest management (IPM) in Australian sorghum production. *Australian Journal of Experimental Agriculture,* 48**,** 1594-1600.

Funk, C. J., Braunagel, S. C. and Rohrmann, G. F. 1997. Baculovirus structure. *In:* Miller, L. K. (ed.) *The baculoviruses.* New York: Plenum Press, pp. 7-32.

Gardiner, G. R. and Stockdale, H. 1975. 2 tissue culture media for production of lepidopteran cells and nuclear polyhedrosis viruses *Journal of Invertebrate Pathology,* 25**,** 363-370.

Gioria, V. V., Jaeger, V. and Claus, J. D. 2006. Growth, metabolism and baculovirus production in suspension cultures of an *Anticarsia gemmatalis* cell line. *Cytotechnology,* 52**,** 113-124.

Glare, T., Caradus, J., Gelernter, W., Jackson, T., Keyhani, N., Kohl, J., Marrone, P., Morin, L. and Stewart, A. 2012. Have biopesticides come of age? *Trends in Biotechnology,* 30**,** 250-258.

Gonzalez, B., Francois, J. and Renaud, M. 1997. A rapid and reliable method for metabolite extraction in yeast using boiling buffered ethanol. *Yeast,* 13**,** 1347-1355.

Goodacre, R., Vaidyanathan, S., Dunn, W. B., Harrigan, G. G. and Kell, D. B. 2004. Metabolomics by numbers: acquiring and understanding global metabolite data. *Trends in Biotechnology,* 22**,** 245-252.

Goodwin, R. H. 1991. Replacement of vertebrate serum with lipids and other factors in the culture of invertebrate cells, tissues, and pathogens. *In Vitro Cellular & Developmental Biology,* 27**,** 470-478.

Granados, R. R. and Hashimoto, Y. 1989. Infectivity of baculoviruses to culture cells. *In:* Mitsuhashi, J. (ed.) *Invertabrate Cell System Applications.* Boca Raton: CRC Press, pp. 3-13.

Grimble, G. K., Rees, R. G., Keohane, P. P., Cartwright, T., Desreumaux, M. and D.B., S. 1987. Effect of peptide chain length on absorption of egg protein hydrolysates in the normal human jejunum. *Gastroenterology,* 92**,** 136-142.

Grob, M. K., O'Brien, K., Chu, J. J. and Chen, D. D. Y. 2003. Optimization of cellular nucleotide extraction and sample preparation for nucleotide pool analyses using capillary electrophoresis. *Journal of Chromatography B-Analytical Technologies in the Biomedical and Life Sciences,* 788**,** 103-111.

Groussac, E., Ortiz, M. and Francois, J. 2000. Improved protocols for quantitative determination of metabolites from biological samples using high performance ionic-exchange chromatography with conductimetric and pulsed amperometric detection. *Enzyme and Microbial Technology,* 26**,** 715-723.

Haas, R. 2004. *Asynchronies in synchronous baculovirus infections.* PhD, The University of Queensland, Brisbane, Australia.

Hans, M. A., Heinzle, E. and Wittmann, C. 2001. Quantification of intracellular amino acids in batch cultures of *Saccharomyces cerevisiae*. *Applied Microbiology and Biotechnology,* 56**,** 776-779.

Harrison, R. and Hoover, K. 2012. Baculovirus and other occluded insect viruses. *In:* Vega, F. & Kaya, H. K. (eds.) *Insect pathology.* Amsterdam: Elsevier.

Heidemann, R., Zhang, C., Qi, H. S., Larrick Rule, J., Rozales, C., Park, S., Chuppa, S., Ray, M., Michaels, J., Konstantinov, K. and Naveh, D. 2000. The use of peptones as

medium additives for the production of a recombinant therapeutic protein in high density perfusion cultures of mammalian cells. *Cytotechnology,* 32**,** 157-167.

Hennere, G., Becher, F., Pruvost, A., Goujard, C., Grassi, J. and Benech, H. 2003. Liquid chromatography-tandem mass spectrometry assays for intracellular deoxy-ribonucleotide triphosphate competitors of nucleoside antiretrovirals. *Journal of Chromatography B-Analytical Technologies in the Biomedical and Life Sciences,* 789**,** 273-281.

Henry, O., Perrier, M. and Kamen, A. 2005. Metabolic flux analysis of HEK-293 cells in perfusion cultures for the production of adenoviral vectors. *Metabolic Engineering,* 7**,** 467-476.

Hewlett, G. 1991. Strategies for optimizing serum free media *Cytotechnology,* 5**,** 3-14.

Hink, W. F. 1970. Established insect cell line from cabbage looper, *Trichoplusia ni. Nature,* 226**,** 466-467.

Hink, W. F., Thomsen, D. R., Davidson, D. J., Meyer, A. L. and Castellino, F. J. 1991. Expression of 3 recombinant proteins using baculovirus vectors in 23 insect cell lines. *Biotechnology Progress,* 7**,** 9-14.

Hitchman, R. B., Possee, R. D., Siaterli, E., Richards, K. S., Clayton, A. J., Birds, L. E., Owens, R. J., Carpentier, D. C. J., King, F. L., Danquah, J. O., Spink, K. G. and King, L. A. 2010. Improved expression of secreted and membrane-targeted proteins in insect cells. *Biotechnology and Applied Biochemistry,* 56**,** 85-93.

Hodson, M. P., Dear, G. J., Griffin, J. L. and Haselden, J. N. 2009. An approach for the development and selection of chromatographic methods for high-throughput metabolomic screening of urine by ultra pressure LC-ESI-ToF-MS. *Metabolomics,* 5**,** 166-182.

Hofmann, C., Sandig, V., Jennings, G., Rudolph, M., Schlag, P. and Strauss, M. 1995. Efficient gene transfer into human hepatocytes by baculovirus vectors *Proceedings of the National Academy of Sciences of the United States of America,* 92**,** 10099-10103.

Hofmann, U., Maier, K., Nicbel, A., Vacun, G., Reuss, M. and Mauch, K. 2008. Identification of metabolic fluxes in hepatic cells from transient C-13-labeling experiments: Part I. Experimental observations. *Biotechnology and Bioengineering,* 100**,** 344-354.

Hu, Y.-C. 2008. Baculoviral vectors for gene delivery: A review. *Current Gene Therapy,* 8**,** 54-65.

Hu, Y. C. 2006. Baculovirus vectors for gene therapy. *In:* Bonning, B. C., Maramorosch, K. & Shatkin, A. J. (eds.) *Advances in virus research.* Academic Press, pp. 287-320.

Huynh, H. T., Chan, L. C. L., Tran, T. T. B., Nielsen, L. K. and Reid, S. 2012. Improving the robustness of a low-cost insect cell medium for baculovirus biopesticides production, via hydrolysate streamlining using a tube bioreactor-based statistical optimization routine. *Biotechnology Progress,* 28**,** 788-802.

Huynh, H. T., Tran, T. T. B., Chan, L. C. L., Nielsen, L. K. and Reid, S. 2013. Decline in baculovirus-expressed recombinant protein production with increasing cell density is strongly correlated to impairment of virus replication and mRNA expression. *Applied Microbiology and Biotechnology,* 97**,** 5245-5257.

Ikonomou, L., Bastin, G., Schneider, Y. J. and Agathos, S. N. 2001. Design of an efficient medium for insect cell growth and recombinant protein production. *In Vitro Cellular & Developmental Biology-Animal,* 37**,** 549-559.

Ikonomou, L., Schneider, Y. J. and Agathos, S. N. 2003. Insect cell culture for industrial production of recombinant proteins. *Applied Microbiology and Biotechnology,* 62**,** 1-20.

Ikonomou, L., Bastin, G., Schneider, Y. J. and Agathos, S. N. 2004. Effect of partial medium replacement on cell growth and protein production for the High-Five (TM) insect cell line. *Cytotechnology,* 44**,** 67-76.

Inlow, D., Shauger, A. and Maiorella, B. 1989. Insect cell culture and baculovirus propagation in protein-free medium. *Journal of Tissue Culture Methods,* 12**,** 13-16.

Jacobson, A., Foster, R., Krupke, C., Hutchison, W., Pittendrigh, B. and Weinzierl, R. 2009. Resistance to Pyrethroid Insecticides in *Helicoverpa zea* (Lepidoptera: Noctuidae) in Indiana and Illinois. *Journal of Economic Entomology,* 102**,** 2289-2295.

Jaki, B. U., Franzblau, S. G., Cho, S. H. and Pauli, G. F. 2006. Development of an extraction method for mycobacterial metabolome analysis. *Journal of Pharmaceutical and Biomedical Analysis,* 41**,** 196-200.

Jardin, B. A., Montes, J., Lanthler, S., Tran, R. and Elias, C. 2007. High cell density fed batch and perfusion processes for stable non-viral expression of secreted alkaline phosphatase (SEAP) using insect cells: Comparison to a batch Sf-9-BEV system. *Biotechnology and Bioengineering,* 97**,** 332-345.

Jarvis, D. L. 2009. Baculovirus-Insect Cell Expression Systems. *Guide to Protein Purification, Second Edition (Methods in Enzymology),* 463, 191-222.

Jehle, J. A., Blissard, G. W., Bonning, B. C., Cory, J. S., Herniou, E. A., Rohrmann, G. F., Theilmann, D. A., Thiem, S. M. and Vlak, J. M. 2006. On the classification and nomenclature of baculoviruses: A proposal for revision. *Archives of Virology,* 151**,** 1257-1266.

Jesionowski, G. A. and Ataai, M. M. 1997. An efficient medium for high protein production in the insect cell baculovirus expression system. *Biotechnology Progress,* 13**,** 355-360.

Jordan, M. and Jenkins, N. 2007. Tools for high throughput medium and process optimization. In Portner, R. and Jenkins, N. (Eds.) *Animal cell biotechnology: Method and protocols.* 2nd ed. Humana press, Totowa, N.J., pp. 193-202.

Kamen, A. A., Bedard, C., Tom, R., Perret, S. and Jardin, B. 1996. On-line monitoring of respiration in recombinant-baculovirus infected and uninfected insect cell bioreactor cultures. *Biotechnology and Bioengineering,* 50**,** 36-48.

King, J. L. and Jukes, T. H. 1969. Non-Darwinian evolution. *Science,* 164**,** 788-798.

King, L. A. and Possee, R. D. 1992. *The Baculovirus Expression System: A Laboratory Guide,* Chapman & Hall, London, UK.

Koek, M. M., Muilwijk, B., van der Werf, M. J. and Hankemeier, T. 2006. Microbial metabolomics with gas chromatography/mass spectrometry. *Analytical Chemistry,* 78**,** 1272-1281.

Kost, T. A. and Condreay, J. P. 2002. Recombinant baculoviruses as mammalian cell gene-delivery vectors. *Trends in Biotechnology,* 20**,** 173-180.

Kost, T. A., Condreay, J. P. and Jarvis, D. L. 2005. Baculovirus as versatile vectors for protein expression in insect and mammalian cells. *Nature Biotechnology,* 23**,** 567-575.

Kumar, S., Wittmann, C. and Heinzle, E. 2004. Minibioreactors. *Biotechnology Letters,* 26, 1-10.

Lecina, M., Soley, A., Gracia, J., Espunya, E., Lazaro, B., Cairo, J. J. and Godia, F. 2006. Application of on-line OUR measurements to detect actions points to improve baculovirus-insect cell cultures in bioreactors. *Journal of Biotechnology,* 125**,** 385-394.

Lin, C.-Y., Lu, C.-H., Luo, W.-Y., Chang, Y.-H., Sung, L.-Y., Chiu, H.-Y. and Hu, Y.-C. 2010. Baculovirus as a Gene Delivery Vector for Cartilage and Bone Tissue Engineering. *Current Gene Therapy,* 10**,** 242-254.

Lindsay, D. A. and Betenbaugh, M. J. 1992. Quantification of cell culture factors affecting recombinant protein yields in baculovirus infected insect cells. *Biotechnology and Bioengineering,* 39**,** 614-618.

Loret, M. O., Pedersen, L. and Francois, J. 2007. Revised procedures for yeast metabolites extraction: application to a glucose pulse to carbon-limited yeast cultures, which reveals a transient activation of the purine salvage pathway. *Yeast,* 24**,** 47-60.

Lu, C., Gonzalez, C., Gleason, J., Gangi, J. and Yang, J.-D. 2007. A T-flask based screening platform for evaluating and identifying plant hydrolysates for a fed-batch cell culture process. *Cytotechnology,* 55**,** 15-29.

Lu, W., Bennett, B. D. and Rabinowitz, J. D. 2008. Analytical strategies for LC-MS-based targeted metabolomics. *Journal of Chromatography B-Analytical Technologies in the Biomedical and Life Sciences,* 871**,** 236-242.

Lua, L. H. L. and Reid, S. 2000. Virus morphogenesis of *Helicoverpa armigera* nucleopolyhedrovirus in *Helicoverpa zea* serum-free suspension culture. *Journal of General Virology,* 81**,** 2531-2543.

Lua, L. H. L. and Reid, S. 2003. Growth, viral production and metabolism of a *Helicoverpa zea* cell line in serum-free culture. *Cytotechnology,* 42**,** 109-120.

Luckow, V. A. and Summers, M. D. 1988. Signals important for high level expression of foreign genes in Autographa californica nuclear polyhedrosis virus expression vectors *Virology,* 167**,** 56-71.

Maharjan, R. P. and Ferenci, T. 2003. Global metabolite analysis: the influence of extraction methodology on metabolome profiles of *Escherichia coli*. *Analytical Biochemistry,* 313**,** 145-154.

Markuszewski, M. J., Otsuka, K., Terabe, S., Matsuda, K. and Nishioka, T. 2003. Analysis of carboxylic acid metabolites from the tricarboxylic acid cycle in *Bacillus subtilis* cell extract by capillary electrophoresis using an indirect photometric detection method. *Journal of Chromatography A,* 1010**,** 113-121.

Mashego, M. R., Rumbold, K., De Mey, M., Vandamme, E., Soetaert, W. and Heijnen, J. J. 2007. Microbial metabolomics: past, present and future methodologies. *Biotechnology Letters,* 29**,** 1-16.

Matindoost, L., Chan, L. C. L., Qi, Y. M., Nielsen, L. K. and Reid, S. 2012. Suspension culture titration: A simple method for measuring baculovirus titers. *Journal of Virological Methods,* 183**,** 201-209.

McIntosh, A. H. and Ignoffo, C. M. 1981. Replication and infectivity of the single-embedded nuclear polyhedrosis-virus, Baculovirus-heliothis, in homologous cell-lines *Journal of Invertebrate Pathology,* 37**,** 258-264.

Mena, J. A. and Kamen, A. A. 2011. Insect cell technology is a versatile and robust vaccine manufacturing platform. *Expert review of vaccines,* 10**,** 1063-1081.

Mendonca, R. Z., Palomares, L. A. and Ramirez, O. T. 1999. An insight into insect cell metabolism through selective nutrient manipulation. *Journal of Biotechnology,* 72**,** 61-75.

Meyer, S., Noisommit-Rizzi, N., Reuss, M. and Neubauer, P. 1999. Optimized analysis of intracellular adenosine and guanosine phosphates in *Escherichia coli*. *Analytical Biochemistry,* 271**,** 43-52.

Micheletti, M., Barrett, T., Doig, S.D., Baganz, F., Levy, M.S., Woodley, J.M. and Lye, G.J. 2006. Fluid mixing in shaken bioreactors: Implications for scale-up predictions from microlitre-scale microbial and mammalian cell cultures. *Chemical Engineering Science,* 61, 2939-2949.

Micheloud, G. A., Gioria, V. V., Perez, G. and Claus, J. D. 2009. Production of occlusion bodies of Anticarsia gemmatalis multiple nucleopolyhedrovirus in serum-free suspension cultures of the saUFL-AG-286 cell line: Influence of infection conditions and statistical optimization. *Journal of Virological Methods,* 162**,** 258-266.

Miller, J. H. 1972. Experiment 48: Assay of B-galactosidase. *In: Experiments in molecular genetics.* New York: Cold Spring Harbor Press, Cold Spring Harbor, pp. 352-355

Moscardi, F. 1999. Assessment of the application of baculoviruses for control of Lepidoptera. *Annual Review of Entomology,* 44**,** 257-289.

Moscardi, F., de Souza, M. L., de Castro, M. E. B., Moscardi, M. L. and Szewczyk, B. 2011. Baculovirus pesticides: Present state and future perspectives. *In:* Ahmad, I., Ahmad, F. & Pitchtel, J. (eds.) *Microbes and Microbial Technology: Agricultural and Environmental Applications.* 1st ed. New York: Springer, pp. 415-445

Mungur, R., Glass, A. D. M., Goodenow, D. B. and Lightfoot, D. A. 2005. Metabolite fingerprinting in transgenic Nicotiana tabacum altered by the *Escherichia coli* glutamate dehydrogenase gene. *Journal of Biomedicine and Biotechnology***,** 198-214.

Murhammer, D. W. 1996. Use of viral insecticides for pest control and production in cell culture. *Applied Biochemistry and Biotechnology,* 59**,** 199-220.

Neermann, J. and Wagner, R. 1996. Comparative analysis of glucose and glutamine metabolism in transformed mammalian cell lines, insect and primary liver cells. *Journal of Cellular Physiology,* 166**,** 152-169.

Nguyen, Q., Nielsen, L. K. and Reid, S. 2013. Genome scale transcriptomics of baculovirus-insect interactions. *Viruses,* 5**,** 2721-2747.

Nielsen, L. K., Smyth, G. K. and Greenfield, P. F. 1991. Hemacytometer cell count distributions-implications of non-poisson behavior *Biotechnology Progress,* 7**,** 560-563.

Nielsen, L. K., Smyth, G. K. and Greenfield, P. F. 1992. Accuracy of the end-point assay for virus titration *Cytotechnology,* 8**,** 231-236.

Nishikawa, N., Yamaji, H. and Fukuda, H. 2003. Recombinant protein production by the baculovirus-insect cell system in basal media without serum supplementation. *Cytotechnology,* 43**,** 3-10.

Nyberg, G. B., Balcarcel, R. R., Follstad, B. D., Stephanopoulos, G. and Wang, D. I. C. 1999. Metabolic effects on recombinant interferon-gamma glycosylation in continuous culture of Chinese hamster ovary cells. *Biotechnology and Bioengineering,* 62**,** 336-347.

O'Reilly, D. R., Miller, L. K. and Luckow, V. A. 1994. *Baculovirus expression vectors - A laboratory manual,* New York Oxford, Oxford University Press.

Ohman, L., Ljunggren, J. and Haggstrom, L. 1995. Induction of a metabolic switch in insect cells by substrate-limited fed batch cultures. *Applied Microbiology and Biotechnology,* 43**,** 1006-1013.

Oldiges, M., Lutz, S., Pflug, S., Schroer, K., Stein, N. and Wiendahl, C. 2007. Metabolomics: current state and evolving methodologies and tools. *Applied Microbiology and Biotechnology,* 76**,** 495-511.

Olejnik, A. M., Czaczyk, K., Marecik, R., Grajek, W. and Jankowski, T. 2004. Monitoring the progress of infection and recombinant protein production in insect cell cultures using intracellular ATP measurement. *Applied Microbiology and Biotechnology,* 65**,** 18-24.

Oliver, S. G., Winson, M. K., Kell, D. B. and Baganz, F. 1998. Systematic functional analysis of the yeast genome. *Trends in Biotechnology,* 16**,** 373-378.

Palomares, L. A., Lopez, S. and Ramirez, O. T. 2004. Utilization of oxygen uptake rate to assess the role of glucose and glutamine in the metabolism of infected insect cell cultures. *Biochemical Engineering Journal,* 19**,** 87-93.

Pan, X. Y., Long, G., Wang, R. R., Hou, S. W., Wang, H. Y., Zheng, Y. T., Sun, X. L., Westenberg, M., Deng, F., Wang, H. L., Vlak, J. M. and Hu, Z. H. 2007. Deletion of a *Helicoverpa armigera* nucleopolyhedrovirus gene encoding a virion structural protein (ORF 107) increases the budded virion titer and reduces *in vivo* infectivity. *Journal of General Virology,* 88**,** 3307-3316.

Pasupuleti, V. K. and Braun, S. 2010. State of the Art Manufacturing of Protein Hydrolysates. *In:* Pasupuleti, V. K. & Demain, A. L. (eds.) *Protein Hydrolysates in Biotechnology.* Dordrecht: Springer, pp. 11-32.

Pedrini, M. R. D., Chan, L. C. L., Nielsen, L. K. and Reid, S. 2006. *In vitro* production of *Helicoverpa armigera* single-nucleocapsid nucleopolyhedrovirus. *Brazilian Archives of Biology and Technology,* 49**,** 35-41.

Pedrini, M. R. S. 2003. *Characterization of few polyhedra mutants of Helicoverpa armigera nucleopolyhedrovirus cultivated in vitro.* PhD, The University of Queensland, Brisbane, Australia.

Pedrini, M. R. S., Wolff, J. L. C. and Reid, S. 2004. Fast accumulation of few polyhedra mutants during passage of a *Spodoptera frugiperda* multicapsid nucleopolyhedrovirus (Baculoviridae) in Sf9 cell cultures. *Annals of Applied Biology,* 145**,** 107-112.

Pedrini, M. R. S., Nielsen, L. K., Reid, S. and Chan, L. C. L. 2005. Properties of a unique mutant of Helicoverpa armigera single-nucleocapsid nucleopolyhedrovirus that exhibits a partial many polyhedra and few polyhedra phenotype on extended serial passaging in suspension cell cultures. *In Vitro Cellular & Developmental Biology-Animal,* 41**,** 289-297.

Pedrini, M. R. S., Reid, S., Nielsen, L. and Chan, L. C. L. 2011. Kinetic characterization of the group II *Helicoverpa armigera* nucleopolyhedrovirus propagated in suspension cell cultures: Implications for development of a biopesticides production process. *Biotechnology Progress,* 27**,** 614-624.

Plassmeier, J., Barsch, A., Persicke, M., Niehaus, K. and Kalinowski, J. 2007. Investigation of central carbon metabolism and the 2-methylcitrate cycle in Corynebacterium glutamicum by metabolic profiling using gas chromatography-mass spectrometry. *Journal of Biotechnology,* 130**,** 354-363.

Possee, R. D., Thomas, C. J. and King, L. A. 1999. The use of baculovirus vectors for the production of membrane proteins in insect cells. *Biochemical Society Transactions,* 27**,** 928-932.

Powell, K. A. and Faull, J. L. 1989. Commercial approaches to the use of biological control agents. *In:* Whipps, J. M. & Lumsden, R. D. (eds.) *Biotechnology of Fungi for Improving Plant Growth.* Cambridge: Cambridge University Press, pp. 259-275.

Power, J. F., Reid, S., Radford, K. M., Greenfield, P. F. and Nielsen, L. K. 1994. Modeling and optimization of the baculovirus expression vector system in batch suspension-culture. *Biotechnology and Bioengineering,* 44**,** 710-719.

Puskeiler, R., Kaufmann, K. and Weuster-Botz, D. 2005. Development, parallelization, and automation of a gas-inducing milliliter-scale bioreactor for high-throughput bioprocess design (HTBD). *Biotechnology and Bioengineering,* 89, 512-523.

Raamsdonk, L. M., Teusink, B., Broadhurst, D., Zhang, N. S., Hayes, A., Walsh, M. C., Berden, J. A., Brindle, K. M., Kell, D. B., Rowland, J. J., Westerhoff, H. V., van Dam,

K. and Oliver, S. G. 2001. A functional genomics strategy that uses metabolome data to reveal the phenotype of silent mutations. *Nature Biotechnology,* 19**,** 45-50.

Rabinowitz, J. D. and Kimball, E. 2007. Acidic acetonitrile for cellular metabolome extraction from *Escherichia coli*. *Analytical Chemistry,* 79**,** 6167-6173.

Radford, K. M. 1995. *Characterisation of the effect of the bioprocess environment on the capacity of the baculovirus expression vector system for recombinantproduct expression.* PhD, The University of Queensland, Brisbane, Australia.

Radford, K. M., Reid, S. and Greenfield, P. F. 1997. Substrate limitation in the baculovirus expression vector system. *Biotechnology and Bioengineering,* 56**,** 32-44.

Raghunand, N. and Dale, B. E. 1999. Alteration of glucose consumption kinetics with progression of baculovirus infection in *Spodoptera frugiperda* cells. *Applied Biochemistry and Biotechnology,* 80**,** 231-242.

Ramautar, R., Demirci, A. and de Jong, G. J. 2006. Capillary electrophoresis in metabolomics. *Trac-Trends in Analytical Chemistry,* 25**,** 455-466.

Reid, S. and Lua, L. H. L. 2005. *Method of producing baculovirus.* International Application Number: PCT/AU2004/001549. International Filing Date: 10/11/2004. Publication Number: WO2005/045014.

Reid, S., Chan, L. C. L. and Van Oers, M. M. 2013. Production of entomopathoginic viruses. *In:* Shapiro, D. E. (ed.) *Mass production of beneficial organisms.* Amsterdam: Elsevier.

Reuveny, S., Kim, Y. J., Kemp, C. W. and Shiloach, J. 1993. Production of recombinant proteins in high-density insect cell cultures. *Biotechnology and Bioengineering,* 42**,** 235-239.

Rhiel, M., Mitchell-Logean, C. M. and Murhammer, D. W. 1997. Comparison of Trichoplusia ni BTI-Tn-5B1-4 (*High Five*(TM)) and *Spodoptera frugiperda* Sf-9 insect cell line metabolism in suspension cultures. *Biotechnology and Bioengineering,* 55**,** 909-920.

Ritter, J. B., Genzel, Y. and Reichl, U. 2006. High-performance anion-exchange chromatography using on-line electrolytic eluent generation for the determination of more than 25 intermediates from energy metabolism of mammalian cells in culture. *Journal of Chromatography B-Analytical Technologies in the Biomedical and Life Sciences,* 843**,** 216-226.

Ritter, J. B., Genzel, Y. and Reichl, U. 2008. Simultaneous extraction of several metabolites of energy metabolism and related substances in mammalian cells: Optimization using experimental design. *Analytical Biochemistry,* 373**,** 349-369.

Roessner, U., Wagner, C., Kopka, J., Trethewey, R. N. and Willmitzer, L. 2000. Simultaneous analysis of metabolites in potato tuber by gas chromatography-mass spectrometry. *Plant Journal,* 23**,** 131-142.

Rohrmann, G. F. 1992. Baculovirus structural proteins *Journal of General Virology,* 73**,** 749-761.

Rohrmann, G. F. 1999. Nucleopolyhedrovirus. *In:* Granoff, A. and Webster, R.G. (ed.) *Encyclopedia of Virology.* New York: Academic Press, pp.146-152.

Rosinski, M., Reid, S. and Nielsen, L. K. 2002. Kinetics of baculovirus replication and release using real-time quantitative polymerase chain reaction. *Biotechnology and Bioengineering,* 77**,** 476-480.

Ryan, D. and Robards, K. 2006. Metabolomics: The greatest omics of them all? *Analytical Chemistry,* 78**,** 7954-7958.

Sangster, T., Major, H., Plumb, R., Wilson, A. J. and Wilson, I. D. 2006. A pragmatic and readily implemented quality control strategy for HPLC-MS and GC-MS-based metabonomic analysis. *Analyst,* 131**,** 1075-1078.

Schlaeger, E. J. 1996. Medium design for insect cell culture. *Cytotechnology,* 20**,** 57-70.

Schwab, W. 2003. Metabolome diversity: too few genes, too many metabolites? *Phytochemistry,* 62**,** 837-849.

Sellick, C. A., Hansen, R., Maqsood, A. R., Dunn, W. B., Stephens, G. M., Goodacre, R. and Dickson, A. J. 2009. Effective Quenching Processes for Physiologically Valid Metabolite Profiling of Suspension Cultured Mammalian Cells. *Analytical Chemistry,* 81**,** 174-183.

Sellick, C. A., Knight, D., Croxford, A. S., Maqsood, A. R., Stephens, G. M., Goodacre, R. and Dickson, A. J. 2010. Evaluation of extraction processes for intracellular metabolite profiling of mammalian cells: matching extraction approaches to cell type and metabolite targets. *Metabolomics,* 6**,** 427-438.

Shan, L., Wang, L., Yin, J., Zhong, P. and Zhong, J. 2006. An OriP/EBNA-1-based baculovirus vector with prolonged and enhanced transgene expression. *Journal of Gene Medicine,* 8**,** 1400-1406.

Shewach, D. S. 1992. Quantitation of deoxyribonucleoside 5'-triphosphates by a sequential boronate and anion-exchange high-pressure liquid-chromatophic procedure. *Analytical Biochemistry,* 206**,** 178-182.

Shryock, J. C., Rubio, R. and Berne, R. M. 1986. Extraction of adenine-nucleotides from cultured endothelial-cells. *Analytical Biochemistry,* 159**,** 73-81.

Shuler, M. L., Hammer, D. A. and Granados, R. R. 1995. Overview of baculovirus insect culture system. *In:* Shuler, M. L., Wood, H. A., Granados, R. R. & Hammer, D. A. (eds.) *Baculovirus Expression Systems and Biopesticides.* New York: Wiley-Liss Inc., pp. 1-11.

Siemensma, A., Babcock, J., Wilcox, C. and Huttinga, H. 2010. Towards an understanding of how protein hydrolysates stimulate more efficient biosynthesis in cultured cells. *In:* Pasupuleti, V. K. & Demain, A. L. (eds.) *Protein Hydrolysates in Biotechnology.* Dordrecht: Springer, pp. 35-54.

Silk, D. B., Grimble, G. K. and Rees, R. G. 1985. Protein digestion and amino acid and peptide absorption. *Proceedings of the Nutrition Society,* 44**,** 63-72.

Slack, J. and Arif, B. M. 2007. The baculoviruses occlusion-derived virus: Virion structure and function. *Advances in Virus Research, Vol 69.* pp. 99-165.

Sommer, R. 1996. Yeast extracts: production, properties and components. 9th International Symposium on Yeasts, 25-30 August, 1996, Sydney, Australia.

Sugiura, T. and Amann, E. 1996. Properties of two insect cell lines useful for the Baculovirus expression system in serum-free culture. *Biotechnology and Bioengineering,* 51**,** 494-499.

Szewczyk, B., Hoyos-Carvajal, L., Paluszek, M., Skrzecz, W. and de Souza, M. L. 2006. Baculoviruses - re-emerging biopesticides. *Biotechnology Advances,* 24**,** 143-160.

Szewczyk, B., Rabalski, L., Krol, E., Sihler, W. and Souza, M. L. d. 2009. Baculovirus biopesticides - a safe alternative to chemical protection of plants. *Journal of Biopesticides,* 2**,** 209-216.

Tabashnik, B. E., Van Rensburg, J. B. J. and Carriere, Y. 2009. Field-Evolved Insect Resistance to Bt Crops: Definition, Theory, and Data. *Journal of Economic Entomology,* 102**,** 2011-2025.

Tanada, Y. and Kaya, H. K. 1993. *Insect Pathology,* San Diego, Academic Press.

Tang, H. R., Wang, Y. L., Nicholson, J. K. and Lindon, J. C. 2004. Use of relaxation-edited one-dimensional and two dimensional nuclear magnetic resonance spectroscopy to improve detection of small metabolites in blood plasma. *Analytical Biochemistry,* 325**,** 260-272.

Taticek, R. A. and Shuler, M. L. 1997. Effect of elevated oxygen and glutamine levels on foreign protein production at high cell densities using the insect cell-baculovirus expression system. *Biotechnology and Bioengineering,* 54**,** 142-152.

Teakle, R. E. 1995. Prospects for the use of baculoviruses as bioinsecticides. *Australasian Biotechnology,* 5**,** 345-348.

Teng, Q., Huang, W. L., Collette, T. W., Ekman, D. R. and Tan, C. 2009. A direct cell quenching method for cell-culture based metabolomics. *Metabolomics,* 5**,** 199-208.

Theobald, U., Mailinger, W., Baltes, M., Rizzi, M. and Reuss, M. 1997. In vivo analysis of metabolic dynamics in Saccharomyces cerevisiae .1. Experimental observations. *Biotechnology and Bioengineering,* 55**,** 305-316.

Tomiya, N., Ailor, E., Lawrence, S. M., Betenbaugh, M. J. and Lee, Y. C. 2001. Determination of nucleotides and sugar nucleotides involved in protein glycosylation by high-performance anion-exchange chromatography: Sugar nucleotide contents in cultured insect cells and mammalian cells. *Analytical Biochemistry,* 293**,** 129-137.

Tran, T. T. B., Dietmair, S., Chan, L. C. L., Huynh, H. T., Nielsen, L. K. and Reid, S. 2012. Development of quenching and washing protocols for quantitative intracellular metabolite analysis of uninfected and baculovirus-infected insect cells. *Methods,* 56**,** 396-407.

Tweeddale, H., Notley-McRobb, L. and Ferenci, T. 1998. Effect of slow growth on metabolism of Escherichia coli, as revealed by global metabolite pool ("Metabolome") analysis. *Journal of Bacteriology,* 180**,** 5109-5116.

Urbanczyk-Wochniak, E., Luedemann, A., Kopka, J., Selbig, J., Roessner-Tunali, U., Willmitzer, L. and Fernie, A. R. 2003. Parallel analysis of transcript and metabolic profiles: a new approach in systems biology. *EMBO Reports,* 4**,** 989-993.

van Oers, M. M. 2006. Vaccines for viral and parasitic diseases produced with baculovirus vectors. *In:* Bonning, B. C. (ed.) *Insect Viruses: Biotechnological Applications.* pp. 193-253.

Vaughn, J. L., Goodwin, R. H., Tompkins, G. J. and McCawley, P. 1977. Establishment of 2 cell lines from insect *Spodoptera-frugiperda* (Lepidoptera-noctuidae). *In Vitro-Journal of the Tissue Culture Association,* 13**,** 213-217.

Villas-Boas, S. G., Hojer-Pedersen, J., Akesson, M., Smedsgaard, J. and Nielsen, J. 2005a. Global metabolite analysis of yeast: evaluation of sample preparation methods. *Yeast,* 22**,** 1155-1169.

Villas-Boas, S. G., Mas, S., Akesson, M., Smedsgaard, J. and Nielsen, J. 2005b. Mass spectrometry in metabolome analysis. *Mass Spectrometry Reviews,* 24**,** 613-646.

Villas-Boas, S. G. and Bruheim, P. 2007. Cold glycerol-saline: The promising quenching solution for accurate intracellular metabolite analysis of microbial cells. *Analytical Biochemistry,* 370**,** 87-97.

Vlak, J. M. 1992. The biology of baculovirus *in vivo* and in culture insect cells. *In:* Vlak, J. M., Schlaeger, E. J. & Bernard, A. R. (eds.) *Baculovirus and Recombinant Protein Processes.* Switzeland: Roche, pp. 2-9.

Wang, M. Y., Wester, K. and Bentley, W. E. 1993. Glutamine determination in insect cell culture media *Biotechnology Techniques,* 7**,** 841-846.

Wang, M. Y., Pulliam, T. R., Valle, M., Vakharia, V. N. and Bentley, W. E. 1996. Kinetic analysis of alkaline protease activity, recombinant protein production and metabolites for infected insect (Sf9) cells under different DO levels. *Journal of Biotechnology,* 46**,** 243-254.

Weibel, K. E., Mor, J. R. and Fiechter, A. 1974. Rapid sampling of yeast-cells and automated assays of adenylate, citrate, pyruvate and glucose-6-phosphate pools. *Analytical Biochemistry,* 58**,** 208-216.

Weiss, S. A., Thomas, D. W., Dunlop, B. F., Georgis, R. and Vail, P. V. *In vitro* production of viral pesticides: key elements. *In:* Monsour, C. J., Reid, S. & Teakle, R. E., eds. *Proceedings Symposium: Biopesticides: Opportunities for Australian Industry*, 1994 Brisbane. University of Queensland, 57-63.

Weiss, S. A., Whitford, W. G., Godwin, G. P., Reid, S. Media design: optimizing of recombinant proteins in serum free culture. *In:* J.M. Vlak, E.J. Schlaeger, a. & Bernard, A. R., eds. *Workshop on Baculovirus and Recombinant Protein Production Processes*, March 29th - April 1st 1992, Interlaken, Switzerland., 306-315.

Wickham, T. J., Davis, T., Granados, R. R., Shuler, M. L. and Wood, H. A. 1992. Screening of insect cell lines for the production of recombinant proteins and infectious virus in the baculovirus expression system. *Biotechnology Progress,* 8**,** 391-396.

Wiendahl, C., Brandner, J. J., Kuppers, C., Luo, B., Schygulla, U., Noll, T. and Oldiges, M. 2007. A microstructure heat exchanger for quenching the metabolism of mammalian cells. *Chemical Engineering & Technology,* 30**,** 322-328.

Winder, C. L., Dunn, W. B., Schuler, S., Broadhurst, D., Jarvis, R., Stephens, G. M. and Goodacre, R. 2008. Global metabolic profiling of Escherichia coli cultures: An evaluation of methods for quenching and extraction of intracellular metabolites. *Analytical Chemistry,* 80**,** 2939-2948.

Wittmann, C., Kromer, J. O., Kiefer, P., Binz, T. and Heinzle, E. 2004. Impact of the cold shock phenomenon on quantification of intracellular metabolites in bacteria. *Analytical Biochemistry,* 327**,** 135-139.

Wong, K. T. K., Peter, C. H., Greenfield, P. F., Reid, S. and Nielsen, L. K. 1996. Low multiplicity infection of insect cells with a recombinant baculovirus: The cell yield concept. *Biotechnology and Bioengineering*, 49, 659-666.

Wong, T. K. K., Nielsen, L. K., Greenfield, P. F. and Reid, S. 1994. Relationship between Oxygen-Uptake Rate and Time of Infection of Sf9 Insect Cells Infected with a Recombinant Baculovirus. *Cytotechnology,* 15**,** 157-167.

Wu, X. H., Yu, H. L., Ba, Z. Y., Chen, J. Y., Sun, H. G. and Han, B. Z. 2010. Sampling methods for NMR-based metabolomics of *Staphylococcus aureus*. *Biotechnology Journal,* 5**,** 75-84.

Wyatt, S. S. 1956. Culture *in vitro* of tissue from the silkworm , *Bombyx mori* L. *Journal of General Physiology,* 39**,** 853-868.

Xie, Q., Michael, P. O., Baldi, L., Hacker, D. L., Zhang, X., Wurm, F. M. 2011. TubeSpin bioreactor 50 for the high-density cultivation of Sf9 insect cells in suspension. *Biotechnology Letters*, 33, 897-902.

Yamaji, H., Tagai, S. and Fukuda, H. 1999. Optimal production of recombinant protein by the baculovirus-insect cell system in shake-flask culture with medium replacement. *Journal of Bioscience and Bioengineering,* 87**,** 636-641.

Yang, D. G., Chung, Y. C., Lai, Y. K., Lai, C. W., Liu, H. J. and Hu, Y. C. 2007. Avian influenza virus hemagglutinin display on baculovirus envelope: Cytoplasmic domain affects virus properties and vaccine potential. *Molecular Therapy,* 15**,** 1736-1736.

Yang, J. D., Gecik, P., Collins, A., Czarnecki, S., Hsu, H. H., Lasdun, A., Sundaram, R., Muthukumar, G. and Silberklang, M. 1996. Rational scale-up of a baculovirus-insect cell batch process based on medium nutritional depth. *Biotechnology and Bioengineering,* 52**,** 696-706.

Zhang, J. Y., Reddy, J., Buckland, B. and Greasham, R. 2003. Toward consistent and productive complex media for industrial fermentations: Studies on yeast extract for a recombinant yeast fermentation process. *Biotechnology and Bioengineering,* 82**,** 640-652.

Zhang, W., Tan, S., Paintsil, E., Dutschman, G. E., Gullen, E. A., Chu, E. and Cheng, Y.-C. 2011. Analysis of deoxyribonucleotide pools in human cancer cell lines using a liquid chromatography coupled with tandem mass spectrometry technique. *Biochemical Pharmacology,* 82**,** 411-417.

APPENDICES

Appendix 1:

Optimization of 50-mL tube bioreactors for insect cell cultures

1. Introduction

As metabolites turnover rapidly (de Koning and van Dam, 1992), the most critical step in the intracellular metabolite extraction procedure is stopping the cell metabolism to preserve the metabolic stage of cells at the point of sampling. Therefore, the cells need to be quenched before extracting intracellular metabolites, and it should be performed as quickly as possible. In order to achieve a quick quenching step, a sufficient amount of culture should be used and poured directly into the quenching solution as soon as it is taken out of the incubator. This step can be performed very quickly using 50-mL tube bioreactors.

Increasing culture throughput for bioprocess development has become progressively important to rapidly screen and optimize process parameters (Chen et al., 2009; Micheletti et al., 2006; Puskeiler et al., 2005). Traditionally, shake flasks and spinner flasks have been used to screen large numbers of clones, cell lines and experimental conditions (Chen et al., 2009; Doig et al., 2006). In recent years, a number of high throughput systems have been developed and reported in the literature including shake flasks, tubes, bubble columns, stirred tank bioreactors and shaken microplates (Betts and Baganz, 2006; Kumar et al., 2004).

The application of 50-mL tube bioreactors with a working volume from 5ml to 20ml, usually 20% of the total volume of the test tube, (Kumar et al., 2004), is a further scaling down step compared with the current widely used system of shaker flasks in dealing with the large number of cultures required for medium optimization processes. The tube culture system was developed by De Jesus et al. (2004), and this work confirmed the usefulness of this system for CHO cells. The main advantage of 50-mL tube bioreactors is the scaling down of the system, while still providing enough sample volume for further analysis and minimizing evaporation problems (Betts and Baganz, 2006; de Jesus et al., 2004; Jordan and Jenkins, 2007). Tube cultures are able to mimic large scale vessel behaviour, as the results discovered from 50ml tube bioreactors can be fitted into the “real” condition found in large scale bioreactors (de Jesus and Wurm, 2009). Recently, 50ml tube bioreactors have been applied widely for work with mammalian cell cultures. Xie et al. (2011) reported the successful application of TubeSpin reactors for Sf9 insect cells infected with a baculovirus.

The aim of this work is to optimize culture conditions for insect cells using high throughput 50-mL tube bioreactors. This step was conducted prior to developing the method for quenching and extraction of intracellular metabolites of cultured insect cells to

investigate the growth of insect cells in tube cultures. The advantage of tube cultures is that it allows conducting the quenching process quickly by pouring immediately the culture in each tube into a cold quenching solution. Since the working volume of a tube culture can be set up at 10 mL, this volume is sufficient for one intracellular extraction sample. As the whole culture can be sacrificed for analysis, sampling and quenching is achieved very rapidly (within seconds). The growth of cells in 50-mL tubes was tested for both HzAM1 and Sf9 cell lines compared with shaker flasks as controls.

2. Materials and methods

2.1 Cell lines, viruses and medium

There were two continuous insect cell lines used in this study. The first cell line was *Helicoverpa zea* (BCIRL-HzAM1), which was derived from the pupal ovarian tissue of *H. zea* (Lepidoptera: Noctuidae) (McIntosh and Ignoffo, 1981). The second insect cell line was *Spodoptera frugiperda* clone 9 cell-line (Sf9; ATCC CRL 1711), which was derived from the ovarian tissue of several fall armyworm pupae (*Spodoptera frugiperda*) (Vaughn et al., 1977). Details of the cell line and stock cell maintenance are described in Chapter 2 of this thesis.

The wild type baculovirus of *Helicoverpa armegia* single nucleopolyhedra virus (HearNPV) was used to infect the HzAM1 cell line, while the recombinant *Autographa californica* multiple nucleopolyhedrovirus which expresses the *Escherichia coli* LacZ gene (rAcMNPV) was used to infect Sf9 cell line. Details of virus isolates and virus stock preparation are described in Chapter 2 of this thesis.

Sf900™II serum free medium (Life Technologies) was used for insect cell propagation.

2.2 Tube culture

Standard 50-mL centrifuge tubes (TPP, Trasadingen, Switzerland) were obtained from Lomb Scientific Australia and used for cell culture. Such a high-throughput culture system allows large multiple-run experiments being carried out with efficient use of resources and labor (de Jesus et al., 2004). This is a modified 50-mL centrifuge tube with a conical bottom and a ventilated cap with a filter. The ventilated cap contains 5 different filtered ventilation holes of different sizes from 0.5 mm in diameter (smallest) to 2 mm diameter (largest). Tubes were stacked into racks mounted on a rotational shaker platform (Thermo Fisher Scientific, USA) with an orbital throw of 25 mm. The set up was installed in

a refrigerated incubator for temperature control at 28^{o}C. In all experiments, cultures in 125 ml shaker flasks (Corning Incorporation, USA) with a working volume of 25 ml were used as the control.

2.3 Experimental procedure

2.3.1 Optimization of 50-mL tube culture for HzAM1 insect cell line

A series of preliminary experiments were conducted to evaluate evaporation rate, and screening for the optimal agitation range for insect cell cultures. The evaporation test over 7 days was conducted with 50-mL tube cultures using a 10 mL working volume and shaking speed of 250 rpm, while the shaker flask culture control was set at 25 mL working volume and shaking speed of 120 rpm. In the preliminary experiment for screening of agitation speeds, insect cell growth in the 50-mL tube culture was first tested at 300 rpm with a seeding cell density of 0.5×10^6 cell/mL. Later on, the shaking speed of 250 rpm was tested with a range of working volumes of 5, 7.5, 10 and 20 mL and two different seeding cell densities of 0.5×10^6 and 1×10^6 cells/mL. Shaker flask cultures were used as a control and were set up at 25 mL, 120 rpm. Experiments were performed in triplicates.

In order to evaluate concurrently the agitation speed and working volume of insect cell growth in 50 ml tube bioreactors, a 2×3 factorial experiment was conducted. In this experiment, insect cells grown in 50 ml tube bioreactors were tested at 2 agitation speeds: 220 and 250 rpm and 3 working volumes: 7.5, 10 and 20 ml. All treatments were done in triplicate. Seeding cell density for this experiment was at 0.5×10^6 cells/ml. Cultures were prepared in a shaker flask and then aliquoted into tubes of different working volumes as per the trial design. Three 125 ml shaker flasks with a working volume of 25 mL were also set up as the control. The total cell density of cultures over 7 days was estimated daily using the Multisizer™4 Coulter Counter.

To optimize the culture conditions for baculovirus infected HzAM1 cells in 50-mL tube bioreactors, an experiment was conducted at two infection cell densities (ICDs) of 0.5×10^6 and 1×10^6 cells/mL and three working volumes of 7.5, 10 and 20 mL at an agitation of 250 rpm. Infections were conducted at a multiplicity of infection (MOI) of at least 6 PFU/cell. Experiments were conducted in triplicate. Shaker flask cultures (in triplicate) were also conducted at the two ICDs mentioned above at a working volume of 25 ml. Volumetric and specific OB yields of infected cultures in 50-mL tube bioreactors were compared with that of the control of infected cultures in shaker flasks.

2.3.2 Optimization of 50-mL tube culture for Sf9 insect cell line

The growth of Sf9 cells in 50-mL tube bioreactor was first investigated at the agitation of 220 rpm and 10 mL working volume as this was shown to be optimal for the HzAM1 cell line. Triplicate cultures were used for each treatment. Shaker flask cultures (in triplicate) at 120 rpm, 25 mL working volume were used as the control. As Sf9 cells in 50-mL tube cultures did not grow as well as those in shaker flask cultures, another experiment was conducted at a range of shaking speeds of 200, 220, 240 and 260 rpm and working volume of 10 mL for Sf9 cells in 50-mL tube bioreactors. Again, shaker flask cultures at 120 rpm, 25 mL working volume were also used as the control. All treatments were conducted in triplicates.

2.4 Assays

Total cell density and total cell volume of all experiments were measured using a Multisizer™4 Coulter Counter (Beckman Coulter Inc., Fullerton, CA, USA). The cell viability was estimated using Typan Blue exclusion method. Details for cell enumeration and cell viability estimation are described in Chapter 2.

Baculovirus occlusion bodies (OBs) were extracted from infected cells using SDS digestion, and were enumerated via microscopy using a hemocytometer, as described in Chapter 2 of this thesis. The OB count for each sample was conducted in technical triplicates.

3. Results and discussion

3.1 Optimization of 50-mL tube culture for HzAM1 insect cell line

The evaporation loss of cultures in 50-mL tubes and shaker flasks is presented in Fig. A1.1. The absolute amount of liquid loss during the culture time was similar in the tubes and shaker flasks. Since the working volume of the shaker flask was more than twice as much as that of the tube culture, the relative liquid loss over the initial volume of the tube culture (10 mL working volume) was nearly double of that of the shaker flask culture (25 mL working volume). Nevertheless, the relative liquid loss through evaporation in tube culture was in an acceptable range, 6.2% over 7 days of culture (Fig. A1.1). The low evaporation rate of 50-mL tube cultures makes them a useful tool for media optimization when dealing with slow-growing animal cells (Betts and Baganz, 2006).

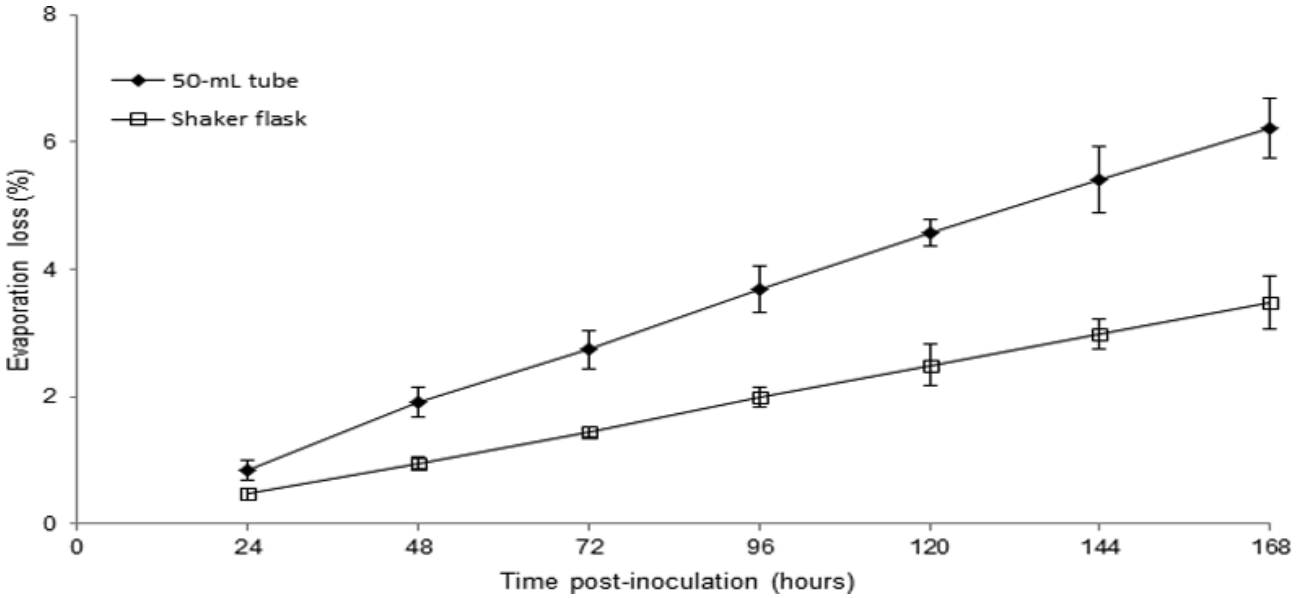

Fig. A1.1 Evaporation loss of cultures of HzAM1 insect cells in 50-mL tube bioreactors at an agitation of 250 rpm and 10 mL working volume versus shaker flasks at 120 rpm and 25 mL working volume. The experiment was conducted in biological triplicates and the error bars are standard deviations of the triplicates.

The 50-mL tube culture was first applied for mammalian cell culture by de Jesus et al. (2004) with a shaking speed of 200 rpm. Since then, 50-mL tube cultures have been used widely for mammalian cell culture with a common shaking speed set at 270 rpm for CHO cells. Initially, it was thought that insect cells required more oxygen than CHO cells (given their larger size) and thus, the shaking speed for insect cells in tube cultures should be higher. Consequently, a shaking speed of 300 rpm was first set up for testing insect cell growth in 50 ml tube cultures. The cell density and viability of HzAM1 cell cultures in 50-mL tube bioreactors, grown at the agitation speed of 300 rpm is shown in Fig. A1.2. The total cell density (TCD) after 24 hours in the tube and shaker flask were similar. However, the TCD of the tube culture was far below that of the shaker flask culture at later times post-inoculation. At 120 hours, the TCD of the culture in the shaker flask was close to 8×10^6 cells/mL, while the TCD of the culture in the 50-mL tube was only around 5×10^6 cells/mL. There was no difference in the viability of the insect cell cultures grown in the 50-mL tube and the shaker flask up to 72 hours post-inoculation. Then, the cell viability in the 50-mL tube cultures significantly reduced after that point (Fig. A1.2). This result shows that the agitation speed of 300 rpm was not suitable for cultures of the HzAM1 cell line in 50-mL tube bioreactors.

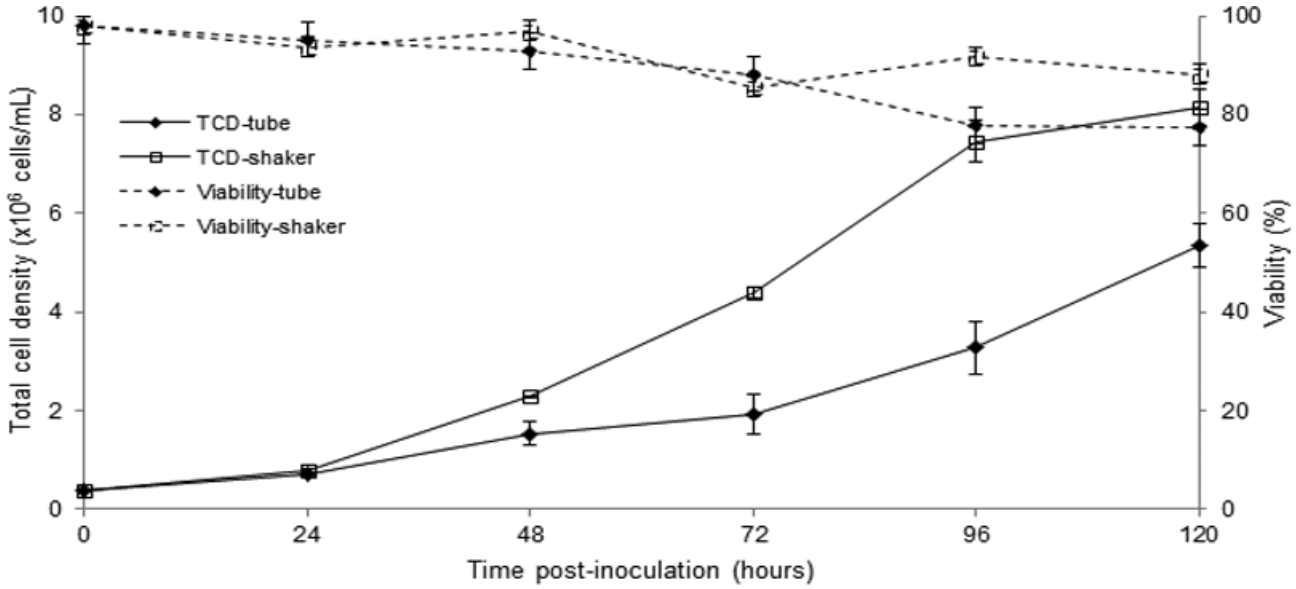

Fig. A1.2 Total cell density and viability of HzAM1 insect cell culture growth in 50-mL tube bioreactors at 10 mL working volume and 300 rpm agitation versus shaker flasks at 25 mL working volume and 120 rpm agitation. Experiment was conducted in biological triplicates and the error bars are standard deviations of the triplicates.

The growth of HzAM1 insect cells in 50-mL tube bioreactors was investigated further at the lower agitation speed of 250 rpm and at various working volumes of 5, 7.5, 10 and 20 mL at the seeding cell density of 0.5×10^6 cells/mL. Result in Fig. A1.3a shows that there was no significant difference among treatments in terms of the total cell density (TCD), except for the lowest working volume in 50-mL tube bioreactors (5 mL). The TCD of uninfected HzAM1 cells in tube cultures was similar to that in the shaker flask control; except for the case of the tube culture at a 5 mL working volume where the TCD was significantly lower than the other cases (Fig. A1.3a). The TCD of uninfected cells in tube cultures at a 20 mL working volume was slightly lower than those in tube culture volumes of 7.5 and 10 mL working volumes and the shaker control. Cell growth in the tube culture at a working volume of 7.5 ml was as good as the 10 mL case. If the working volume is too low (5 mL) or too high (20 mL) then the tube culture does not support cell growth as well as the shaker control. For the total cell volume (TCV), Fig. A1.3b shows that TCV of tube cultures at a working volume of 7.5, 10 and 20 mL were similar to that of the shaker flasks. However, the TCV of uninfected HzAM1 cells in 50-mL tube bioreactors at a low working volume (5 mL) was significantly lower than the other cases. From this preliminary experiment, it can be concluded that the HzAM1 insect cell line can grow well in 50-mL tube bioreactors at an agitation speed of 250 rpm and a working volume of 7.5 to 10 mL.

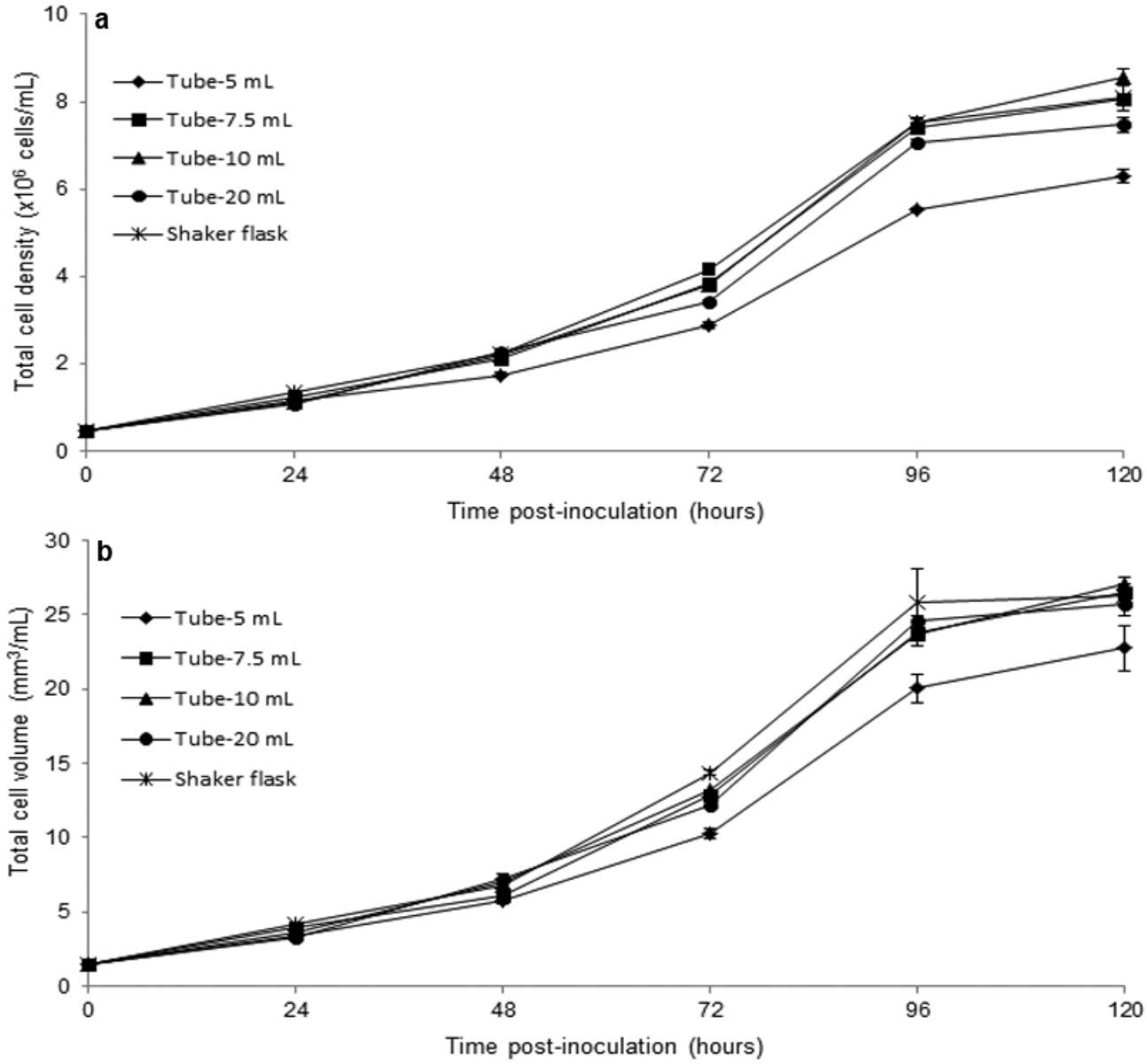

Fig. A1.3. Total cell density (a) and cell volume (b) of HzAM1 insect cell cultures seeded at 5×10^5 cells/mL and grown in 50-mL tube bioreactors at 250 rpm and at the indicated working volumes versus shaker flasks at 120 rpm and 25 mL working volume. All values represent the average of the three biological replicates, and the error bars indicate the standard deviation of the biological triplicates.

The cell growth results of a final tube optimization experiment, in which two different agitation speeds (220 and 250 rpm) was tested against three working volumes (7.5, 10 and 20 mL) are shown in Fig. A1.4. In this case, there was no difference in the TCD (Fig.A1.4a) and TCV (Fig. A1.4b) between insect cell cultures in tubes and shaker flasks for all conditions investigated. In 50-mL tube bioreactors, the TCD and TCV of the cultures at the two different shaking speeds of 250 and 220 rpm were similar.

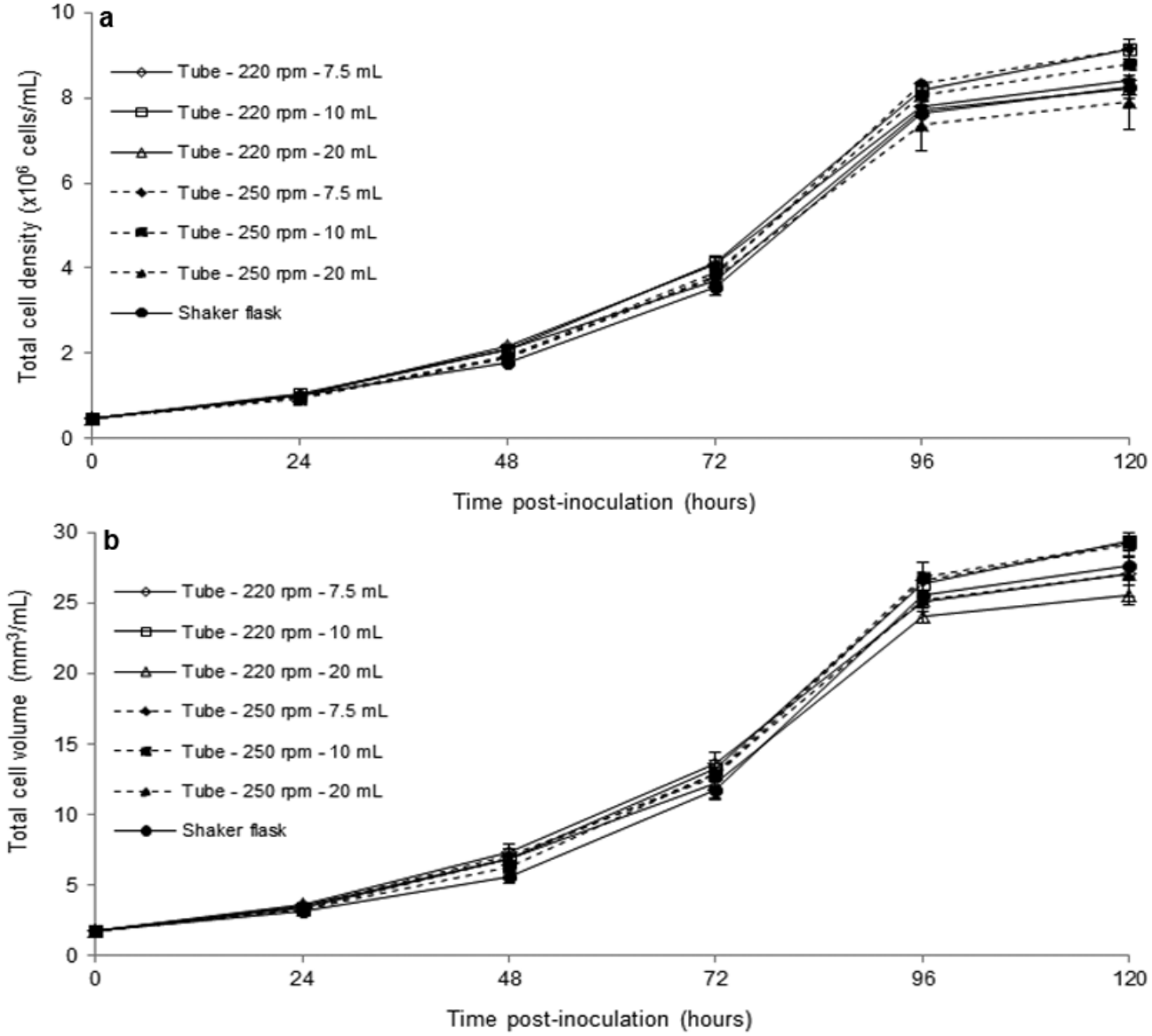

Fig. A1.4. Total cell density (a) and cell volume (b) of insect cell cultures seeded at 0.5×10^6 cells/mL, grown in 50-mL tube bioreactors at 220 and 250 rpm (at the indicated working volumes) vs shaker flasks at 120 rpm and 25 mL working volume. All values represent the average of the three biological replicates, and the error bars indicate the standard deviation of the biological triplicates

In summary, the result in Fig. A1.1 indicates that evaporation rates by tube cultures are within acceptable levels, (10 mL working volume, 250 rpm). Fig. A1.2 shows that excessive mixing (10 mL working volume, 300 rpm), results in poor cell growth. Fig. A1.3 indicates that 7.5 to 10 mL is the best working volume for tube cultures (seeded at 0.5×10^6 cells/mL, 250 rpm), while too low (5 mL) or too high (20 mL) a working volume of cultures produce a less optimal result. Fig. A1.4 indicates that 220 rpm is as good as 250 rpm for 7.5 and 10 mL cultures in 50-mL tube bioreactors. This figure shows that a 20 mL working

volume is also good for tube cultures, but when considering all the data together, it is advisable to work with 7.5-10 mL culture volumes.

Kumar et al. (2004) concluded that the best working volume for 50-mL tube bioreactors was from 5 mL to 20 mL and the most suitable working volume was usually 20% of the total volume of the test tube. It could be concluded from this work (Fig. A1.1-4) that a shaking speed of 220 to 250 rpm and a working volume of 7.5 to 10 mL are the most suitable for HzAM1 insect cell growth in 50-mL tube bioreactors.

The results above showed that uninfected HzAM1 insect cells grow well in 50-mL tube bioreactors at a shaking speed of 220 rpm and a working volume of 7.5 to 10 mL. At this agitation speed, however, baculovirus infected HzAM1 insect cells clumped and precipitated on the bottom of the tube. Therefore, 250 rpm was chosen for infected cultures in 50-mL tubes.

Volumetric and specific OB yields of infected cultures in 50-mL tube bioreactors at 250 rpm and various working volumes of 7.5, 10 and 20 ml are shown in Fig. A1.5. The cell density increase post-infection for the case of infected cells in 50-mL tube bioreactors at the 7.5 and 10 mL working volumes and the shaker flask control was in the range of 76-93% and 64-82% for the infection cell density (ICD) of 0.5×10^6 and 1×10^6 cells/mL, respectively. There was no difference in cell density increase post-infection and the average cell volume between tube cultures at 7.5 and 10 mL working volumes and the shaker culture (Fig. A1.5a). For the case of infected cultures in 50-mL tube bioreactors at the working volume of 20 mL, the cell density decreased post-infection (Fig. A1.5a). At the high working volume (20 mL) in 50-mL tube cultures, infected cells were found to precipitate in the bottom of the tube. Hence, the cell population reduced, presumably as there was not enough oxygen for the precipitated cells. This result indicates that a 20 mL working volume in 50-mL tube cultures is too much to allow proper mixing of the infected HzAM1 cells. At this high working volume, infected cells clumped and settled on the bottom of the tube as the 250 rpm shaking speed was not enough to keep the virus induced clumped cells in suspension for such a high volume in the tube culture. The average cell volume of infected cultures at an ICD of 0.5×10^6 cells/mL was larger than that at an ICD of 1×10^6 cells/mL (Fig. A1.5a). The larger cell volume resulted in a higher cell specific yield (Fig A1.5a, b). Generally, however, there was no difference in the OB yield of infected cells grown in shaker flasks or in 50 ml tube bioreactors at 250 rpm with a working volume of 7.5 or 10 mL (Fig. A1.5b). The specific OB yield for cultures at an ICD of 0.5×10^6 cells/mL were higher than that at an ICD of 1×10^6 cells/mL as found for the average cell volume.

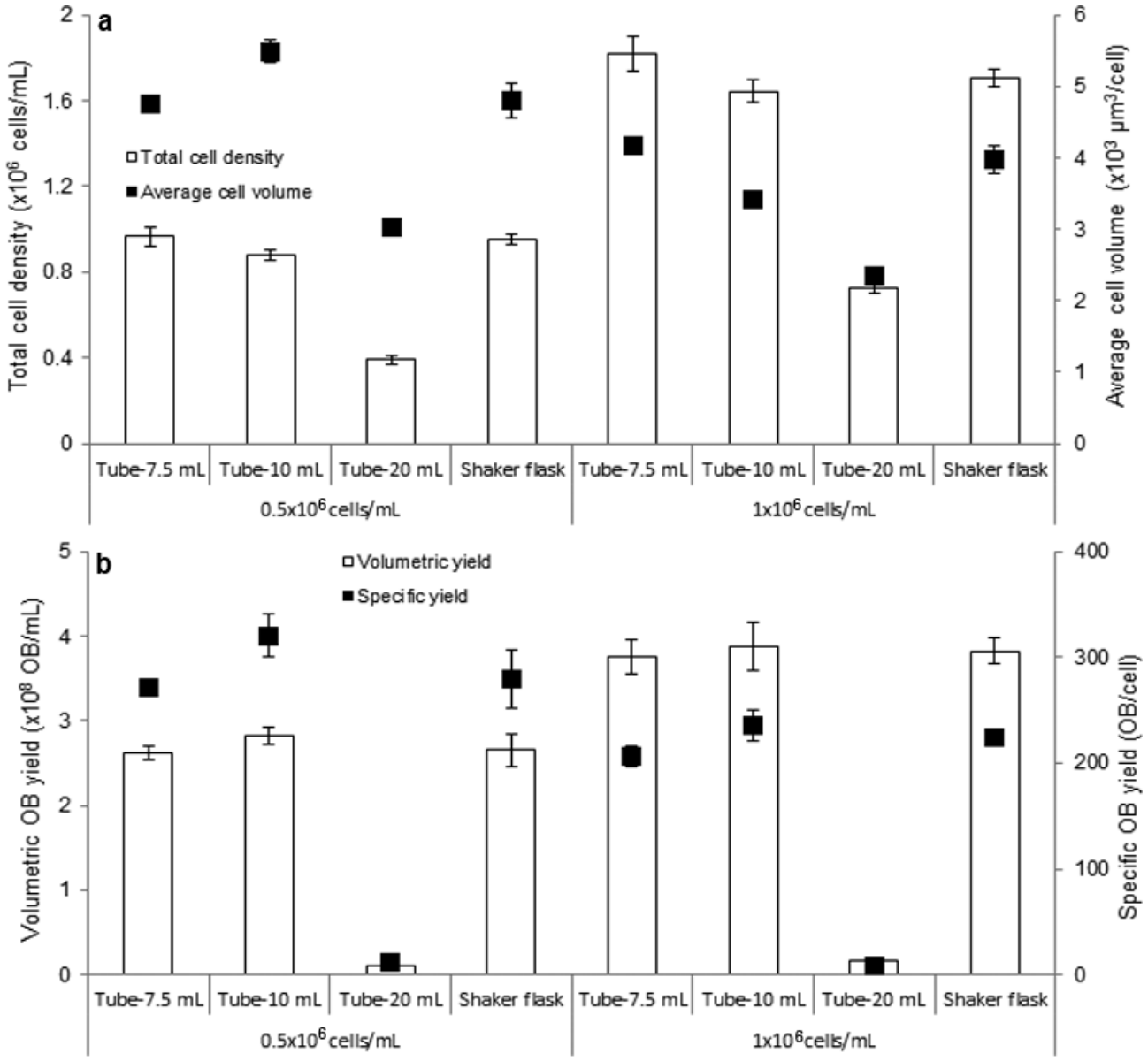

Fig. A1.5. Total cell density and average cell diameter (a) and volumetric and specific OB yields (b) of infected HzAM1 insect cell cultures in 50-mL tube bioreactors at 250 rpm (at the indicated working volumes) vs shaker flasks at 120 rpm, 25 ml working volume. Two infection cell densities (ICDs) were used of 0.5×10^6 and 1×10^6 cells/mL. Infections were conducted at a multiplicity of infection (MOI) of at least 6 PFU/cell using the supernatant of P2 virus stock. All values represent the average of the three biological replicates, and the error bars indicate the standard deviation of the biological triplicates

3.2 Optimization of 50-mL tube culture for Sf9 insect cell line

As found above, HzAM1 insect cells can grow well at the shaking speed of 220 rpm and 10 mL working volume. Therefore, the cell growth of uninfected Sf9 cells in 50-mL tube bioreactors was tested at this agitation and working volume and the result is presented in Fig. A1.6. Unlike HzAM1 cells, Sf9 cells did not grow well in 50-mL tube

bioreactors. Cell growth in 50-mL tubes seemed to be similar to that of the shaker flasks over the first day. After that however the total cell density in 50-mL tube cultures increased only slightly, while cells nearly doubled every day, as normal, in shakers (Fig. A1.6). The viability of cells in 50 ml tube cultures also dropped quickly, while they remained at a high level in shaker flask cultures. Although Sf9 cells seemed to double over the first day in 50-mL tube cultures, these cells already were likely to be in a suboptimal condition and this would not be suitable for intracellular metabolite studies.

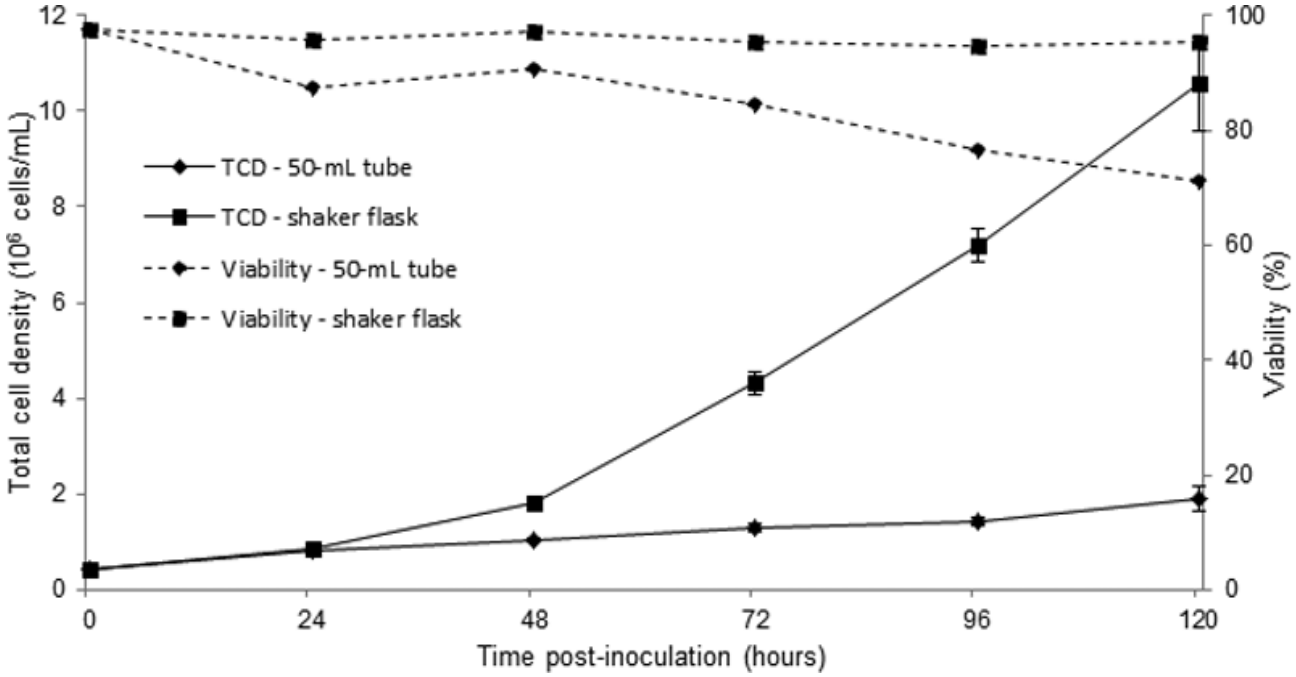

Fig. A1.6 Total cell density (TCD) and viability of uninfected Sf9 cells grown in 50-mL tubes at 220 rpm, 10 ml working volume, and in shaker flasks at 120 rpm and 25 ml working volume. The seeding cell density was at 0.5×10^6 cells/mL using SF900II medium. All values represent the average of three biological replicates, and the error bars indicate the standard deviation of the biological triplicates.

A further investigation was conducted under the wide range of shaking speeds of 200, 220, 240, and 260 rpm for growing Sf9 cells in 50-mL tube bioreactors and the result is shown in Fig. A1.7. The result here indicates that 50-mL tube bioreactors seem to be not suitable for Sf9 insect cells as no response was found with different shaking speeds. However, Xie et al. (2011) reported that Sf9 insect cells grew well in 50-mL tube bioreactors at an agitation of 200 rpm and 10 mL working volume where the cell viability was maintained over 90% and the uninfected cell grew up to 1.6×10^7 cells/mL in Sf900™II medium. The reason why the Sf9 cells in the current study did not grow in 50-mL tube cultures is unclear.

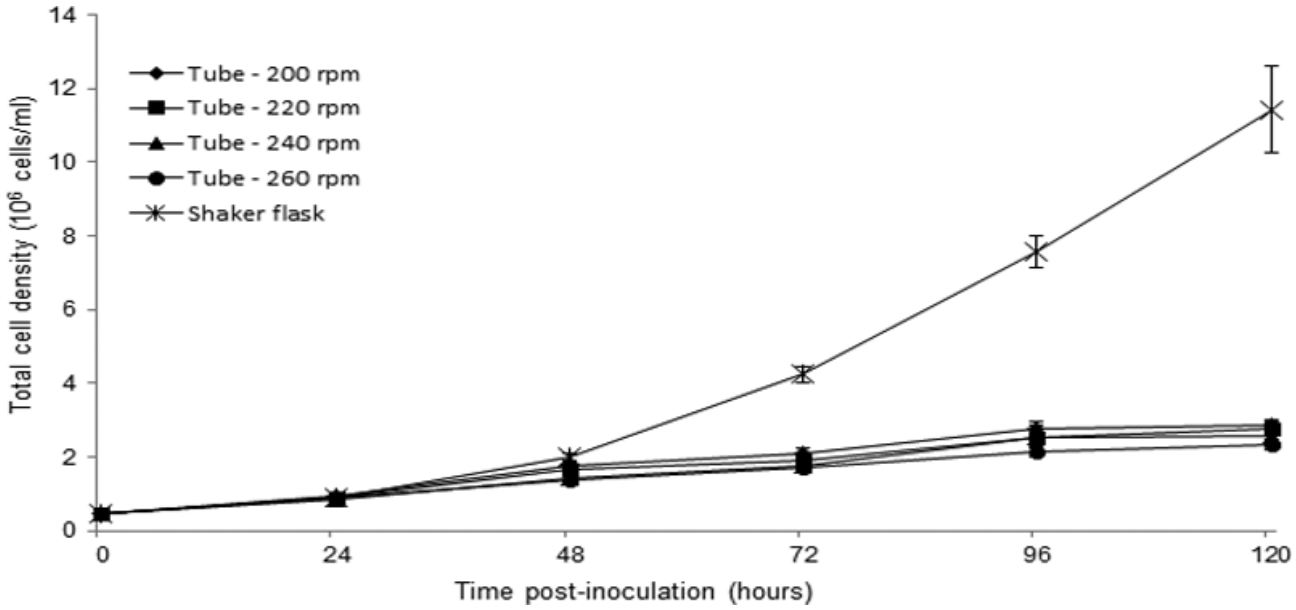

Fig. A1.7 Total cell density (TCD) of uninfected Sf9 cells grown in 50 ml tubes (10 mL working volume) at different shaking speeds of 200, 220, 240 and 260 rpm and in shaker flasks (25 mL working volume, 120 rpm). The seeding cell density was at 0.5×10^6 cells/mL using SF900II medium. All values represent the average of three biological replicates, and the error bars indicate the standard deviation of the biological triplicates.

4. Conclusions

The high throughput means of 50-mL tube bioreactors are useful for the process of screening and optimization of cell culture conditions as they allow more replication of treatments using the same amount of lab resources (incubator space, medium), while providing sufficient culture volumes for sampling. Tube cultures also provide an opportunity for quick handling of intracellular metabolite quenching and extraction processes as the addition of quenching solution and centrifugation can be done using the same tube for cell culture. Therefore, if insect cells can grow well in 50-mL tube bioreactors as mammalian cells do, it provides a good opportunity for the intracellular metabolite extraction protocol to be performed in a quick and accurate manner. Results from the current study confirm that 50-mL tube bioreactors can support both uninfected and infected HzAM1 insect cells where the cell growth and baculovirus yield were as good as found in shaker flask controls. Therefore, 50-mL tube bioreactors can be used for intracellular metabolite studies for this insect cell line. In contrast, the Sf9 insect cell population used in these studies did not grow well in 50-mL tube bioreactors under the conditions employed, despite a previous report indicating Sf9 cells can grow well in tube cultures. For this case, therefore, shaker cultures should be used for intracellular metabolite extraction studies for Sf9 cells of both uninfected and infected cultures.

Appendix 2:

Glucose and amino acid concentrations post-infection/ inoculation - Sf9/AcMNPV system in Sf900™III medium

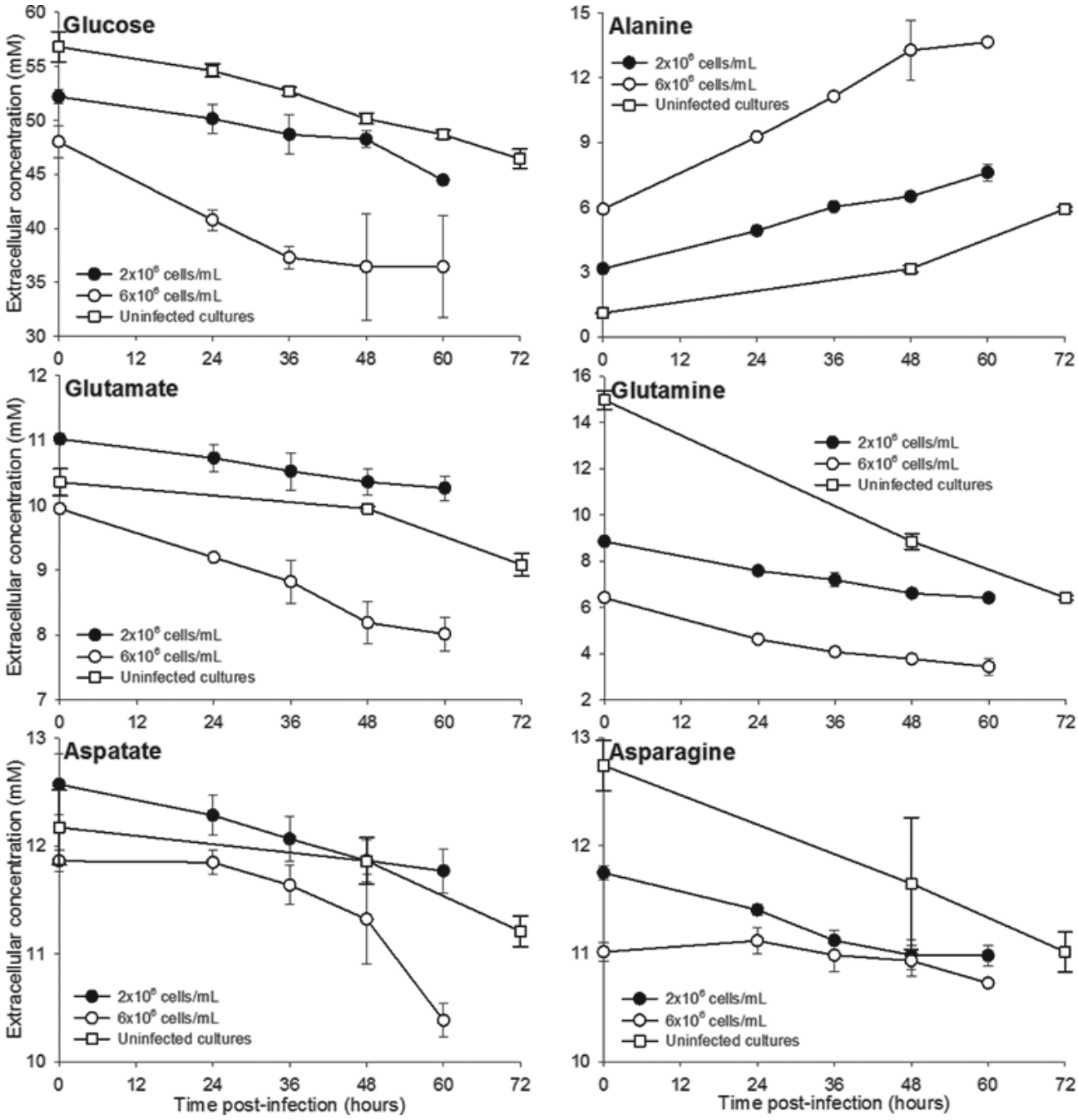

Fig. A2.1 Glucose, alanine, glutamate, glutamine, aspatate and asparagine concentrations at various times post-infection/inoculation for the infected and uninfected Sf9 cell/rAcMNPV system in Sf900™III medium. Infection cell densities (ICDs) investigated included a low (2×10^6 cells/mL) and a high (6×10^6 cells/mL) ICD by seeding a culture at an initial cell density of 0.5×10^6 cells/mL letting them grow and then infecting at different times post-inoculation to obtain the targeted ICDs. Infections were conducted at an MOI of 10 PFU/cell. The uninfected culture was set up at a seeding cell density of 0.5×10^6 cells/mL and left to grow until the peak cell density was obtained. The experiment was conducted in shaker-flask suspension cultures. Each data point is the average from three biological replicates, and the error bars represent the standard deviation.

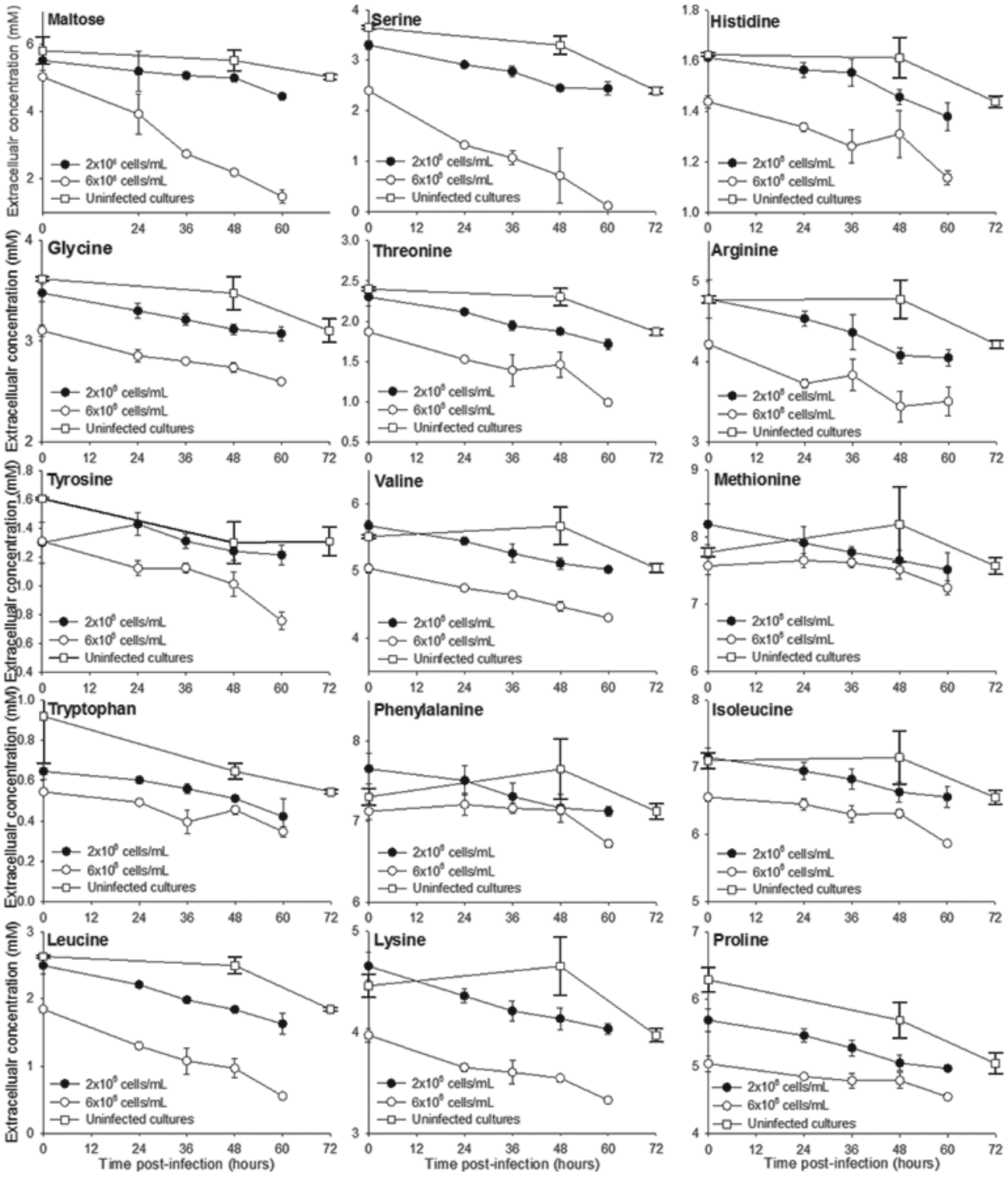

Fig. A2.2 Maltose and various amino acid concentrations at various times post-infection/ inoculation for the infected and uninfected Sf9 cell/rAcMNPV system in Sf900™III medium. Conditions were as for Fig. A2.1.

Appendix 3:

Glucose and amino acid concentrations post-infection/ inoculation - Sf9/AcMNPV system in chemically defined medium (CDM)

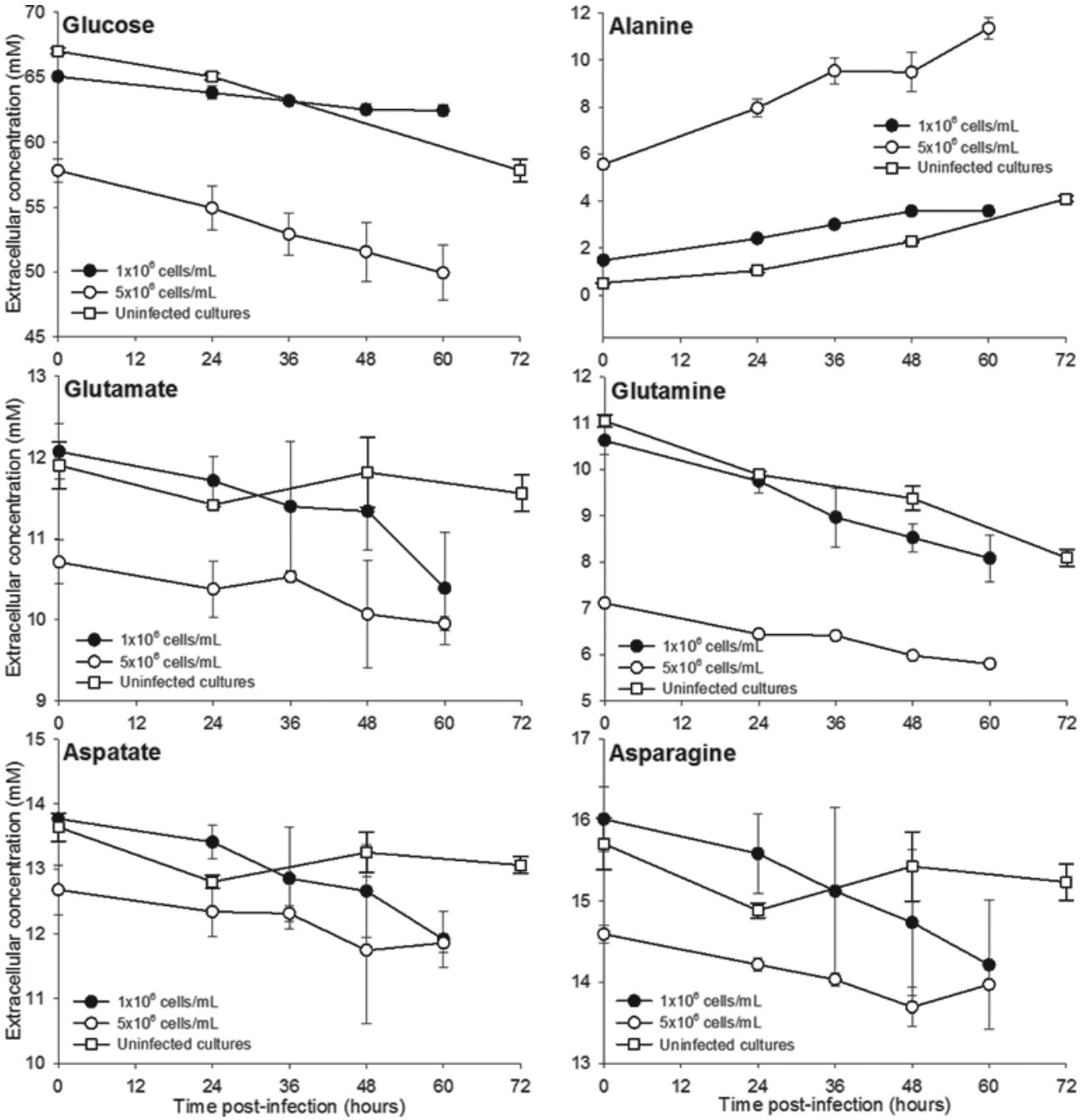

Fig. A3.1 Glucose, alanine, glutamate, glutamine, aspatate and asparagine concentrations at various times post-infection/inoculation for the infected and uninfected Sf9 cell/rAcMNPV system in CDM. Two infection cell densities (ICDs) were investigated including a low (1×10^6 cells/mL) and a high (5×10^6 cells/mL) ICD by seeding a culture at an initial cell density of 0.5×10^6 cells/mL, letting them grow and then infecting them at various times post-inoculation to obtain the targeted ICDs. Infections were conducted at an MOI of 10 PFU/cell. The uninfected culture was set up at a seeding cell density of 0.5×10^6 cells/mL and left to grow until the peak cell density was obtained. The experiment was conducted in shaker-flask suspension cultures. Each data point is the average from three biological replicates, and the error bars represent the standard deviation.

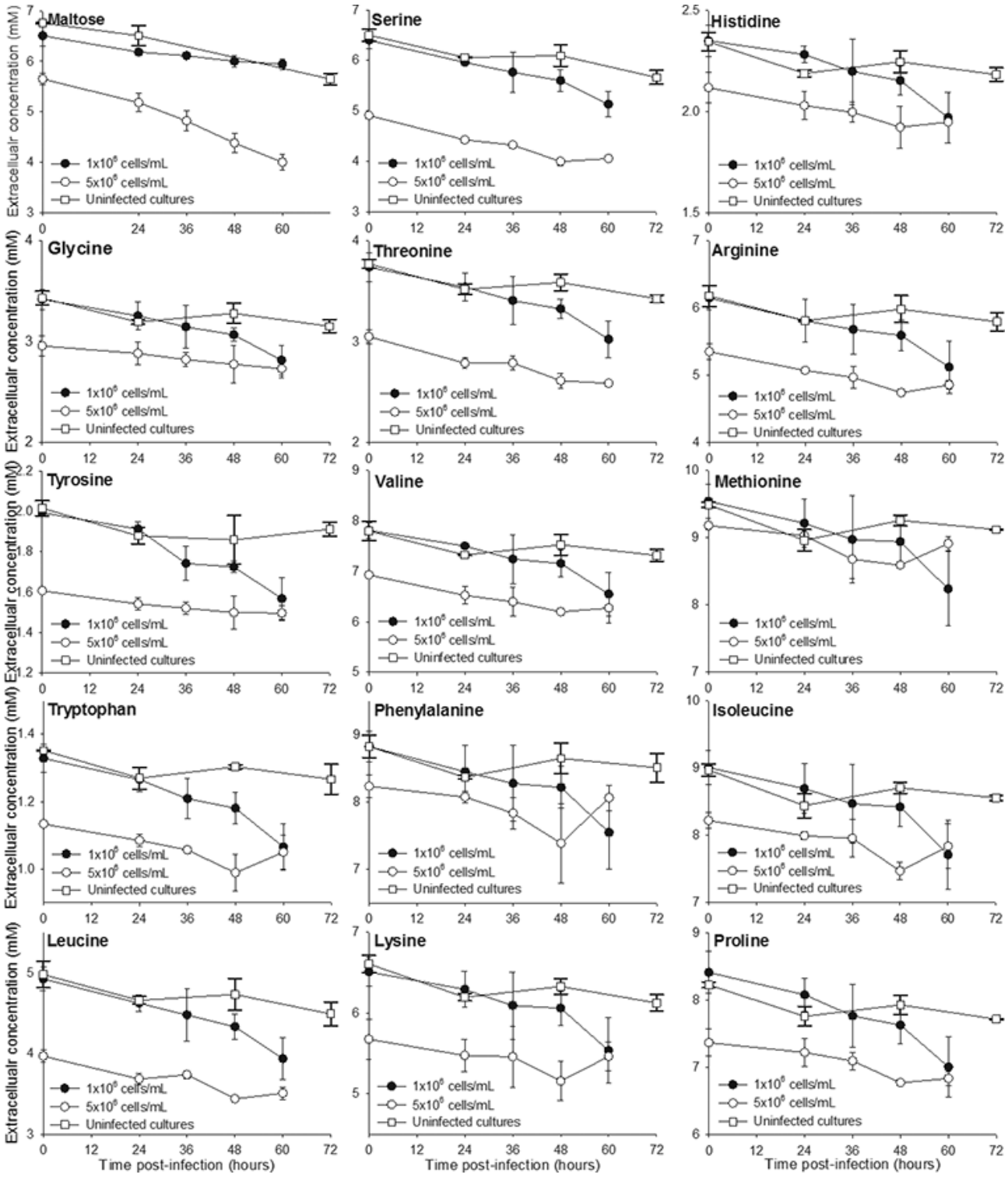

Fig. A3.2 Maltose and various amino acid concentrations at various times post-infection/ inoculation for the infected and uninfected Sf9 cell/rAcMNPV system in CDM. Conditions were as for Fig. A3.1.

Appendix 4:

Glucose and amino acid concentrations post-infection/ inoculation - HzAM1/HearNPV system in Sf900™III medium

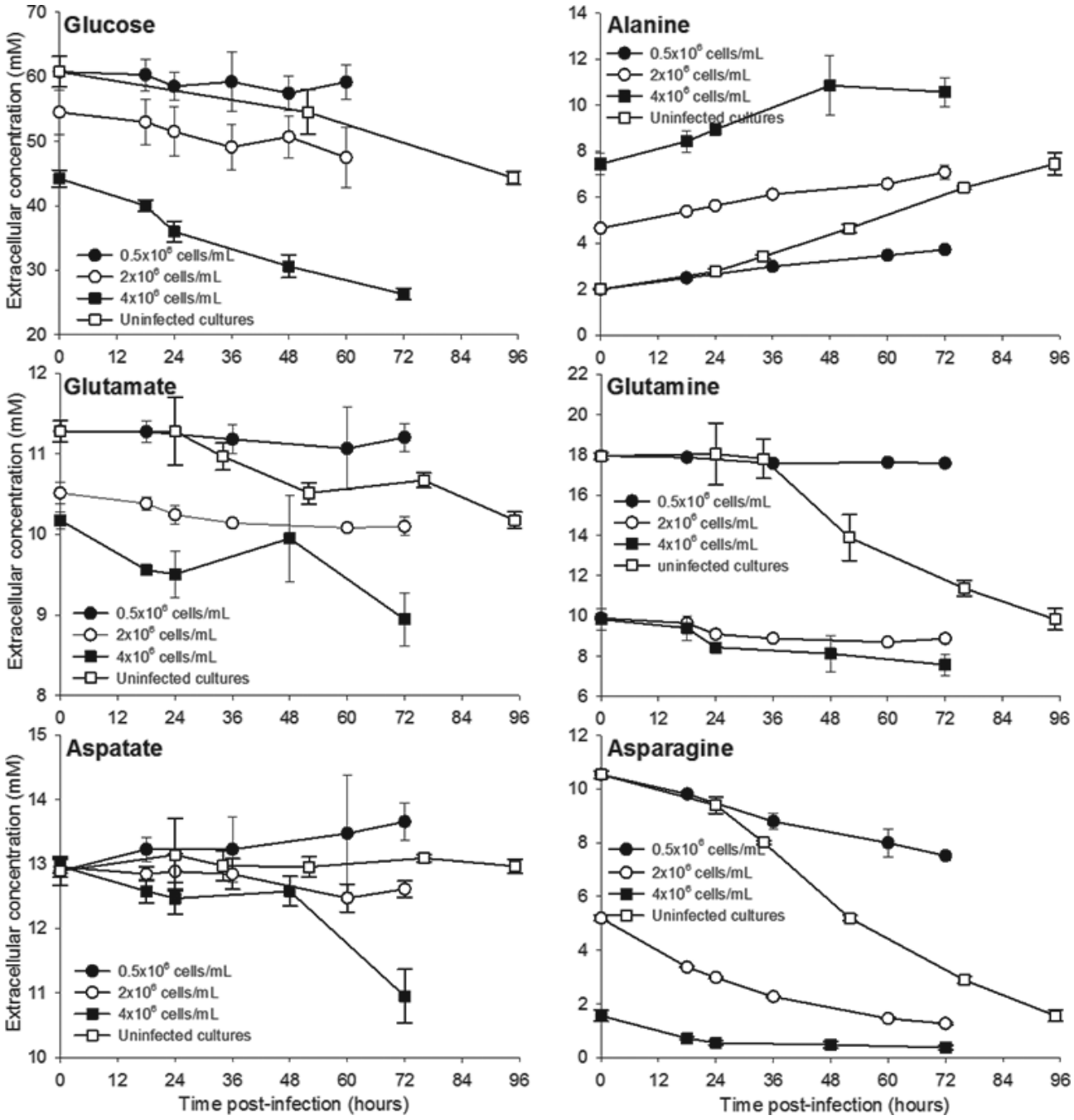

Fig. A4.1 Glucose, alanine, glutamate, glutamine, aspatate and asparagine concentrations at various times post-infection/inoculation for the infected and uninfected HzAM1 cell/HearNPV system in Sf900™III medium. Various infection cell densities (ICDs) were investigated including 0.5, 2 and 4×10^6 cells/mL by seeding a culture at an initial cell density of 0.5×10^6 cells/mL, letting them grow and then infecting them at various times post-inoculation to obtain the different ICDs. Infections were conducted at an MOI of 5 PFU/cell. The uninfected culture was set up at a seeding cell density of 0.5×10^6 cells/mL and left to grow until the peak cell density was obtained. The experiment was conducted in shaker-flask suspension cultures. Each data point is the average from three biological replicates, and the error bars represent the standard deviation.

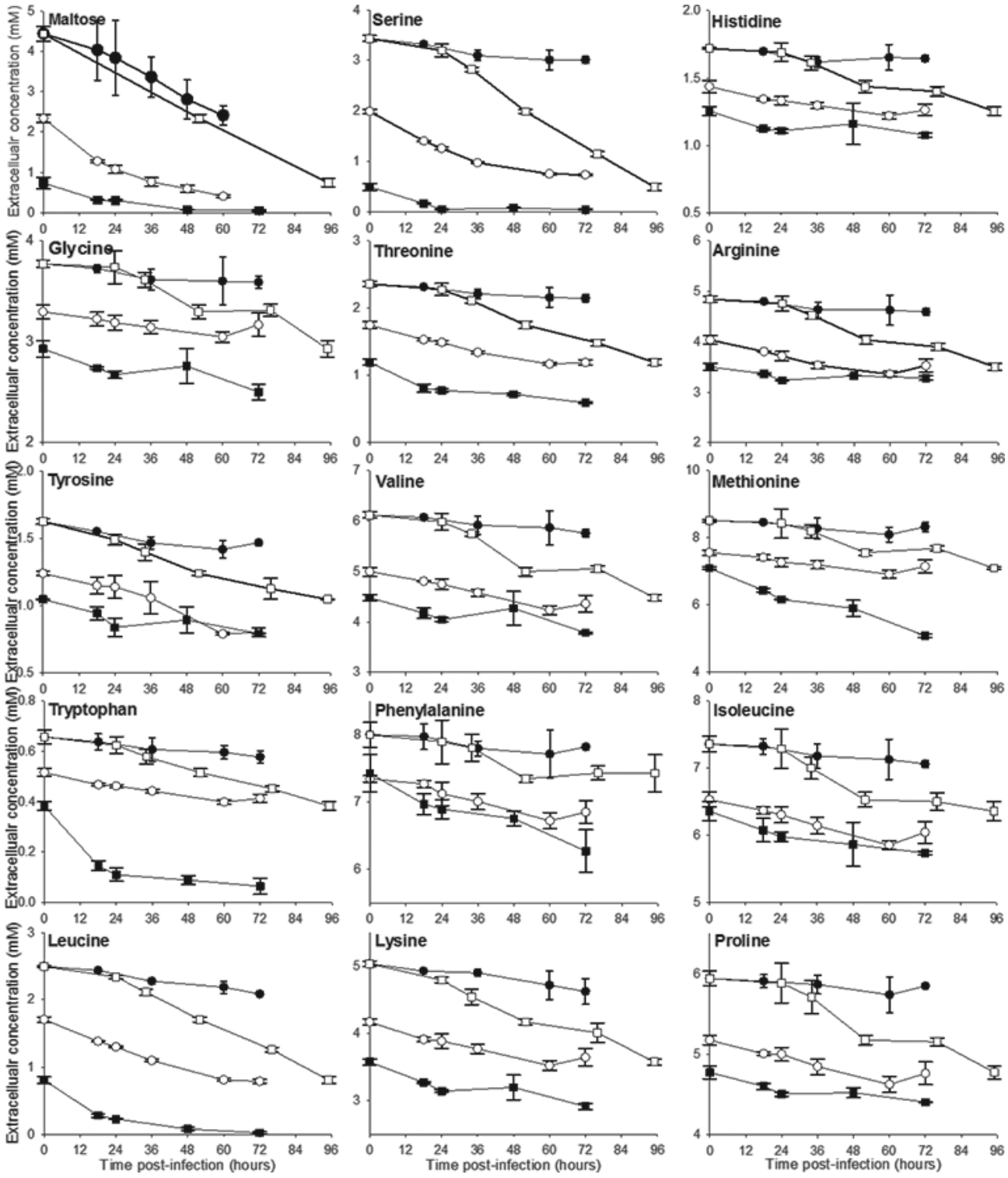

Fig. A4.2 Maltose and various amino acid concentrations at various times post-infection/ inoculation for the infected and uninfected HzAM1 cell/HearNPV system in Sf900™III medium. Various infection cell densities (ICDs) have been investigated including 0.5 (●), 2 (O) and 4 (■) $\times 10^6$ cells/mL. Conditions were as for Fig. A4.1.